Investigation of the antioxidative and radical scavenging impact of natural compounds *in-vitro* and on cell metabolism

I n a u g u r a l d i s s e r t a t i o n

zur Erlangung des akademischen Grades eines

Doktors der Naturwissenschaften (Dr. rer. nat.)

der

Mathematisch-Naturwissenschaftlichen Fakultät

der

Universität Greifswald

vorgelegt von

Dana Alexandra Thal

geboren am 15.09.1989

in Hamburg

Greifswald, 23.05.2018

Dekan: Prof. Dr. Werner Weitschies

1. Gutachter: PD Dr. Heike Kahlert

2. Gutachter: Prof. Dr. Uwe Schröder

Tag der Promotion: 08.10.2018

Content

Abstract

In an aerobic environment the occurrence of reactive oxygen species (ROS) is a common phenomenon. The diverse roles of ROS in cellular function and in diseases make them a target of interest in many research areas. Substances capable of directly or indirectly reducing the (harmful) effects of ROS are referred to as "antioxidants". However, the term is applied miscellaneously in the chemical and the biological context to describe different attributes of a substance. In this work the potential of an electrochemical assay to detect different ROS *in-vitro* was explored. The method was optimized to investigate the radical scavenging activities (antioxidant potential) of trolox and different plant compounds (ascorbic acid, caffeic acid, epigallocatechin gallate, ferulic acid, kaempferol, quercetin, rutin, and *Gynostemma pentaphyllum* extract) *in-vitro*. The obtained data was compared to established antioxidant *in-vitro* assays. Further, the impact of the plant substances on cellular parameters was evaluated with the electrochemical assay and established cell assays.

The optimization of the electrochemical assay allowed the reproducible detection of ROS. The sensor electrode proved differently sensitive towards individual ROS species. The highest sensitivity was recorded for hydroxyl radicals while superoxide and hydrogen peroxide had little impact on the sensor. Extracellular ROS concentrations could be detected from cell lines releasing elevated ROS into the extracellular space. The antioxidant activity of the investigated plant substances could be demonstrated with all *in-vitro* assays applied. However, the absolute as well as the relative activity of the individual substances varied depending on the experimental parameters of the assays (pH, radical species, phase, detection method).

The plant compounds modified redox related intracellular parameters in different cell lines. However, a direct correlation between intracellular and extracellular effects of the plant compounds could not be established.

The work demonstrates the feasibility to use the electrochemical assay to sense ROS as well as to evaluate the radical scavenging activity of molecules. The *in-vitro* antioxidant activities demonstrated for the individual plant substances are not reliable to predict the cellular effects of the molecules.

Figures

Tables

Abbreviations

% v/v	volume percentage
°C	degree Celsius
°K	degree Kelvin
µg	microgram
µL	microliter
µM	micro molar
µm	micrometer
^{1}H-NMR	1H-nuclear magnetic resonance
A	ampere
A	amplitude or integral intensity of an IR absorption mode or absorbance (see context)
AA	ascorbic acid
AAPH	2,2'-azobis(2-amidinopropane) dihydrochloride
ABTS	2,2'-azino-bis(3-ethylbenzothiazoline-6-sulphonic acid)
AC	alternating current
ACV	alternating current voltammetry
ADP	adenosine diphosphate
AFM	atomic force microscopy
ANOVA	analysis of variance
AOx	antioxidant
c	concentration
C	capacity
C_{10}SH	1-decanethiol
C_{16}SH	hexadecanethiol
C_{8}SH	octaethiol
CA	caffeic acid
CAPE	phenethyl ester of caffeic acid
CAT	catalase
CBA	carotene bleaching assay
CCVK-I	Cell counting viability kit-one
CE	counter electrode
CGA	chlorogenic acid
CHAPS	3-[(3-cholamidopropyl)dimethylammonio]-1-propanesulfonate
CL	chemiluminescence
cm	centimeter
COX	cyclooxygenase
CV	cyclic voltammetry
Cyp P450	cytochrome P450 enzymes
DMSO	dimethyl sulfoxide
DNA	deoxyribonucleic acid
DPPH	2,2-diphenyl-1-picrylhydrazyl)
DPV	differential pulse voltammetry
E	electric potential
E_0	standard reduction potential
ECS	electrochemical stripping
EDTA	ethylenediaminetetraacetic acid

e.g.	for example
EGCG	epigallocatechin gallate
eqn.	equation
ER	endoplasmic reticulum
ERO1	endoplasmic reticulum oxireductin 1
ET	electron transfer
eV	electronvolt
F	Faraday constant
FA	ferulic acid
FCS	fetal calf serum
FRAP	ferric ion reducing/antioxidant power
fwhm	full width at half maximum
g	gram
g	gravitational acceleration
GFP	green fluorescence protein
GOD	glucose oxidase
GP	Gynostemma pentaphyllum
GPx	glutathione peroxidase
GR	glutathione reductase
Grx	glutaredoxins
GSH	glutathione
GSSG	glutathione disulphide
GST	glutathione S-transferase
h	hour
HaCaT	human adult low calcium high temperature keratinocyte cell line
HAT	hydrogen atom transfer
HEK293	human embryonic kidney 293 cell line
HER	hydrogen evolution reaction
HIF	hypoxia inducible factor
HRP	horseradish peroxidase
HyPer	(genetically encoded) hydrogen peroxide sensor
I	electric current
IL-6	interleukin-6
IRS	infrared reflection spectroscopy
K	kaempferol
k	SAM destruction rate
L	liter
L-012	8-amino-5-chloro-7-phenyl-pyrido[3,4-d]pyridazine-1,4(2H,3H)dione
LMWA	low molecular weight antioxidant
Log2	logarithm to base 2
LPO	lipoxygenase
M	molar
M	mediator
MHz	megahertz
min	minute
mL	milliliter
mm	millimeter

MPO	myeloperoxidase
mRNA	messenger ribonucleic acid
Msr	methionine sulfoxide reductases
MΩ	mega-ohm
n	number of samples/electrons
NADH	nicotinamide adenine dinucleotide
NADPH	nicotinamide adenine dinucleotide phosphate
nm	nanometer
NOX	NADPH oxidase
OD	optical density
ORAC	oxygen radical absorbance capacity
P/S	penicillin/streptomycin
PBS	phosphate buffered salt solution
Pb-UPD	underpotential lead deposition
PDI	protein disulfide isomerase
pH	negative decadic logarithm of the molar hydrogen ion concentration
p*K*a	negative decadic logarithm of the acid dissociation constant
PKC	protein kinase C
PM IRRAS	polarization modulation-infrared reflection-adsorption spectroscopy
PMA	phorbol 12-myristate 13-acetate
p-NDA	p-nitrosodimethylaniline
Prx	peroxiredoxin
PUFA	polyunsaturated fatty acid
Q	quercetin
R	rutin
R	universal gas constant
R^2	coefficient of determination
R_a	average roughness
RD	reductive desorption
RE	reference electrode
RFU	relative fluorescence units
RLU	relative light units
ROS	reactive oxygen species
RPMI-1640	Roswell Park Memorial Institute medium
RT	room temperature
s	seconds
SAM	self-assembled monolayer
SD	standard deviation
SE	standard error
SECM	scanning electrochemical microscopy
SEM	standard error mean
SOD	Superoxide dismutase
SSL	simulated sunlight
STM	Scanning tunneling microscopy
t	time
T	temperature
TAZ	tafazzin knock out C6 glioma cells

*t*BHP	tert-butyl hydrogen peroxide
TC	tetracycline
TEAC	trolox equivalent antioxidant capacity
TNF-α	tumor necrosis factor alpha
Trx	thioredoxin
U	unit
UME	ultramicroelectrode
UV	ultraviolet
V	volt
WE	working electrode
WST-8	2-(2-methoxy-4-nitrophenyl)-3-(4-nitrophenyl)-5-(2,4-disulfophenyl)-2H-tetrazolium monosodium salt
WT	wild-type C6 glioma cells
XO	xanthine oxidase
XPS	X-ray photoelectron spectroscopy
YFP	yellow fluorescence protein
y-Gr	yeast glutathione reductase
θ	surface coverage
λ	light wavelength
ν_{as}	asymmetric stretching mode
ν_{s}	symmetric stretching mode

1. Aim of the thesis

Redox biology is an important component in cell function and disease. The regulatory redox system seems to be more complex than first anticipated, but the modulation of redox systems by antioxidants still seems to hold some potential for disease prevention or treatment. A natural source of antioxidant substances are plants [1]. However, even though a great variety of approaches to assess the antioxidant activity of plant compounds or extracts exists, its informative value for biological systems is often limited. Scholz et al developed an electrochemical assay to quantify oxygen radicals [2]. The technique opens the opportunity to compare the capacity of substances to scavenge these oxygen radicals and to hinder their generation. The method seems highly sensitive and suited to assess biologically relevant oxygen radicals [3]. Therefore, this project was aimed at adapting the electrochemical assay to be applicable in a cell culture experiment. For this purpose, the assay was further optimized, the reproducibility of the method was tested and the experimental parameters altered to simulate cell culture conditions. Different isolated plant compounds as well as a more complex plant extract were compared for their antioxidant activity in cell culture (glia and keratinocyte cell lines) as well as in a cell-free experimental set-up. The results were then compared to the electrochemical assay results. In summary the following points were addressed by the thesis:

(i) further characterization of the electrochemical sensor electrode;
(ii) behavior of the sensor at different experimental parameters;
(iii) assessment of known plant antioxidants with the electrochemical sensor;
(iv) comparison of results with established antioxidant assays;
(v) possibility to transfer the assay to a cell culture experimental set-up;
(vi) intracellular effects of the antioxidants.

Conclusively, the aim of the thesis was to evaluate the informative value of the electrochemical assay on the antioxidant activity of plant activities, its applicability to cell culture experiments and to investigate possible correlations with intracellular effects.

2. Introduction

2.1. Reactive oxygen species (ROS)

2.1.1. Formation and occurrence

Aerobic living organisms depend on the presence of oxygen in the atmosphere for energy generation. Ground state molecular oxygen is a paramagnetic biradical, because its outer electrons in the π-orbital have the same spin direction. Therefore, oxygen preferentially accepts one electron at a time during redox reactions due to the spin restriction rule. This behavior can easily lead to the generation of reactive oxygen species (ROS). The term ROS is a collective term to describe a heterogeneous group of radical and non-radical oxygen containing molecules that derive directly or in a second reaction from the partial reduction of oxygen. The species included within the group vary considerably in their half-life times and their reaction rates. In the literature the superoxide anion radical ($O_2^-\cdot$), hydrogen peroxide (H_2O_2), the hydroxyl radical ($HO\cdot$), hypochlorous acid ($HClO$), hypobromous acid ($HOBr$), singlet oxygen ($^1O_2$), the peroxyl radical ($ROO\cdot$), the alkoxyl radical ($RO\cdot$), carobonate ($CO_3^-\cdot$) as well as hydroperoxide ($ROOH$) are included within the group of ROS ([4], [5]).

As diverse as the group itself are the sources of ROS. In an extracellular environment ROS can be generated by UV light, ionizing radiation, transition metals, heavy metals, ozone or chemicals (drugs, pollutants, pesticides, industrial solvents). Those chemicals might either react to form peroxides or ozone, promote the formation of superoxide (e.g. quinones, nitroaromatics or bipyrimidiulium herbicides), or release iron and copper that can promote the formation of hydroxyl radicals (see Fenton reaction, equation 1.1) ([4], [6], [7]).

In eukaryotic cells the named external sources can promote intracellular ROS formation, or some chemicals can be further metabolized to radicals (e.g. polyhalogenated alkanes). Additionally, ROS are formed naturally at multiple intracellular sites [8]. One source is the mitochondrial electron transport chain (especially complex I (nicotinamide adenine dinucleotide (NADH) ubiquinone oxidoreductase) and complex III (ubiquinone-cytochrome C oxidoreductase)) [9], where one-electron reduction of O_2 can lead to the formation of superoxide. The production of superoxide at the mitochondria is therefore coupled to the metabolic rate and the electron transfer competence. Other sources are the peroxisomal β-oxidation [10] and the endoplasmic reticulum (ER) [11]. Those three compartments are the main locations of metabolic oxygen consumption and hence contribute significantly to intracellular ROS generation.

Other important intracellular sources of ROS are nicotinamide adenine dinucleotide phosphate (NADPH) oxidases (NOX) and dual oxidases (DUOX). Those flavoproteins can produce superoxide by passing electrons from NADPH to molecular oxygen via two heme groups in their

transmembrane domains. The superoxide can further react to form hydrogen peroxide. In humans seven enzymes belonging to this family have been identified so far. They are distributed throughout various tissues fulfilling different functions [12].

In addition to NOX enzymes there are several other enzymes present in different compartments of the eukaryotic cell, which catalyze ROS generating reactions. Examples are:

- → superoxide dismutase (SOD): There are three major SOD families, depending on their metal cofactor which is either copper and zinc (Cu/Zn type), iron or manganese (Fe/Mn type) or nickel (Ni type). In mammalians the Cu/Zn type as well as the Mn type can be found. The other forms are restricted to bacteria and prokaryotes. The enzymes dismutates superoxide to form hydrogen peroxide and molecular oxygen (table 1). Since the enzyme reduces the load of intracellular superoxide, it has been titled an "antioxidant" enzyme [13]. However, this classification neglects that SODs produce hydrogen peroxide as a product, which is an important factor in redox signaling and can further react to form hydroxyl radicals.
- → endoplasmic reticulum oxireductin 1 (ERO1): ERO1 is involved in the oxidative protein folding in the endoplasmic reticulum (ER). It accepts electrons from the reduced protein disulfide isomerase (PDI) chaperones to transfer them to molecular oxygen producing H_2O_2 in the process [14].
- → the heme containing myeloperoxidase (MPO): MPO is most abundant in neutrophil granulocytes. The enzyme catalyzes the conversion of chloride and hydrogen peroxide to form hypochlorite [15].
- → several oxidases such as xanthine oxidase (XO), acyl-CoA oxidase, glucose oxidase (GOD).
- → lipoxygenase (LPO).
- → cyclooxygenase (COX).

Their catalyzed reactions, that have ROS as a natural product, are listed in table 1. The enzymes are examples for the deliberate and controlled ROS generation in cells. Another scenario for ROS generation are uncoupling events, like in the respiratory chain in mitochondria, for which the monooxygenation reaction of substrates by members of the cytochrome P450 enzymes (Cyp P450) is another enzymatic example. The family of Cyp P450 enzymes is essential in performing biotransformation processes. They are involved in drug metabolism as well as in steroid hormone synthesis, and polyunsaturated fatty acid (PUFA) metabolism. During the normal reaction cycle, Cyp P450 use NADPH and dioxygen molecule as substrates and release an oxygenated product as well as a water molecule. However, when the electron transport is uncoupled from substrate oxygenation, superoxide (one electron reduction), hydrogen peroxide (two electron reduction)

or water (four electron reduction) can be released in three "unproductive reaction pathways" from the enzyme. [16] The rate of uncoupling events is dependent on the specific enzyme as well as on external factors [17].

Table 1: List of ROS producing enzymes in eukaryotic cells with their ROS producing catalyzed reactions

enzyme	catalyzed reaction
acyl-CoA oxidases	acyl-CoA+O_2→trans-2,3-dehydroacyl-CoA+H_2O_2
AO	R–CHO+H_2O+O_2→R–COOH+H_2O_2+H^+
CypP450	liberation of ROS via uncoupling events during substrate monooxygenation reactions
ERO1	$FADH_2$+O_2+2e^-→H_2O_2+FAD
GOD	β-D-glucose+O_2→ D-glucono-1,5-lacton+H_2O_2
LPO	PUFA+O_2→fatty acid hydroperoxide
MPO	H_2O_2+Cl^-→H_2O+ClO^-
NOX/ DUOX	NADPH+O_2→$NADP^+$+2 $O_2^-\cdot$+H^+
SOD	2 $O_2^-\cdot$+2H^+→ O_2+H_2O_2
XO	hypoxanthine+O_2+H_2O→xanthine+ $O_2^-\cdot$+2H^+
	xanthine+O_2+H_2O→uric acid+ $O_2^-\cdot$+2H^+

AO: aldehyde oxidase, COX: cyclooxygenase, CypP450: cytochrome P450 enzymes, DUOX: dual oxidase, ERO1: endoplasmic reticulum oxireductin 1, GOD: glucose oxidase, LPO: Lipoxygenase, MPO: myeloperoxidase, NOX: nicotinamide adenine dinucleotide phosphate (NADPH) oxidases, PUFA: polyunsaturated fatty acid, SOD: superoxide dismutase, XO: xanthine oxidase

Another potential source of ROS formation might be free transition metal ions such as iron from iron-sulfur clusters, heme groups or metal-storage proteins. In the presence of hydrogen peroxide iron ions can act as redox partner to form hydroxyl radicals in the Fenton reaction (1.1) [18].

$$H_2O_2 + Fe^{2+}(Cu^{1+}) \rightarrow OH^- + HO\cdot + Fe^{3+}(Cu^{2+}) \quad (1.1)$$

2.1.2. Biological role of ROS

The biological effects of ROS depend (i) on their reactivity (electron configuration, redox potential), (ii) on their site of generation (proximity to sensitive target molecules), and (iv) on the local concentration (generation vs. degradation rate). Hydrogen Peroxide for example is relatively stable under physiological conditions, is membrane permeable and might diffuse away from the site of its formation. It can act as a signaling molecule and serves as a substrate in enzymatic reactions. However, in the presence of metal ions it can be converted into the much more reactive

hydroxyl radical (1.1). The hydroxyl radical, with a one-electron reduction potential of +2.33 V, is a strong oxidant reacting at diffusion control rates randomly with biomolecules nearby such as lipids, proteins or DNA. [19] This can cause lipid peroxidation, alter enzyme or transcription factor activities, receptor binding properties, alter gene expression or cause mutations [20]. Ultimately, this can lead to cell damage and cell death [21]. It has also been proposed that accumulation of ROS induces cell damage that might play a role in aging ([22], [7]), though the hypothesis is controversial [23]. Nevertheless, several pathological conditions have been associated with altered cellular ROS levels/redox statuses and consequently with altered redox signaling in the cell. Among those are cancer [20], diabetes ([24], [25]) and chronic inflammations [26]. Also, harmful effects of excessive exercise have been associated to an increased production of ROS ([27], [28]).

2.1.2.1. Cellular ROS protection system

To prevent damaging effects of ROS, aerobic living cells are equipped with a sophisticated system to control the levels of ROS and to implement them in cellular signaling events. The manifestation of the systems varies between different cell types as well as different cell compartments, making them differently sensitive towards ROS.

One component of the cell to actively control the effects of ROS are redox enzymes such as glutathione peroxidases (GPx), glutathione reductase (GR), methionine sulfoxide reductases (Msr) [29], peroxiredoxins (Prx), catalases (CAT), thioredoxins (Trx), glutaredoxins (Grx) and superoxide dismutase (SOD) (see table 2 for catalyzed reactions) [30]. SOD can be found among the ROS detoxifying enzymes as well as among the ROS producing enzymes (table 1), because it reacts with superoxide but produces hydrogen peroxide in the process. The enzymatic system controls the ROS flux, translates the signals into protein modifications or is involved in the recycling of LMWAs. Under conditions of elevated ROS levels many of the redox enzymes are upregulated. [23] Among the redox enzymes, Prx are one of the most important ones. They are highly abundant in mammalian cells (up to 1% of the cellular soluble protein fraction [31]) and their thiolates have a high reaction rate with hydrogen peroxide. The human Prx2 for example, present in the cytosol and the nucleus, exhibits a reaction rate of $k = 110^8 \times \mathrm{M}^{-1}\mathrm{s}^{-1}$, which is 3.800.000 times higher than the reaction rate of cysteine with hydrogen peroxide. [32] Additionally, the high rate constants of Prx for the reduction of alkyl hydroperoxides and peroxynitrite make them an important enzyme during inflammation processes. According to a model based on Jurkat cells 76% of intracellular steady state flux of hydrogen peroxide are converted by Prx and GPx [33].

Apart from the redox enzymes that control ROS effects in the cell, there are also non-enzymatic components of the cell that are involved in redox regulation. As with the enzymes their occurrence

is cell type specific, as well as cell component dependent. They can either be produced by the organism itself or must be provided exogenously, such as vitamin E and C. The three classes of non-enzymatic redox regulators in eukaryotic cells are:

i. radical scavengers, which by formation of relatively stable radicals terminate radical chain reactions (e.g. α-tocopherol);
ii. reducing agents, such as the most abundant intracellular thiol compound glutathione (GSH, γ-L-glutamyl-cysteinyl-glycine), ascorbic acid or cysteine;
iii. antioxidant synergists often in interaction with enzymes. Antioxidant synergist can influence redox status indirectly by alteration of gene expression, enzyme activities or by reduction of oxidized molecules [34].

Table 2: Overview of important redox enzymes in eukaryotic cells and their catalyzed reactions

enzyme	catalyzed reaction
CAT	$H_2O_2+Fe^{3+}\text{-}E \rightarrow H_2O+O=Fe^{4+}\text{-}E^{+}$
	$H_2O_2+O=Fe^{4+}\text{-}E^{+} \rightarrow H_2O+Fe^{3+}\text{-}E+O_2$
GPx	$2GSH+H_2O_2 \rightarrow GSSG+2H_2O$
GR	$GSSG+NADPH+H^{+} \rightarrow 2GSH+NADP^{+}$
Grx	$Grx\text{-}(SH)_2+protein\text{-}S_2 \rightarrow Grx\text{-}S_2+protein\text{-}(SH)_2$
Msr	$methionine\ S\text{-}oxide+Msr\text{-}(SH)_2 \rightarrow methionine+Msr\text{-}S_2+H_2O$
Prx	$Prx_{reduced}+H_2O_2 \rightarrow Prx_{oxidized}+2H_2O$
SOD	$M^{(n+1)}+SOD+O_2^{-}\cdot \rightarrow M^{n}+SOD+O_2$
	$M^{n}+SOD+O_2^{-}\cdot+2H^{+} \rightarrow M^{(n+1)}+SOD+H_2O_2$
	with M= Cu(n=1); Mn(n=2); Fe(n=2); Ni(n=2)
Trx	$E_{oxidized}+Trx_{reduced} \rightarrow E_{reduced}+Trx_{oxidized}$

CAT: catalases, E: enzyme, GR: glutathione reductases, Grx: glutaredoxins, GST: glutathione-S-transferases, GPx: glutathione peroxidases, Msr: Methionine sulfoxide reductases, Prx: Peroxiredoxins, SOD: superoxide dismutases, Trx: thiooredoxins, M: metal in active center

2.1.2.2. Redox signaling

Although ROS can cause cell damage, the discovery that ROS themselves can function as cellular signaling molecules and the fact that they are deliberately generated within the cell, let to the conclusion that the presence of ROS is required for normal cell function. Over the last years mounting evidence has been collected to demonstrate that the purposeful and deliberate endogenous production of ROS, for example by NOX and DUOX enzymes, is an essential

component of cellular signaling and cell homeostasis to regulate host defense, growth, apoptosis, angiogenesis, endocrine functions and protein modifications among others [12]. As mentioned before, seven different NOX enzymes as well as various isoforms have been identified in humans. NOX exist either constitutively active, providing a constant flux of oxidants, or agonist-dependent, providing ROS in response to various signals (growth factors, cytokines, calcium) [35].

The redox regulatory system depends on regulatory redox couples (thiol/disulfide redox couples, thioredoxins, glutathione/glutathione disulfide (GSH/GSSG) and cysteine/cystine (Cys/CySS)), which can serve as redox sensors as well as signal transducers. The different systems do not always act in synergy but can also function in parallel pathways [36]. The translation of redox signals into biological function can be achieved via protein cysteine residues which serve as thiol switches being sensitive to reversible oxidation, nitrosylation, glutathionylation, acylation, sulfhydration or metal binding [37].

The rate of oxidation/reduction events in the cell is a complex system that is not only determined by the pure thermodynamics of the reaction, as expressed in the redox potential (E) by the Nernst equation (1.2), but also by the kinetics. [31] Therefore, the state of oxidation at a certain location at a certain time point in the cell is a complex function of redox potentials, reaction rates (determined in a cellular system by enzyme activity), and the concentration of oxidants, reductants and protein abundance [38]. In fact, the reaction rates of protein thiols with H_2O_2 for example can vary over several orders of magnitude, depending on their specific nature [32].

$$E = E^0 + \frac{RT}{nF} \times \ln \frac{a_{ox}}{a_{red}} \tag{1.2}$$

With E= reduction potential; E^0 = standard reduction potential; R= universal gas constant = 8.31447 J mol^{-1} K^{-1}; T= temperature; n = number of transferred electrons; F= Faraday constant = 96485.34 C mol^{-1}; a_{red}= activity of reduced species; a_{ox}= activity of oxidized species

The complexity of the system allows an independent regulation of the redox environment for different cell compartments that depend on the relative kinetics of the electron transfer reactions. The resulting non-equilibrium conditions between the subcellular compartments (micro and macro) as well as between different cell types are in direct relation to cell functions. Rapidly dividing cells for example exhibit more reduced potentials [36]. Another functional relation can be seen in the ER. The presence of oxidant equivalents is a critical parameter for the oxidative protein folding in the eukaryotic ER. To control the ER redox environment the membrane associated flavoprotein Ero1 provides oxidizing equivalents to allow disulfide bond formation and protein folding. Disulfide formation is essential for protein activity, structure stabilization and protein translocation. The activity of Ero1 is regulated by oxidative and reductive shifts in the ER environment, which are translated into the redox status of two different regulatory cysteine

residues within the protein (thiol-disulfide switches) [39]. Over this “shuttle disulfide” cysteine pair in Ero1 the disulfide-bond formation can be transported in a cascade onto the protein disulfide isomerase (PDI) and from there onto target proteins. ERO1 function is essential for disulfide bond formation in yeast, whereas in mammals its function is compensated for by alternative pathways [39]. The produced hydrogen peroxide is detoxified via GPx8 located near the generation side [40].

In general protein activity control via redox signaling or redox sensing can be considered a redox sensitive complement to protein control by phosphorylation. In fact, there is a cross talk between redox-regulated pathways with phosphorylation and calcium-dependent ones [6]. The presence of hundreds of specific cysteine residues within proteins sensitive to the physiological state of the cell give an explanation why ROS can be important signaling molecules to translate external stimuli into adaptive responses of the cell, like for example physical exercise in the skeletal muscle into mitochondrial biogenesis [41]. The protein cysteine residues that are affected by redox modifications via the formation of disulfides are not necessarily part of the active center of the protein nor do they comply to the rules postulated by Richardson and Thornton ([42], [43]) for the location of disulfides within protein structures. Indeed, according to rules of Richardson and Thornton, redox sensitive disulfides are often so called “forbidden disulfides”, like cross-strand disulfides (CSDs). This can be explained by the fact that disulfide formation in proteins were believed to be primarily a way of protein structure stabilization. However, the functional role of redox sensitive disulfides does not necessarily require them to stabilize the protein structure, which explains why they can also be found in positions within the protein structure formerly thought impossible. In fact, redox active disulfides often possess a high torsional energy, while structural ones exhibit low torsional energy [44]. The oxidation of disulfides can be catalyzed by enzymes (e.g. Trx) or via autocatalytic activity of the protein (e.g. auto-reduction through conformational changes). In general, the redox activity is dependent on the redox potential of the individual disulfides. Considering that the redox potential varies between different cell compartments, the translocation of a protein might already be sufficient to reduce/oxidize its thiols. The different redox potentials of disulfides are also a key factor in signaling cascades (downhill flow of electrons). However, as mentioned before, in a biological context the kinetics of the redox reaction must not be neglected. That means even though a reaction is thermodynamically favorable it can only occur if the activation energy is low enough. This factor is often determined in a biological setting by protein activities/abundance, which presents another possibility for the cell to modify redox statuses between compartments.

Often disulfide formation in redox signaling induces conformational changes that are translated to altered enzyme activities. They can lead to an inactivation as well as an activation of the enzyme [44]. But the role of redox switches goes beyond the function of simple on and off switches with

many different functional consequences possible such as altered transcription factor binding, ligand binding, protein trafficking and protein degradation [36]. Furthermore, some redox switches in proteins are irreversible [44]. A very important parameter for the involvement of thiols in redox signaling is their accessibility. Beyond that the redox chemistry is influenced by external factors such as Zn^{2+}, which can lower the pK_a values of certain cysteines upon binding [45]. Together the different reaction rates of protein thiols and their accessibilities for oxidants of enables specificity in signaling and permits oxidation even at relatively reduced steady state conditions [38]. The abundance of cysteines is higher in higher evolved organisms [46]. This might be a hint towards the evolution of redox signaling as a sophisticated control pathway in more complex organisms.

2.1.2.3. Immune system

Another factor that underlines the requirement of ROS for normal cell function in aerobic living organism is their involvement in the host defense system of the immune system. One example is the NOX of phagocytes (Phox) that can be found mainly in neutrophils and macrophages. The enzyme is activated upon the exposure to microorganisms. The activated enzyme produces superoxide in the so called "oxidative burst" to fend off the pathogens. [12] Other important enzymes in this immune response system that utilize ROS is the defense against pathogens are the myeloperoxidase (MPO) and the eosinophil peroxidase. They are involved in the disruption of bacterial cell walls, and the post-translational modification of protein amino acid residues. The enzymes produce bactericidal ROS, namely hypohalous acids (hypochlorous, hypobromous and hypothiocyanous acids) from hydrogen peroxide. The acids are very potent antimicrobial oxidants. However, in higher concentrations they can have cytotoxic effects, which is why they can be problematic during chronic inflammation [15].

2.2. Plant Antioxidants

2.2.1. General definition of antioxidants

Considering the importance of ROS in normal cell function as well as in disease, the idea arose to modify the intracellular redox status by external supplementation with so called "antioxidants". The term "antioxidant" is used by many different disciplines and is not uniformly defined. In food chemistry an "antioxidant" describes a substance that can reduce lipid peroxidation of a food product increasing its shelf life or a substance added to a product to promote consumer's health by decreasing adverse effects of ROS. In the cosmetic industry an "antioxidant" is utilized to prevent rancidity of lipid-based cosmetics or it is sold as a valuable ingredient that can protect the skin from free environmental radicals and decrease skin aging. In the oil industry "antioxidants" are added to gasoline and other fuels to prevent polymerization reactions. A museum curator will use "antioxidants" to preserve organic artefacts. In the fabrication process of polymers

"antioxidants" are added to optimize the process and to make the product more robust against environmental influences such as ultraviolet light. Taking these applications together an "antioxidant" might be defined as a reducing agent that inhibits oxidation [47] or a substance that slows down the rate at which something decays because of oxidization [48]. Another definition defines an antioxidant as "any substance that, when present at low concentrations compared to those of an oxidizable substrate, significantly delays or prevents oxidation of that substrate" [49].

Taking the term "antioxidant" into the biological/medical field the issue becomes even more complex. Up to a few years ago the concept of "oxidative stress" prevailed in scientific publications. The background for this term arose from the hypothesis that the cell holds a balance between oxidants and antioxidants. In case of increased levels of oxidants, the balance could be maintained by counteracting the higher concentration with elevated levels of antioxidants. If the oxidants level rose above a certain threshold the balance would tip over and cause cell damage and cell death. According to this concept increasing the amount of cellular antioxidants would be a suitable approach to counteract oxidative damage in the cell and prevent ROS related pathological conditions. However, the concept neglects two important facts: (i) the redox status of a cell cannot be considered as one, because of compartmentalization; therefore, the balance of antioxidants and oxidants of the complete cell oversimplifies the matter; (ii) oxidants are not only harmful for the cell but primarily important signaling molecules and essential for redox signaling. Interruption of signaling pathways by increased antioxidant's concentration might be counterproductive. In any case, the definition for an antioxidant in the biological sense needs to go beyond being a substance that simply inhibits or slows down oxidation. The complexity of a biological environment extents the term antioxidant to a substance which alternatively:

- directly scavenges biologically relevant ROS;
- is capable of recycling intracellular antioxidants;
- induces upregulation of the expression/activity of antioxidant enzymes;
- beneficially influences cellular ROS protection/adaption pathways;
- chelates free ions that might catalyze radical formation;
- increases the intracellular content of antioxidants, e.g. by being a precursor for their synthesis;
- or prevents the formation of ROS.

Furthermore, the following requirements need to be fulfilled for an antioxidant to be biologically effective: (i) the effective concentration range for the antioxidant must not be toxic to the cell as well as its reaction products; (ii) the antioxidant must be able to reach the target site (polarity and pharmacokinetics); (iii) the reaction rate constants and reduction potential must outcompete

the ones of other molecules present, (iv) the reaction product of the antioxidant must not be harmful to the cell.

2.2.2. Antioxidants in higher plants

Living under aerobic conditions the evolution of ROS from partial oxygen reduction also takes place in higher plants. Besides exposure to environmental factors such as UV light, toxins, drought etc. can trigger the formation of ROS within plant cells [50]. Like in eukaryotic cells ROS are responsible for wanted (redox signaling) and unwanted (cell damage) effects within plant cells [51]. The logical consequence is that higher plants also possess enzymatic and non-enzymatic antioxidant components such as glutathione, ascorbate, α-tocopherol, proline and betaine [52]. But also outside the antioxidant defense system other substances that naturally occur in plants have been classified as antioxidants. Most of these plant substances belong to the class of plant secondary metabolites meaning that they are not mandatory for primary cell functions. They fulfill a variety of functions that are not necessarily related to redox regulation such as floral pigmentation, repelling natural enemies or alluring animals/insects to promote reproduction. They were classified as antioxidants because they exhibit some oxidation lowering or ROS-quenching properties in a cellular environment or in cell-free settings. Most are phenolic compounds, such as flavonoids, phenolic acids, tannins, coumarins, xanthonoids or stilbenes (see figure 1), but also carotenoids belong to this group. The abundance of antioxidant substances is tissue and plant specific. Furthermore, their concentration within plants is influenced by environmental factors such as light exposure, climate (e.g. altitude), the soil (nutrient/salt content/toxins), water availability and the temperature ([53], [54], [1]).

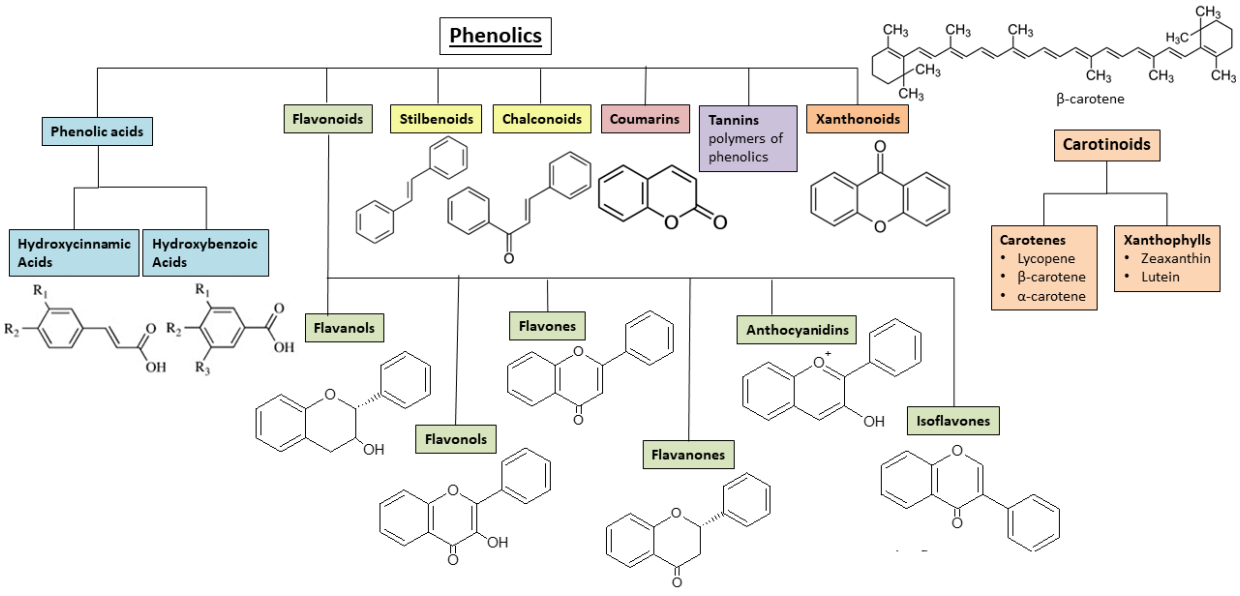

Figure 1: Overview of secondary plant metabolite classes with reported antioxidant activities. The main classes of phenolics and carotenoids are shown together with their structural backbone molecules.

2.2.3. (Chemical) properties of plant antioxidants

The chemical structures of non-enzymatic antioxidant molecules from higher plants are divers. They can broadly be classified in phenolic and non-phenolic components. Among the nonphenolic components are some low molecular weight antioxidants (LMWA) such as proline, betaine and glutathione. Furthermore, vitamins such as ascorbic acid (vitamin C), α-tocopherol (vitamin E) or carotenes (provitamin A) can be found in many plants. Carotenes belong together with xanthophylls to the group of carotinoids, which are isoprenoid compounds with up to 14 conjugated double bonds. While carotenes are purely hydrocarbons, xanthophylls also contain oxygen. Their ability to scavenge radicals is determined by the presence of functional groups as well as by the number of double bounds in the molecule [55]. In plants they are an important class of pigments, that take part in photosynthesis and help to buffer excessive light energy (prevent photodamage) [56]. In humans they make up the macula pigments (zeaxanthin and lutein) and some carotenes have provitamin A function meaning that they can be metabolized to retinoids in the human body [57].

The phenolic substances are made up to a great extent from flavonoids. They are a family of plant secondary metabolites that include more than 9,000 different molecules. All flavonoids have a carbon ring structure (two phenyl rings and one heterocyclic ring). Their diversity arises from substituted groups that can be bound to ten different carbons of the flavonoid skeleton [58]. Depending on the position and the type of added groups flavonoids are classified into flavanols, flavonols, flavones, flavanones, anthocyanidins and isoflavones (see Figure 1). The substituted groups determine their polarity as well as their reduction potentials. Active groups (e.g., NH_2 or OH) in ortho, meta and para position differently influence radical scavenging activities of the molecules [59]. Structural features that have been claimed to increase the radical scavenging abilities of flavonoid species are the ortho 3',4'-dihydroxy groups in the B ring (e.g. in quercetin), the meta 5,7-dihydroxy groups in the A ring (e.g. in kaempferol) as well as the 2,3-double bond in combination with the 4-ketogroup and the 3-hydroxyl group in the C ring and the o-dihydroxy in the B ring [60]. Due to their electron donating capacities flavonoids have high reaction rates with superoxide radicals. The products of this reaction are hydrogen peroxide and a flavonoid phenoxyl radical [61]. Both products still possess some cell damaging capacity and need to be neutralized *in-vivo,* however they are less reactive than superoxide itself. Flavonoids also exhibit high rate constants for the reaction with singlet oxygen at physiological pH [62]. Their ABTS[1] radical scavenging potential in aqueous media was reported to outcompete those of ascorbate and trolox (water-soluble vitamin E analog) [63]. However, under physiological pH conditions another study found them inferior electron donors [64]. Besides their radical scavenging ability flavonoids can

[1] 2,2'-azino-bis(3-ethylbenzothiazoline-6-sulphonic acid)

also chelate metal ions such as iron and copper, thereby inhibiting transition metal-catalyzed free radical formation. In the plant flavonoids are usually present in glycosylated forms, which reduces their reactivity with free radicals but increases their water solubility [60]. Relevant flavonoids in the human diet that will be discussed further in this work are epigallocatechin gallate (EGCG), quercetin, rutin and kaempferol.

Phenolic acids are another important group within plant phenolics. They are synthesized from L-phenylalanine or L-tyrosine and can be divided into two major groups: hydrobenzoic acids and hydroxycinnamic acids. Their characteristic structural features are at least one aromatic ring with at least one substituted hydroxyl group (figure 1). Depending on the number and position of the hydroxyl groups they exhibit different antioxidant activities. Two important hydroxycinnamic acids in the human diet are ferulic and caffeic acid. They are present in a great number of foods, mostly in glycosylated or esterized forms. [65]

2.2.4. Biological effects

The reported biological effects of plant components are diverse. It has been widely acknowledged that their antioxidant effects go beyond direct scavenging of ROS, especially because the concentration reached in tissue after oral intake are often incompatible to kinetic requirements of biologically relevant reactions [66]. The antioxidant effects also rely on their ability to activate antioxidant enzymes, to chelate metal ions, to inhibit enzymatic ROS production or to reduce intracellular LMWAs among others. In the following, an overview of the antioxidant effects of selected plant substances relevant for this thesis will be presented. However, first some general consideration for the biological effects of plant antioxidant are mentioned:

(i) the oral uptake of plant antioxidant substances greatly dependent on the intake of fruits and vegetables as well as on tea and coffee consumption. The resulting bioavailability depend on matrix effects, cellular uptake, transformation processed and excretion rate. It is known that most polyphenols are extensively metabolized after absorption resulting in methylated, glucuronidated or sulfated metabolites. These biotransformation processes have an impact on the antioxidant activity of the substances. [65]

(ii) the chemical properties of the antioxidant determine its antioxidant activity under specific conditions. Therefore, its effects are site specific (different activities at the membrane, in cytosol, in the ER etc.).

(iii) to outcompete or at least support the intracellular antioxidant system in the direct scavenging of ROS molecules, the supplied antioxidant needs to reach the side of ROS generation and show higher reaction rates than the natural occurring antioxidants present.

(iv) the complexity of the cell requires the evaluation of synergistic/antagonistic effects with other cell components.

(v) reactivation of antioxidant molecules after reduction might require energy equivalents such as NADPH or cellular antioxidants such as ascorbate. This might lead to energy depletion or to the depletion of antioxidants within the cell.

(vi) the fate of the reaction products of radical scavenging events need to be considered. The products might be less reactive than the initial reaction partners but might still be potentially harmful for the cell.

In the following some reported biological effects of representative antioxidant plant substances relevant for this thesis are summarized.

2.2.4.1. Vitamins: ascorbic acid and vitamin E (trolox)

L-Ascorbic acid ($AscH_2$, vitamin C) is one of the most abundant antioxidants in plants, where it serves multiple functions in redox regulation and as enzyme cofactor [67]. During evolution humans lost the functional gene encoding the enzyme of the last step of ascorbic acid biosynthesis (L-gulono-1,4-lactone oxidase, GLO). Thus, it became a vitamin, an essential component of the human diet. Its concentration in the human body is regulated by intestinal absorbance, tissue transport and renal excretion regulated via GLUT family transporters and sodium-vitamin C cotransporters (SVCT 1 and 2) [68]. However, high doses can be toxic due to oxalate formation [69]. Blood plasma levels normally vary between 40 and 120 µM (dependent on health status, gender, dietary intake [70]) and can accumulate in tissue to mM concentrations. Chemically, ascorbic acid is a water-soluble sugar acid that can act as hydrogen and electron donor. It possesses two ionizable hydroxyl groups. (see figure 2) The ascorbate monoanion ($AscH^-$) is the dominant form at physiological pH. The molecule can undergo two consecutive, one-electron oxidations to form the ascorbate radical ($Asc^- \cdot$) and dehydroascorbic acid (DHA). The radical is relatively unreactive (resonance stabilization of the unpaired electron) and can dismutate to ascorbate and DHA [71]. DHA itself does not possess antioxidant or free radical scavenging properties and is unstable at physiological conditions. Therefore, the cell needs to reduce it back to ascorbate (e.g. by GSH, mitochondrial electron transport chain [72]) [69]. The electron donating ability of ascorbate along with its high abundance explains its important role as antioxidant *in-vivo* and its ability to serve as enzyme cofactor. As such it is involved in histone demethylation, the HIF (hypoxia inducible factor) system and essential for many hydroxylases (e.g. for carnitine and collagen synthesis) [71]. Furthermore, an involvement of ascorbate in the immune system has been suggested based on the observations that it possesses anti-inflammatory effects, is accumulated in activated T lymphocytes and shows anti-viral activity (reviewed in [73]). But ascorbate does not only function as antioxidant but depending on the concentration and on the

circumstances, it acts as a pro-oxidant. Especially in the presence of metal ions (iron, copper, vanadium, cobalt, chromium) ascorbate can induce the formation of hydrogen peroxide, superoxide and hydroxyl radicals by promotion of oxygen and hydrogen peroxide reduction (see 1.3 to 1.5) [71]. In the absence of metal ions autooxidation of ascorbate dianion (Asc^{2-}) forming superoxide can occur. However, at physiological pH the reaction has a very low rate constant (k= 300 $M^{-1}\ s^{-1}$) [74].

$$AscH^- + Fe^{3+} \rightarrow Asc^- \cdot + Fe^{2+} \tag{1.3}$$

$$Fe^{2+} + O_2 \rightarrow Fe^{3+} + O_2^- \cdot \tag{1.4}$$

$$2O_2^- \cdot + H^+ \rightarrow H_2O_2 + O_2 \tag{1.5}$$

The pro-oxidant properties of ascorbate are desired for oxidative protein folding in the ER and protein thiol modifications [69]. The fact that the circumstances determine whether vitamin C acts as an antioxidant or pro-oxidant nicely mirrors the challenges of antioxidant research and is a phenomenon that always needs to be considered for antioxidants in complex systems. The term “redox modulator” instead of “antioxidant” might therefore be more suitable.

An interplay of ascorbate with other LMWAs such as GSH and vitamin E in cellular redox regulation has been suggested. An ascorbate-GSH-cycle for the reactivation of DHA to ascorbate has been proposed as an essential part of H_2O_2 signaling [75]. The crosstalk between the two molecules is also supported by the influence of ascorbate concentration on mitochondrial GSH content [72]. A proposed crosstalk between vitamin C and vitamin E is likely to exist *in-vitro* but proof for its significance *in-vivo* is missing.

Vitamin E is a collective term for four naturally occurring tocopherols (α, β, γ, and δ) and four tocotrienols (α, β, γ, and δ). Of those eight substances RRR-α-tocopherol is the biological most active form in the body, because of its preferred transport by the α-tocopherol transfer protein and its lower degradation and elimination rate compared to the other vitamers. From all the vitamins vitamin E is the most enigmatic one because its full biological function is still not understood [76]. Much of its physiological role has been attributed to its action as a radical scavenger in the lipophilic phase [66] preventing lipid peroxidation in membranes [67]. A mechanism for the peroxyl radical scavenging of vitamin E at membranes has been proposed with the resulting tocopheroxyl radical being reduced in turn by vitamin C in the hydrophilic phase. However, though the reaction is possible *in-vitro*, its biological relevance has not been proven, yet. Others attribute the biological effects of vitamin E to its regulation of signaling cascades and gene expression as a redox sensor [79]. An argument in favor of vitamin E being more than just an antioxidant *in-vivo* would be that α-tocotrienol is a more potent antioxidant than α-tocopherol

in-vitro but that α-tocopherol is more potent in treating vitamin E deficiency syndromes *in-vivo* [78] (see [80] for further discussion of this controversy). In this work the water-soluble vitamin E derivate, trolox, is used, thus omitting the controversy of vitamin E function and focusing on the radical scavenging ability of this molecule. In the trolox molecule (6-hydroxy-2,5,7,8-tetramethylchroman-2-carboxylic acid) the trimethyltridecan carbon chain of tocopherol is replaced by a carboxylic acid residue (see figure 2). The substance is used in many antioxidant assays as a positive control such as the TEAC and the FRAP assay (see chapter 1.3.).

2.2.4.2. Phenolic acids: ferulic acid and caffeic acid

The phenolic acids can be subdivided into hydrobenzoic and hydrocinnamic acids (see Figure 1). Caffeic acid (3,4-dihydroxycinnamic acid, CA) belongs to the later. It is a highly abundant polyphenol that can be found for example in coffee beans, blueberries, apples or ciders. The free acid presents the smallest part of naturally occurring CA. Mostly it occurs bound to other biomolecules [81]; e.g., as chlorogenic acids (CGA, mono-, di, tri-esters with quinic acid (1L-1(OH),3,4/5-tetrahydroxycyclo- hexane carboxylic acid), esters of other hydroxy acids, esters of sugars, glycosides or amides [82]. The conjugates of CA possess different bioactivities and antioxidant capacities. Upon reaction with a radical CA can form a resonance stabilized phenoxy radical. In comparison to other phenolic acids its resulting antioxidative activity is rather high. That is explained by its second hydroxyl group in the *ortho* position (see figure 2), which increases antioxidative activity in comparison to monophenols or polyphenols with the second hydroxyl group in *meta* position [83]. The antioxidative properties of CA *in-vitro* are expanded by *in-vivo* studies that report positive effects of the phenethyl ester of caffeic acid (CAPE) against *t*BHP-induced hepatotoxicity that might be related to its ability to scavenge ROS and protect DNA from oxidative damage [84]. Furthermore, CAPE was reported to be a specific inhibitor of NF-κB [85] and to inhibit 5-lipoxygenase activity as well as to block superoxide production in PMA (phorbol 12-mysistate 13-acetate) stimulated human neutrophils and superoxide production in a cell-free xanthine/xanthine oxidase system [86]. However, autooxiation of *ortho*-dihydroxy phenolics, such as CA, is related to the formation of superoxide. This autooxidation is pH dependent and occurs preferentially at high pH values, but oxidation can also be catalyzed by transition metal ions, such as Fe^{3+} [87]. The reduced metal ions can induce hydroxyl radical formation via the Fenton reaction (see eqn. 1). It has been proposed, that via this phenomenon as well as by the promotion of reductive iron release from ferritin [88] and depletion of intracellular GSH and ascorbate pools by the formed phenoxyl radical or quinon, *ortho*-dihydroxy phenolics might induce pro-oxidative effects *in-vivo* [89].

Another widely distributed hydrocinnamic acid in the plant kingdom is ferulic acid (FA). It is present in many vegetables and grains as free acid but primarily it occurs in conjugated forms

[90]. In Japan it is approved as a food additive to decrease oxidation and as a functional food component [91]. In comparison to CA, ferulic acid only possesses one hydroxyl group (see figure 2). The second one is replaced by a methoxy group. Therefore, FA exhibits lower antioxidative activity *in-vitro* [92]. A study on human embryonic kidney 293 cells (HEK293) demonstrated a beneficial effect of FA treatment prior to H_2O_2 exposure. FA treatment improved cell survival, increased catalase (CAT) and superoxide dismutase (SOD) levels and decreased malondialdehyde (MDA) levels [93]. However, in the study design H_2O_2 and FA were present together in the cell medium. Therefore, direct extracellular scavenging of H_2O_2 in the media might be responsible for some of the FA effects. Another study on Neuro-2a cells reported a positive effect of FA released from a chitosan/gelatin/β-glycerol phosphate (C/G/GP) hydrogel on H_2O_2 treated cells. They reported fewer DNA fragmentation and the down-regulation of inflammatory and apoptosis marker's mRNA levels. [94] Exploring the underlying mechanisms for the cellular effects of FA a study by Itagaki et al suggested the chain-breaking activity of FA to play an important role in its protective effect against oxidative injury in cell studies [91]. They found its radical scavenging and xanthine oxidase inhibition effect to be less pronounced in comparison to EGCG and ascorbic acid. However, as already mentioned for CA, some plant phenols (FA, gallic acid, catechin and p-coumaric acid) were shown to promote the reductive release of ferritin bound iron [88]. Considering the important role of iron ions in ROS generation via the Fenton reaction, this might be an indicator for a potential prooxidative effect of FA *in-vivo*.

2.2.4.3. Flavonoids: kaempferol, quercetin, epigallocatechin gallate and rutin

In the following one flavanol (epigallocatechin gallate, EGCG) and three flavonols (rutin, quercetin and kaempferol) from the heterogenous group of flavonoids will be discussed further.

EGCG is the most abundant catechin in green tea (*Camellia sinensis*) [87]. Due to its chemical structure (see figure 2) it can act as a radical scavenger both in ET and HAT reactions via its hydroxyl groups in the B- and D-ring. The resulting resonance stabilized semiquinone radical is less reactive and can therefore function as radical chain breaker. (reviewed in [87]) However, as already mentioned for FA and CA the autooxidation or metal catalyzed oxidation of phenols results in the formation of superoxide as well as semiquinone radicals and quinones. At high concentrations the oxidized forms of EGCG can form conjugates with cysteine and glutathione [95] or react with protein thiolates (Cys) and selenolates (selenocysteines, Sec) nucleophiles that have low p*K*a values. For example the quinone of EGCG can react with the reduced states of Trx and TrxR resulting in the formation of EGCG-Trx1 (Cys32) and EGCG-TrxR (Cys/Sec) conjugates [96]. This can lead to an inhibition of the enzymes [97]. But the reported biological effects of EGCG go beyond its redox activity. In fact, EGCG has been demonstrated to modulate signal transduction

pathways, transcription factors, DNA methylation, mitochondrial function, and autophagy [98]. EGCG is regarded as a potential drug candidate for cancer prevention and treatment ([99],[87]).

Kaempferol (3,5,7-trihydroxy-2-(4-hydroxyphenyl)-4H-1-benzopyran-4-one) is a flavonol that can be found in a variety of edible plants and medical herbs. Mostly it occurs in the form of glucosides, conjugated with different sugar molecules [100]. A positive correlation between the intake of kaempferol-rich foods and reduced risk for different cancer types has been reported by epidemiological studies ([101],[102]). However, the complex nature of the food compositions makes it impossible to ascribe the positive health effect to kaempferol alone. Synergistic effects with other food components might play a role. A combined treatment of Madin-Darby canine kidney (MDCK) cells with quercetin and kaempferol, for example, increased the bioavailability of quercetin in the cells because both flavonoids are excreted from the cells via the same transporter (breast cancer resistance protein (Bcrp, Abcg2)), which has a higher affinity for kaempferol [103]. *In-vitro* studies on pure kaempferol demonstrated its scavenging ability towards HOCl, superoxide [104], and peroxyl radicals [105]. Cell based studies reported that Kaempferol stimulates glucose uptake in 3T3-L1 adipocytes [106], increases gene expression of TrxR 1 and Trx (TXN and TXNR1) in human keratinocytes [107], reduces CM-H_2DCFD detected ROS levels in H_2O_2 stimulated mouse-derived hippocampal neuronal HT22 cells [108], reduces Abeta (amyloid beta protein) initiated activation of caspase cascades and reactive oxygen species accumulation in rat cortical neurons [109], and reduced lipid peroxidation in 2-deoxy-D-ribose stimulated HIT-T15 pancreatic β-cells [110] to name just a few studies. More studies reporting the anti-inflammatory, anti-diabetic, anti-oxidative, and anti-cancer effects of kaempferol are reviewed in [111],[112],[111] and [113].

The structure of quercetin (2-(3,4-Dihydroxyphenyl)-3,5,7-trihydroxy-4H-chromen-4-one) is equal to the one of kaempferol with the exception that it possesses a second hydroxy group in the B ring (catechol structure, see figure 2). The combination of the catechol structure, the double-bond in the C-ring along with the 3-OH, and 5-OH groups in the A-ring explains its good radical scavenging capacity *in-vitro*, which is also supported by its low half peak reduction potential ($E_p/2$) of 0.03 mV [60]. In the TEAC assay the radical scavenging ability of quercetin was reported to be 6.24-fold higher than for trolox [114]. The molecule shows similar electrochemical oxidation behavior to kaempferol with the difference that the oxidation product of quercetin is more stable, which can be advantageous in radical chain breaking reactions [115]. Furthermore, quercetin possesses the ability to chelate metal ions [116]. Quercetin is highly abundant in many fruits and vegetables where it mostly occurs as glycosides. In the 1970 the substance was classified as being cancerogenic, but the high abundance of the molecule in the human diet as well as preceding studies refuted this statement. Only at unphysiologically high concentration quercetin demonstrated detrimental effects. Adverse effects might arise from its oxidized form, the

quercetin-quinone, which can react with protein thiols or GSH ([117], [118]). A role of quercetin in the treatment/prevention of cardiovascular diseases has been proposed. Studies demonstrated reduced inflammatory markers, improved plasma lipid concentrations, a better insulin-secretion from pancreatic β-cells as well as an impact of quercetin supplementation on arteriosclerosis events in different cell and animal models (reviewed in [119]). Furthermore, a potential use of quercetin in cancer therapy is debated, relying on the selective induction of cell death or cell cycle arrest in cancer cells. Epidemiological studies indicate that quercetin supplementation is only beneficial for diseased patients and has no impact on healthy individuals (reviewed in [119], [120]).

The last flavonoid discussed here is rutin. Rutin is a glycoside of quercetin with an attached disaccharide (α-L-rhamnopyranosyl-(1,6)-β-D-glucopyranose). Rutin demonstrated weaker radical scavenging activity in the DPPH assay than quercetin [121], which can be explained by the fact that its 3-OH group in the C-ring is blocked by the bound glycoside. Nonetheless, rutin inhibits lipid peroxidation in an *in-vitro* set-up by scavenging superoxide and peroxyl radicals and by chelating iron ions in relatively stable complexes [116]. Furthermore, it can scavenge hydroxyl radicals [122] Supplementation of streptozotocin (STZ)-induced diabetic rats with rutin beneficially influenced blood glucose and insulin levels and increased enzymatic and non-enzymatic antioxidants in liver, kidney and brain tissue of the animals [123].

Rutin, kaempferol and quercetin have all been reported to interact with lipid membrane models and to alter membrane fluidities ([124], [125]). However, the significance of this observation on *in-vivo* effects has not been established, yet.

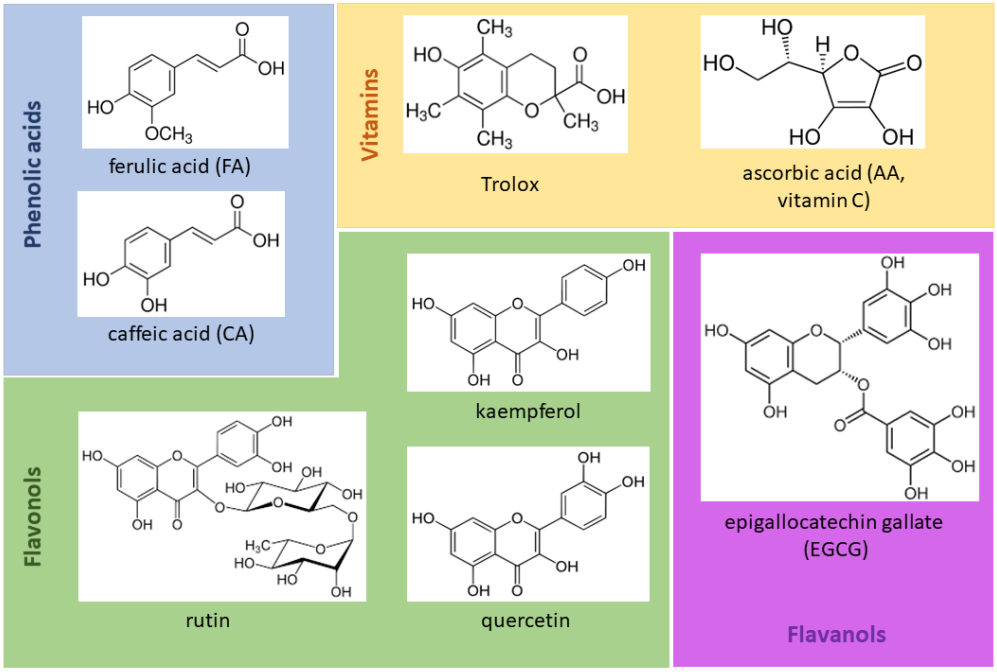

Figure 2: Chemical structures of the plant substances investigated in this work (see chapter 1.2. for further description)

2.2.4.4. Plant extracts: *Gynostemma pentaphyllum*

As mentioned before the content and type of antioxidant substances found in plants is plant specific. Some plant species exhibit component profiles that are believed to be especially beneficial for health like *Gynostemma pentaphyllum* (Thunb.) Makino (GP, chinese name 'jiaogulan'). GP is a medicinal herb that has been used in the Asian region for several centuries to treat a wide range of pathological conditions [126]. Much research has been undertaken to understand effect mechanisms and to identify active substances within GP [127]. *In-vitro* studies demonstrated the antioxidant effects of the plant. Those effects are mainly attributed to flavonoids and other phenolics (especially rutin and quercetin) [128], but also some antioxidant activity of contained polysaccharides are reported [129]. The radical scavenging capacity vary significantly between samples due to natural fluctuations in the phytochemical composition. The antioxidant content is affected by (i) the plant part (higher in leaves than in stem); (ii) the genotype (diploid, tetraploid) [130]; (iii) the extraction method (lipophilic or hydrophilic components) [131]; (iv) the growing conditions (toxins, water, UV-radiation, humidity, soil quality) [128]; and (v) matrix effects for whole plant samples.

The physiological effects reported for GP are mainly attributed to saponins (dammarane-type gypenosides [132]) but studies are also based on the application of whole plant extracts or crude polysaccharides ([133], [134]). GP extracts or isolated compounds are reported to effect (i) inflammatory events via effects on mRNA expression of proinflammatory factors like TNF-α, IL-6 and Ptgs2 and other cytokines [130], COX-2 [135], interleukins, alteration of macrophage redox

status, NK cell activity, elevation of CD4+ T lymphocyte counts as well as the CD4+/CD8+ ratio [134], inhibition of iNOS activity in murine macrophages [136]; (ii) the lipid metabolism via modulation of lipoprotein lipase (LPL) activity [137], insulin sensitivity, decreased triglyceride and total cholesterol levels [138], elevated levels of phosphatidylcholine and decreased levels of trimethylamine N-oxide (TMAO) [139]. Furthermore, an impact on adipogenesis and increased weight loss in obese patients were reported in this context [140]; (iii) cardiovascular parameters such as vasorelaxation in bovine endothelial cells via eNOS stimulated NO release [141]; (iv) cancer by induction of nonapoptotic cell death in cancer cells (modulation of intracellular ROS production via ROS-ER-Ca^{2+} induced cell death [142]), inhibition of cancer cell proliferation [143], cell cycle arrest [144], apoptosis [145], inhibition of invasion and metastasis, inhibition of glycolysis and immunomodulating activities (reviewed in [146]). Further studies report antidepressant-like effects [147], inhibition of human cytochrome P450 enzymes [148], reduced physical fatigue after exercise [133] as well as neuro-protective properties of GP [149].

It is obvious that the antioxidant effects of GP *in-vitro* are not directly translatable into antioxidant effects *in-vivo*. The physiological effects of GP are harder to predict than antioxidant activities *in-vitro* since they cannot simply be foreseen from chemical properties of the extract components and they may vary significantly between different cell lines and tissues. Furthermore, bioavailability, metabolization events as well as toxicity and antiproliferative effects must be considered to predict biological effects of GP. However, the reported effects of GP on pathological conditions related to altered intracellular redox status, such as cancer, inflammation or diabetes, open the possibility that the physiological effects of the plant are connected to modulation of intracellular redox parameters.

2.3. Assessment of antioxidant activity

2.3.1. General considerations

The assessment of antioxidant activities/capacities especially intracellular and *in-vivo* is an ambitious endeavor. The broad definition of antioxidants increases the number of possible parameters to be tested. An antioxidant assay might test for the radical scavenging capacity of a substance, for its radical chain breaking ability, for its ability to protect a target molecule from oxidation, for its ROS lowering effects by enhanced cellular degradation or reduced cellular production, for its capacity to repair ROS inflicted damage or for the impact of the redox status of a single protein. Along with this complex definition of the assays' targets come some methodological challenges that must be addressed: the short lifetime of ROS, the compartmentalization of redox biology that requires location specific techniques, direct reaction of reporter molecules with ROS that by itself influences ROS levels, the requirement of specific probes/sensors for defined ROS species and the low intracellular concentrations that require

sensitive methods. Nevertheless, a great number of studies dealing with the assessment of antioxidant capacities *in-vitro* as well as *in-vivo* exist in the literature. They investigate single compounds or mixtures, such as plant extracts, to consider synergistic effects. There is a great variety in the experimental conditions and in turn in their biological relevance.

2.3.2. *In-vitro* assays

In-vitro antioxidant assays are a tool often applied in the food industry or as a first screening of compounds for their antioxidant potential. They mainly focus on the ability of a substance to neutralize or reduce the number of active radicals in a system. From a mechanistically point of view *in-vitro* antioxidant assays can basically be divided into two main groups: assays that rely on electron transfer (ET) reactions and assays that are based on hydrogen atom transfer (HAT) reactions [150]. In ET assays the antioxidant activity of a substance is evaluated by its ability to donate an electron to a radical becoming a cation radical itself. The important parameter that determines the antioxidant efficiency in ET assays is therefore the ionization potential (IP) of the tested substance. It HAT based assays the hydrogen transfer from the antioxidant substance to the radical is the essential step. Therefore, the bond-dissociation energy (BDE) for the OH bond of the investigated substance is of interest. [151] Popular examples for ET assays are: TEAC (Trolox equivalent antioxidant capacity) [152], FRAP (ferric ion reducing/antioxidant power) [153], DPPH (diphenyl-1-picrylhydrazyl) reduction capacity assay ([154], [155]), p-NDA (N,N-Dimethyl-4-nitrosoaniline) oxidation assay [156], the PCL assay (photo chemiluminescence) [157], the DMPD (*N,N*-dimethyl- *p*-phenylendiamine) assay [158] or the total phenol assay by Folin-Ciocalteu reagent [159]. Among the HAT assay are the ORAC (oxygen radical absorbance capacity), the crocin bleaching method, inhibition of lipid oxidation and the TRAP (total radical trapping antioxidant parameter). Furthermore, some assays focus on the metal chelating capacity of a substance that could prevent transition ion induced radical formation. Among those are the HORAC (hydroxyl radical antioxidant capacity, [160]), and the luminol (5-Amino-2,3-dihydrophthalazine-1,4-dione) assay if the radicals are produced by the Fenton reaction. The named assays are listed together with their measured reactions, some advantages and limitations in table 3. Most of them measure the reaction of a substance with a radical. In the case of ABTS (2,2'-azino-bis(3-ethylbenzothiazoline-6-sulphonic acid)), DPPH (2,2-diphenyl-1-picrylhydrazyl) and AAPH (2,2'-Azobis(2-amidinopropane) dihydrochloride) they are artificial radicals that are rather stable and have no biological relevance. The great variety of available methods to assess antioxidants as well as the variation in experimental protocols, materials, reference standards and measured parameters in one assay often complicate comparison of the obtained results [161]. Other shortcomings that stand in the way of obtaining biological relevant data are non-physiological pH values or the absence of complex reaction media that could model conditions *in-vivo*. Besides, other antioxidant effects that can be achieved by the recycling of

intracellular antioxidants, the induction of cellular pathways, the interaction with enzymes, the increased bioavailability of other substances among others are neglected. Another way of antioxidant assessment *in-vitro* are electrochemical measurements that are further discussed in chapter 1.3.5.

Table 3: List of popular antioxidant assays *in-vitro* (summary of [162], [163], [164])

assay	radical	Measured reaction	advantages	limitations
ET (electron transfer) assays				
TEAC	ABTS	Reduction of ABTS radical (dark blue color) to colorless $ABTS^{2-}$	Broad database on measured substances	End-point assay: no information on reaction rates; ABTS radical rather stable: no biological relevance
FRAP	Fe^{3+}	Reduction of Fe^{3+} to Fe^{2+}	Fe^{3+} biological relevant	Measurements at acidic pH (3.6); problematic to assess metal chelators; longer reaction times required (4 min)
DPPH assay	DPPH	Reduction of colored DPPH radical	Information on reaction kinetics	DPPH radical rather stable, no biological relevance; some reactions with DPPH reversible
Total phenol assay (FCR)		Reduction of Mo^{6+} to blue colored Mo^{5+} compound	Little interference with matrix components at measured wavelength (734 nm)	Measurements at basic pH (10); not specific for phenols (reflects FCR reducing capacity of a sample); not applicable for lipophilic antioxidants
p-NDA assay	Hydroxyl radical	Absorbance shift from the reaction of p-NDA with radical	Hydroxyl radical biological relevance	pH dependency of probe
PCL Assay	superoxide	Scavenging ability of superoxide radical generated by optical excitation (luminol as reporter probe)	Superoxide biological relevance; applicable to detect antioxidants in the nanomolar range	Measurement at basic pH (10.5)
DMPD	DMPD	Decrease of the absorbance of the purple radical cation $DMPD^{\cdot+}$	Very stable endpoint	Measurements at acidic pH (5.25); not suitable for hydrophobic substances; interferences from organic acids
HAT (hydrogen atom transfer) assays				
ORAC	AAPH	Prevention of AAPH radical reaction with fluorescein solution	Broad database on measured substances; suitable for antioxidants with and without lag phases/ complex samples	Unsuited for lipophilic substances; AAPH radical no biological relevance
TRAP	AAPH	Prevention of AAPH radical reaction with fluorescein solution with	Data standardized to Trolox as reference substance	Variation in lag time phases can lead to under-/ overestimation; AAPH radical no biological relevance
Crocin bleaching	AAPH	Prevention of Crocin bleaching by AAPH radical	Considers both the concentration of antioxidants and their reaction rate constants	Not suited for reactions with lag phase; Crocin not standardized (mixture of natural pigments); AAPH radical no biological relevance

Inhibition of lipid oxidation	Cu^{2+}; azo compounds	Inhibition of Cu^{2+} or azo initiator induced lipid autooxidation	Process biological relevance	Azo compounds quite aggressive and can form different radicals [165]; possible formation of micelles
Luminol assay	Hydroxyl radical	Inhibition of chemiluminescence from the radical reaction with luminol	Hydroxyl radical biological relevance	pH dependency of luminescence; luminescence can be quenched by NO and enhanced by peroxynitrite
Metal chelating ability assays				
HORAC	Hydroxyl radical	Prevention of Co^{2+} complex induced Fenton like reaction fluorescein decay	Hydroxyl radical biological relevance	Metal chelating capacity often outcompete hydroxyl radical scavenging
Other assays				
TOSC	Peroxyl radicals	Capacity of a substance to inhibit the oxidation of alpha-keto-gamma-methiolbutyric acid (KMBA) to ethylene	Peroxyl radicals biological relevant; applicable to tissue probes and fat-soluble antioxidants	Not specific to one ROS (KMBA can also be oxidized by HOCl and peroxynitrite [166])

AAPH: 2,2'-Azobis(2-amidinopropane) dihydrochloride, ABTS: 2,2'-azino-bis(3-ethylbenzothiazoline-6-sulphonic acid, DMPD: *N,N*-dimethyl-*p*-phenylendiamine, DPPH: 2,2-diphenyl-1-picrylhydrazyl, FCR: Folin–Ciocalteu reagent; FRAP: ferric ion reducing/antioxidant power, HORAC: hydroxyl radical antioxidant capacity, ORAC: oxygen radical absorbance capacity, PCL: photochemiluminescence, *p*-NDA: N,N-Dimethyl-4-nitrosoaniline, TEAC: Trolox equivalent antioxidant capacity, TRAP: total radical trapping antioxidant parameter

2.3.3. Cellular and *in-vivo* assays

The complexity of *in-vivo* measurements or cell models also increases the number of possible targets for an antioxidant assay. Depending on the anticipated effect of an antioxidant intracellular assays concentrate either on measuring ROS concentrations, ROS damage products, redox couple's ratios, redox protein abundance or protein redox statuses. Basically, the approaches can be divided into two different groups: the ones that directly measure ROS and the ones that focus on the measurement of ROS reaction products.

Direct ROS measurements can be realized using fluorescence probes or by using genetically encoded ROS sensors. On the market many different fluorophores are available that go into a fluorescent state after reaction with ROS. Some examples are Amplex® Red (10-Acetyl-3,7-Dihydroxyphenoxazin), $DCFAH_2$ (dichlorodihydrofluorescein), rhodamine derivates (e.g. DHR: dihydrorhodamine 123), or Tempo-9-AC [2]. Those probes are available from various companies and are used frequently to measure ROS. However, there are some severe limitations to these probes. Most of them are unspecific (react with different ROS), pH sensitive and can undergo spontaneous autooxidation or overoxidation states (over-/underestimation of ROS concentration). Besides their direct reaction with ROS means that they manipulate intracellular ROS levels. Another disadvantage of most of the probes is that their fluorescence is often

[2] 4-((9-acridine-carbonyl)amino)-2,2,6,6-tetramethylpiperidin-oxyl

dependent on third parties such as enzyme activities, metal ions or the presence of oxygen. This makes their read out ambiguous to interpret because it is not exclusively dependent on ROS concentration. (reviewed in [167]) One example is Amplex® Red, which is used to detect H_2O_2. The conversion of the probe in the presence of H_2O_2 to the fluorescent resorufin is catalyzed by horseradish peroxidase (HRP) and therefore the signal is directly dependent on the activity of the enzyme. Besides, it was demonstrated that exposure of the probe to light [168] or interference of dietary antioxidants can lead to false positive results [169]. To overcome some of the limitations of the first generation of fluorophores, new fluorophores have been developed like boronates or organic fluorophores attached to nanoparticles or polymers. (reviewed in [170]). Other detection methods rely on the use of chemiluminescence probes like luminol, lucigenin, or *Cypridina* luciferin analog (MCLA[3]). One example is the luminol-based chemiluminescence probe L-012 [4] [171], that has been widely used to detect superoxide from cells in various settings. However, the chemiluminescence reaction seems to require an initial oxidation step by peroxidases and H_2O_2 which leaves some doubt on the specificity of the probe [172]. Another way of ROS detection are sensor electrodes. This possibility is discussed further on.

Another approach to assess intracellular ROS levels are protein-based genetically encoded sensors. They have the advantage that they can be targeted to specific sites within the cells giving information on compartment and sub-compartment specific processes. Further, they enable measurements in living cells/organism and enable to follow very fast processes in real-time measurements. The sensors encode fluorescence proteins, such as the green fluorescence protein (GFP), or yellow fluorescence protein (YFP). GFP and YFP have the unique ability of self-catalyzed chromophore formation, thus their fluorescence is independent of external factors [173]. Introduction of the GFP/YFP gene into an organism lead to the expression of the fluorophore that can be detected within the living cell by fluorescence-based methods. Fluorescence proteins have applications in many areas. To use them as genetically encoded redox probes the proteins are integrated into ROS/redox sensitive domains. One example is the HyPer sensor with the circularly permuted YFP (cpYFP) inserted into the hydrogen peroxide sensitive OxyR regulatory domain (OxyR-RD) from E.coli [174]. In the presence of hydrogen peroxide a disulfide formation in OxyR-RD lead to a conformational change that can be measured in a ratiometric excitation spectrum change of the cpYFP. The ratiometric detection makes the sensor independent of expression rates. Further advantages are the sensitivity of the sensor (nanomolar range of hydrogen peroxide) and the fast-reaction rates with hydrogen peroxide (10^5 $M^{-1}s^{-1}$) that allow real-time measurements. (reviewed in [175]) HyPer has been targeted to the ER [176], mitochondria, the cytosol [177] as well as to peroxisomes [178] to study site specific hydrogen peroxide levels. Other important

[3] 2-Methyl-6-(4-methoxyphenyl)-3,7-dihydroimidazo[1,2-a]pyrazin-3-one, hydrochloride
[4] 8-amino-5-chloro-7-phenyl-pyrido[3,4-d]pyridazine-1,4(2H,3H)dione

genetically encoded ROS sensors are the redox sensitive YFP (rxYFP) and the redox sensitive GFPs (roGFPs). Both FPs have additional Cys residues in proximity of the chromophore. Therefore, the oxidation/ reduction of the protein lead to spectral changes. While the changes for rxYFP are intensiometric, the roGFPs allow ratiometric fluorescence measurements. ([179], [180], [181]) Reaching an equilibrium with the intracellular thiol pool can be rather slow for roGFP and rxYFP. To overcome this problem Gutscher at al fused roGFP with Grx1. The availability of Grx to catalyze the thiol/disulfide exchange between the intracellular thiol pool and roGFPs as a rate limiting factor is omitted this way, thus creating a sensor for the intracellular GSH/GSSG ratio (Grx1-roGFP2) [182]. Fusing the yeast peroxidase Orp1 to roGFP (Orp1-roGFP) created a sensitive sensor for hydrogen peroxide and demonstrated that peroxidases can catalyze the oxidation of Cys residues that are not reactive enough to be oxidized by hydrogen peroxide alone in a cellular environment [183].

A disadvantage of genetically encoded sensors is their pH sensitivity. In most GFP like proteins a Tyr residue externally accessible can be either protonated or deprotonated depending on the environmental pH. The protonated or deprotonated forms of the chromophore have different excitation peaks. Therefore pH changes can be misinterpreted as reduction/oxidation of the probe [177]. Another disadvantage of genetically encoded sensors is that they might have an impact on the cells phenotype.

An indirect measurement of ROS is the detection of ROS reaction products. Here different groups of target molecules can be addressed, namely proteins, lipids, or DNA molecules. Protein modifications induced by ROS can be nitrations, carbonylations, glutathionylations or thiol modifications. Protein tyrosin nitration is caused by peroxynitrite ($ONOO^-$) formed from the reaction of of nitric oxide (NO) and the superoxide radical ($O_2^- \cdot$) [184]. Detection of the formed nitrotyrosin is possible by HPLC analysis, fluorescent detection, [185] or ELISA kits (e.g. OxiSelect™ Nitrotyrosine ELISA Kit, Cell Biolabs). The interaction of hydroxyl radicals with biomolecules can lead to the formation of reactive carbonyl groups like aldehydes and ketones. The resulting products can be divided into high molecular weight (HMW) carbonyls and low molecular weight (LMW) carbonyls. LMW carbonyls are generated in oxidative cleavage reactions, while in HMW carbonyls the reactive carbonyl group is formed in a target molecule, e.g. a protein [186]. Protein carbonylations are irreversible modifications that might lead to a loss of protein function, depending on the degree of carbonylation [187]. However, the great variety of potential products that can form in carbonylation reactions is accompanied by a great variety of possible detection methods. Therefore, standards in carbonyl analysis are crucial to overcome orders of magnitude variances between reported results [188]. For both carbonylation and nitration analysis of proteins the sample treatment during the analysis is often quite harsh, which might alter the initial status of the samples. Other protein modifications that can be evaluated are

glutathionylations or thiol modifications. The later can be assed for example by one-/two-step labeling of the thiols with subsequent analysis of the samples by western-blot. Other techniques are the biotin-switch assay, redox-DIGE, OxiCAT, IodoTMT or R-SOH labeling to evaluate intracellular thiol modifications. Focusing on the interaction of ROS with lipids the lipid peroxidation can be assessed. This can be done via quantification of F_2-isoprostanes [189] or with the fatty acid analog C11-BODIPY™ 581/591 [190]. The interaction of ROS with DNA can be evaluated by the measurements of the inflicted DNA base damage via the quantification of 8-OHdG (8-hydroxydeoxyguanosine). The indirect assessment often lacks information on the ROS species that introduced the modifications (an exception is the carbonylation of proteins, which can only be induced by hydroxyl radicals). Furthermore, the methods do not allow a direct quantification of ROS. The evaluated oxidation products can also accumulate to a certain degree within the cell. The assays are end-point measurements giving no information on the temporal dimensions of the reactions that led to the detected products.

Another indirect way of antioxidant effect evaluation is the assessment of redox protein abundance or the evaluation of redox couple ratios, e.g. GSH/GSSG or protein disulfides/protein thiols. Especially the ratio of GSH to GSSG within the cell has often been used as a parameter for the redox status of a cell. However, this approach neglects that the oxidized GSSG can be pumped out of the cell, bound to proteins or be enzymatically reduced within the cell. Therefore, an endpoint assay for the determination of the intracellular GSH/GSSG ratio might lead to biased results. Cell assays that include cell lysis to evaluate the intracellular GSH/GSSG ratio often yield different results than intracellular assays (e.g. with Grx1-roGFP2), possible due to the fast reaction rates of the intracellular pool with atmospheric oxygen.

The main challenges to be addressed by all presented methods are their specificity, their sensitivity, their time and local resolution and their invasiveness to the investigated system. Because many methods fail to do so, many ambiguous and biased results have been published in the redox research field. The genetically encoded sensors are the first techniques at hand to follow intracellular redox processes *in-vivo* in real-time measurements. Further development of the encoded sensors will be the next step in obtaining less biased and more informative results [175].

2.3.4. Electrochemical antioxidant assays

2.3.4.1. General aspects

Another way to assess antioxidant activities is by electrochemical measurements. Electrochemistry offers three areas in the investigation of antioxidants. The first is the direct investigation of the antioxidant potential of a substance by determining their redox properties at relevant pH values. Looking at different molecules in comparison, it is possible to predict the

antioxidant active moiety of more complex molecules (e.g. of polyphenols) [64]. However, the oxidation potential itself does not necessarily correlate well with antioxidant activities for example in the DPPH assay [191], but in combination with other reaction parameters such as the number of transferred electrons (*n*) the oxidation potential allows to make predictions on the antioxidant activity (E_{50} value) of a substance [192]. It is also a valuable tool for a quick screening of plant extract for their antioxidant potential. However, the obtained potentials depend on the selection of the electrolyte solution (aqueous or non-aqueous, composition). Therefore, the predictive value for biological systems is often limited.

The second option is to determine the interaction of any ROS or other radical with a potential antioxidant via cyclic voltammetry to investigate reaction mechanisms and kinetics ([193], [194], [195]). However, since this is only a two-component system the reaction parameters are not necessarily transferable to *in-vivo* conditions.

The third option for the use of electrochemistry in antioxidant research are electrochemical sensors for ROS detection/ quantification or the detection of ROS inflicted damage products via the sensor. The idea behind it is that the ROS concentration or damage product's concentration decreases in the presence of an antioxidant. The scientific literature offers a great range of proposed sensor electrodes on the basis that they allow rapid measurements and that instrumentations are mostly inexpensive in comparison with fluorescence detection. [196] One class of sensors relies on enzymes that are immobilized on the sensor electrode surface. For the detection of superoxide two different enzymes, cytochrome *c* (cyt *c*) and SOD have been proposed. Cyt *c* oxidizes superoxide to form O_2. Its own heme iron is regenerated after the reaction at the electrode surface. The current that results from the electron flow of the radical to the electrode via the attached cyt *c* is proportional to the radical concentration [197]. To increase the current cyt *c* is often attached in multilayers to the electrode surface [198]. However, since cyt *c* is not specific to superoxide and can also reduce for example H_2O_2, which is often present in biological samples, SOD has been proposed as a more specific sensor for superoxide. SOD catalyzes the dismutation of superoxide to H_2O_2 and O_2. The detection can either rely on the direct electron transfer from SOD to the electrode [199] or on the detection of the generated H_2O_2. The H_2O_2 quantification can be achieved by amperometric measurements [200] or by another second enzyme system such as horseradish peroxidase (HRP) embedded in a polypyrrole layer [201].The fixation of enzymes to electrode surfaces requires experimental conditions that enable proper enzyme activity (pH, temperature) and positioning of the enzyme that allow electron transfer at high rate constants (right location of the active center).

Another class of electrochemical sensors omits these challenges that are involved with the use of enzymes and focuses on ROS inflicted damage. For example, electrodes that immobilize double stranded DNA (dsDNA) can assess the ROS inflicted damage by measuring the guanine oxidation

peak between 0.8 and 1.0 V (vs. Ag/AgCl) by square wave voltammetry (SWV). The signal decreases upon the exposure of the electrode to oxidizing ROS [202]. The use of dsDNA is justified by arguing that ROS inflicted damage to DNA can cause mutations *in-vivo* and is therefore biologically relevant. Other sensors assess the damage ROS inflict on biological less relevant material such as polypyrrole. In response to the overoxidation by hydroxyl radicals the material loses its conductivity which can be monitored electrochemically [203].

2.3.4.2. SAM based sensor electrode

2.3.4.2.1. Principle

The use of dsDNA or Cyt *c* on electrochemical ROS sensors has been introduced in the previous section. Fixing DNA to an electrode surface requires positive potential to achieve the electrostatic binding of negatively charged DNA [202], while Cyt *c* binding requires a linker molecule to immobilize the enzyme on the surface. Those linker molecules are often alkylthiols that can form self-assembled monolayers (SAMs) on gold surfaces. During SAM formation the sulfur atoms chemisorb to the gold surface. Proving sufficient time van de Waals forces as well as hydrophobic effects of the alkylthiol carbon chains with hydrophile solvents promote the formation of well-ordered SAMs. SAM formation can occur in the gas as well as in the liquid phase. Because of their relative ease of preparation as well as their stability alkylthiol SAMs on gold surfaces are popular in biosensor fabrication. Often, they are applied as linker molecules or further modified to individual requirements by the introduction of functional groups. However, as was demonstrated by Scholz et al [204] alkylthiols themselves are sensitive to oxygen radical attack. This discovery let to the development of an electrochemical sensor for hydroxyl radicals composed of an alkylthiol SAM covered gold electrode. The exposure of such prepared electrodes to oxygen radicals let to the degradation of the SAM proportional to radical concentration and exposure time. The extent of damage to the SAM can be assessed by differential pulse voltammetry (DPV) measurements in an electrolyte containing a resolved redox couple such as $Ru(NH_3)_6^{3+/2+}$ ions. The measurements take place in a three-electrode set-up consisting of the sensor electrode as working electrode (WE), a counter (CE) and a reference electrode (RE) to control the potential applied at the working electrode. Working in a potential range that corresponds to the redox potential of the ions in solution, the measured currents reflect the reduction of the ions at the WE surface. In case of an undamaged SAM the reduction of the ions in solution at the gold electrode is blocked. After radical exposure the amount of exposed gold sites or SAM defect sites correlates with the reduction current measured at the electrode. Using DPV measurements also small defects in the SAM can be detected. That is because in DPV the potential is applied in a waveform and the current is measured twice, before and after application of the potential pulse. This eliminates much of the noise from background and capacity current [205]. Because of its sensitivity the method is a

promising tool for the assessment of biologically relevant ROS, such as hydroxyl radicals, at physiologically concentrations [2]. Introduction of an antioxidant to the radical solution opens the opportunity to assess the radical scavenging capacity of the antioxidant, which is translated into less damage to the SAM and ultimately into lower peak currents measured at the electrode in DPV [3] (figure 3).

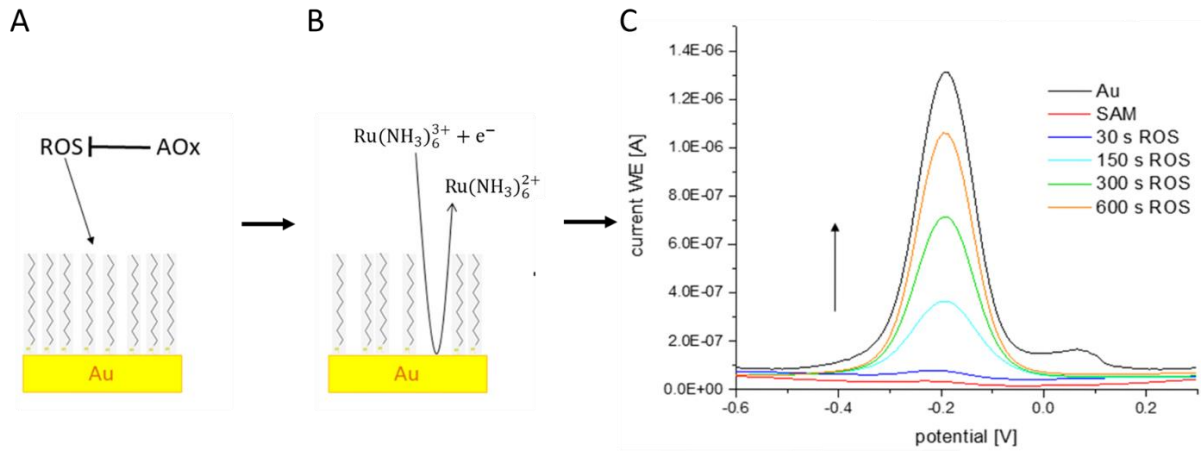

Figure 3: Measurement principle at the SAM modified sensor electrode. (A) Polycrystalline Au electrodes are covered with a $C_{10}SH$ SAM. The sensor is exposed to reactive ROS and antioxidants (AOx). (B) The resulting partial destruction of the SAM enables the reduction of $Ru(NH_3)_6^{3+}$ at the exposed Au sites in DPV measurements. (C) The resulting reduction currents measured at the electrodes increase with exposure time and ROS concentration.

2.3.4.2.2. Data evaluation

The described methods allow to indirectly quantify the concentration of ROS present in a solution by evaluation of the degree of damage to the SAM. This is measured is reflected in the height of the $Ru(NH_3)_6^{3+}$ ions reduction current measured after radical exposure in DPV and plotted against exposure time. The slope from the obtained graph is evaluated and used as in indicator for the concentration of radicals in solution. The steeper the slope the higher the ROS concentration. For the investigation of the antioxidant activity of a plant compounds the SAM covered gold electrode is exposed to oxygen radicals in the presence of the plant compound. The scavenging activity of the compound is reflected in the inhibition of the SAM degradation process compared to the SAM destruction rate in the absence of the compound. The steeper the slope the lower is the antioxidant activity.

3. Methods

All chemicals were of analytical grade. All experiments were performed using ultrapure water (resistivity=18.2 MΩ cm).

3.1. Electrochemical assay

For the studies alkanethiol SAM covered polycrystalline gold electrodes were applied as ROS sensors as initially proposed by Scholz et al [2]. For the presented work the electrode pretreatment, the SAM coverage, the ROS quantification and the electrode cleaning were further characterized and adapted to the requirements of antioxidant activity measurements in a biological context.

3.1.1. Electrode pretreatment

Polycrystalline gold electrodes with a radius of 2 mm (±0.1 mm) embedded in polyether ether ketone (PEEK) (Metrohm AG, 6.1204.140) and polycrystalline gold electrodes with a radius of 0.5 mm embedded in a glass corpus were pretreated before alkanethiol SAM coverage. First, potential contaminants were removed from the gold surface electrochemically via reductive desorption (RD) (cyclic voltammetry (CV) from −0.5 V to −1.5 V for 10 cycles in 0.1 M NaOH at 0.5 V s^{-1}). Second, the 2 mm electrodes were cleaned mechanically by polishing them with MicroPolish II Alumina Powder (0.3 μm; 0.05 μm; Buehler, an ITW Company) for 10 min with each grinding size. Loosely attached alumina particles were removed in an ultrasonic bath (Emmi 20 Eco, EM AG). The step was omitted for the 0.5 mm electrodes following the manufacturer's instructions (Metrohm AG). Afterwards the electrodes were subjected to a visual control for scratches and impurities under a light microscope (100: 1 objective, Leitz Laborlux 12 Pol S). The electrochemical cleaning was performed via CV in 0.1 M H_2SO_4 (scan rate 0.1 V/s; 0 V to 1.5 V) until a stable voltammogram was obtained. As a last step, gold oxides, that might have been generated during the pretreatment procedures, were removed from the gold surface via the "electrochemical electrode stripping" (ECS) procedure proposed by Tkac et al [206] (CV in 0.1M H_2SO_4, scan rate 0.1 V/s; range 0.2 V to 0.75 V; 10 cycles).

The $Ru(NH_3)_6^{3+}$ reduction signal at the cleaned Au electrodes was measured by differential pulse voltammetry (DPV) in 1 mM hexaammineruthenium(III) chloride ($[Ru(NH_3)_6]Cl_3$, Sigma-Aldrich) solution in 0.1 M acetate buffer (pH = 4.7; −0.6 V to 0.3 V; step potential 0.01 V; interval time 0.2 s).

All electrochemical measurements were performed in deareated electrolytes (600 s N_2 purging prior to measurement). The voltammetric measurements were performed with a 663 VA stand in combination with an Autolab PGSTAT 20 and an Eco Chemie IME 303 (Metrohm AG). A glassy

carbon (GC) electrode served as counter electrode and an Ag/AgCl (3 M KCl) electrode as reference. Data were recorded with NOVA 1.11 and NOVA 2.0 software (Metrohm AG). Data analysis was performed with OriginPro 2016 (OriginLab Cooperation).

3.1.2. SAM preparation

The cleaned gold electrodes were rinsed with water and ethanol and immersed into 2 mM ethanolic 1-octodecanthiol, 1-decanethiol or 1-hexadecanethiol solution (Sigma Aldrich) and kept at room temperature in the dark for 17 hours. After the SAM formation process the electrodes were again rinsed with water and ethanol. The integrity of the formed SAM was tested in DPV measurements in 1 mM $[Ru(NH_3)_6]Cl_3$. The coating procedure was assumed successful in case of the absence of the $Ru(NH_3)_6^{3+}$ reduction signal. To further verify the coating procedure for SAM formation, Au (111) plates were prepared by hydrogen flame annealing gold on quartz plates. The plates were incubated in thiol solutions under the described conditions. Afterwards, images of the formed SAM were taken with a scanning tunneling microscope (STM) using a STM/AFM (PicoSPM (Molecular imaging)) with NanoScope E Scanning Probe Microscope Controller (di Digital Instruments, Veeco Metrology Group) with STM tips cut from Pt/Ir wire. The pictures taken with STM were analyzed with Gwyddion 2.41 software.

3.1.3. Further characterization

The gold surface structure before, after and during the SAM removal process by radical attack was investigated with AFM (atomic force microscopy) and Pb-UPD (underpotential lead deposition).

3.1.3.1. Atomic force microscopy (AFM)

The impact of the cleaning procedure and SAM coverage/removal cycles on the electrode's gold surface were investigated with atomic force microscopy (AFM). AFM images were taken with a Nanosurf EasyScan 2 (Nanosurf Inc.) in non-contact mode with NANOSENSORS™ PPP-NCLR cantilevers at C=48 N·m^{-1} and f_0=190 kHz. The images of the electrodes were taken after the cleaning procedure, after SAM removal via radical treatment, and after SAM removal via reductive desorption. The roughness average (Ra) of the Au surface was calculated from AFM data using Gwyddion 2.41 software.

3.1.3.2. Underpotential lead deposition (Pb-UPD)

The nature of the gold surface before, during and after SAM coverage was further investigated with Pb-underpotential deposition (Pb-UPD) measurements in 0.1 M $NaClO_4$+0.01 M $HClO_4$+0.001 M $Pb(ClO_4)_2$. The measurements were performed in a potential range of −0.45 V to 0.5 V for uncoated gold electrodes at 0.02 V s^{-1} at a 663 VA stand (Metrohm AG). For coated electrodes the range was restricted from −0.38 V to 0.5 V. Data was recorded with GPES 4.9 007.

3.1.4.Evaluation of ROS induced SAM degradation

In addition to monitoring the impact of ROS on the SAM by DPV measurements the process was followed by different other techniques to obtain a more detailed picture of the processes at the sensor electrode's surface.

3.1.4.1. Cyclic voltammetry (CV)

Cyclic voltammograms (CVs) in 1 mM $[Ru(NH_3)_6]Cl_3$ in 0.1 M acetate buffer as well as in 0.1 M H_2SO_4 were recorded from −0.5 V to 0.3 V at 0.05 V/s after each radical exposure interval. From the voltammograms the anodic and cathodic peak potentials and currents were determined. The general set-up for the measurements was as described before (see section 3.1.1.).

3.1.4.2. Alternating current voltammetry (ACV)

The gold surface coverage by the formed SAM after repetitive exposure to oxygen radicals was measured with selective alternating current voltammograms (ACV) (0.45 to −0.55 V vs. Ag/AgCl; sinusoidal perturbation voltage at frequency (f) = 20 Hz, amplitude (A) of 0.01 root-mean-squared voltage (V_{RMS}), 5 mV/s) recorded in 0.1 M acetate buffer (pH 4.7). From the in-phase (0°) and quadrature (90°) component of the measured AC current potential dependent differential capacity curves were calculated:

$$C = \frac{\left(E / I_{90^\circ}\right)}{\frac{2}{\pi} \times A \times 2\pi \times f} \tag{2.1}$$

SAM surface coverage of the Au electrode (θ) was derived from the differential capacity values using the following formula:

$$\theta = \frac{C_0 - C}{C_0 - C_{perfect}} \tag{2.2}$$

With C_0= differential capacity of cleaned Au surface under experimental conditions, $C_{perfect}$ = theoretical differential capacity of defect free $C_{10}SH$ (1.32 µF/cm²) or $C_{16}SH$ (0.83 µF/cm²) monolayer and C = differential capacity of the SAM monolayer measured in experiments.

3.1.4.3. Scanning electrochemical microscopy (SECM)

Polycrystalline gold plates were prepared by thermal evaporation of gold on chrome coated quartz plates under vacuum conditions (film thickness 150–160 nm; Mini Coater, Tectra GmbH, Germany). The plates were coated with alkanethiol SAMs as described before and exposed to oxygen radicals photolytically generated by UV light (λ=365 or 254 nm) from 1 mM H_2O_2 in

aqueous solution. Electrochemical SAM removal was performed in 0.1 M NaOH (−0.3 to −1.2 V vs. Ag/AgCl; 0.1 V/s; 10 cycles).

i. Fabrication and testing of the microelectrodes

Microelectrodes used for SECM measurements were manufactured at the laboratory from Pt-wire with a diameter of 25 µm sealed in a glass capillary and pulled under vacuum conditions. Prior to use electrodes were polished with Al_2O_3 powder (grain size 0.05 µm; Buehler, Germany) and tested via CV measurements in 1 mM $Ru(NH_3)_6Cl_3$ in 0.1 M acetate buffer and in 0.1 M Na_2SO_4 (2 cycles; −0.5 to 0.3 V vs. Ag wire; 0.025 V/s; CE: Pt wire; CHI Potentiostat).

ii. Approach curves and imaging

The electrolyte and the gold substrate were connected via a gold wire (Ø=10 µm). The cell potential was fixed to −0.42 V (vs. Ag) and the surface was approached at 0.5 µm/s using PIHera linear precision positioner (Physik Instrumente (PI) GmbH & Co. KG) until a current maximum was reached. Data were fitted to the model of Lefrou and Cornut [207] for $RG=r_{glass}/r_T=7$ and the microelectrode tip radius $r_T=10$ µm. The currents measured at the electrode tip i_T were normalized for the current in bulk solution ($i_{T\infty}$):

$$I_T = \frac{i_T}{i_{T\,i\infty}} \tag{2.3}$$

I_T was plotted against the distance from the probe d in relation to r_T ($L=d/r_T$). Taking the obtained data from the approach curves, the microelectrode was retrieved from the surface by the distance d=10 nm for imaging and imaging data were analyzed with MIRA software (Microscopic Image Rapid Analysis; Gunther Wittstock).

3.1.4.4. X-ray photoelectron spectroscopy (XPS)

The elemental composition on the surface of the SAM coated polycrystalline gold plates after radical treatment (UV) and after reductive desorption (RD) in comparison to untreated SAM areas on the same samples (no UV; no RD) were analyzed with X-ray photoelectron spectroscopy (XPS) under vacuum conditions (ESCALAB 250 Xi (Thermo Fisher). For each treatment the signals of Au 4f, S 2p, C 1s und O 1s at 40 x 900 µm area scans were recorded. Data were normalized for background signal and signal intensities were normalized according to Scofield [208], the transmission function (device manual, Thermo Fisher) and attenuation length (AL) according to Laibinis [209].

3.1.4.5. PM IRRAS

Orientation of the absorbed thiol molecules at the gold surface were investigated by polarization modulation Fourier transform infrared reflection absorption spectroscopy (PM IRRAS) measurements in air (Vertex 70 (Bruker), Polarization Modulator (Hinds Instruments), external reflection setup (custom made) as described before [210]. Each probe was measured 6×500 times at λ^{-1}=1,600 nm and 2×500 times at λ^{-1}=2,900 nm. Data was analyzed with OPUS software (Bruker).

3.1.5.ROS sensing

Radical exposure of successfully coated electrodes was performed in quartz test tubes (Metrohm AG; Ø=15.6 mm) filled with varying concentrations of H_2O_2 (30%, Merck, 1 mM up to 1 M) in distilled water. Radicals were generated by photolysis of H_2O_2 by UV light radiation (UVB/UVC: 705 UV Digester, Metrohm AG; UVC: λ=254 nm, Obsytec). The SAM radical removal process was followed by DPV (parameters as described before) and Pb-UPD measurements (0.1 M $NaClO_4$+0.01 M $HClO_4$ +0.001 M $Pb(ClO_4)_2$; −0.38 V to 0.5 V for coated electrodes and −0.45 V to 0.5 V for uncoated electrodes at 0.02 V s^{-1}). The electrodes were exposed to the radical solution for treatment intervals of 30 seconds. Afterwards they were transferred into the electrolyte solution to measure DPV or Pb-UPD signals at the electrodes. The peak currents of the $Ru(NH_3)_6^{3+}$ reduction signal in DPV measurements (I_t) were divided by the initial currents measured at the cleaned electrodes (I_0) and the logarithm of the inverse was plotted against the radical treatment time (t)to evaluate the signal regain dynamics: $\ln\left[1-\left(\frac{I_t}{I_0}\right)\right]$.

The slope of the resulting function (k) was determined of the plot by a linear fit (software OriginPro 2015G). From the k values the kinetics of the ROS induced SAM degradation process at the electrodes were evaluated. As negative control the experiments were performed without the addition of H_2O_2.

The impact of oxygen on the reaction was evaluated by purging the reaction solution, containing H_2O and H_2O_2, in the quartz tubes with N_2 or O_2 for 20 minutes prior to H_2O_2 addition and exposure of the electrodes.

The role of different cell media and cell buffers as buffering agents in the destruction of the SAM by reactive species were evaluated by replacing the distilled water in the quartz test tubes during H_2O_2 photolysis by RPMI (Roswell Park Memorial Institute (RPMI) 1640 medium (with and without phenol red, Sigma), DMEM (Dulbecco's Modified Eagle's medium, PAN Biotech, cat. no: P04-01550), HBSS (Hank's balanced salt solution, D8264, Lot RNBC8868, Sigma) or PBS

(phosphate buffered saline, D8662, Lot RNBD3943, Sigma). The experiments were taken as an indicator for the behavior of the electrode in a cell culture set-up.

The importance of individual ROS for the destruction of the SAM on the electrode's surface was investigated by the preferential generation of superoxide at TiO_2 particles in aqueous media. For this purpose superoxide radicals were generated *in-vitro* at TiO_2 nanoparticles (particle size 4 to 8 nm; 200 mg L^{-1}; Carl Roth) via radiation with simulated sunlight (SSL, 300–700 nm) as reported before [211]. As solvent for the TiO_2 nanoparticles water and preheated HT buffer (37 °C; pH=7.4) were used. Radiation took place in 12 mL quartz test tubes (Metrohm AG). The formation of superoxide was verified by its reduction of nitro blue tetrazolium chloride (NBT; 0.1 mM; Carl Roth) into insoluble formazan. The resulting decrease of NBT absorbance at 260 nm in the solution over a period of 2 hours was measured in acryl cuvettes ($10 \times 10 \times 45$ mm; Sarstedt AG & Co) at a photometer (Specord 50 photometer; Jena Analytik). The TiO_2 particles with the precipitated formazan were filtered out of the solution prior to absorbance measurements with 0.2 µm pore sized filters (Filtropur S 0.2 syringe filter, Sarstedt).

The generated superoxide radicals at TiO_2 particles were then investigated with the SAM modified Au electrodes. The electrodes were exposed to the freshly stirred TiO_2 suspension radiated for 20 minutes with SSL. After incubation with the TiO_2 particle solution the electrodes were rinsed with H_2O and ethanol and transferred into a $[Ru(NH_3)_6]Cl_3$ solution to measure the $Ru(NH_3)_6^{3+}$ ion reduction signal via DPV at the electrodes.

3.2. Evaluation of antioxidant activities *in-vitro*

Eight different plant substances, one vitamin derivate and one plant extract were chosen as representative plant substances to be investigated for their antioxidant activities in the different experimental settings:

(i) standardized *Gynostemma pentaphyllum* (Makino) extract powder (GP) obtained by extraction of dried aerial parts with 75% ethanol/ 25% H_2O (from Herbasin (Shenyang) Co., Ltd. (China) [212]; kindly provided for by Prof. Lorenz Schild, Otto-von-Guericke-University, Magdeburg) diluted in DMSO to a final maximal concentration of 0.5% DMSO and 120, 60 or 30 µg/mL (GP)
(ii) ascorbic acid (AA, 99%, Sigma-Aldrich)
(iii) caffeic acid (CA, 98%, Carl Roth GmbH + Co. KG),
(iv) (-)- epigallocatechin gallate (EGCG, Sigma-Aldrich)
(v) *trans*-ferulic acid (FA, 99%, Sigma-Aldrich)
(vi) kaempferol (Kaem, Glentham Life Sciences Ltd)
(vii) quercetin dihydrate (97%, Alfa Aesar)

(viii) (+)-rutin trihydrate (97%, Alfa Aesar)

(ix) Trolox (6-hydroxy-2,5,7,8-tetramethylchroman-2-carboxylic acid, 97%, Acros Organics)

Further details about the individual substances can be found in the introduction. To accord for the potential effects of the solvent all substances were diluted in a 1:4 mixture of DMSO (dimethyl sulfoxide, >99.9%, Sigma-Aldrich) and water. The final concentration of DMSO in all solutions was > 0.8% v/v.

3.2.1. Electrochemical assay

For the evaluation of antioxidant activities of plant substances and extracts with the electrochemical assay, the substances were added in different concentrations (10 to 500 µM) to the radical solutions in the quartz test tubes (see 2.2.4.). The scavenging capacity of the substances towards ROS in aqueous solution were measured indirectly by the slope of the function ln[1-(I_t/I_0)] vs. t representing the SAM destruction rate (k_{AOx}) in comparison to the rate of destruction in the absence of the antioxidant substance (k):

$$\text{scavenging}[\%] = \left[\frac{(k - k_{AOx})}{k}\right] \times 100 \qquad (2.4)$$

The parameter k was determined in the linear section of the function from 30 to 300 seconds treatment time.

3.2.2. Luminol assay

The luminol assay relies on the chemiluminescence (CL) emitted from the exited state of the luminol dianion upon oxidation. For the reaction 60 mM luminol in 0.5 M NaOH (Carl Roth) were mixed together 1:10 with a 2 mM Fe-EDTA solution (ethylenediaminetetraacetic acid (EDTA)-Na_2 ˟2 H_2O (Thermo Fisher Scientific GmbH) in 0.1 M acetate buffer+$(NH_4)_2Fe(SO_4)_2$˟6 H_2O (Merck) in water) and varying concentrations of the plant substances in aqueous solution. The reaction was initiated by the addition of 2˟10^{-3} M H_2O_2. After 10 seconds in the dark the CL was measured in a portable tube luminometer (Junior LB 9509, Berthold Technologies GmbH & Co. KG). For each condition, 10 independent measurements were performed and the mean value calculated.

3.2.3. *p*-NDA assay

The oxygen radical scavenging activity of the investigated plant substances was further determined using *N,N*-Dimethyl-4-nitrosoaniline (*p*-NDA) as a probe. The bleaching of *p*-NDA due to oxidation can be observed as decreasing absorption at 440 nm [156]. For the assay 50 µM *p*-NDA in 0.1 M phosphate buffer (pH=7.2) were bleached by hydroxyl radicals, that were generated

with the Fenton reaction using 330 µM $Fe(II)Cl_2 \times 4\ H_2O$ (Merck) in phosphate buffered solution with 0.01 M H_2O_2. The antioxidant plant substances were added in different concentrations (50 to 200 µM) to the reaction solution. In order to account for the formation of reactive species and Fe^{3+} ions in the aerated solutions at the chosen pH due to autoxidation the blank measurements were performed in the presence of iron ions [213]. Afterwards the decrease of the absorbance A at λ=440 nm was monitored on a spectrophotometer (Specord 50, Jena Analytics) over a period of 2.5 hours. The spectra were recorded with the manufacturer's software (WinASPECT, version 1.7.0.79, Jena Analytics). For each condition 4 independent measurements were performed. Data was standardized to the blank measurements and the decrease of the absorbance (A_{A0x}) in relation to the control sample without plant compound $(A_{H_2O_2})$ for the individual time points was calculated.

3.2.4. Carotene bleaching assay (CBA)

β-Carotene is a naturally occurring plant pigment with an intense red/ orange color. It is itself considered an antioxidant because it can scavenge ROS and can absorb excessive energy from ultraviolet, violet, and blue light (see introduction). However, upon oxidation the molecule is decolorized. The process can be monitored by the decrease of its absorption maximum at $\lambda = 460$ nm. The decolorization process can be reduced by the addition of an antioxidant to the solution. In the literature different versions of the carotene bleaching assay (CBA) can be found. For this study the assay proposed by Miller et al was applied [214]. Briefly, a 400 mM β-carotene (≥97%, Sigma-Aldrich) solution in trichlormethan (chloroform, 99%, Carl Roth) was prepared and mixed 1:20:200 with linoleic acid sodium salt (≥98%, Sigma-Aldrich) and Tween® 20 emulsifier (polyethylene glycol sorbitan monolaurate, Sigma-Aldrich). Chloroform was removed by evaporation and 23% v/v distilled water were added under vigorous stirring. The emulsion was then diluted 1:3 with water and pipetted into spectrometer acrylic cuvettes (10 × 10 × 45 mm, Sarstedt) together with 4% v/v antioxidant solution that was prepared 1:1 with ethanol and water. The extinctions of the samples were measured from 400 to 520 nm directly after addition of the antioxidant substances at t=0 minutes on a spectrophotometer (Specord 50, Jena Analytics). The spectra were recorded with the manufacturer's software (WinASPECT, version 1.7.0.79, Jena Analytics) and standardized to a blank measurement containing the solution without ß-carotene or any antioxidant. Afterwards the samples were placed in a 50°C water bath and the decolorization of the solution was monitored by measurements every 10 minutes over a period of 60 minutes. For each condition four independent measurements were performed.

3.3. Cell assays

3.3.1. Cell lines

Apart for the antioxidant assays the plant substances were tested for cellular effects. For this reason and for testing the sensor electrode in cell culture experiments, five different cell lines were used in the study for different purposes:

(i) human keratinocytes (HaCaT, Sigma) [215];

(ii) rat C6 glioma cells with encoded mitochondrial HyPer Red (Mito-Hyper; Hyper WT);

(iii) rat C6 glioma cells with encoded mitochondrial Hyper Red and tafazzin (TAZ) knock out (Hyper TAZ), obtained by lentivirus transfection. The cell lines (ii) and (iii) were kindly provided by the working group of Prof. Lendeckel from Institute of Medical Biochemistry and Molecular Biology, University Medicine Greifswald and Prof. Elsner/ Prof. Lenzen from the University Medicine Hannover;

(iv) human embryonic kidney 293 cell line (HEK 293) expressing human NADPH oxidases Nox4 (Nox4-HEK293) with a tetracycline-inducible tet-on operator (Nox4-pDEST30) [216]; and

(v) Nox5 (Nox5-HEK293), generated via lentiviral transfection and selection [6]. The cell lines (iv) and (v) were kindly provided by the lab of Prof. Dr. Katrin Schröder at the Cardiovascular Research Center in Frankfurt.

HaCaT cells were cultivated in RPMI-1640 cell medium (R8758, Lot RNBD7303, Sigma) with 8% v/v fetal calf serum (FCS, Lot 044M3395, Sigma) and 1% v/v penicillin-streptomycin (P/S). Glia Hyper cells were cultivated in DMEM (low glucose, PAN Biotech, cat. no: P04-01550) supplemented with 3% v/v FCS, 1% v/v P/S and 0.2 µL/mL puromycin (invivogen). Nox-HEK293 cells were kept in Dulbecco's Modified Eagle Medium (DMEM, Gibco) supplemented with 10% v/v FCS and 1% v/v P/S. All cells were kept in humidified atmosphere (37 °C; 5% CO_2). During ROS measurements Nox-HEK293 cells were kept in HEPES Tyrode buffer (HT; containing in g/L: 2.33 HEPES; 0.2 CaCl; 0.1 MgCl; 0.2 KCl; 8 NaCl; 0.05 NaH_2PO_4; 1 D-glucose).

3.3.2. Metabolic activity assay - WST-8

To determine the effects of each antioxidant substance on the metabolic activity of HaCaT cells the WST-8 assay (Colorimetric Cell Viability Kit I; PromoCell GmbH) was applied. The assay relies on the conversion of 2-(2-methoxy-4-nitrophenyl)-3-(4-nitrophenyl)-5-(2,4-disulfophenyl)-2H-tetrazolium monosodium salt to the water-soluble orange-colored formazan dye. The reduction is performed by dehydrogenases present in viable cells via an electron carrier (1-methoxy PMS[5]). [217] The absorbance of the formazan dye is proportional to the number of metabolically active

[5] phenazine methyl sulfate

cells and therefore an indicator for the cell number. [218] For experiments HaCaT cells between passages 10 to 20 were plated in flat bottomed 96-well plates (TPP Techno Plastic Products AG, Germany) at a density of 5000 cells/ well. The cells grew for 24 h or 48 h (37°C, 5% CO_2) before treatment with 10 µL of antioxidant substances at variant concentrations diluted in H_2O and DMSO (< 0.8%). As control cells were treated only with water and DMSO. The cells were then incubated for 1 h, 24 h or 48 with the substances. After treatment the cell medium was removed, and the cells were washed twice with phosphate buffer saline (1✕PBS with 5 mM EDTA) and incubated for 1 hour with 2 to 15% v/v ethanol/ DMSO, 100 µM *t*BHP (*tert*-butyl hydrogenperoxide), 100 µM H_2O_2 or H_2O as control in HBSS. To each well 10 µL of WST-8 CCVK I solution were added and the optical density (OD) was measured after another 4 h incubation time at λ=450 nm in a fluorescence plate reader (Varioskan™ Flash Multimode Reader, Thermo Scientific, USA). To verify the dependence of OD signal on the cell number cells were plated out in different densities (10,000–500 cells/ well) and OD was measured after 48 h incubation. All tests were performed on a minimum of three biological replicates. Values were corrected for blank (cell buffer + CCVK-I solution) and standardized to the mean value of untreated cells (control).

3.3.3. Cell proliferation

Cell proliferation of HaCaT cells was monitored with CASY cell counter and analyzer (Roche AG). Cells were plated at a density of 5000 cells/ well in 96-well cell culture plates (flat-bottomed, TPP Techno Plastic Products AG) and grown for 24 hours. Afterwards cells were treated with plant substances and incubated for another 24 to 48 hours. For the last hour of incubation cells were additionally stimulated with 50 µM H_2O_2 or 100 µM *t*BHP. Afterwards cells were washed twice with PBS/EDTA and incubated 5 minutes with 0.05% trypsin/0.02% EDTA. The trypsin aided cell detachment was stopped by adding complete media, and the cells were centrifuged (3 min, 230✕ *g*, room temperature (RT), Heraeus Multifuge X3R, Thermo Scientific) and resuspended in cell medium. The cell suspension was diluted 1: 100 with CasyTon (REF 5651808, OMNI Life Science GmbH & Co KG) and analyzed for cell number, cell viability, debris content, average cell volume and cell diameter (CASY TT, parameters: sample volume 400 µL; capillary 150 µm; X-axis 60 µm; Y-axis auto; 3 cycles; dilution 101; evaluation cursor 11.7–60 µm; norm. cursor 6.15–60 µm).

The proliferation of Hyper cells was monitored with the cell permeable Hoechst 33258 nucleic acid stain (phenol, 4-[5-(4-methyl-1-piperazinyl)[2,5'-bi-1H-benzimidazol]-2'-yl]-, trihydrochloride, Thermo Fisher Scientific). The Hoechst 33258 stain emits blue fluorescence when bound as a minor-groove binder to dsDNA and can therefore be applied to determine the relative cell number by staining the cell nuclei [219]. For the assay Hyper WT cells were platted at a density of 7,000 cells/well and Hyper TAZ at a density of 14,000 cells/well in 96-well cell culture plates (clear flat bottom, black polystyrene plate, Sigma Aldrich). After 24 hours

incubation cells were treated with plant substances (dissolved in DMSO and water) and incubated for additional 24 hours. Afterwards cells were washed twice with PBS. To each well 50 µL PBS containing 5 mM glucose and 50 µL Hoechst 33258 reagent (final concentration 2 µg/mL) were added. The cells were kept in the dark on a shaker for 7 minutes before the fluorescence signal was measured in a fluorescence microplate reader (Infinite® 200 PRO, Tecan Trading AG, excitation 470 nm, emission 570 nm, 4×4 measurements/ well). The spectra were recorded with i-control™ software (Tecan Group Ltd.). For each treatment the mean relative fluorescence units (RFU) of four different wells were calculated.

Additionally, growth curves of the Hyper cells were obtained by counting the cells with a hemocytometer. The cells were platted at an initial density of 40,000 cells/mL/well for Hyper TAZ and 20,000 cells/mL/well for Hyper WT in 12 well plates (Greiner Bio One). The cells were either incubated in DMEM + 3% FCS + 1% P/S supplemented with 50 µM trolox every 24 hours or no supplementation (control). Additional external stress was induced to the cells by the addition of 20 µM H_2O_2 every 24 hours prior to cell harvest. After 24, 48, 72, and 96 hours cells were washed twice with PBS, detached by 1× Trypsin (3 min incubation at 37°C, 5% CO_2), and resuspended in DMEM. The cells were centrifuged (5 min, 1450 × *g*, RT) and the cell pellet resuspended in a defined volume DMEM to obtain a cell density that allowed the counting of > 100 cells. The cell suspension was mixed 1:1 with trypan blue solution, incubated for 1 minute and pipetted into a hemocytometer (Neubauer improved, LO-Laboroptik Ltd.). The cells (alive: unstained, dead: stained blue) were counted under a light microscope (100× magnification, cell counting protocol according to [220]).For each treatment the mean cell number per mL was calculated from four different wells.

3.3.4. ^{1}H-NMR analysis

For the evaluation of extracellular metabolome changes induced by the plant substances treatment extracellular metabolome studies for Hyper and HaCaT were performed by ^{1}H-nuclear magnetic resonance (^{1}H-NMR) analysis. For this purpose, HaCaT cells were cultivated for 24 hours in cell dishes (60×16 mm, 22.1 cm^2 growth area, TPP Techno Plastic Products AG) at a density of cells/mL. After 24 hours they were treated with antioxidant substances diluted in DMSO and water (final DMSO concentration $< 0.4\%$ v/v). Control cells were treated with DMSO and water only. After 24 hours 1 mL of the cell medium was removed for sterile filtration (syringe filtration unit Filtropur S 0.2 with a polyethersulfone membrane, pore size 0.2 µm, Sarstedt). The probes were stored at -20°C until measurement. The cells were detached from the dishes and counted with a CASY cell counter as described before. The NMR analysis of the samples was performed as described before [221]. Briefly, the metabolome samples were diluted 2:1 with sodium hydrogen phosphate buffer (0.2 mol L^{-1}, pH 7.0) containing 50% D_2O containing 1 mM 3-trimethylsilyl-

[2,2,3,3-D_4]-1-propanoic acid as an internal standard. The samples were measured in a Bruker Avance II-600NMR spectrometer (Bruker Biospin), operating at a proton frequency of 600.27 MHz. The spectra were recorded with TOPSPIN 3.2 software (Bruker Biospin). The metabolite signals were referenced according to the internal standard. Data analysis was carried out using AMIX v3.9.12 software (Bruker Biospin), as described in [221]. The relative concentration of each metabolite was normalized using the following formula (from [222]):

$$\frac{\left(C_t / C_{t0}\right)}{N_t} \tag{2.5}$$

with C_t: the relative concentration after time t incubation of the cells with the plant substances or the control; C_{t0}: the relative concentration in the initial medium; N_t the cell number after time t

From the values the logarithm to base 2 (Log_2) was calculated to demonstrate the fold changes in the samples in comparison to the untreated control [222]. Statistical analysis and graphs were obtained with MetaboAnalyst 4.0 software (Xia Lab, McGill University, Canada).

3.3.5.Intracellular GSH/GSSG ratio

The intracellular ratio of GSH to GSSG in HaCaT cells was determined with the Promega GSH/ GSSG-Glo™ assay system (Promega Corporation) in accordance to the producer's protocol [223] and previous experiments [224]. Briefly, the cells were seeded in 96 well cell culture plates at a density of 5,000 cells/ well and allowed to grow for 24 hours. Afterwards the medium was removed and fresh medium containing varying amounts of the investigated plant substances was added for 24 hours. The medium was then replaced by HBSS containing 100 µM tBHP. After 1-hour incubation the buffer was removed and 50 µL total glutathione or oxidized glutathione Lysis reagent were added to each well. Cells were shaken for 5 minutes before adding 50 µL of Luciferin Generation reagent. After 30 minutes 100 µL Luciferin detection solution were added to the wells and the cells were kept for 15 minutes in the dark at room temperature before the luminescent signal of each well was measured in a spectral scanning multimode plate reader (Varioskan Flash Multimode Reader with SkanIt™ Software, Thermo Scientific). For each condition four independent replicates were measured. All reagents were mixed freshly before the experiment. The dependence of the measured fluorescence signal upon the amount of GSH in the probe was verified with a GSH standard curve that was generated using 0 to 16 µM GSH diluted in water. The calculation of the GSH/GSSG ratio for each cell treatment was calculated from the RLU (relative light units) of the luminescence signals of the total and oxidized glutathione measurements as follows:

$$\frac{GSH}{GSSG} = \frac{RLU_{total} - RLU_{GSSG}}{\left(RLU_{GSSG} / 2\right)} \tag{2.6}$$

3.3.6. Total cellular GSH content

The determination of total intracellular GSH in HaCaT cells was carried out with an assay developed by the group of Dr. Lillig (Institute of Medical Biochemistry and Molecular Biology, University Medicine Greifswald) modified from Akerboom and Sies [225]. HaCaT cells were cultivated for 24 hours in RPMI-1640 and another 24 hours in the presence of plant substances, diluted in water and DMSO. One hour prior to cell harvest the cell medium was replaced by 100 µM *t*BHP in HBSS. The cells were washed twice with PBS/ EDTA, harvested by incubation with 0.05% trypsin/0.02% EDTA for 5 minutes and centrifuged (3 min, 230 ᵡ *g*, RT). The cell pellet was resuspended in HBSS and centrifuged again (5 min, 250 ᵡ *g*, RT). The cells were lysed by the addition of 50 µL lysis buffer (250 mM Tris, 0.1% Triton X-100, pH=7.4), 1 µL protease inhibitor and 2% CHAPS (3-[(3-Cholamidopropyl)dimethylammonio]-1-propanesulfonate). After 20 minutes the cells were frozen to –80 °C for 5 minutes before being centrifuged again (25 min, 300 ᵡ *g*, RT). The supernatant without the upper lipid layer was transferred into fresh Eppendorf tubes. The protein content of the cell lysates was determined with a Bradford assay, using the Bradford Coomassie brilliant blue G-250 protein-binding dye [226]. Briefly, a concentration series of the cell lysates was prepared in TE buffer (Tris/EDTA buffer, pH=8) and 5 µL of the samples were pipetted in duplicate in four different dilutions into a 96 well plate along with a protein standard series of bovine serum albumin (BSA, Albumin fraction V, Carl Roth). To each well 195 µL Bradford reagent (Quick Start™ Bradford 1x Dye Reagent #5000205, Bio-Rad) were added and the plate was incubated for 5 minutes in the dark. The absorbance of each well was measured at 595 nm in a microplate photometer (Thermo Scientic Multiskan EX, Thermo Fisher). From the BSA absorbance values a protein concentration standard curve was obtained from which the protein concentration of the cell lysates was determined. The samples were diluted with TE buffer to a protein concentration of 1 µg/µL. Protein precipitation was achieved by the addition of 4% v/v sulfosalicylic acid overnight on ice. The samples were centrifuged (300 ᵡ *g*, 30 min) and the supernatant was transferred into fresh Eppendorf tubes and neutralized with 1 M NaOH/HCl to a pH of 7. For the determination of the GSH content concentration series of the probes and a GSH standard were made and pipetted in duplicate into a 96-well plate. To each well 1.5 mM Ellman's reagent (5,5'-dithiobis-(2-nitrobenzoic acid, DTNB) in TE-buffer were added. DTNB reacts with thiols in a 1:1 stoichiometry to form the yellow colored 2-nitro-5-thiobenzoate dianion (TNB^{2-}). The amount of TNB^{2-} was measured via its absorbance at 412 nm (Infinite® 200 PRO, i-control™ software, Tecan Group Ltd.). Afterwards 1.5 mM NADPH and yeast glutathione reductase (y-Gr, 1:50, Sigma-Aldrich) were added to each well. The absorbance increase at 412 nm was monitored over a period of 30 minutes. From the endpoint value of the second measurement (2 values before saturation) the values of the first measurement were subtracted for each well. The measured absorbance values of the GSH standard series were plotted versus the GSH concentration. The

resulting standard curve was fitted to a non-linear 4 parameter function (qt-grace software, non-linear fit):

$$f(x) = y = \frac{(a-d)}{\left(1+\left(\frac{x}{c}\right)^{b}\right)} \tag{2.7}$$

With the resulting parameters *a*, *b*, *c* and *d* from the fit the concentrations of GSH in the individual samples were calculated from their measured absorbance values *y*:

$$[GSH] = \left(\left(\left(\frac{a-d}{y-d}\right)-1\right)^{\frac{1}{b}}\right) \times c \tag{2.8}$$

For each sample the intracellular total GSH content [nmol/mg protein] was calculated.

3.3.7. Assessment of superoxide production (L-012)

Superoxide production from Nox5-HEK293 was verified with the chemiluminescence probe L-012 (8-amino-5-chloro-7-phenyl-pyrido[3,4-d]pyridazine-1,4(2H,3H)dione) in a real time measurement [8]. The basal signal of L-012 in solution was monitored in darkness in a Berthold 6-channel tube luminometer (LB9505, Berthold, Wildbad, Germany) until a stable signal was obtained. Cells were washed with 1 X PBS, trypsinated, resuspended in HT buffer and injected into the L-012 solution (final L-012 concentration 200 µM). After reaching a stable light emission signal 100 nM phorbol 12-myristate 13-acetate (PMA) were injected to stimulate Nox-5 superoxide production. Superoxide dismutase (SOD) was given to the cell suspension to quench the fluorescence signal. A blank measurement was performed without HEK293 cells. Data was recorded with LumiCounter 1.0 software.

3.3.8. Assessment of hydrogen peroxide production (AmplexRed)

The production of hydrogen peroxide from Nox4-HEK293 after TC stimulation was verified with Amplex Red reagent (Thermofisher; A12222), which can be converted by horseradish peroxidase (HRP) in the presence of H_2O_2 to the fluorescent molecule resorufin. Induction of Nox4 with 1 µg/mL tetracycline was performed for 24 h in HEPES Tyrode buffer (HT; containing in g L^{-1}: 2.33 HEPES; 0.2 CaCl; 0.1 MgCl; 0.2 KCl; 8 NaCl; 0.05 NaH_2PO_4; 1 D-glucose). After 24 hours incubation the cells were washed with PBS and incubated 30 minutes in HT buffer containing 50 µM Amplex Red and 2 U/mL HRP. 200 µL of the cell supernatant were transferred into a 96 well plate (Greiner 96 Flat Bottom Transparent Polystyrene) and fluorescence signal was measured at 545 nm

excitation/590 nm emission in a TriStar2 Multimode Reader (LB942, Berthold, Wildbad, Germany). Data was recorded with Tecan i-control™ software.

3.3.9. Assessment of mitochondrial ROS (mitoHyPer)

The relative mitochondrial ROS concentration was measured in C6 glioma TAZ Hyper and WT Hyper cells (see chapter 3.3.1.). The cells were incubated for 24 hours in 96-well microplates (black, clear-bottomed, Greiner Bio One) in DMEM + 3% FCS + 1% P/S and an additional 24 hours with the addition of cell substances diluted in H_2O and DMSO as described before. Afterwards the cells were washed twice with 1 x PBS. To each well PBS containing 5 mM glucose and 0 to 50 µM H_2O_2 were added. The fluorescence signal was measured directly after H_2O_2 addition at 390 and 458 nm (Infinite® 200 PRO, Tecan Trading AG, excitation 390/485 nm, emission 510/535 nm, 4 × 4 measurements/well). The spectra were recorded with i-control™ software (Tecan Group Ltd.). For each well the HyPer signal (fluorescence at 485 nm) was normalized to the cell number (fluorescence at 390 nm).

3.3.10. Electrochemical assay (in cell culture)

The possibility to assess the extracellular ROS concentration with the SAM modified Au electrodes was explored with HaCaT, Nox4-HEK293 and Nox5-HEK293 cells. HaCaT cells were plated in 60 x 15 mm dishes (TPP®) for 24, 48 or 72 hours before treatment with ethanol, 100 µM *t*BHP, 50 µM H_2O_2 or H_2O. The treatment was performed in RPMI-1640, HBSS or PBS. After one hour the SAM coated electrodes were exposed to the cell medium/buffer for a defined time. Additionally, the cells were lysed after treatment by the addition of a cell lysis buffer and the electrodes were exposed to the cell lysate. The electrodes were washed with ethanol and water and transferred into an 1 mM $[Ru(NH_3)_6]Cl_3$ containing electrolyte to measure the DPV signal of the $Ru(NH_3)_6^{3+}$ ion reduction signal at the electrodes. The same was done for Nox4-HEK293 in HT buffer 24 hours after addition of 1 µg/mL TC and for Nox5-HEK293 cells 20 minutes after addition of 100 nM PMA to the cells.

3.4. Statistical analysis

Statistical analysis of the data were performed with OriginPro 2016 unless stated otherwise. Student's t-test with $p<0.05$ of mean values ±SEM was used to compare $n=2$ independent samples. For multiple comparison of $n>2$ independent samples one-way ANOVA was performed. Data were tested for normal distribution and variance homogeneity prior to data analysis. For graphical purposes data are presented as mean ±SD unless stated otherwise. Individual details of statistical analysis are described in the corresponding method/results section.

4. Results and discussion

4.1. Optimization and characterization of the electrochemical assay

The first part of the work consisted of the optimization and further characterization of the electrochemical ROS assay developed by Scholz et al [2]. The work focused on the sensor electrode: a polycrystalline gold electrode covered with an alkanethiol SAM. Interaction of ROS with the monolayer introduces defect sites within the layer. The degree of destruction is followed by the increase of current measured at the electrode due to the reduction of a soluble redox couple at the exposed gold sites in DPV measurements. The aim was to adapt the assay to more physiological requirements (low ROS concentrations, buffered cell culture media), and to obtain a better understanding of the interaction of ROS with the sensor electrode.

4.1.1. Optimization of the electrode preparation

4.1.1.1. Gold electrode surface

Besides the thiol molecules themselves, the underlying gold surface has an impact on the properties of the formed SAM. The crystallographic orientation of the surface, impurities [206], structural defect sites as well as the average microscopic roughness of the surface influence the quality of the SAM [227]. Polycrystalline gold is a heterogeneous material that exhibits various crystallographic orientations and can vary significantly in its roughness depending on the previous treatment of the material. To fabricate reproducible SAMs on polycrystalline gold the pretreatment of the gold electrodes has to be performed in a way that a surface with comparable characteristics is produced every time. The optimized pretreatment protocol developed consisted of the following steps [228]: adsorbed molecules were first removed from the surface by reductive desorption (RD), followed by polishing with Al_2O_3, restructuring of the gold surface by CV and removal of gold oxides by "ECS" [206]. After this initial treatment cycle, the surface was covered with a SAM, which was removed again from the surface by oxygen radicals generated from the photolysis of H_2O_2 in aqueous solution.

The removal of the SAM by ROS influences not only the attached thiol molecules but also the underlying gold surface. The interaction of ROS with gold surfaces has been investigated before. ROS treatment of polycrystalline gold lead to the preferential removal of grain boundaries and asperities present on the surface, which has a smoothening effect [229], [230]. We observed the same effect for SAM covered gold [228], though, the effect we observed was less pronounced. The lower degree of gold surface smoothening by ROS can be explained by two factors. First, we exposed our electrodes to lower ROS concentrations in comparison to the previous study. Second, the gold surface is partly protected by the attached thiol molecules still attached to the surface. However, radical treatment in combination with the described pretreatment of the gold

electrodes significantly decreased the average roughness of the gold surface as demonstrated with AFM images before SAM coverage. The roughness was lower than for surfaces that were polished and for surfaces from which the SAM was removed by reductive desorption (RD) instead of radical treatment (figure 4). After the initial treatment cycle of the gold surface and the first removal of the SAM by radicals, the surface properties of the polycrystalline electrodes remained stable. The lower surface roughness remained after repetitive SAM coverage/radical removal cycles, thus providing ideal conditions for reproducible SAM formation at the same electrodes [228].

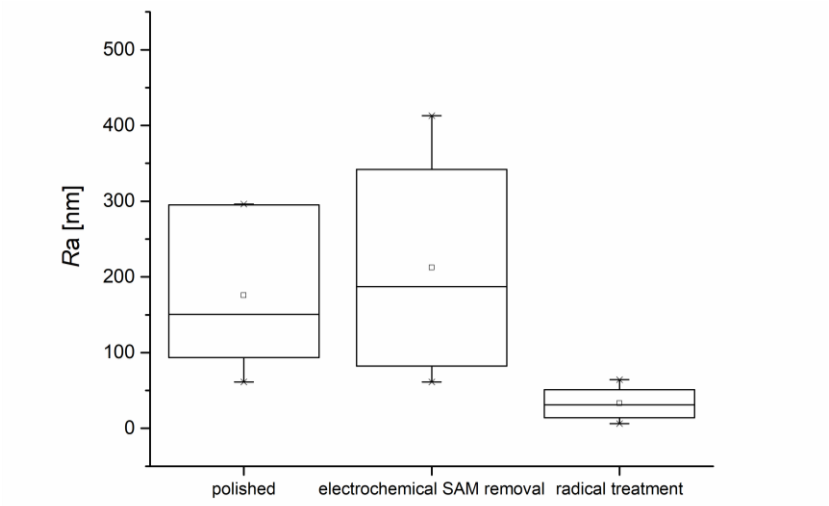

Figure 4: Average roughness (*R*a) of polycrystalline gold surfaces measured from AFM image after mechanical polishing (polished), electrochemical SAM removal and removal via photolytically generated oxygen radicals (radical treatment). Picture was taken from [228].

The obtained SAMs under the chosen experimental conditions are not flawless. STM images revealed some pinholes within the SAM structure of about 0.4 nm depth [228]. We assume that those represent monoatomic steps within the SAM. Obtaining defect-free monolayers on polycrystalline gold is impossible due to the roughness of the surface and the atomic steps which are characteristic for polycrystalline gold. However, for the purpose of the work, the reproducibility of the SAM's quality and its behavior towards ROS is the essential parameter.

4.1.1.2. Crystalline gold structure

Our results demonstrate that the treatment cycles produce a smoothened surface that maintains its properties over numerous treatment cycles. As stated, we used polycrystalline gold surfaces that are characterized by heterogeneous activity and binding energies. Therefore, we investigated if the polycrystalline character of the surface could be retained over several SAM coverage/removal cycles. Furthermore, we tested if thiol molecules attached to differently orientated gold atoms were affected equally by the ROS treatment.

In Pb-UPD measurements we obtained voltammograms that exhibited the characteristic stripping peaks from the Au(111), Au(110) and Au(100) face, as expected for a polycrystalline surface

(figure 5 A) [159]. At electrodes that underwent SAM coverage and removal cycles the characteristic features of a polycrystalline gold surface remained (figure 5 A). We therefore assume that the polycrystallinity of the gold surface is conserved during the treatment cycles.

Further Pb-UPD measurements focused on the specific effects of ROS exposure on the crystalline structure of the gold. The recorded voltammograms in figure 5 B demonstrate the characteristic peaks for different gold sites (Au(110), Au(111) and Au(100) face). The stripping peaks are suppressed at SAM covered electrodes and gradually regained at all gold sites in correlation to ROS exposure time. This suggests that either thiols bound to all sites were removed equally by ROS or that after ROS exposure a reformation process of the mobile thiol molecules at the surface occurred. In both cases, the SAM coverage of the gold remained homogenous over the surface. There are no indicators suggesting the irreversible blocking of certain sites on the gold surface. We take this observation as another argument in favor of reusing the electrodes for multiple measurements.

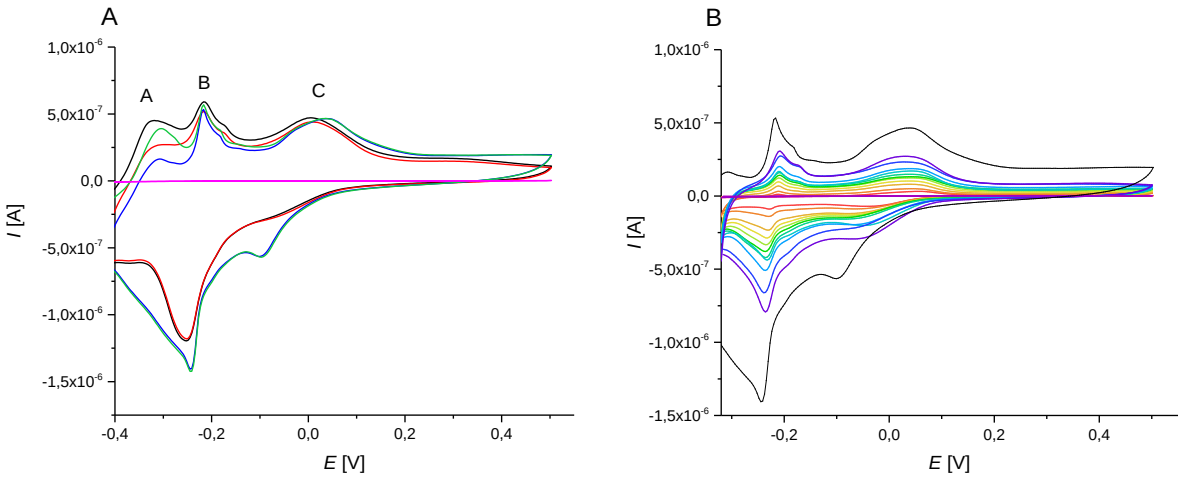

Figure 5: Pb-UPD signal at polycrystalline gold electrodes A) bevor (blue and green lines) and after SAM coverage and radical removal (black and red lines). B) Pb-UPD signal before SAM coverage (black line), after SAM coverage (red line) and after exposure to oxygen radicals for increasing time periods (30 seconds (orange) to 10 minutes (purple). Graphic taken from [7].

Figure 5 B indicates that the ROS treatment failed to produce the same current maxima as before SAM coverage at the electrodes. Apparently, some thiol molecules remain fixed to the gold thus blocking the surface and reducing the electrochemically active electrode's surface. The observation is in line with DPV measurements, where the final $Ru(NH_3)_6^{3+}$ ion reduction current after ROS treatment always remained slightly below the current value measured at the cleaned electrode (see chapter 4.1.1.2.1.).

4.1.1.3. Alkylthiols for SAM preparation

4.1.1.3.1. Behavior in DPV and CV measurements

Different alkanethiols were tested for SAM preparation in hindsight of their ease of preparation and their sensitivity towards ROS. Many publications demonstrate that the carbon chain length of the thiol influences the SAM formation process. Longer chains profit from a more pronounced hydrophobic effect as well as from stronger van-der-Waals forces that promote the formation of ordered SAM structures [231]. Though, the formation process required more time than for shorter thiols, the obtained SAM is more ordered and stable [232]. Our results obtained in DPV measurements agree with this observation. Using hexadecanethiol ($C_{16}SH$) SAM the gold surface remained blocked after exposure to low ROS concentrations (10^{-4} M H_2O_2; UV-B), while the same treatment of 1-decanethiol ($C_{10}SH$) covered electrodes altered the SAM structure in a way that allowed the penetration of $Ru(NH_3)_6^{3+}$ ions to be reduced at the gold surface (figure 6). CV measurements in the same electrolyte support the DPV data by showing the same behavior of equally treated electrodes. SAM coverage totally blocked the redox signal of $Ru(NH_3)_6^{3+/2+}$ ions. The signal could be regained at $C_{10}SH$ SAM covered electrodes by exposure to photolytically generated ROS (figure 7 A) but not at $C_{16}SH$ covered electrodes (figure 7 B). We therefore assume, that the longer alkyl chains were not sufficiently influences by the ROS to allow the penetration of $Ru(NH_3)_6^{3+}$ ions or electrons to the Au surface. Therefore, no reduction current was measurable after ROS treatment at the electrodes in CV and DPV. This phenomenon can be explained by:

(i) a more ordered SAM that limit the penetration of ROS and therefore the number of attack sites for ROS,

(ii) the longer alkyl chains that increase the distance from the electrolyte to the gold surface, reducing the number of electron tunneling events over this barrier,

(iii) the longer alkyl chains that might still function as a barrier in case of carbon chain breaks induced by ROS.

The witnessed behavior of $C_{10}SH$ and $C_{16}SH$ SAMs towards ROS is in good agreement with the general assumption that longer alkyl chains (number C-atoms>10) increase the organization and stability of thiol-SAMs on Au surfaces [231]. The $C_{16}SH$ SAM proves more resistant towards ROS treatment. As mentioned before, electron-channeling processes are also more likely to occur at shorter alkyl chains. However, this phenomenon is only relevant at SAM containing low numbers of defect sites, because tunneling current should be small relative to that arising from direct electron transfer at defect sites [233].

The initial current maximum was not regained at $C_{10}SH$ covered electrodes after ROS treatment up to 50 minutes. Previous experiments with hexacyanoferrate(II) as redox probe and C_6SH or

$C_{16}SH$ SAMs demonstrated that a complete removal of the SAM with hydroxyl radicals generated by the Fenton reaction could not be achieved [2]. Since the ROS concentrations in our experiments were even lower, we assumed that complete SAM removal is unrealistic in our experimental setting. With octathiol (C_8SH) covered electrodes we obtained high standard deviations for our measurements (data not shown).

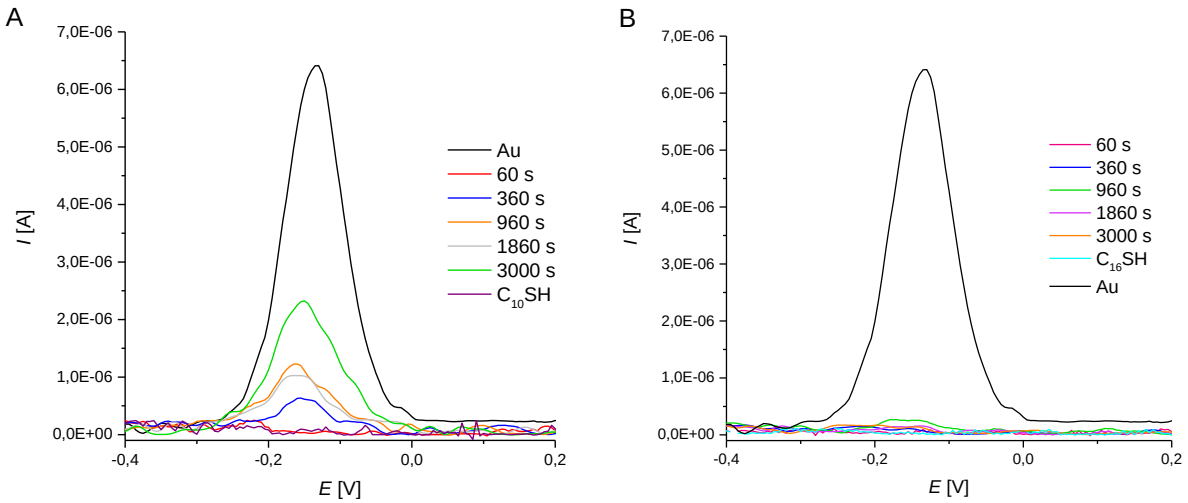

Figure 6: DPV currents measured for the reduction of $Ru(NH_3)_6^{3+}$. The graphs show the current measured at cleaned Au surfaces (black lines) and at $C_{10}SH$ (A, purple line) and $C_{16}SH$ SAMs (B, turquoise line). The exposure of the SAM covered electrodes to photolytically generated ROS let to a regain of the signal at $C_{10}SH$ SAM covered electrodes (A). At $C_{16}SH$ SAM covered electrodes the signal remained suppressed (B).

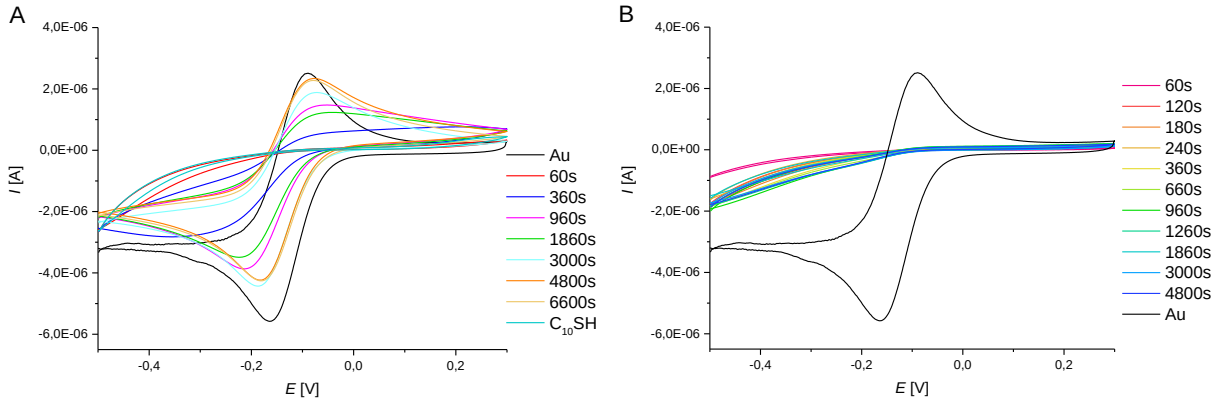

Figure 7: CVs recorded at (A) $C_{10}SH$ coated Au electrode before and after 60 to 6,600 seconds exposure to radicals and (B) CVs recorded at the $C_{16}SH$ coated Au electrode before and after 60 to 4800 seconds exposure to radicals. Measurements were performed in 1 mM $Ru(NH_3)_6^{3+}Cl_3$ solution from −0.5 to 0.3 V vs. Ag/AgCl at 0.05 V s^{-1} on a 600E Potentiostat/Galvanostat (CH Instruments) and data was recorded with CHI 660 software.

4.1.1.3.2. Influence on surface coverage

To obtain an idea on the extent of SAM coverage that remained after ROS treatment on the gold surfaces, we performed ACV measurements in acetate buffer. From the in phase and out-of-phase components of the AC signal differential capacity curves were calculated for the individual SAM covered electrodes. The differential capacity decreases near the point of zero charge (pzc) as the coverage of the gold surface increases [234]. Therefore, the method allows to calculate the coverage of the gold surface with the thiol molecules [235]. In comparison to the theoretically calculated differential capacity value for a $C_{10}SH$ monolayer, the experimental value was slightly higher (1.32 vs. 2 $\mu F/cm^2$). It confirmed that the SAM formed on the polycrystalline Au surface is not defect-free. However, initial treatment of the SAM with radicals slightly decreased the differential capacity values to around 1 $\mu F\ cm^{-2}$ (table 4; figure 8 A+B). This might be an indicator for some rearrangements of the liquid phase thiol molecules on the surface leading to an apparent increased surface blockage. A major destruction of the SAM with a lower energetic UV light source (UV-A, λ=365 nm) could not be achieved within a treatment period of 5 hours. However, a lower wavelength (λ=256 nm) and the associated increase of the amounts of reactive species within the treatment solution led to a decrease of initial surface coverage by 15% after 1 hour of treatment (table 4; figure 9). Short-term treatment (30 to 120 seconds) resulted in the same behavior as witnessed for lower energetic UV light with an initial decrease of the calculated differential capacity currents that correspond to an increase surface blockage. $C_{16}SH$ SAM covered gold did not exhibit the same behavior. The longer alkyl chains presented a more stable monolayer for the ROS molecules to destroy. ROS treatment up to 80 minutes altered the initial surface coverage by less than 1% (table 4; figure 8 C +D). These results indicate that the longer alkyl-chains form a more stable SAM that is more resistant towards ROS attack (as demonstrated before by CV and DPV measurements). Furthermore, the longer chains present a higher energy barrier limiting the possibility of ion tunneling events to occur over the SAM [236].

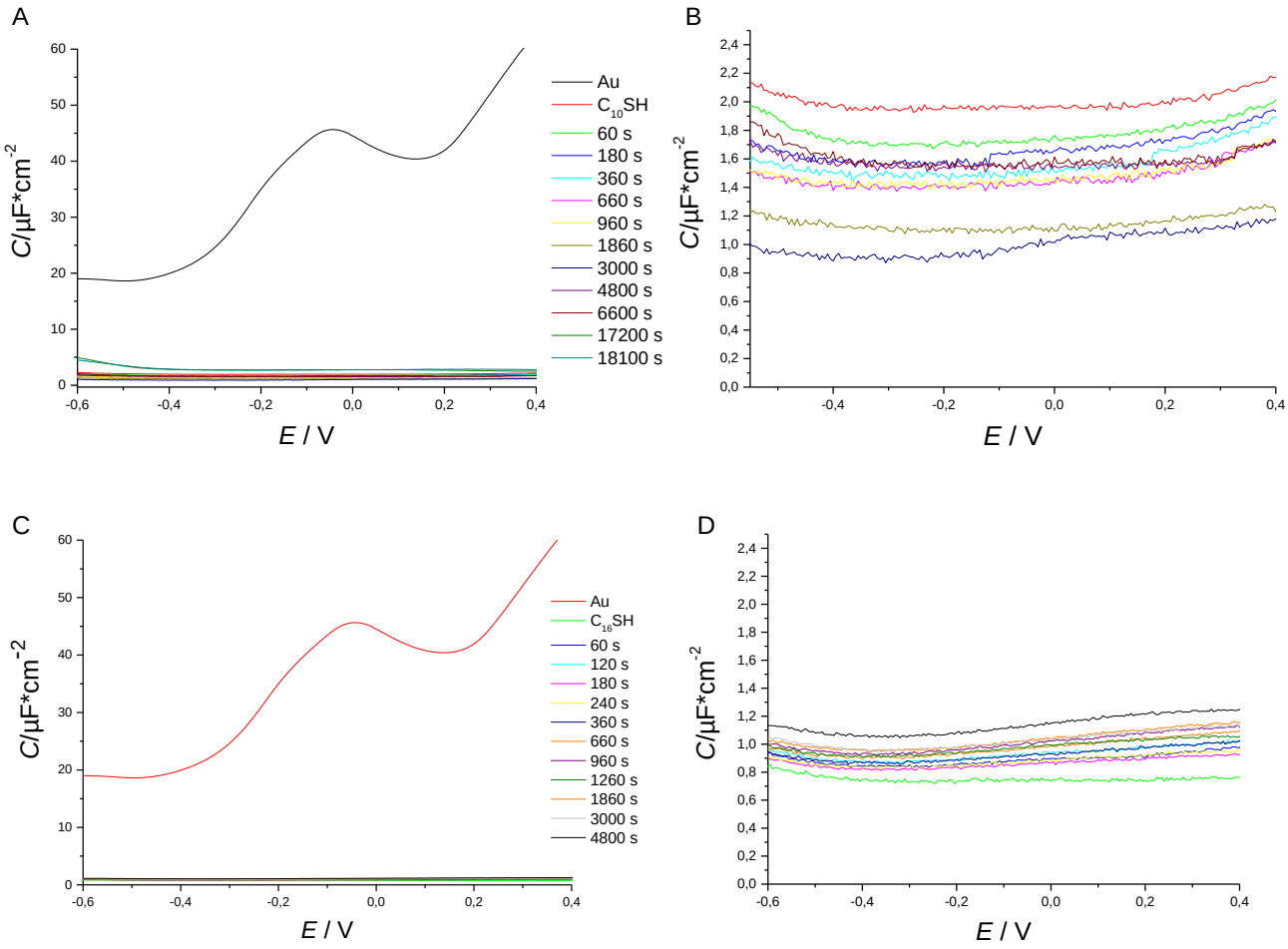

Figure 8: Differential capacity curves calculated from phase-selective ACV measurements in 0.1 M acetate buffer (pH=4.7). AC voltammograms were recorded from 0.45 to −0.55 V vs. Ag/AgCl with a sinusoidal perturbation voltage at a fixed frequency (*f*) of 20 Hz and an amplitude (*A*) of 0.01 V root mean square (V_{RMS}) at 5 mV s^{-1}. Graphs represent calculated curves for $C_{10}SH$ covered electrodes (A, B) and $C_{16}SH$ covered electrodes (C, D) after different exposure times towards photolytically generated radicals by UV light (λ=365 nm).

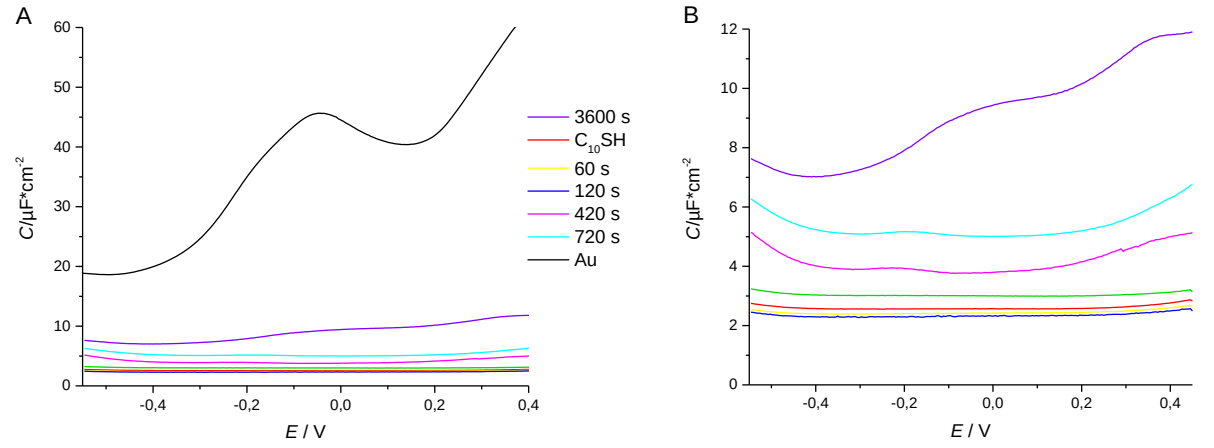

Figure 9: Differential capacity curves calculated from phase-selective ACV measurements in 0.1 M acetate buffer (pH=4.7; 0.45 to −0.55 V vs. Ag/AgCl; frequency=20 Hz; amplitude=0.01 V root mean square (V_{RMS}); 5 mV s^{-1}). Graphs represent calculated curves for $C_{10}SH$ covered electrodes after different exposure times towards photolytically generated radicals (256 nm UV light source).

Table 4: Changes of $C_{10}SH$ and $C_{16}SH$ SAM coverage on Au electrodes due to radical exposure. The surface coverage (Θ) is calculated from ACV measurements' data as described before [235]. Experiments were performed with two different UV light sources (λ=366 nm or 256 nm).

UV light λ=254 nm		UV light λ=365 nm		
$C_{10}SH$		$C_{10}SH$		$C_{16}SH$
ROS treatment [s]	coverage [%]	ROS treatment [s]	coverage [%]	coverage [%]
0	97.1	**0**	98.5	100.1
30	97.2	**30**	99	99.9
60	97.5	**180**	99.2	99.9
120	97.6	**360**	99.5	99.8
180	97.8	**480**	99.7	99.7
420	94.4	**960**	99.6	99.6
480	88.6	**1,860**	100.5	99.6
720	91.7	**3,000**	100.7	99.6
780	84.8	**4,800**	99.5	99.3
3,600	82.1	**18,100**	96.7	

4.1.1.3.3. Elementary composition analysis

To test if the surface coverage, demonstrated in ACV measurements, was due to thiol molecules that were still attached to the gold surface, we performed XPS measurements. In XPS the sample is radiated with photons of a specific energy to excite the electronic states of atoms below the surface of the sample. Electrons ejected from the surface are filtered for their energy before a detector records the intensity of a defined energy. The resulting energy spectra exhibit resonance peaks characteristic of the electronic structure for atoms at the sample's surface up to a depth of 10 nm. The spectra contain information on the binding energy of the electronic states of atoms as well as the chemical environment of the atoms at the surface (energy shifts of the peak energies) [237].

XPS analysis were performed on SAM covered gold samples on which the SAMs were treated in a certain area either by reductive desorption (RD) or by photolytically generated ROS. The other part of the sample remained untreated. Afterwards we measured the XPS signals for gold, sulfur, carbon and oxygen (Au 4f, S 2p and C 1s and O 1s). The results demonstrate that also after longer treatment with oxygen radicals the signals for all four elements (Au, S, O, C) could be detected in the spectra (table 5). The S 2p spectra exhibits a double peak at 162±1 eV that is characteristic for alkanethiol SAM/ Au binding energies [238]. The C 1s spectra demonstrate intense signals for C-C/C-H/C-S-bonds at around 285±1 eV as well as slightly more energetic binding energies at

287±1 eV of partly oxidized C-atoms (figure 10), corresponding to binding energies reported in the literature before [239]. The data support the presence of thiol molecules on the gold surface also after the treatment with radicals or removal of the SAM by RD. This indicates that the removal process via ROS is not complete as demonstrated before by CV, DPV and ACV measurements. The treatment with oxygen radicals increased the relative peak intensity (I) for oxygen on the treated surfaces in comparison to the samples from which the thiol SAM was removed electrochemically by RD (I≒9.89 vs 48.03; table 5). While the removal process via RD is considered to be a one electron reaction leaving behind neutral gold atoms ($AuSR+1e^{-}+Au(0)+RS^{-}$, [240]), the products that might arise from radical treatment are numerous. The formation of several oxides is a possible explanation for the higher oxygen content on the radical treated samples. The hypothesis is further supported by the binding energies of partly oxidized C-atoms represented in the measured spectra.

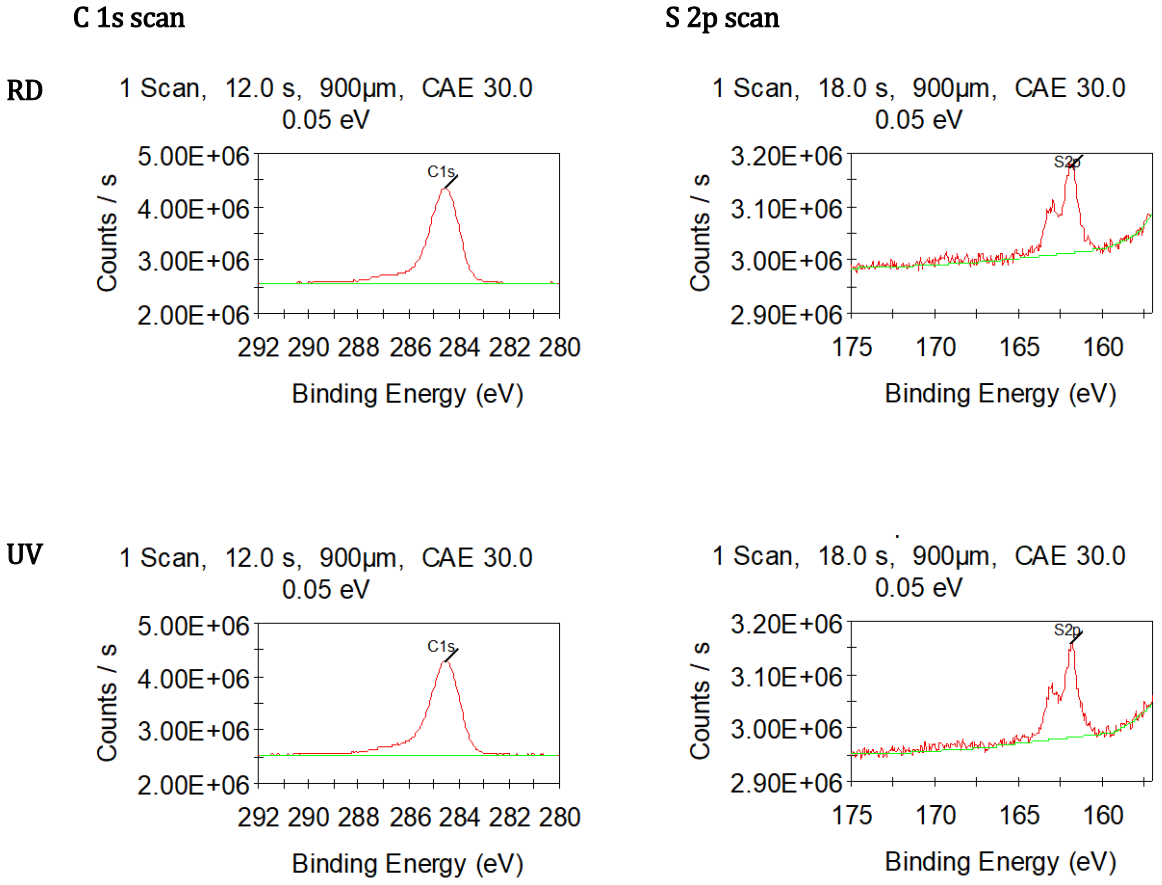

Figure 10: XPS spectra for the C 1s and S 2p signals of $C_{10}SH$ SAM covered gold substrates treated by RD or with UV generated ROS (red lines). The spectra are corrected for the background signal (green line).

Table 5: Signal intensities measured for the Au 4f, S 2p, C 1s and O 1s signals with XPS. The data represent the relative intensities calculated from XPS spectra corrected for the background signal, normalized according to Scofield, the transmission function (device manual ESCALAB 250 Xi, Thermo Fisher) and attenuation length (AL). The relative intensities are shown for $C_{10}SH$ SAM covered Au samples after treatment with RD or photolytically generated ROS (UV) on one site of the sample and the corresponding untreated site (no RD/no UV). The resulting ratios from the elements signals are presented on the right site of the table.

	no RD	RD	no UV	UV		no RD	RD	no UV	UV
Au 4f	107.75	93.75	94.68	94.98	**C/S**	14.18	17.74	15.47	15.77
S 2p	7.01	6.53	4.75	4.65	**C/Au**	0.92	1.24	0.78	0.77
C 1s	99.41	115.76	73.71	73.29	**S/Au**	0.07	0.07	0.05	0.05
O 1s	3.97	9.89	46.95	48.03	**O/S**	0.57	1.51	9.86	10.33

Comparison of treated and untreated areas on the gold samples revealed little differences. This holds also true for the ratios of C/S, C/Au, S/Au calculated from the relative signal intensities (table 5). Only the Au 4f in the RD treated sample area is lower than in the untreated area (I'=93.75 vs. 107.75) and the O 1s signal is higher in the RD treated area ((I'=3.97 vs. 9.89). Two processes might be responsible for the lack of difference between the treated and the untreated areas of the samples: (ii) Lateral movement of thiol molecules might have occurred after the treatment resulting yet again in a homogenous distribution of thiol molecules on the surface. (ii) Absorption of thiol molecules from the air might have occurred on the samples prior to XPS measurements. This phenomenon is due to the high free energy of metal surfaces that promote the adsorption of atmospheric contaminants [241]. The probability increases in laboratories where thiols are employed frequently. The two processes would lead to a homogeneous distribution of the attached thiol molecules on the treated and untreated surface areas. This could also explain why RD treatment, which has been found quite efficient for the removal of thiol molecules from gold [242], still leaves behind so many thiol molecules on the investigated gold surface in this setting. Furthermore, the samples contained some iodide and silver contamination that could be detected in the XPS spectra. The source of these contaminants is not known.

4.1.1.3.4. Molecular orientation/alkyl-chain tilt

Further investigations of the impact of radical treatment on the attached thiol molecules on the gold electrodes were undertaken with infrared reflection-absorption spectroscopy (PM IRRAS) measurements. The measurements were performed in air on SAM covered Au plates. PM IRRAS is a method that allows investigating the tilt angle of the attached thiol molecules in relation to the gold surface.

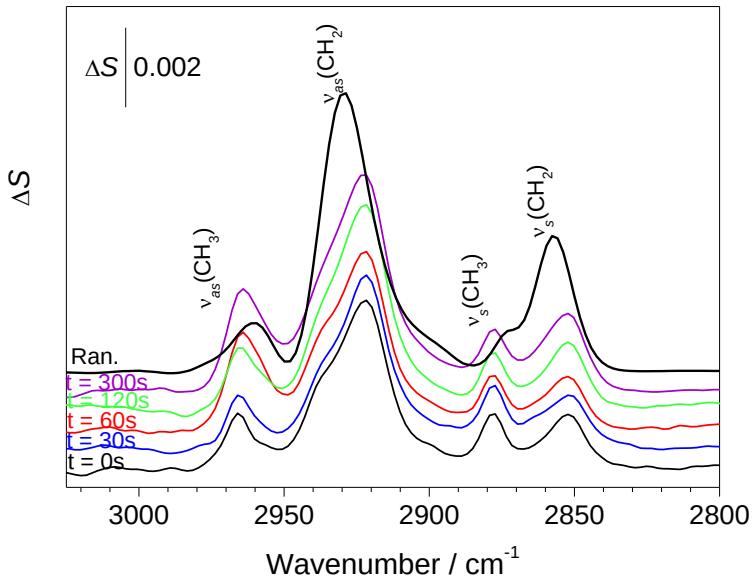

Figure 11: PM IRRA spectra in the CH stretching modes region of $C_{10}SH$ monolayer on Au after different times of exposure (as marked in the figure) to photolytically generated ROS.

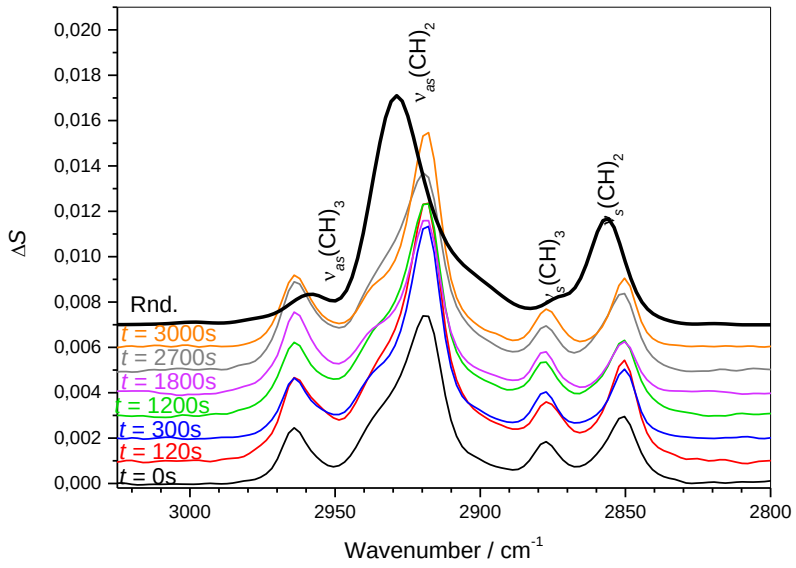

Figure 12: PM IRRA spectra in the CH stretching modes region of $C_{16}SH$ monolayer on Au after different times of exposure (as marked in the figure) to photolytically generated ROS.

Figures 11 and 12 show the PM IRRA spectra in the CH stretching modes region of the $C_{10}SH$ and $C_{16}SH$ SAM on Au after different times of ROS treatment (0 to 3,000 seconds). All spectra exhibit four well resolved IR absorption modes arising from the methyl and methylene asymmetric and symmetric stretching modes. The asymmetric $\nu_{as}(CH_3)$ stretching mode of the terminal methylene group in both studied monolayers is centered at 2,963.8±1.2 cm^{-1}. The corresponding symmetric

$\nu_s(CH_3)$ mode is centered at 2,978.0±0.5 cm^{-1}. The positions of the methylene stretching modes depend on the length of the alkane chain in the SAM. In the $C_{10}SH$ monolayer the $\nu_{as}(CH_2)$ mode is asymmetric. From the high frequency mode around 2,936 cm^{-1}, it is overlapped with the Fermi resonance (FR) between the symmetric methyl stretching mode and the overtone of the symmetric methyl bending mode [243]. A weak shoulder at the low frequency side of the $\nu_{as}(CH_2)$ mode arises from FR between the symmetric methylene stretching mode and the overtone of the methylene bending mode. The $\nu_{as}(CH_2)$ mode is centered at 2,921.5±1.5 cm^{-1} and its full width at half maximum (fwhm) is equal to 17.5±1.2 cm^{-1}. The $\nu_s(CH_2)$ mode is centered at 2,851.5±1.2 cm^{-1} and its fwhm is equal to 12.3±0.8 cm^{-1}. In the $C_{16}SH$ monolayer the $\nu_{as}(CH_2)$ mode is centered at 2,918.1±0.5 cm^{-1} and its fwhm is equal to 11.2±1.0 cm^{-1}. The $\nu_s(CH_2)$ mode is centered at 2,850.4±0.5 cm^{-1} and its fwhm is equal to 11.0±0.8 cm^{-1}. The thick lines in figures 8 and 9 correspond to the calculated PM IRRA spectra of randomly distributed $C_{10}SH$ or $C_{16}SH$ molecules, respectively, within a monolayer thick film. These spectra were calculated from isotropic optical constants of corresponding alkanethiol molecules. In these spectra the methylene stretching modes are blue-shifted comparing to the PM IRRA spectra of SAMs. The $\nu_{as}(CH_2)$ mode is centered at 2,928.4±0.4 cm^{-1} and its full width at half maximum (fwhm) is equal to 21.0±1.0 cm^{-1}. The $\nu_s(CH_2)$ mode is centered at 2,856.8±0.3 cm^{-1} and its fwhm is equal to 15.6±0.3 cm. These frequencies of the methylene stretching modes are characteristic for the hydrocarbon chains existing in a liquid state [244]. Solidification of a hydrocarbon chain restricts its mobility and hinders its rotational freedom leading to a stretched all-trans conformation [245]. In IRS these changes lead to a red-shift of the methylene stretching modes [243]. The positions of the methylene stretching modes in the $C_{16}SH$ monolayer correspond to a crystalline hydrocarbon chain in the all-trans conformation. The shorter $C_{10}SH$ molecules in the monolayer on the Au surface are present in a so-called liquid-ordered phase ([246], [247]). It means that the hydrocarbon chains of decanethiol adapt a stretched conformation. However, next to the predominant all-trans conformation a few gauche defects are still present.

The figures 11 and 12 show that both monolayers react differently towards the ROS treatment. In case of the $C_{10}SH$ monolayer the integral intensities of the methylene stretching modes increases monotonically with time of the ROS treatment. The ROS treatment of the $C_{16}SH$ monolayer leads initially to an increase in the intensity of the methylene stretching modes (time of radiation $<$ 1,200 s). Afterwards the intensities of the methylene stretching modes decrease until radiation times of 2,700–3,000 seconds they increase again. In addition, capacitance measurements indicate that during the investigated treatment time with UV-A light (365 nm) the surface coverage of the Au electrode does not change by more than 1%. These changes indicate that the hydrocarbon chains change their orientation. Since in both studied monolayers the hydrocarbon chains adapt the stretched conformation, the tilt of the hydrocarbon chains in the freshly prepared as well as

irradiated SAMs of alkanethiols could be calculated. In an isotropic film, such as an alkanethiol monolayer, transition dipole vectors of each IR absorption mode have a strictly defined orientation. According to the surface selection rule of IRRAS [248], the integral intensity of an IR absorption mode (*A*) can be described as follows:

$$\int A d\nu \infty \Gamma \left| \vec{\mu} \times \vec{E} \right|^2 = \Gamma \times \left| \vec{\mu} \right|^2 \times \left| \vec{E} \right|^2 \times \cos^2 \phi \tag{3.1}$$

A is proportional to the surface concentration of these molecules on the electrode surface (Γ) and the square of the absolute values of the dot product of the transition dipole vector ($\vec{\mu}$) of a given absorption mode and the electric field vector of the incident light ($\vec{E}$). The integral intensity of a given absorption band depends on the angle ϕ between the $\vec{\mu}$ and $\vec{E}$ vectors. On the Au electrode surface, the $\vec{E}$ vector of the *p*-polarized light is directed normal to the interface. Therefore, changes of the integral intensity of an absorption band reflect the tilt of the $\vec{\mu}$ vector of a given vibrational mode with respect to the surface normal (direction of $\vec{E}$) ([249], [250]). Equation 3.2 was used to calculate the angles ϕ between the direction of transition dipole vectors of the methylene stretching modes and the surface normal:

$$\cos^2 \phi = \frac{\int A_{\text{exp}} d\nu}{3 \int A_{\text{random}} d\nu} \tag{3.2}$$

With $A_{\text{exp}} d\nu$ and $A_{\text{random}} d\nu$ being the intensities of the corresponding IR absorption modes of either $C_{10}SH$ or $C_{16}SH$ molecules in monolayer assemblies on Au and for the random distribution of the molecules in the film, respectively. The results of these calculations are shown in figure 13.

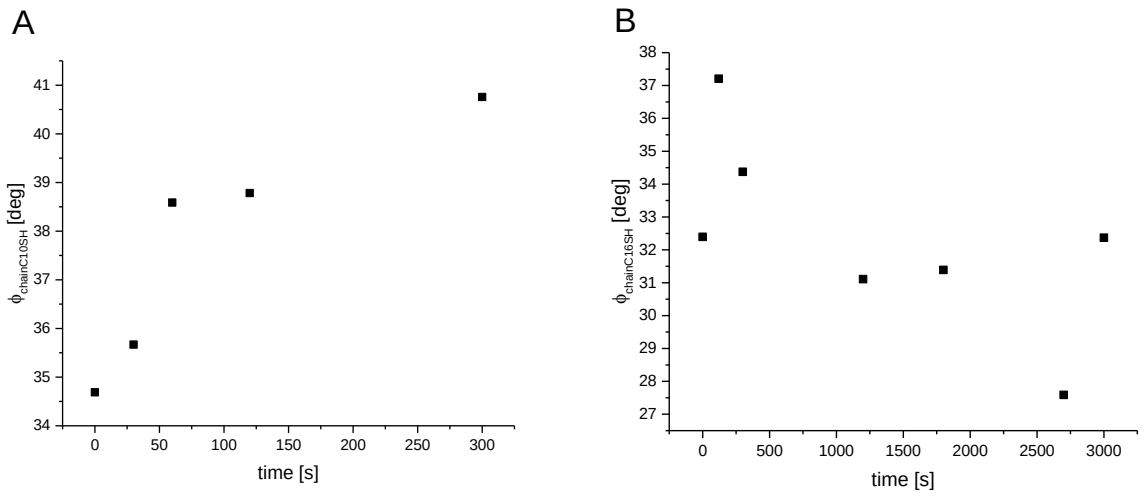

Figure 13: Tilt angle of the hydrocarbon chain of the A) $C_{10}SH$ and B) $C_{16}SH$ molecules in a SAM on Au as a function of time of the sample treatment with photolytically generated ROS.

In the $CH_{10}SH$ monolayer, despite constant surface coverage, the tilt of the hydrocarbon chains increases as a function of sample treatment time. In the freshly prepared monolayer the tilt angle is equal to 34.5° vs. surface normal. This is in good agreement with values reported in the literature for alkanethiol alkyl chains in all-trans conformation assembled in a monolayer exhibiting an average tilt angle of 28 to 40° to the surface [251]. After 300 s of sample treatment the tilt angle increases to ca. 41° vs. surface normal. These changes indicate that the hydrocarbon chains change their orientation in the monolayer on the Au surface. Interestingly, electrochemical measurements show a decrease in the capacitance minimum (see ACV measurements) with a simultaneous increase in the permeability of the monolayer to $Ru(NH_3)_6^{3+}$ cations in DPV measurements. On first sight, these results appear contradictory. However, a possible explanation for the obtained data is that the treatment of the SAM with ROS induces defect sites in the monolayer. The defects sites induce a reorientation of the mobile thiol molecules, which induces the increase in the tilt angle of the alkyl chains seen in PM IRRAS. Desorbed thiol molecules might accumulate on top of the monolayer, increasing the film thickness and attribute to the altered capacitance measured at the treated samples. This is also observed in the PM IRRA spectra as an increase in the intensities of the methylene stretching modes (consistent with an average "more parallel orientation" to the Au surface of alkanethiol molecules). Though the film thickens, the induced micro-defect sites are mature enough to allow the penetration of $Ru(NH_3)_6^{3+}$ ions to be reduced at the gold surface. Therefore, a regain of the redox signal in DPV measurements can be detected (figure 14 A).

In the freshly prepared $C_{16}SH$ monolayer the hydrocarbon chains have an average tilt of 32° vs. surface normal, being in excellent agreement with literature [251]. At initial times of the sample

ROS treatment the tilt of the hydrocarbon chains increases to roughly 36 to 37° vs. surface normal. It suggests that $C_{16}SH$ monolayers become more tilted towards the metal surface. The radical attack does not lead to desorption of alkanethiol molecules from the Au surface. With longer times of treatment, the tilt angle decreases again to ca. 30° vs. surface normal. Putting these results in context to the data obtained from XPS, DPV and ACV measurements, it seems that the $C_{16}SH$ SAM is affected only little by the treatment. The monolayer is not permeable to the $Ru(NH_3)_6^{3+}$ ions and the capacitance gradually increases (figure 14 B). The capacitance minimum after 3000s of irradiation increases to 1.0–1.2 µF cm^{-2} and the film remains impermeable to the ions. If any, only small amounts of the $C_{16}SH$ molecules are removed from the monolayer not affecting its structure, orientation and permeability. It has been reported before that partly oxidized alkanethiol SAMs retain their blocking characteristics toward electron transfer [231]. Comparing the behavior of $C_{16}SH$ and $C_{10}SH$ SAMs it can be concluded that the physical state of the alkane chain plays a very important role in the reaction with ROS.

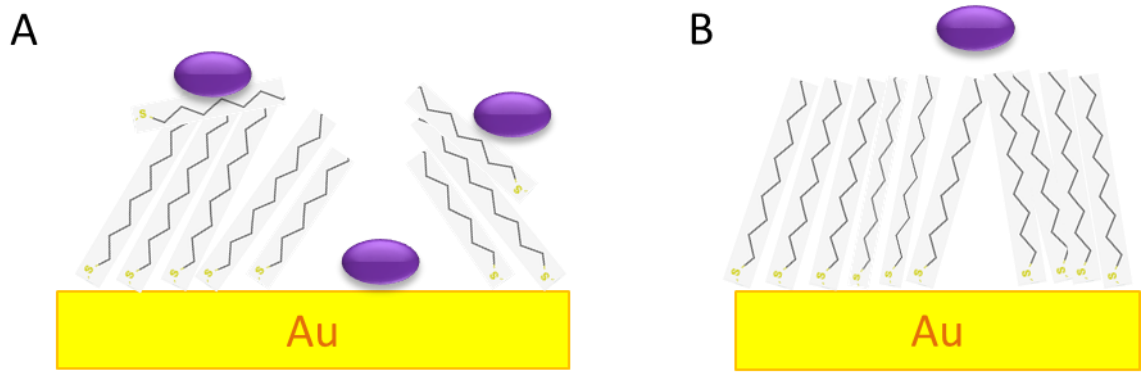

Figure 14: Possible molecular assembly of $C_{10}SH$ (A) and $C_{16}SH$ (B) molecules on gold surfaces after treatment with photolytically generated ROS. A) In a $C_{10}SH$ SAM, defect sites allow the penetration of $Ru(NH_3)_6^{3+}$ ions (purple ellipses). Detached thiol molecules accumulate on the monolayer increasing the film thickness. (B) Defect sites in a $C_{16}SH$ induced by ROS treatment are not sufficient to allow the penetration of the ions to the gold surface.

Taking the obtained results for the behavior of the C_8SH, $C_{10}SH$ and $C_{16}SH$ SAMs on polycrystalline gold together, we conclude that the chain length has an impact on the sensitivity of the formed SAM towards ROS. C_8SH SAMs were not further investigated because we obtained high standard deviations in the measurements with C_8SH SAMs. SAMs formed with $C_{16}SH$ proved to be rather stable against ROS treatment. They were affected only slightly by the ROS treatment in terms of surface coverage and chain tilt angle. Most importantly, the ROS treatment failed to regain the reduction current of $Ru(NH_3)_6^{3+}$ ions at $C_{16}SH$ SAM covered electrodes in DPV and CV measurements. $C_{10}SH$ SAM also proved rather stable against radical attack concerning surface

coverage and modification of the tilt angle. However, the induced defects in the formed $C_{10}SH$ SAMs by ROS allowed the penetration of dissolved $Ru(NH_3)_6^{3+}$ ions, which can be reduced at the gold surface.

From our results, we conclude that $C_{10}SH$ are best suited for ROS sensing in our experimental set-up. Therefore, we proceeded in further experiments using $C_{10}SH$ for SAM formation on the sensor electrodes.

4.1.1.4. Impact of SAM removal on the electrochemical surface activity

The electrochemical properties of the SAM covered gold surfaces before and after treatment were evaluated by scanning electrochemical microscopy (SECM). In SECM an ultramicroelectrode (UME; $r_T \leq 25$ µm) can be positioned with high precision in the *x*, *y* or *z* direction to measure electrochemical reactions at solid/liquid, liquid/gas or liquid/liquid interfaces [252]. We used the technique at the solid/liquid interface of the SAM covered gold electrodes (sample) in solution containing $Ru(NH_3)_6^{3+}$ ions (mediator, *M*). The geometry of UME determines that the mass transport occurs by hemispherical diffusion. Applying a potential at the UME at which the mediator is reduced a diffusion-limited steady state current ($i_{T\infty}$) is obtained at the electrode in a position far away from the sample. The steady state current is defined as:

$$i_{T\infty} = 4 \times n \times F \times D \times c \times r_T \tag{3.3}$$

With n = number of electrons; F = Faraday constant; D = diffusion coefficient; c = bulk concentration of mediator; r_T = UME tip radius

Operating SECM in the "feedback mode" the technique allows discriminating between conducting, insulating and semiconducting surfaces. This can be achieved by bringing the UME close to the sample. In case of a conducting sample the mediator *M* can be recycled (reduced/oxidized) at the samples surface increasing the flux of *M* to the UME. Hence, the measured relative current value increases (positive feedback). At an insulating surface *M* is not recycled. The surface hinders the diffusion of *M* from the bulk solution to the UME, thus limiting the flux of *M* to the electrode. Therefore, the measured current value decreases (negative feedback). For semiconducting surfaces, intermediate states are measured. [253] Recording the current as a function of the distance to the sample (d), a so called approach curve, and fitting the measured values of the approach curve to the theoretical model of Cornut and Lefrou [254], allows to calculate the heterogeneous reaction rate constant κ for the mediators regeneration [254]:

$$\kappa = \frac{k_{\text{eff}} r_T}{D} \tag{3.4}$$

With k_{eff} = apparent heterogeneous rate constant of the mediator

From the fit the kinetics of the mediator's reaction at the UME at close proximity d of the substrate are apparent. With this approach, we investigated the insulating properties of the $C_{10}SH$ SAM on gold before and after photolytically generated ROS treatment. In our case, the mediator M was $Ru(NH_3)_6^{3+}$ that was reduced at the UME to $Ru(NH_3)_6^{3+}$ at a constant applied potential of -0.42 V (experimental scheme depicted in figure 15).

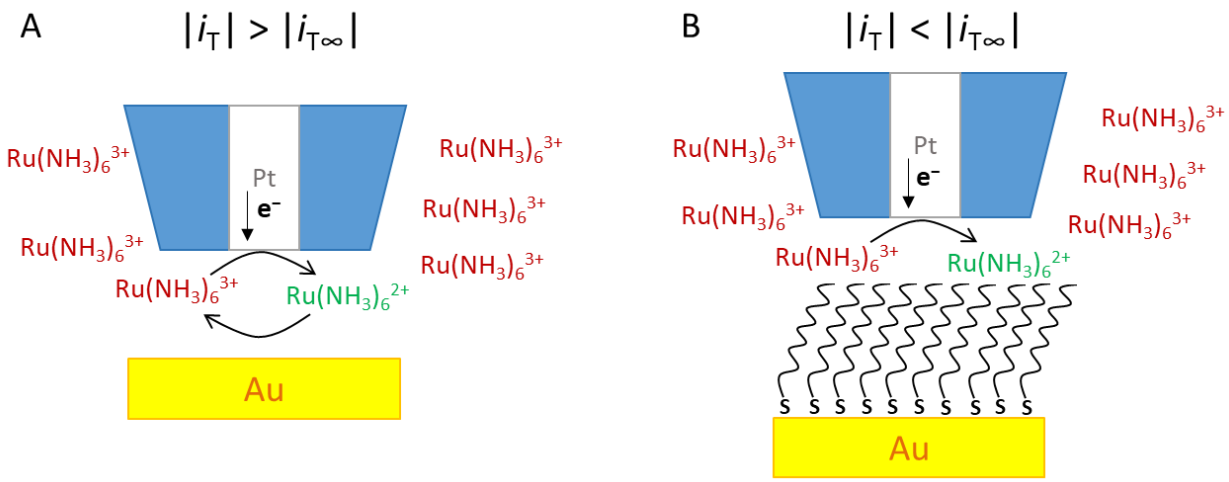

Figure 15: Experimental set-up for SECM measurements. A constant potential of -0.42V was applied at the Pt-working electrode. A) Approaching a conducting surface would increase the measured current (i_T) in comparison to the current measured in bulk solution ($i_{T\infty}$). B) Approaching an insulating surface (SAM covered gold) would lead to a current decrease.

For measurements, the geometry of the UME tip is important because it directly influences the reaction kinetics at the electrode tip. Therefore, the UME used in SECM was characterized in CV measurements in the electrolyte containing the mediator as well as by optical inspection under an electron microscope. An image of the electrode tip along with is geometric characteristics is shown in figure 16. The Pt wire embedded into the glass corpus is clearly visible in the center of

the electrode tip. The ideal geometry for an UME tip of this type is a perfect circle with the Pt wire

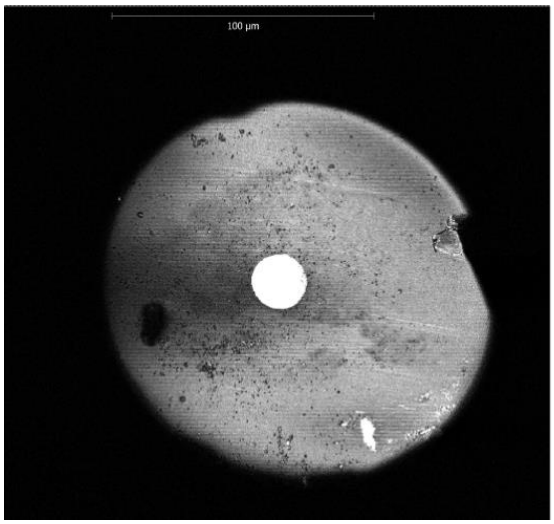

Radius glass (r_{glass})	71.25 µm
Radius Pt-tip (r_T)	10.37 µm
$RG = \frac{r_{glass}}{r_T}$	6.87

Figure 16: Electron microscope image of the UME. The image clearly shows the Pt wire (white circle) embedded in the glass corpus. The radius of the Pt wire (r_T), the glass corpus and the resulting *RG* value for the electrode were measured with imageJ software.

in the very center. This would allow equal diffusion distances for the mediator from each side to the electrode. The depicted electrode is slightly elliptic but does not differ much from the ideal. The r_T and the radius of the glass corpus obtained from the image were 10.4 µm and 71.3 µm, respectively. The resulting *RG* value, calculated from the radius of the glass divided by r_T, was 6.9. The measurements were initially performed using the same mediator $Ru(NH_3)_6^{3+}$ and the same electrolyte (acetate buffer, pH=4.7) as in the previous electrochemical experiments to increase the comparability of the data. It has been demonstrated before that the ion's properties influence the penetration abilities of the ion at SAM´s defect sites [236]. Important parameters are:

a) the hydrated diameter (D_H)=effective diameter of a hydrated ion in solution [255]
b) Stokes diameter (D_S)= diameter of a hard sphere that diffuses at the same rate as the ion [256]
c) Pauling diameter (D_P)=bare ion crystal diameter [255]
d) solvation enthalpy (ΔH_S) defines the interaction between an ion and solvent molecules; small $-\Delta H_S$ values indicate that hydrated ions easily undergo dehydration [257]
e) ionic mobility (U_0)=uniform velocity acquired by an ion under unit potential gradient.

Ions with small D_S values, small $-\Delta H_S$ values and large U_0 values can easily permeate into the SAMs. For example Cl^- (D_S=2.42 Å; $-\Delta H_S$=350 kJ mol^{-1}; U_0 =7.91×10^{-8}m^2 s^{-1} V^{-1}) have higher permeation ability than F^- (D_S=3.38 Å; $-\Delta H_S$=485 kJ mol^{-1}; U_0 =5.67 ×10^{-8}m^2 s^{-1} V^{-1}) [236].

However, since the working electrode in SECM was a Pt wire instead of gold, the potential for hydrogen evolution reaction (HER) in acidic media was shifted into the redox potential area of the mediator. The resulting current overlaid with the mediator`s CV current (figure 17 A). Therefore,

we decided to use Na_2SO_4 as alternative electrolyte. The resulting CV current at the UME was lower than in acetate buffer and corresponding to the expected theoretical values. Only some overlaying reaction current was measurable in the negative potential range (figure 17 B).

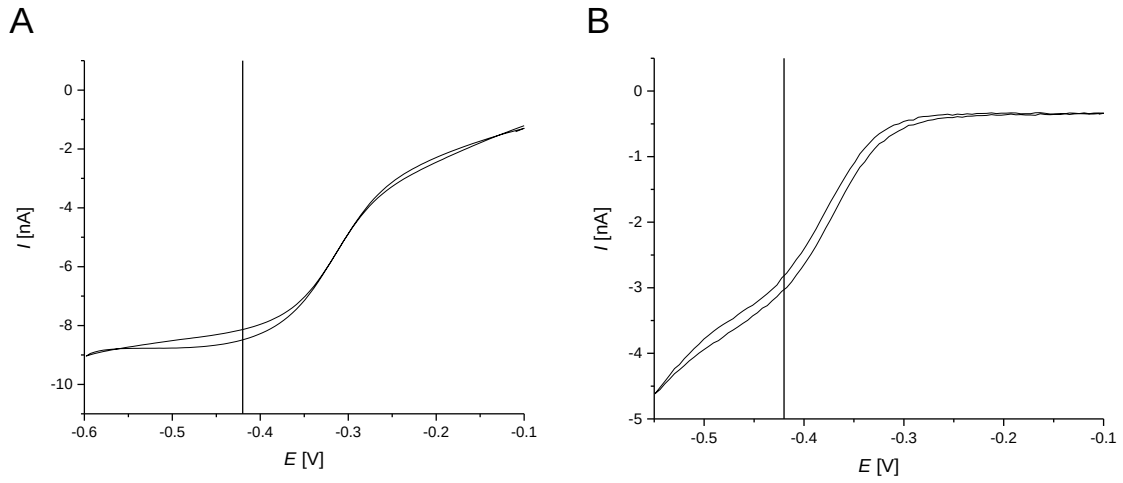

Figure 17: CVs recorded at the UME in 1 mM $(Ru[NH_3]_6)Cl_3$ in A) acetate buffer and B) Na_2SO_4. The vertical black line in the graphs marks the potential fixed at the UME during SECM measurements.

Approach curves on the SAM covered electrodes demonstrated the passivating behavior of the SAM against the $Ru(NH_3)_6^{3+/2+}$ redox couple. In comparison to approach curves that were recorded on glass as substrate, some surface activity was detected expressed in different values for the parameter κ to modulate the current limiting behavior close at the substrate with first order irreversible redox kinetics (κ=0.001 vs. κ=0.05; figure 18 A). It demonstrates that the passivating effect of the SAM is not complete and that some defect sites present in the SAM allowed oxidation of the redox couple in solution as demonstrated before in ACV measurements. The fact that alkanethiol SAMs do not function as complete electrochemical isolators, especially on surfaces exhibiting a lattice like gold, has been reported before [236]. To estimate the pinhole size that contribute to the $Ru(NH_3)_6^{3+}$ ion reduction signal following parameters are considered: (i) the radius of the $Ru(NH_3)_6^{3+}$ ion; (ii) the kinetics of an outer sphere electron reaction; (iii) currents resulting from direct ion exchange reactions overweight ion tunneling events over the SAM. Taking these parameters into consideration, the size of potential pinholes that contribute to the current signal was estimated to be ≥5 Å^2 per cm^2 [258]. Using an UME with a r_T of 10 µm the measured current is the sum of several differently sized defects sites within the SAM. Nonetheless, in sum the SAM still serves as a passivating film on top of the gold. Treatment with oxygen radicals altered the redox kinetics at the electrode tip close to the substrate resulting in positive approach curves. However, in comparison to clean gold surfaces the reaction was still hindered (figure 18 A+B) indicating that still many active gold sites remained blocked by adsorbed thiol molecules

limiting the recycling of the $Ru(NH_3)_6^{3+/2+}$ redox couple at the gold substrate. Longer treatment with oxygen radicals only slightly increased κ values from 1.7 to 2.1 but failed to regain values of clean gold. Removal of the thiol SAM via reductive desorption let to positive approach curves. The obtained kinetic parameters did still not resemble the ones for a cleaned gold surface (κ_{RD}=4.2 vs. κ_{Au}=10; figure 18 C+D). Therefore, it is assumed that the electrochemical SAM removal still leaves behind some thiol molecules or other impurities on the gold surface reducing its electrochemical activity of the gold (supported by the previous presented XPS, PM-IRRAS, CV, DPV data). However, a clear distinction between RD and ROS treated samples is visible ($\kappa_{ROS\ 180s}$ =1.9 vs. κ_{RD}=4.2 and 4.4). In comparison to radical treatment, the electrochemical thiol SAM removal process is capable of (a) removing more thiol molecules from the gold substrate and/or (b) leaving behind electrochemically (more) active gold sites. The SECM data does not allow distinction between gold sites blocked by thiol molecules, sites blocked by other contaminations and electrochemically less active gold. However, the elementary composition of the surface after ROS treatment obtained from the XPS data (chapter 4.1.1.2.3.) suggests that the blocking molecules on the surface are indeed thiol molecules.

Modeling the currents measured while approaching the substrate to the obtained model parameters demonstrate the small differences in the reaction kinetics between different radical exposure times (figure 18 B) as well as the strong effect of RD on the insulating properties of the SAM (figure 18 D).

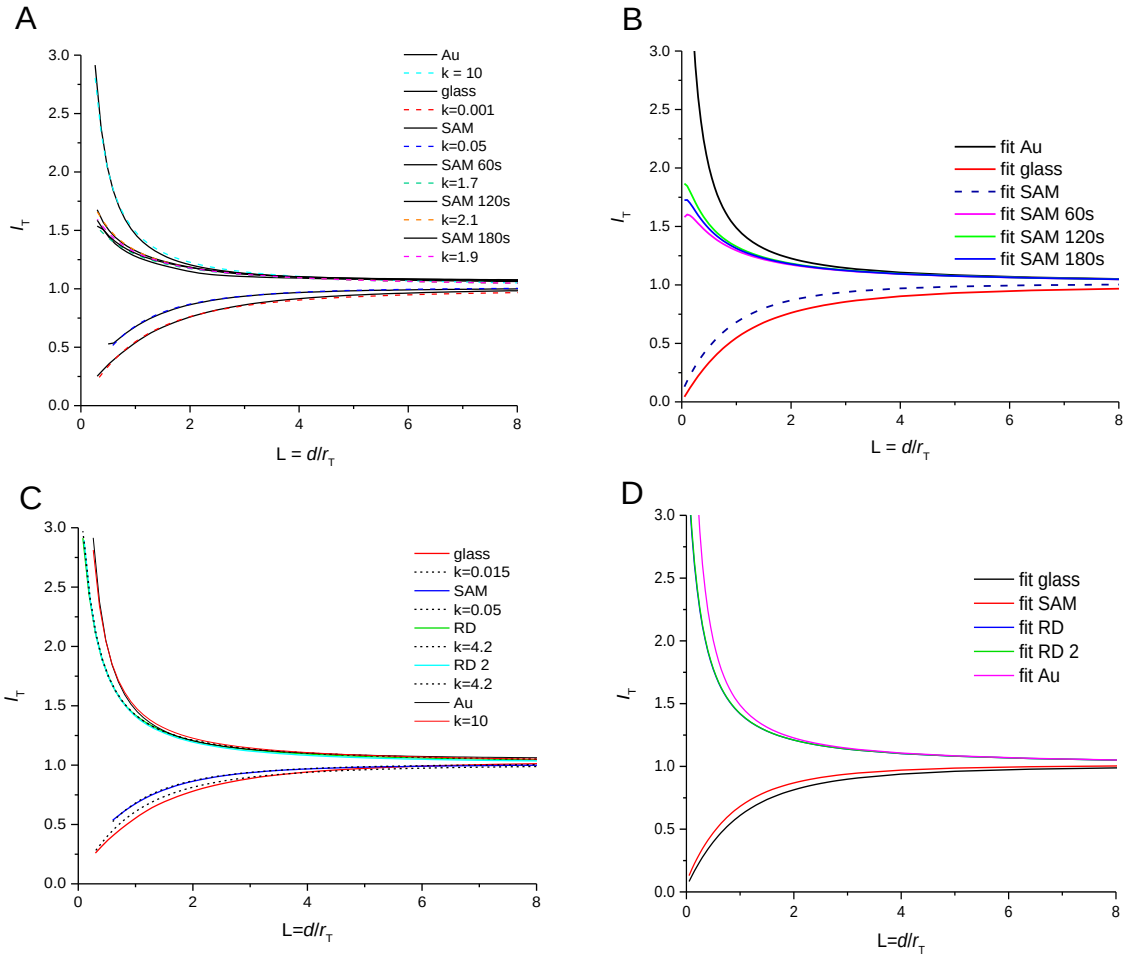

Figure 18: Approach curves on $C_{10}SH$ covered Au surfaces. A) Measurements were taken before (SAM, blue line) and after 60 seconds (green line), 120 seconds (orange line) and 180 seconds (pink line) exposure towards photolytically generated ROS. B) Fitted SECM approach curves corresponding to the data shown in A. C) Approach curves at $C_{10}SH$ coated gold samples after reductive desorption of the SAM (RD; RD 2). D) Fitted SECM approach curves corresponding to the data shown in C. All measurements were recorded in 1 mM $[Ru(NH_3)_6]Cl_3$ in 0.1 M Na_2SO_4 and fitted to the model of Cornut et al. [254] for RG=7 and r_T = 10 for different κ values (dashed lines) and represent currents measured at the electrode tip i_T normalized for the current in bulk solution $i_{T,\infty}$. ($I_T = i_T / i_{T,\infty}$) plotted against the distance from the probe (d) in relation to r_T. Approach curves on a glass plate are taken as a negative control and on a cleaned Au surface as positive control.

In SECM imaging the current at the UME is recorded while the tip is moved over the sample in parallel to the surface. Combining the data of several lateral scans yields a picture mapping the electrochemical activity of the scanned sample area. The attainable resolution in SECM imaging depends upon the tip radius and distance d between tip and sample [259]. The distance d was determined from the approach curves and fixed for imaging at 10 nm. The tip radius r_T and the RG value, defined as the radius of the insulating glass corpus at the UME tip divided by r_T, was determined from an electron microscope image of the UME (figure 16). The image revealed that

the UME had some minor defect sites and the Pt wire was not centered perfectly within the glass corpus. Therefore, the diffusion distance was not equal from all sites to the electrode. However, obtained images of differently treated SAM surfaces confirmed the first impression obtained from approach curves. On RD treated samples only small inactive sites (i_T=(−4) nA) were recorded (figure 19 A). Most of the surface exhibited high electrochemical activity (i_T=(−12) nA). The high electrochemical activity suggests that RD treatment exposed active gold sites. We attribute the inactive sites to adsorbed thiol molecules or other insulating impurities attached to the surface. The obtained image supports the kinetic data from the fitted approach curves that suggest a similar electrochemical behavior of the electrodes after SAM removal via RD to the one of a cleaned gold surface. The reaction kinetics are only slightly hindered by the remaining molecules attached to the surface represented in the image by the inactive sites.

SAM covered gold substrates treated with oxygen radicals exhibited a more heterogeneous electrochemical activity (i_T=(−2.8) to (−3.6) nA; figure 19 B). Since the average electrochemical activity represents a partly insulating surface, we conclude that most of the surface is still covered with the SAM molecules and that the difference to the reaction kinetics of a glass surface (complete insulator) are due to defect sites within the SAM. That assumption is in agreement with the kinetic parameters obtained with the approach curves showing only slight modifications in the kinetics at the surface upon prolonged radical treatment. The images do not show the exact size of the uncovered areas in the SAM because the electrode radius is expected to be larger than individual defect sites. Therefore, the obtained electrochemical activity "image" is interpreted as the cumulative response of numerous defect sites in the SAM distributed randomly over the substrate. The obtained electrochemical activity of the surface is the average from SAM covered and uncovered regions of the underlying gold substrate.

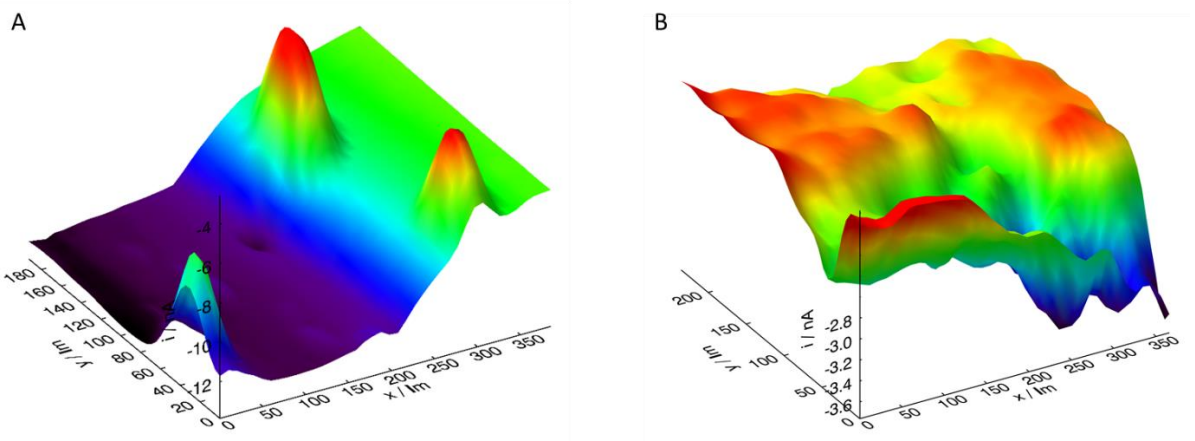

Figure 19: SECM images taken of a $C_{10}SH$ SAM covered gold sample after A) reductive desorption (RD) and B) after 5 minutes treatment with photolytically generated oxygen radicals.

4.1.2. Adaption of ROS concentration

In previous work, the electrochemical sensor electrode was employed to measure non-physiologically, high concentrations of ROS (0.5 M H_2O_2 in Fenton reaction [260]; 1 M H_2O_2 in photolysis [261]). Scholz et al reported a ROS detection limit for their alkanethiol SAM covered gold electrode of 10^{-5} M H_2O_2 in the Fenton reaction [2]. However, in their work they employed C_6SH SAMs. As stated before, we obtained inconsistent results employing C_nSH with $n \leq 8$. Therefore, we tested if we could obtain the same or lower detection limit with $C_{10}SH$ SAMs as reported by Scholz et al. The ROS concentrations expected in a biological context are in the nM and under some specific conditions in the µM range. We focused our work on the µM concentration range. Figure 4 A shows the standardized current increase of the $Ru(NH_3)_6^{3+}$ ion reduction signal at SAM covered gold electrodes in dependence of the treatment time with ROS. Employing an initial concentration of 10^{-2} M H_2O_2 in water let to a gradual regain of the current measured in DPV. Reducing the concentration to 10^{-5} M still let to a signal regain at the SAM covered electrode. However, the signal increase did not exceed to more than $10 \pm 3\%$ of the initial current maxima measured at the cleaned electrode (figure 20 B).

Hilgemann et al employed the electrochemical assay to measure radical scavenging capacity of plant extracts [3]. For data evaluation they plotted the logarithm of the standardized DPV peak currents against the treatment time ($\ln(1-[I/I_0])$ vs. time). For the resulting function, they obtained two distinct linear sections describing the exponential decay of the curve: a fast decay from 0 to 5 minutes (k_1) and a slower decay from 5 to 30 minutes (k_2). They formulated the hypothesis, that k_1 describes the effective attack of hydroxyl radicals at unordered SAM domains at the Au electrode surface, leading to a fast regain of the current signal. In the second range from 5 to 30 minutes the attack at the remaining highly ordered SAM domains would then take place much slower, resulting in the slow decay k_2. For a SAM that was prepared by a longer annealing time (70 h), they only witnessed a slow decay described by k_2. However, their hypothesis neglects the mobility of the thiol molecules on the gold surface and possible reordering processes of the SAM that might occur.

Figure 20 B shows the logarithmic increase of the $Ru(NH_3)_6^{3+}$ ion reduction signal in dependence of the treatment time in our experimental setting. Unlike the data reported by Hilgemann et al the signal resurgence at high H_2O_2 concentrations (10^{-2} M and 10^{-3} M) takes place much faster (as described by k_2) until a plateau is reached were no further current increase was measured. At lower H_2O_2 concentrations, the plateau is reached at a later time point and the final current stays below the initial current measured at the cleaned gold electrodes. Evaluating the slope k in the initial minute of the resulting function we found the steepest slope for the measurements with

10^{-2} M H_2O_2 becoming less pronounced with lower H_2O_2 concentrations ($k_{10^{-2}} = -0.0322; k_{10^{-3}} = -0.0026; k_{10^{-4}} = -0.0024; k_{10^{-5}} = -0.0007$ linear fit 0 to 60 seconds). The differences in the kinetics of SAM destruction measured by Hilgemann et al and ours can be due to differences in the experimental set-ups:

(i) the generation of ROS (photolytically vs. Fenton reaction),

(ii) the H_2O_2 concentration (0.5 M vs. 10^{-2} to 10^{-5} M),

(iii) the type of thiol molecules for SAM preparation (C_6SH vs. $C_{10}SH$),

(iv) the gold pretreatment,

(v) the SAM annealing time (15 minutes vs. 17 h),

(vi) the protocol actually applied for ROS treatment.

Especially (vi) might have an impact on the SAM degradation process. Hilgemann et al exposed their SAM covered electrodes always for 5 minutes to freshly prepared Fenton solution. It must be assumed that over the treatment period the concentration of hydroxyl radicals decays. Since we applied shorter treatment times, the decay of radicals in the treatment solution does not occur to the same extent during electrode treatment. We therefore assume that the prolonged treatment time is not equal to the prolongation of the effective intensity of ROS attack of the SAM.

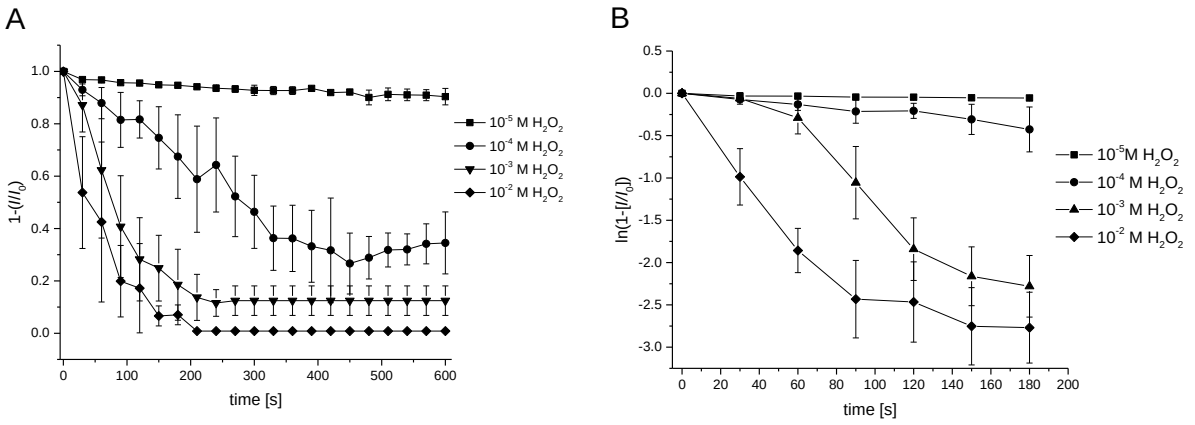

Figure 20: Increase of the $Ru(NH_3)_6^{3+}$ ion reduction signal at SAM covered gold electrodes in dependence of the treatment time with ROS. The graphs show the normalized currents (A) and the logarithm of the values from which the *k* values are determined (B). ROS were generated from photolysis of H_2O_2 in water. The initial concentration of H_2O_2 ranged from 10^{-5} M to 10^{-2} M.

Looking at the dependence of the percentage increase of the $Ru(NH_3)_6^{3+}$ ion reduction signal at the ROS treated electrodes on the initial concentration of H_2O_2 in the treatment solution yielded a sigmoidal shaped curve (figure 21 A). The shape of the function is in agreement with data published before by Scholz et al [2]. However, their data refers to a treatment time of 300 seconds with 0 to 200 mM H_2O_2 employed in the Fenton reaction. We witnessed the same behavior at our electrodes at a treatment time of 150 seconds with 0 to 10 mM H_2O_2 in photolysis. Because the generation of ROS is different, the concentration of H_2O_2 in the experiments is not directly

comparable. Therefore, direct statements on the sensitivity of the electrodes towards ROS are problematic. The relevant parameter, the concentration of ROS that interact with the SAM, is not clearly defined in both experimental settings.

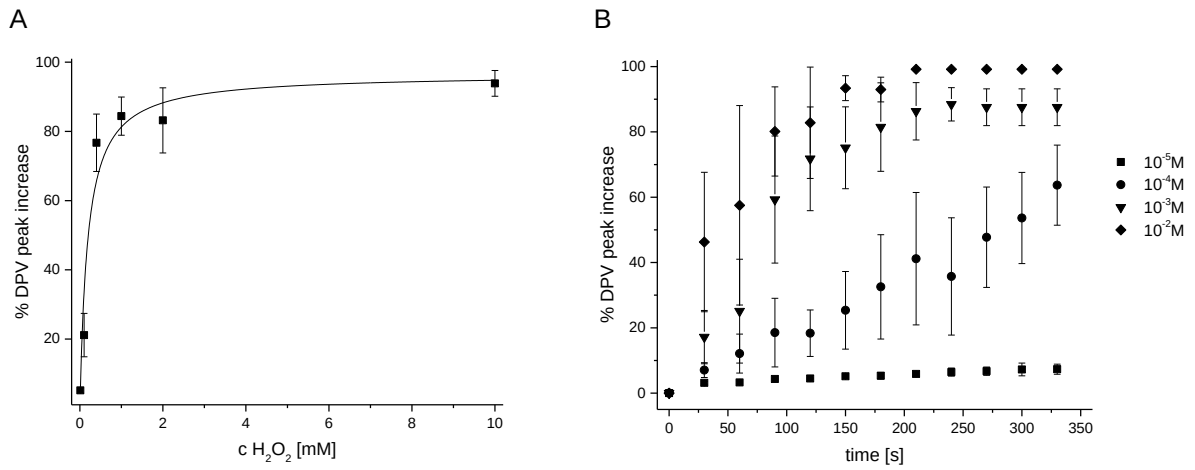

Figure 21: Dependence of the DPV peak increase at the SAM covered Au electrodes on A) the concentration of H_2O_2 at 150 seconds treatment time and B) on the treatment time with ROS for different H_2O_2 concentrations (10^{-5} to 10^{-2} M). ROS were generated from photolysis of H_2O_2 in water.

The photolysis of H_2O_2 took place in a reaction volume of 10 mL. The process generates hydroxyl radicals (eqn. 3.5) that can further react to form other ROS [262].

$$H_2O_2 \xrightarrow{h\nu} OH^- + OH\cdot \tag{3.5}$$

Hydroxyl radicals are very powerful oxidants, with a standard reduction potential of 2.8 V [263]and react with many molecules at a diffusion controlled rate. The diffusion coefficient for the hydroxyl radical has been reported as 2.1 $cm^2\ s^{-1} \times 10^5$ [264]. Because of this high reactivity, it is likely that only hydroxyl radicals generated in proximity to the sensor electrode will react directly with the SAM, while others will form secondary ROS. Calculating the exact concentration of ROS that interact with the SAM is therefore troublesome. However, since it is unlikely that the effective ROS concentration much outnumbers the initial concentrations of H_2O_2 employed in the experiments, we conclude that the sensitivity of the $C_{10}SH$ SAM covered electrodes towards ROS in water is sufficient to determine ROS at 10^{-5} M concentration.

4.1.3. Environmental influence factors

To transfer the electrochemical assay to biological relevant experimental setting, the influence of different environmental factors on the SAM degradation process on the sensor electrodes had to be investigated. Due to osmotic effects, cells cannot be cultivated in pure water. Cultivation and measurements on cells must take place in buffered solutions containing certain nutrients and ions. For cultivation the cells are kept in cell media that contain amino acids, vitamins, inorganic salts

and often glucose as energy source. In addition, the medium is often supplemented with serum (mostly from fetal calves) that provides the growth factors, hormones, and attachment factors required for cell cultivation. The function of the medium is to provide the cells with the necessary factors to enable cell growth and to maintain the osmolality and the pH during cultivation. Depending on their composition, artificial media can be divided into (i) balanced salt solutions (e.g. PBS, DPBS[6], HBSS, EBSS[7]), (ii) basal media (e.g. MEM[8] DMEM) and (iii) complex media (e.g. RPMI-1640, IMDM[9]). Balanced salt solutions are mainly used for immediate survival of the cells (for example during the performance of an assay). Basal and complex media are employed to achieve prolonged cell survival, indefinite growth and to promote specific cell functions. [265] Many of these cell media/cell buffer components are capable of scavenging or interacting with ROS themselves. Therefore, we assessed the ability of the electrochemical sensor electrode to sense ROS (generated by photolysis of 10^{-4} M H_2O_2) in different cell media employed in cell culture experiments.

Figure 20 shows the current increase at SAM covered electrodes in dependence on ROS exposure time. Figure 22 A shows the mean signal increase at electrodes exposed to ROS in HBSS. As can be seen from the large standard deviations at the individual time points the behavior of the SAM towards the generated ROS varied significantly. Especially at later time points, some SAMs were affected by ROS while others only showed minor modifications. In figure 22 B the data from 5 individual measurements of electrodes exposed to ROS in RPMI-1640 are shown. Apart from one individual measurement (electrode 5, figure 22 B), the procedure failed to degrade the SAM. The peak current measured in DPV (I) did not exceed $1.6\pm1\%$ of the initial peak current (I_0) measured at the clean gold electrode. Only in one out five measurements, I increased to 54.9% of I_0 after 450 seconds exposure to ROS. In comparison measurements with the same concentration of H_2O_2 (10^{-4} M) in water did lead during the same exposure time (480 s) to a signal regain of 72 ± 8 % (figure 22 B).

RPMI-1640 belongs to the category of complex media. In our measurements we used RPMI-1640 without phenol red (phenolsulfonphthalein, used as a pH indicator), because the molecule can interact with ROS at its hydroxyl groups. Nonetheless, RPMI-1640 still contains several molecules that can interact with ROS such as amino acids, glutathione, glucose or vitamins. The measurements in HBSS demonstrate that a less complex media increases the probability that the ROS interact with the SAM. In contrast to complex media, the cell buffer does only contain inorganic salts. This explains why we were able to obtain current increases like the ones measured

[6] Dulbecco's Phosphate-Buffered Saline
[7] Earle`s Buffered Salt Solution
[8] Minimum Essential Media
[9] Iscove's Modified Dulbecco's Media

in water (72±8% in H_2O vs. 69±12% in HBSS at t=480 s). However, the standard deviations for measurements in HBSS are 4% higher than in water. Measurements in HT buffer, which contains apart from some inorganic salts, an organic buffering agent and some glucose (see method section), yielded similar results to measurements in HBSS. In summary, the data demonstrate that complex cell media, like RPMI-1640, possess protective effects towards the SAM. Measurements in less complex media, like HBSS, enable the gradual degradation of the SAM on the electrode surface. However, the increase in possible reaction partners for the generated ROS increases the variety in the SAM degradation process. This is reflected in the large standard deviations of the measurements in HBSS especially at later time points (270 to 480 s).

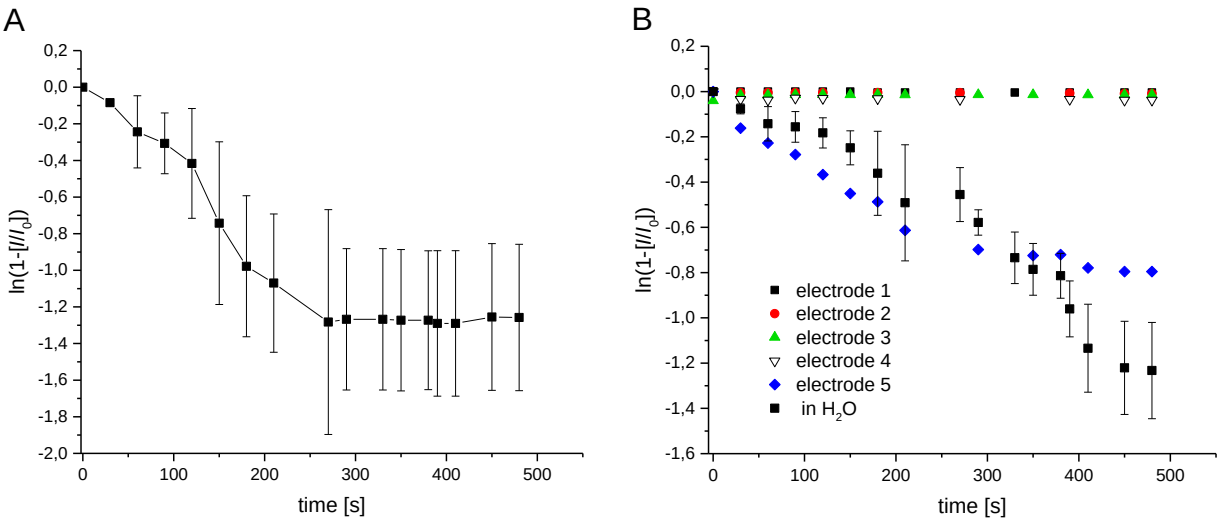

Figure 22: Increase of the $Ru(NH_3)_6^{3+}$ ion reduction signal at SAM covered gold electrodes exposed to ROS in different media. A) Mean current±SD of 4 independent measurements in HBSS. B) Five individual measurements in RPMI-1640 (electrode 1 to 5) and the mean of 4 independent measurements±SD in H_20 are shown. ROS were generated by photolysis of 10^{-4} M H_2O_2 in the respective media.

Cellular medium contains less oxygen than the normal atmospheric air because the cells are incubated at elevated CO_2 levels (5%). The generation of ROS is directly dependent on the O_2 availability. Altering the O_2 concentration in solution during ROS generation had a strong impact on the SAM removal process (see chapter 4.1.4.).

4.1.4. Detection of different ROS

As stated already in the introduction the term ROS defines a heterogeneous group of molecules. Our method of choice for *in-vitro* ROS generation, the photolysis of H_2O_2, generates hydroxyl radicals (eqn. 1.1). Due to their high reactivity the radicals can form several reaction products that can interact with the SAM covered sensor electrodes. The phenomenon is a general challenge of ROS assays because ROS can be converted into each other making the distinction between primary and secondary ROS troublesome. However, to determine if the sensor exhibits different

sensitivities towards individual ROS we choose various experimental set-ups that favor the evolution of specific ROS.

In a first step, we investigated if UV radiation of H_2O without H_2O_2 present in the treatment solution can degrade the SAM. The treatment did not result in a current increase measured at the electrodes in DPV (figure 23). Therefore, we assume that the hydroxyl radicals that are produced from H_2O_2 induce the degradation process and not the UV light itself. Radiation of water with UV light can lead to the generation of ozone. However, this only occurs at wavelengths of 185 nm and below. Since we operate the UV light at 254 nm, we do not expect ozone to be formed in our experimental setting.

Purging the water before and during ROS generation with nitrogen had the same effect as leaving the H_2O_2 out of the system. We could not detect any significant changes to the SAMs reflected in the absence of the $Ru(NH_3)_6^{3+}$ ion reduction signal at the electrodes in DPV. Increasing the amount of oxygen in the system on the other hand, by purging the water before and during the ROS generation with O_2 resulted in an immediate regain of the DPV signal at the exposed electrodes. In comparison to water that was not purged with the same amount of H_2O_2 (10^{-4} M), the degradation of the SAM was accelerated by the increased oxygen content in the treatment solution. The accelerated SAM degradation is expressed in the increase of the slope k for the normalized current values ($\ln(1-[I/I_0])$ plotted against the radical exposure time (figure 22): $k_{O_2+H_2O_2} = -0.0301, k_{N_2+H_2O_2} = 4\times10^{-7}, k_{H_2O_2} = -0.0113, k_{noH_2O_2} = -0.00003$.

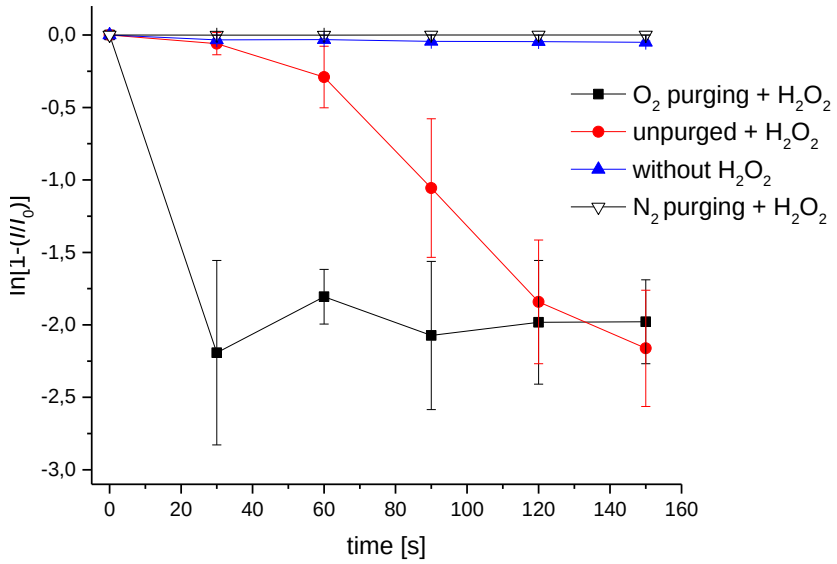

Figure 23: Effect of the oxygen and nitrogen concentration during ROS generation and treatment on the SAM degradation process at gold electrodes. The normalized peak current of the $Ru(NH_3)_6^{3+}$ ion reduction in DPV (I) is plotted against treatment time in UV light radiated water containing 10^{-4} M H_2O_2 (or without

H_2O_2). The water was either unpurged or purged for 20 minutes before and during the ROS generation with O_2 or N_2.

We therefore assume that oxygen availability is an essential parameter for the SAM degradation process. Further, the data suggest that reactive nitrogen species (RNS) do not play a role in the SAM degradation process since UV radiated N_2 saturated solutions had no impact on the SAM.

Another important physiological ROS is superoxide. In comparison to the hydroxyl radical it is less reactive. This property enhances its lifetime and therefore also its detection window. We generated superoxide radicals in a cell free environment at TiO_2 nanoparticles with simulated sunlight (SSL) in HT buffer and in water. The formation of superoxide was monitored with NBT. A decrease of NBT absorption at 260 nm was measured over time as an indirect parameter for superoxide generation, which reacts with NBT to form an insoluble formazan at the TiO_2 nanoparticles [211] (figure 24 A). After 1 hour, the NBT signal decreased in water and to a lesser extent in HT buffer (H_2O A_{260}: 1.68 vs. 1.60; HT A_{260}: 1.51 vs. 1.45; figure 24 B). This is an indicator for the superoxide formation under the described experimental condition in water and to a lesser extent in HT buffer. The total values for the absorption at 260 nm in HT were smaller than reported in previous work [211], which can be explained by interference of the HT buffer. The shift of the absorbance curves with the HT buffer is due to the fact, that the recorded spectra were standardized to a reference solution containing only buffer or water. Therefore, the baseline was different for both conditions. The absolute concentration of superoxide formed at TiO_2 nanoparticles in aqueous solution reported in the literature vary depending on the concentration of TiO_2 nanoparticles, the measurement time and the light source. For a solution containing 100 mg L^{-1} TiO_2 irradiated 30 minutes with 365 nm light a concentration of 180 nM for long-lived superoxide radicals was reported [266]. Another study that used 5 mg L^{-1} TiO_2 nanoparticle solution irradiated with 365 nm light for 2 hours reported a superoxide concentration of 8 µM and a total ROS concentration (OH^-, $^1O_2$, $O_2^-\cdot$) of 443 µM [267]. As indicated by the later study, it must be assumed that apart from superoxide radicals also hydroxyl radicals, hydrogen peroxide and singlet oxygen are formed at the TiO_2 particles. However, their contribution is smaller under the chosen light wavelength [211]. If the expected concentrations generated with this method are indeed in the µM-range, the ROS amounts should be within the detection limit of the sensor electrode.

However, exposure of SAM coated Au electrodes towards the generated superoxide did not affect SAM integrity in a measurable way in HT buffer. Furthermore, the SAM degradation process by superoxide in water had only little effects on the measured DPV signals at the electrodes in comparison with treatment of ROS generated from10^{-4} M H_2O_2 (figure 24 C). In HT buffer no measurable $Ru(NH_3)_6^{3+}$ ion reduction occurred up to an exposure time of 35 minutes at the

electrodes (figure 24 D). The results were verified by CV measurements of the electrodes after TiO_2 exposure in H_2SO_4 were the measured gold signal was minor compared to the initial signal indicating that most of the surface was still coated by the SAM (figure 24 E). We confirmed that the blockage of the gold surface is indeed due to thiol molecules still attached to the surface by RD measurements in NaOH. The resulting voltammograms exhibited the characteristic reduction peaks of the thiol molecules. The irreversible removal of the adsorbed molecules decreased the reduction current proportional to the number of CV scans. The size of the initial reduction peak indicates that most of the thiol molecules were still attached to the gold surface after superoxide/TiO_2 exposure (figure 24 F). A possible explanation for the small impact of the formed superoxide on the SAM would be the low concentration of superoxide generated at the TiO_2 nanoparticles that were unlikely to exceed 10 µM in addition to the buffering capacity of the HT buffer. This could also explain the small reduction of NBT absorbance in general (figure 24).

Conclusively, the experimental data suggest that the SAM degradation process requires the presence of oxygen in the treatment solution and can be suppressed by high nitrogen saturation/low oxygen concentration. H_2O_2 and superoxide itself have only little effect on the SAM, while hydroxyl radicals generated from photolysis of H_2O_2 seem to have the strongest impact on the SAM. The absolute ROS concentrations generated by the individual methods are expected to differ. Therefore, the data are not reliable for quantitative comparison. However, qualitive data evaluation suggests that the sensor is differently sensitive towards individual ROS.

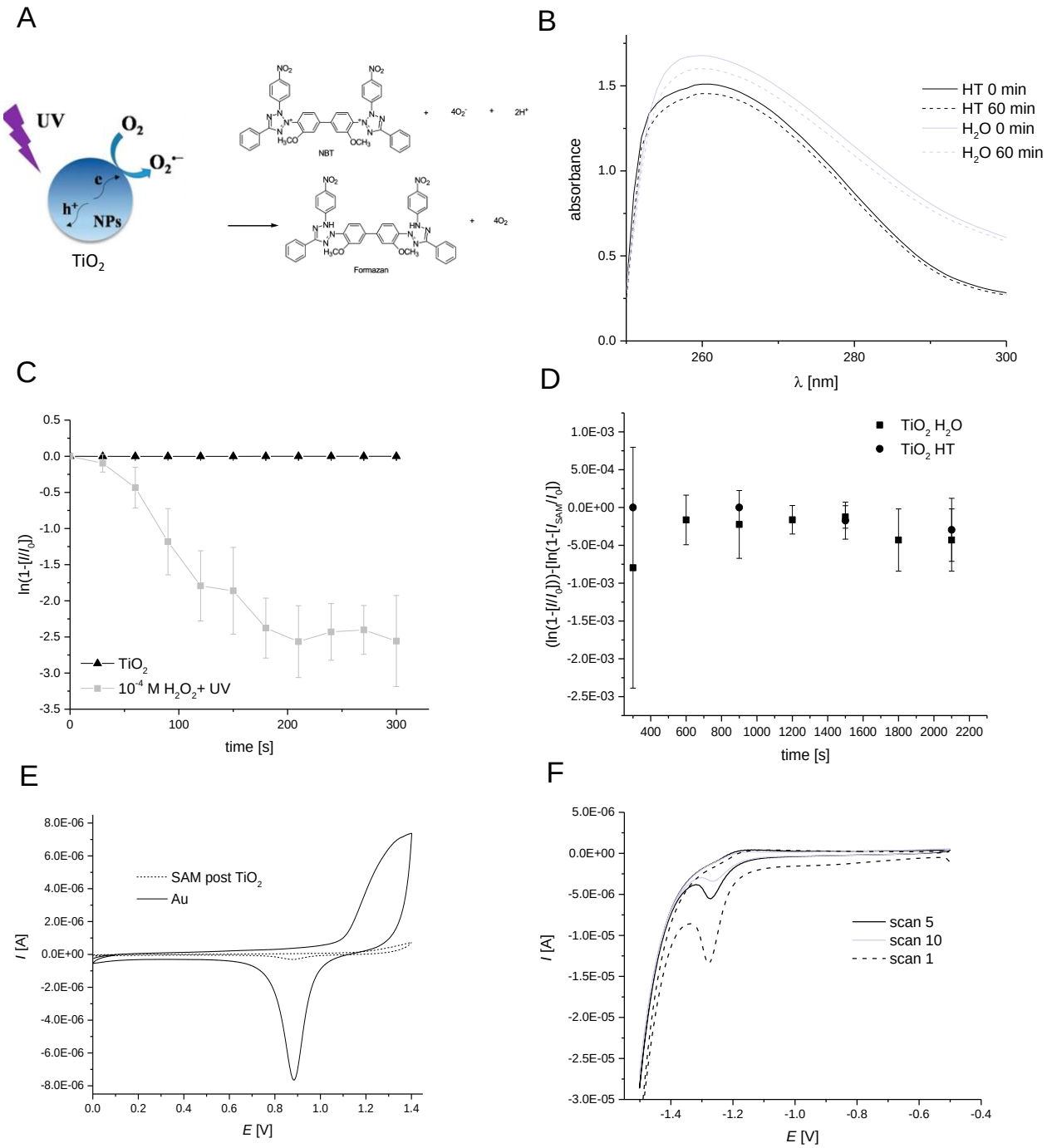

Figure 24: A) Principle of superoxide generation at TiO_2 particles in solution. B) Absorbance measurements of 0.1 M NBT with 200 mg L^{-1} TiO_2 nanoparticles in water (grey lines) and HT buffer (black lines) after 0 and 60 minutes radiation with simulated sunlight (SSL). C+D) Peak height of the $Ru(NH_3)_6^{3+}$ ion reduction signal at SAM covered Au electrodes in DPV after incubation with superoxide from TiO_2 nanoparticles in H_2O and in HT buffer in comparison to treatment with ROS from photolysis of H_2O_2. E) CV measurements at the cleaned gold electrode and at SAM covered electrode after exposure to TiO_2 generated superoxide in 0.1 M H_2SO_4 at 0.1 V s^{-1}. F) RD voltammograms at the SAM covered electrodes in 0.1 M NaOH after exposure to TiO_2 generated superoxide.

4.2. Evaluation of antioxidant activities of plant substances *in-vitro*

The first experiments on the characterization of the electrochemical sensor assay were the fundament for the application of the sensor in the evaluation of the antioxidant activities of

different plant substances/extracts as already performed by Hilgemann et al [260]. In their work, they compared the results of the electrochemical assay to results they obtained for the same plant extracts with the DPPH assay. Though they could obtain linear dependencies between the radical scavenging properties and the concentrations of the plant extracts with both assays, the results differed significantly between both assays. The authors ascribe this to the different radical probes (DPPH radical vs. OH radical) they used in the experimental settings. Therefore, we decided first to evaluate the plant substances in assays that do not use the rather stable DPPH radicals, which have no biological relevance.

In a first step, the plant substances (ascorbic acid (AA), caffeic acid (CA), epigallocatechine gallate (EGCG), ferulic acid (FA), kaempferol, quercetin, rutin, trolox) and an ethanolic extract of the plant *Gynostemma pentaphyllum* (GP) were assessed for their antioxidant activities in different established chemical *in-vitro* antioxidant assays.

4.2.1. Luminol assay

Chemiluminescence (CL) describes the generation of light emission by a chemical reaction. Several CL-based methods for the evaluation of antioxidant activity exists. One common chemiluminescent reagent is luminol[10]. One variant of the luminol assay measures the capacity of a substance to scavenge hydroxyl radicals generated in the Fenton reaction [268]. Scavenging of the radicals inhibits the oxidation of the luminol dianion into an electronically exited state. To go back into the ground state, the molecule emits excessive energy in form of a photon. The emitted photons cause the CL of the probe. [269] Adding a substance to the reaction it is assumed that the higher the measured CL the lower the radical scavenging activity of the substance [268]. The oxidation of luminol can also be caused by H_2O_2, $O_2^{-}\cdot$ and $ONOO^{-}$. Therefore, the method is not specific for one ROS [270].

We performed measurements adding the individual plant substances in different concentrations to the reaction solutions. All of the tested substances reduced the CL, indicating that they all possess radical scavenging activity in the experimental setting. At the highest concentration (100 µM) the radical scavenging activity of the substances ranged between 90 to 99%. Only FA ($70\pm5\%$) and rutin ($77\pm3\%$) exhibited lower activities. Plotting the antioxidant concentration against their radical scavenging activity indicates that at 100 µM most substances reached the non-linear dynamic range of the correlation function between concentration and scavenging activity (no linear correlation visible anymore) (figure 25 A).

[10] 5-Amino-2,3-dihydrophthalazine-1,4-dione

At lower concentrations of the plant substances (50 µM) the differences between the individual compounds become more distinct. CA, EGCG, quercetin, and kaempferol still exhibited high scavenging activities at 50 µM (98%; 91±2%; 86±5%; 92±2%). AA, FA, and rutin had intermediate scavenging activities (71±3%; 54±1%; 65±7%). At 50 µM all of the substances, apart from trolox, were above the EC_{50} value (concentration required to decrease the initial chemiluminescence intensity by 50%). Trolox had the lowest scavenging activity in the measurements (40±8%, figure 25 B). The great number of experimental protocols for CL measurements with luminol impedes the possibility of direct data comparison in the literature. EC_{50} values reported for trolox (10.0±0.4 µM), AA (23.7±0.4 µM) and quercetin (0.9 µM) in one publication differ from our results [271]. However, the initial H_2O_2 concentration in the assay, the ROS generation mechanism as well as the buffer solution were different from ours. The parameters have been reported to have an impact on the measured CL from luminol [272]. This can explain the discrepancies between the reported results. The data agree in terms of quercetin being a more potent radical scavenger than the other two substances in this setting. Referring to the results obtained with this assay, the ranking of the plant compounds for their radical scavenging activity at 50 µM is as follows:

CA > kaempferol ≥ EGCG > quercetin > trolox > AA > rutin > FA.

The radical scavenging activity of the GP extract correlates to the employed concentration (0 to 600 µg/mL, figure 25 C). The slope of the fitted linear function ($f(x)=bx$ with $b=0.155\pm0.01$) corresponds to parameters reported before for other plant extracts. Between the individual measurements of the extract, high standard deviations were recorded. This can be due to the higher complexity of the sample and possible interferences between the different plant compounds.

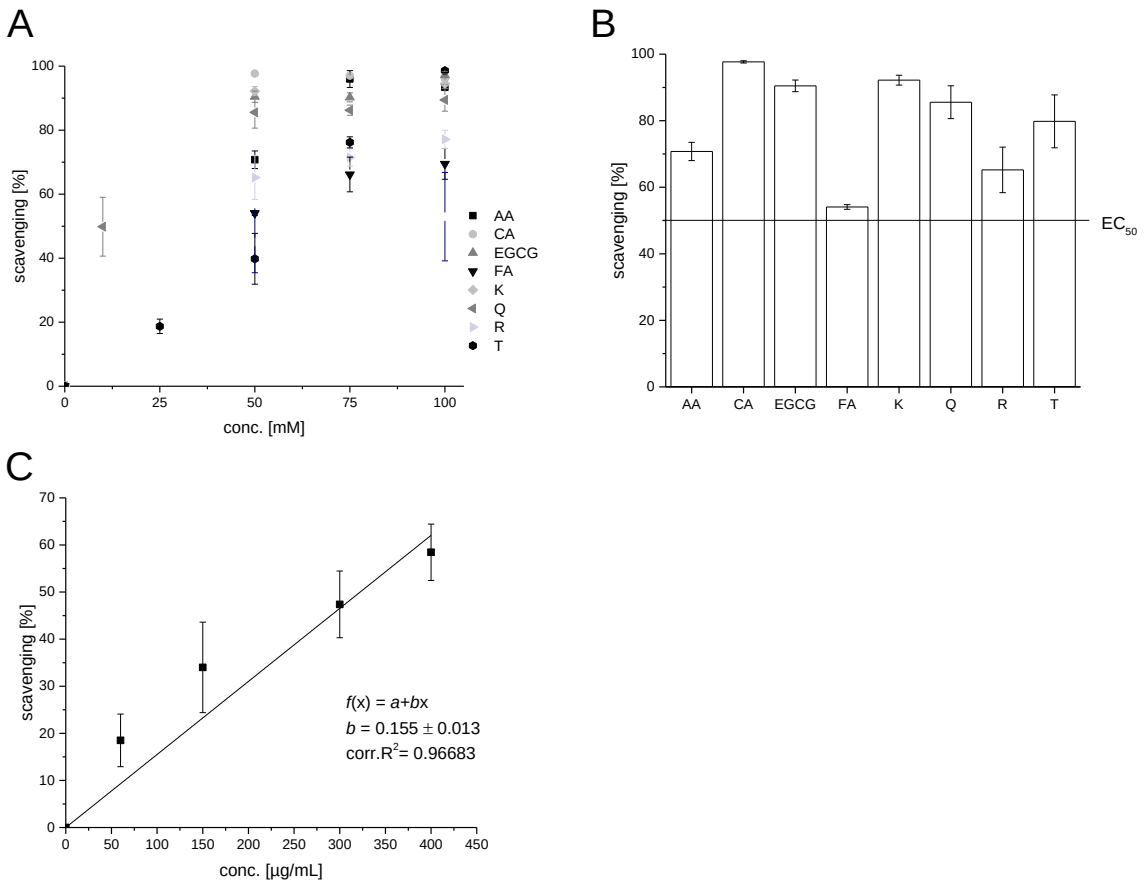

Figure 25: Radical scavenging activities of different plant substances in the luminol assay. A) Radical scavenging in dependence on the concentration of plant substance (0 to 100 µM). B) Comparison of radical scavenging activity of plant substances at 50 µM. C) Radical scavenging activity of GP extract at different concentrations. Data represent the mean of n=10 independent measurements normalized to a blank measurement and standardized to measurements without plant substance. AA: ascorbic acid; CA: caffeic acid; EGCG: epigallocatechine gallate; FA: ferulic acid; K: kaempferol; Q: quercetin, R: rutin; T: trolox, GP: *Gynostemma pentaphyllum* extract.

The advantage of the luminol assay is that it evaluates the scavenging activity towards the biological relevant hydroxyl radical. However, generation of the radical via the Fenton reaction make a distinction between the radical scavenging ability of a substance and its metal chelating ability impossible. Both, metal chelating of the iron ions at well as scavenging of the hydroxyl radicals, result in a reduction of the effective radical concentration in the system and therefore in a decrease of the measured CL.

Several experimental parameters influence the luminol-based CL. Hastings at al demonstrated that different cell culture media can influence the CL from luminol [273]. We observed the same phenomenon assessing the scavenging ability of GP extract in RPMI-1640 cell culture medium. The presence of the media significantly altered the CL values measured in the experiments.

4.2.2. *p*-NDA assay

In neutral or alkaline media *p*-nitroso-*N*,*N*-dimethylaniline has a large extinction coefficient (3.4×10^{-4} $M^{-1}cm^{-2}$) at λ=440 nm [274]. The reaction with hydroxyl radicals can destroy the

chromophore leading to a bleaching of *p*-NDA, which can be monitored by the reduction of the absorption at 440 nm. Adding a radical scavenger to the solution will decrease the rate of bleaching induced by the radicals [274].

Like in the luminol assay the bleaching of *p*-NDA does not require the use of rather stable radicals, like ABTS or DPPH that do not possess any biological significance. Rather it assesses the ability of molecules to interact with the biologically relevant hydroxyl radical. The measured absorbance values were normalized to measurements without H_2O_2. Relating the decrease of the *p*-NDA signal over time (0 to 150 min) to the data obtained without the addition of a plant substance, yielded the reduction of the radical induced bleaching effect by the plant compound:

$$\text{decrease bleaching [\%]} = ((A_{\text{AOx}} - A_{H_2O_2}) / A_{H_2O_2}) \times 100$$

with: A_{AOx} =normalized absorbance of *p*-NDA solution with plant compound; $A_{H_2O_2}$ =normalized absorbance of *p*-NDA solution without plant compound.

The results of this assay demonstrate that all of the tested plant compounds were able to reduce the bleaching effect of the *p*-NDA molecule by hydroxyl radicals at a concentration of 100 µM. Rutin, kaempferol, EGCG and trolox were the most potent substances in this assay. In the presence of 100 µM of the substances the bleaching after 150 minutes decreased by 250±5%, 137±7%, 130±4% and 125±4%, respectively. Addition of AA, CA, FA and quercetin did also decrease p-NDA bleaching measured after 150 minutes but to a lesser extent (30±3%; 37±6%; 75±6%; 26±6%; figure 26 B).

In figure 26 A the decrease of *p*-NDA bleaching by the individual substances is shown over time. The temporal development allows a distinction of the individual substances into three different groups. The first group of substances exhibits more or less constant bleaching decreasing activity over 150 minutes (FA and EGCG). In the second group the activity decreases over time (CA, quercetin and AA). In the third group the activity increases over time (rutin, kaempferol and trolox).

We corrected the data for blank measurements without H_2O_2 that also included iron ions in order to subtract the effects of auto bleaching of the *p*-NDA molecule in the aerated solutions at the chosen pH [213]. Therefore, the bleaching effect observed is attributed to the effects of the radicals. The results are an indicator for the capacity of the substances to interact with hydroxyl radicals in at a physiological pH value.

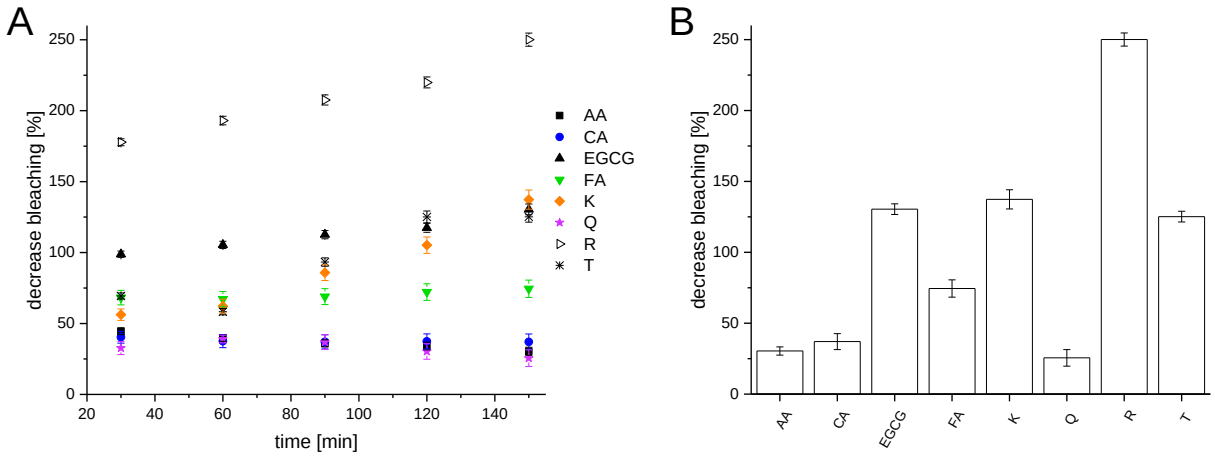

Figure 26: Reduction of the hydroxyl radical induced bleaching of *p*-NDA by different plant compounds. A) The decrease of bleaching by the plant compounds in a solution containing 50 mM *p*-NDA. B) The decrease of *p*-NDA bleaching in comparison to the control after 150 minutes. Data represent the mean of $n=4$ independent measurements ±SD at 100 µM plant compound concentration. The data is corrected for the blank measurement and related to the values obtained without the addition of plant compound (control).

Comparison of the results obtained with this assay yield quite a different ranking for the radical scavenging activity of the substances at 150 minutes reaction time:

rutin > kaempferol ≥ EGCG > trolox > FA > CA > AA > quercetin.

One important parameter for the radical scavenging activity of molecules are the number and position of functional groups ([275]; see also introduction and chapter 4.2.1.3.). Rutin and EGCG possess the highest number of OH-groups from the investigated substances (10 and 8 OH-groups, respectively). This could contribute to their high activity in this assay.

The order of activity in the *p*-NDA assay is different from the one obtained with the luminol assay. Especially the radical scavenging activities of rutin, CA, quercetin and FA are ranked differently by the two methods. On the other hand, the ranking of kaempferol and EGCG is equal with both assays. The main differences between the two assays were the initial concentration of H_2O_2 (luminol: 2×10^{-3} M vs. *p*-NDA 10^{-2} M), the source of iron ions (Fe-EDTA vs. $Fe(II)Cl_2$), the pH (5.5 vs. 7.2) and the fact that *p*-NDA, in comparison to luminol, is rather specific for hydroxyl radicals.

Measurement of the GP extract with the *p*-NDA method was not possible because the extinction of the plant extracts overlay with the extinction of *p*-NDA at 440 nm.

4.2.3. Carotene-bleaching assay

The luminol assay as well as the *p*-NDA bleaching assesses radical scavenging processes in the aqueous phase. To obtain corresponding data on the behavior of the plant compounds in the lipid phase, we choose as a third reference method for the evaluation of the plant compounds *in-vitro*

the carotene-bleaching assay (CBA). As mentioned in the introductory part β-carotene is a plant chromophore with a distinct orange/red color. Upon oxidation the molecule is decolorized, which can be followed via the decrease of its absorption maximum at λ=460 nm. Addition of a radical scavenger will slow down or inhibit the bleaching. Unlike in the other two reference assays, the radicals were not generated by the Fenton reaction but by the heat induced coupled oxidation of linoleic acid and β-carotene in an emulsified, aqueous solution ([276], [214]). The peroxyl radical formed from the linoleic acid (LOO·) does react with the β-carotene molecule to form a radical adduct (eqn. 3.6, [277]).

$$\beta\text{-carotene} + \text{LOO}\cdot \rightarrow \beta\text{-car-OOR}\cdot \qquad (3.6)$$

The results of the assay demonstrate that all the investigated substances decreased the rate of β-carotene bleaching over a period of 2 hours. The concentration of the plant substances was 50 µM. Figure 27 A shows the decrease of the absorption at 460 nm over time. In the sample without plant substance (control) the absorption is reduced to 44±2% of the initial signal. Addition of the different plant compounds (50 µM) slowed down the bleaching rate. After 120 minutes the measured absorption was still between 74 and 95 % of the initial signal (AA: 74±9%; CA: 78±13%; FA: 81±10%; EGCG: 88±12%; rutin: 95±4%; kaempferol: 83±11%; quercetin: 90±1%; GP extract: 85±2%). Especially, rutin was very potent in reducing the bleaching of β-carotene in the system. The percentage reduction of the bleaching effect induced by the coupled oxidation of linoleic acid and β-carotene in comparison to the control measurement after 120 min is shown in figure 27 B. The reduction of bleaching for the different plant compounds was as follows: AA: 13±8%; CA: 20±4%; FA: 24±8%; EGCG: 30±5%; rutin: 38±8%; kaempferol: 29±5%; quercetin: 30±6%; GP: 26±11%.

Plotting the reduction of bleaching obtained for each plant compound against the number of OH-groups within the individual molecules yields a positive linear correlation between the two parameters (figure 27 C; linear fit; R^2=0.7417). This indicates that the number of functional OH groups is an important parameter for the radicals scavenging activity of a molecule. The importance of the number as well as of the position of OH groups of a molecule for its radicals scavenging potential has been demonstrated before [275]. The only substance that does not obey the rule in this experimental setting is AA. However, in comparison to the other molecules AA has a much higher water solubility (333 g L^{-1} [278]), while it is insoluble in fats or oils [279]. AA is therefore less likely to interact with radicals in the lipid phase. This does also explain why AA has the lowest activity in this assay. The order of the investigated plant substances according to their reduction of β-carotene bleaching at a concentration of 50 µM is as follows:

rutin> kaempferol ≥ EGCG ≥ quercetin> FA> CA> AA.

The order differs from the results of the luminol assay. However, apart for the ranking of quercetin the results correspond to the activity order obtained with the *p*-NDA assay.

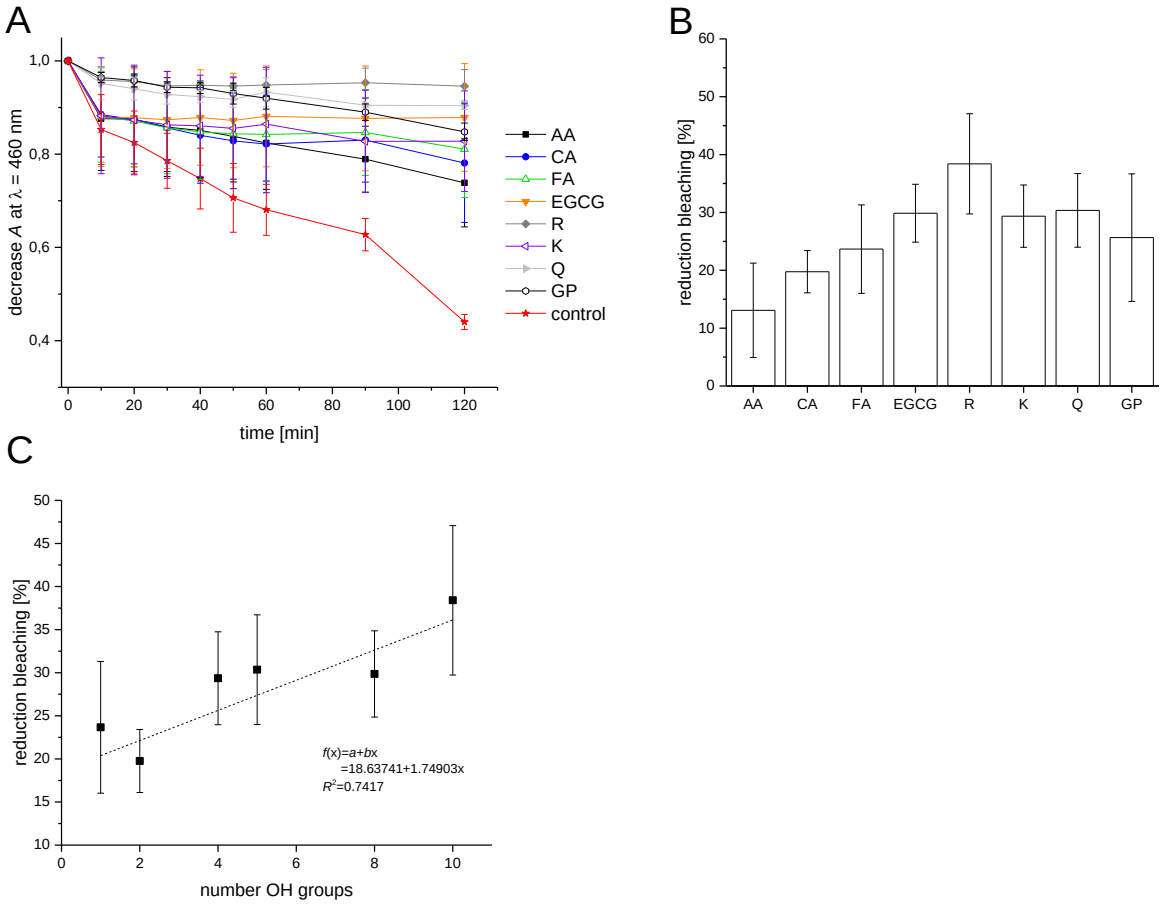

Figure 27: A) Decrease of the absorption signal of β-carotene solution at 460 nm upon heat induced oxidation. B) The reduction of carotene bleaching by the addition of individual plant in comparison to the control measurement after 120 minutes. C) Correlation between the reduction of bleaching to the number of OH groups within the individual molecules (linear fit; Origin software; R^2=0.7417; exception: AA). Data represent the mean values from n=4 independent measurements ±SD.

4.2.4. Evaluation with the electrochemical sensor assay

The radical scavenging activities of the individual plant substances were evaluated in a fourth experimental setting by the electrochemical assay. Measurements with rutin, kaempferol and quercetin produced very high standard deviations and showed no concentration dependency. All three substances belong to the group of flavonoids and share the same molecular structure of the flavone backbone (2-phenyl-1,4-benzopyrone). Flavonoids absorb strongly in the UV-B region of the light spectrum thus playing an important part in the photo-protection of plant parts exposed to sunlight [280]. The direct interaction with UV-radiation in the experiment could prevent the generation of ROS from photolysis. Therefore, the measurements might reflect the prevention of ROS generation instead of the ROS scavenging activity. In case of quercetin the low water solubility of the molecule (0.06 g L^{-1}; [281]) might be an additional factor for its inconsistent performance as radical scavenger in the assay. Rutin is a glycoside of quercetin with the added disaccharide

rutinose (see introduction). UV-B and UV-C light induced degradation of the molecule might lead to a cleavage of the disaccharide moiety [282]. This would explain the similar behavior of quercetin and rutin in the electrochemical assay. Kaempferol differs from quercetin only in its degree of hydroxylation (mono- instead of dihydroxylated). The molecule demonstrates therefore similar (slightly enhanced) UV-B adsorbing properties [283].

All of the other substances could slow down the process of ROS induced degradation of the SAM. From the slope of the function (current increase at the SAM covered electrodes vs. ROS exposure time from 30 to 300 seconds) the radical scavenging activities were calculated. The data was compared to measurements without plant compound. For all substances the standardized logarithm of the measured currents ($\ln(1-[I/I_0])$ changed linearly within the first 300 seconds. In the measurements with added plant compounds, the linear section of the function was elongated. However, since the control measurements often reached a plateau after 300 seconds treatment the radical scavenging activity was determined from the data up to 300 seconds.

Figure 28 shows the typical current increase in DPV measurements at SAM covered electrodes with different concentrations of plant compound added (in this case 50 to 200 µM AA). The more plant compound added the flatter the corresponding curve becomes, indicating that the current increase and therefore the SAM destruction rate by ROS at the electrode is slowed down. From the slope of the curve the radical scavenging activity of the individual plant substance at its respective concentration is calculated. The resulting radical scavenging activity calculated for AA from this graph are AA 50 µM: 58±7%, AA 100 µM: 82±3% and AA 200 µM: 88±2%.

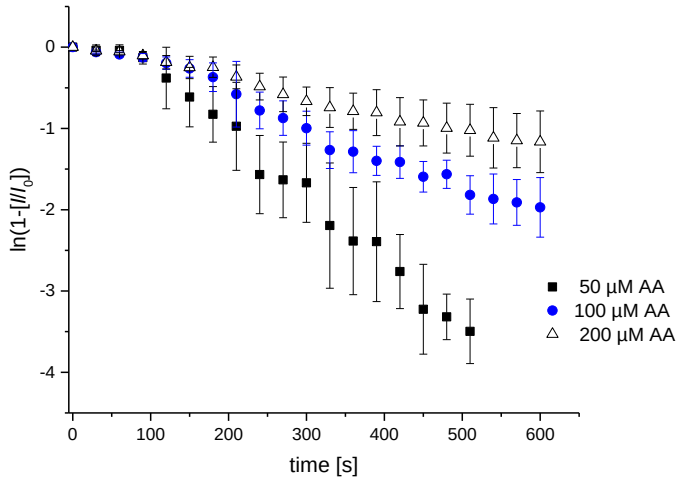

Figure 28: DPV currents (I) measured at $C_{10}SH$ SAM covered gold electrode in the presence of AA after different exposure times to photolytically generated ROS.

At a concentration of 100 µM all of the investigated plant substances showed significant radical scavenging activities against 10^{-3} M H_2O_2 in photolysis (AA: 82±3%; CA: 97%; FA: 75±4%; EGCG: 94%; trolox: 99%; figure 29 A). The activities of the substances were concentration dependent as

demonstrated in figure 28 for AA. The order of radicals scavenging activity for the individual plant compounds calculated from the data of the electrochemical assay is as follows:

trolox> CA> EGCG> AA> FA.

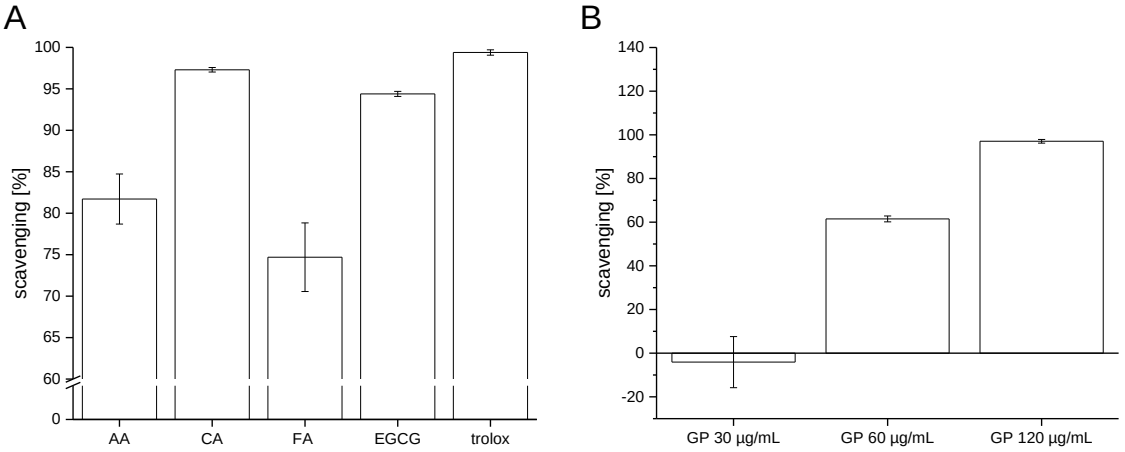

Figure 29: A) Radical scavenging activities calculated for A) different plant substances (conc. 100 µM) and B) different concentrations of *G. pentaphyllum* extract (GP). Scavenging values are calculated from the slope of the current regain in DPV measurements in comparison to the control.

The ethanolic GP extract exhibited radical scavenging activity in a dose-dependent manner. At the lowest concentration (30 µg/mL) the extract had no radical scavenging properties and large standard deviations between individual measurements were recorded, with some measurements even demonstrating prooxidative activity of the plant extract ($-4\pm11\%$ radical scavenging activity). However, at higher concentrations (60 and 120 µg/mL) the radical scavenging activity of the extract increase with the employed concentration in the electrochemical assay ($62\pm1\%$ and $97\pm1\%$, figure 29 B). Hilgemann et al assessed with a slightly different version of the electrochemical assay the radical scavenging of five different medicinal plant extracts (*Cymbopogon citratus, Psidium guajava, Achyrocline satureoides, Baccharis genistelloides, Matricaria chamomilla*) against ROS generated in the Fenton reaction [3]. At a concentration of 100 µg/mL the different plant extracts exhibit radical scavenging activities between 50 to 73%. The highest activity reported in this assay was at 86% for 200 µg/mL *Matricaria chamomilla.* Taking this value as reference, the radical scavenging of GP is very high in comparison to other medicinal plant extracts. However, the comparison has some limitation because the plant extracts investigated by Hilgemann et al [3] are obtained by aqueous extraction (30 minutes with boiling water), while the GP extract is an ethanolic extract. Therefore, the profile of contained substance classes in both extracts is expected to be different. Previous studies demonstrated that the mode of extraction significantly influences the radical scavenging activity of the plant extract [284]. Furthermore, it must be considered that the generation of radicals was different in the two experimental set-ups (Fenton reaction vs. photolysis).

4.2.5. Comparison of the *in-vitro* antioxidant assays

The comparison of the electrochemical assay with the DPPH assay in previous work demonstrate the differences in the radical scavenging activities determined with both methods [2].The data obtained from the luminol assay, the *p*-NDA assay, the CBA and the electrochemical assay demonstrate the antioxidant activities of the plant substances. However, the absolute values of ROS scavenging activity as well as the order of activity for the investigated substances differ between the assays (table 3). This observation can be explained by the fact that all assays have slightly different experimental parameters. Considering the different techniques of ROS generation in the antioxidant assays, it is obvious that their results also reflect the UV absorption or Fe^{2+}-chelation properties of the substances along with their ROS scavenging activities. The contribution of UV absorption and/or Fe^{2+}-chelation on antioxidant assay results has been reported before [285].

Quercetin, rutin, kaempferol and CA have been demonstrated to act as Fe^{2+}-chelators at neutral pH [285], [286]. The ability to chelate iron ions inhibits the Fenton reaction and is, therefore, an attribute that enhances the antioxidant activity of a compound in the Fenton reaction. However, changes in the pH affect the metal-chelating properties of quercetin, rutin and kaempferol [286]. Other studies demonstrate the ability of quercetin, rutin and kaempferol to reduce iron ions under specific conditions, which has a prooxidative effect in the Fenton reaction [287]. The observed effects of the substances on the Fenton reaction and the related extent of hydroxyl radical formation depend on the pH and the concentration ratio of the compounds to the number of iron ions [287]. Besides, the nature of the transition metal ions is a relevant parameter. While flavonoids failed to enhance the Fenton reaction in the presence of pure ferric salt, ferric-ADP or ferric citrate, they intensify the reaction in the presence of EDTA–ferric ions [288]. This observation is of interest because in the luminol assay the Fenton reaction was accomplished with Fe-EDTA while in the *p*-NDA assay we applied $Fe(II)Cl_2$.

Additionally, flavonoids are known to adsorb UV light [283]. The later might explain why the electrochemical assay was not suited to evaluate the radical scavenging activities of the three flavonoids quercetin, rutin and kaempferol. The radicals that are required for the destruction of the SAM on the electrodes in this experimental setting are generated by the photolysis of H_2O_2. Substances that adsorb the UV light prevent the generation of ROS. Therefore, the measured current at the SAM covered electrodes is no longer an indicator for the radical scavenging ability of the plant compound but of its ability to prevent the generation of ROS in the first place.

As demonstrated in figure 27 C the antioxidant activity of the plant compounds (apart from AA) in the CBA assay correlate to the number of OH groups within the individual molecules. The assay is the only one that detects the antioxidant activity of the substances in the lipid phase. This can

explain the weak performance of AA in the assay. Comparison of the activity rankings obtained for each assay (table 6) shows the highest conformity between the ranking of the CBA and the *p*-NDA assay.

Table 6: Radical scavenging activity in four different in-vitro assays of different plant substances and *Gynostemma pentaphyllum* extract. Listed are the source of ROS in the individual assays, the phase of antioxidant interaction and the performance of the individual substances in the assay

assay	ROS source	phase	Activity order (at 50 to 100 µM)	Effects GP extract
Luminol	$2x10^{-3}$ M H_2O_2; Fenton	aqueous	CA> kaempferol≥ EGCG> quercetin> trolox> AA> rutin> FA	Antioxidant; conc. dependent
***p*-NDA**	10^{-2}M H_2O_2; Fenton	aqueous	rutin > kaempferol ≥ EGCG > trolox > FA > CA > AA > quercetin	Not measurable
CBA	Heat induced oxidation	lipid	rutin> kaempferol≥ EGCG≥ quercetin> FA> CA> AA	Antioxidant
Electro-chemical	10^{-3} M H_2O_2; UV	aqueous	trolox> CA> EGCG> AA> FA	Antioxidant; conc. dependent

The activity values of kaempferol and EGCG are very similar in the CBA, luminol and *p*-NDA assay, respectively. The similarity of the substances is not directly derivable from their molecular structure (number of OH groups) nor from their physical properties (molecular mass, water solubility).

In summary, the antioxidant activity assay *in-vitro* yield different relative as well as absolute radical scavenging activities for the individual plant substances.

4.3. Measurements in cell culture

After evaluation of the electrochemical assay and the radical scavenging activities of the different plant compounds in a cell-free environment, the experiments were transferred to cell culture-based set-ups.

4.3.1. Electrochemical assay measurements

4.3.1.1. Assessment of ROS from human keratinocytes (HaCaT)

We tested the behavior of the electrochemical assay in cell culture measurement. The objective was to measure enhanced levels of extracellular ROS from stimulated cells. The experiments were first performed on a human keratinocyte cell line (HaCaT). Skin cells are a model of interest for redox processes because they serve as the first line of defense against environmental factors such as UV light or toxins. HaCaT cells contain/release different ROS damage product such as 8-Isoprostane and exhibit enhanced carbonylated protein content after H_2O_2 or UV-B light

stimulation [289]. Another chemical to induce redox changes in HaCaT cells is *t*BHP. It induces the continuous stepwise productions of intracellular radical substances and its effects are therefore longer lasting [290].

Treatment with sublethal concentrations of *t*BHP (<200 µM) has been reported to affect the intracellular GSH/GSSG ratio, to promote hydroxyl radical formation, [291] and to increase intracellular ROS measured with the fluorescent probe CDCFH[11] [292].

We tested if the effects, induced by 1 hour-treatment with 100 µM *t*BHP in HBSS, could be detected by the sensor electrode. The $Ru(NH_3)_6^{3+}$ ion reduction current at the SAM covered electrodes was measured after 30, 60, 90, 360 and 600 seconds exposure to the treated cells. Figure 30 shows the development of the current (I) measured at the electrodes normalized to the initial current at the cleaned gold electrode (I_0) over time. After an initial current increase, the electrode reached its initial state again. The maximum current I measured after 360 seconds is only 0.2% of I_0. The increase of I is not linear to the exposure time. One possible explanation for the observed behavior is the low concentration of ROS expected in the measurements. The decrease of I measured at the electrodes after 600 s incubation with the cells can be interpreted as the reorganization of the SAM or alternately as the adsorption of molecules from the cell culture. Although the medium was washed off before the measurements and the HBSS components (KCl, KH_2PO_4, $NaHCO_3$, NaCl, Na_2HPO_4, D-Glucose) are not likely to interact with the SAM, artefacts from the cells or the medium can still interact with the electrodes. Repetitive measurements at *t*BHP, H_2O_2 or ethanol stimulated HaCaT cells demonstrated that the procedure could not affect the SAM to the extent that I would increase by more than 0.4% of I_0.

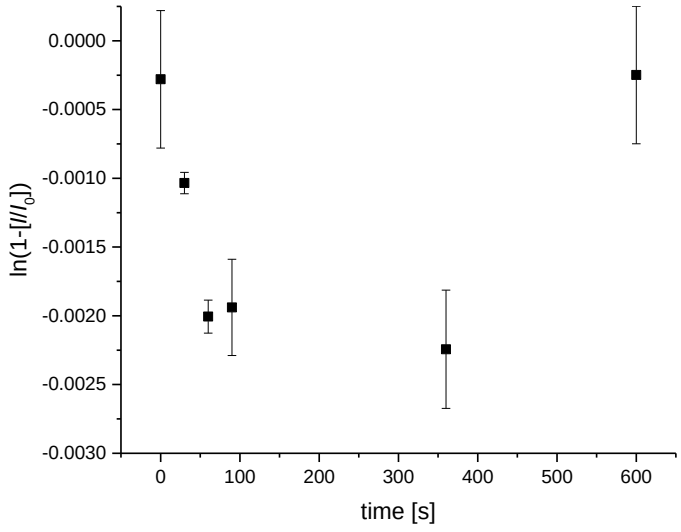

Figure 30: Temporal development of the $Ru(NH_3)_6^{3+}$ ion reduction signal at SAM covered gold electrodes after exposure to 100 µM *t*BHP stimulated HaCaT cells in HBSS. The current measured at the electrodes (I)

[11] 6-caboxy-2',7'-dichlorodihydrofluorescein diacetate

was related to the initial current measured at the cleaned gold electrodes (I_0). Data represent the results of n = four independent measurements ±SD.

Since we assumed that the concentrations of ROS released by stimulated HaCaT were below the detection limit of the electrochemical assay, we focused on cells that released elevated amounts of ROS into the extracellular space.

4.3.1.2. Detection of superoxide release from Nox5-HEK293 cells

It has been shown that the NADPH oxidase Nox5 produces superoxide radicals upon PMA stimulation via protein kinase C (PKC) activation [293]. The superoxide release from Nox5-HEK293 was monitored in a real-time measurement with the fluorescence probe L-012. After a stable baseline signal Nox5-HEK293 were injected into the test solutions. The injection resulted in an initial spiking of the signal caused by external light and oxygen until the signal stabilized again at around 1,900 RLU. Injection of PMA significantly increased the emitted light. The increase was most pronounced 500 s after injection (about 100-fold) and light emission stayed elevated onwards at around 160,000 RLU. The increased light emission from L-012 demonstrates that PMA could stimulate superoxide release from the cells over a longer period. Addition of SOD immediately reduced the emitted light by 98% supporting the assumption that the fluorescence signal was caused by superoxide in this system (figure 31 A).

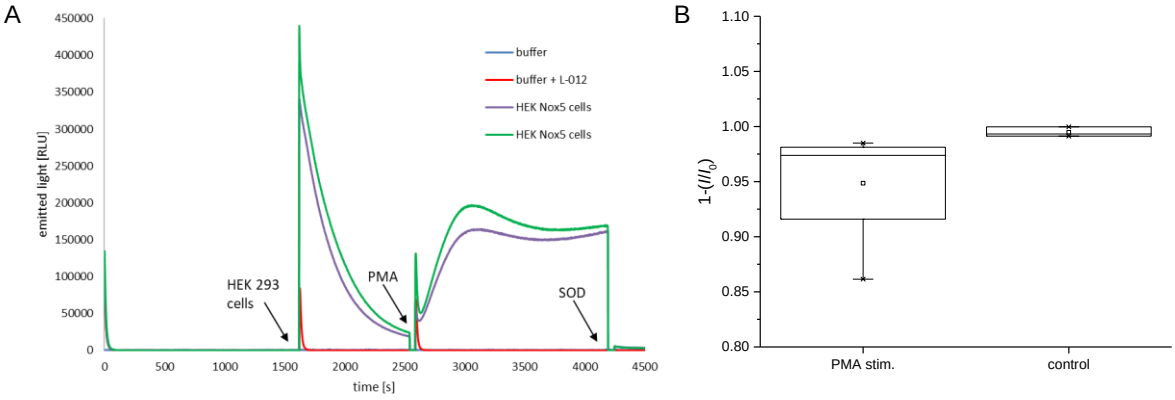

Figure 31: Superoxide production from Nox5-HEK293 cells in HT buffer measured with the fluorescence probe L-012. Arrows indicate the time points of injection to the L-012 solution (cells; PMA; SOD). Measurements were performed with HT buffer (blue line), L-012 + buffer (red line) and buffer + L-012 + HEK Nox5 cells (purple and green lines). B) Increase of the $Ru(NH_3)_6^{3+}$ ion reduction current at SAM coated Au electrodes after 300 s incubation with Nox5 HEK 293 cells in HT (stimulated with PMA 20 min prior measurement or unstimulated). Boxplots present data of n=3 independent measurements.

The measurements with the fluorescence probe L-012 verified that under the experimental conditions the PMA stimulated HEK Nox5 cells release measurable concentrations of superoxide into their environment. In a next step, we tested if the superoxide was detectable with the electrochemical assay. We exposed the SAM coated Au electrodes to PMA stimulated cells in HT

buffer for 300 seconds. A higher $Ru(NH_3)_6^{3+}$ ion reduction signal could be recorded at the electrodes after exposure to PMA stimulated cells compared to unstimulated ones (0.0051 ± 0.0025 vs. 0.0109 ± 0.0054, figure 31 B). This suggests that the higher concentration of superoxide released from stimulated cells influenced the SAM degradation process leading to a regain of the $Ru(NH_3)_6^{3+}$ ion reduction signal at the electrodes. However, the changes were only little suggesting only minor defects in the SAM. Further, it has to be noted that the sample size was too low to allow statistically reliable conclusions.

As demonstrated in a previous chapter (4.1.5.), we tested if the SAM degradation process could indeed be caused by superoxide itself. The superoxide radicals were generated in a cell free environment at TiO_2 nanoparticles with SSL in HT buffer and in water. The formation of superoxide was monitored with NBT. A decrease of NBT absorption at 260 nm was measured over time as an indirect parameter for superoxide generation, which reacts with NBT to form an insoluble formazan at the TiO_2 nanoparticles [211]. The exposure of SAM coated Au electrodes towards the generated superoxide did not affect SAM integrity in a measurable way in HT buffer and also the SAM degradation process by superoxide in water had only little effects on the measured DPV signals at the electrodes. In HT buffer no measurable $Ru(NH_3)_6^{3+}$ ion reduction occurred up to an exposure time of 2100 s at the electrodes (figure 24). A possible explanation would be the low concentration of superoxide generated at the TiO_2 nanoparticles. Though the concentration of superoxide released by Nox5-HEK293 cannot be expected to be higher, potential secondary reaction partners as well as other cell metabolites might interact with the SAM. At this point is must be considered that ROS generation at TiO_2 nanoparticles is not limited to superoxide anions. Hydroxyl radicals, hydrogen peroxide and hydroperoxyl radical are also expected to form [211], though their contribution is smaller under the chosen light's wavelength [211]. However, the results indicate that the SAM degradation process and consequently the regain of the $Ru(NH_3)_6^{3+}$ ion reduction signal at the electrodes is not primarily caused by superoxide itself.

Therefore, the difference between electrochemical measurements at the control and the PMA cells must be explained by secondary ROS that arise from the released superoxide from stimulated cells. At this point it is noteworthy that though L-012 has been titled a sensitive CL probe for $O_2^- \cdot$ [171], later studies demonstrate that peroxidase and H_2O_2 induce L-012-derived CL in the presence of oxygen. In fact, $O_2^- \cdot$ alone does not react with L-012 to emit luminescence [172]. Since L-012 is not specifically detecting $O_2^- \cdot$ the increased L-012 CL signal measured at PMA stimulated cells might already entail ROS other than $O_2^- \cdot$ that contribute to the destruction of the SAM on the sensor electrodes.

4.3.1.3. Detection of hydrogen peroxide release from Nox4-HEK293 cells

In a third approach we exposed the sensor electrodes to a Nox4-HEK293 cell line expressing NOX4 upon tetracycline (TC) induction [216]. TC induces a rapid increase in NOX4 mRNA in the cell line followed by a release of ROS [216]. In contrast to other Nox enzymes, Nox4 primarily produces H_2O_2 instead of superoxide. The changed pattern in ROS production has been attributed to the third extracytosolic loop (E-loop) of Nox4, which sets it apart from Nox1 or Nox2. [216], [294] 24 hours after NOX4 induction with TC the amount of H_2O_2 released from the cells was quantified with AmplexRed. In figure 32 A the increase in the AmplexRed fluorescence signal in comparison to the baseline signal for TC stimulated and unstimulated cells is shown. The increase in the fluorescence signal was 56 ± 2 times for TC induced cells and 1.2 ± 0 times for cells not treated with TC. We therefore assume that the TC induction was successful and resulted in an elevated release of H_2O_2 from the cells in the extracellular space.

In the next step, we tried to detect the released H_2O_2 from the cells with the sensor electrode by exposing the SAM covered electrodes towards TC treated and untreated cells for 1 to 20 minutes. In figure 32 B the development of the current measured in DPV at the electrodes (I) normalized to the initial current measured at the electrodes (I_0) in dependence on the exposure time is shown. The current measured at electrodes exposed to unstimulated cells did not change significantly over the treatment time (figure 32 B, grey data points). The current measured at electrodes exposed to the stimulated cells on the other hand, increased slightly (figure 32 B, black data points). After 12 minutes of exposure, however, no further increase could be detected. We therefore assume that the released H_2O_2 induced SAM modifications at the sensor electrodes that resulted in higher currents measured in DPV. The sample size needs to be increased to verify the observed tendency. The higher standard deviation of the data from the stimulated cells indicate that the process of the SAM modification was heterogeneous, either because of variations in H_2O_2 concentrations released from the cells or because of differences in secondary effects at the electrodes (formation of secondary ROS, interaction of metabolites/buffer components with the electrode).

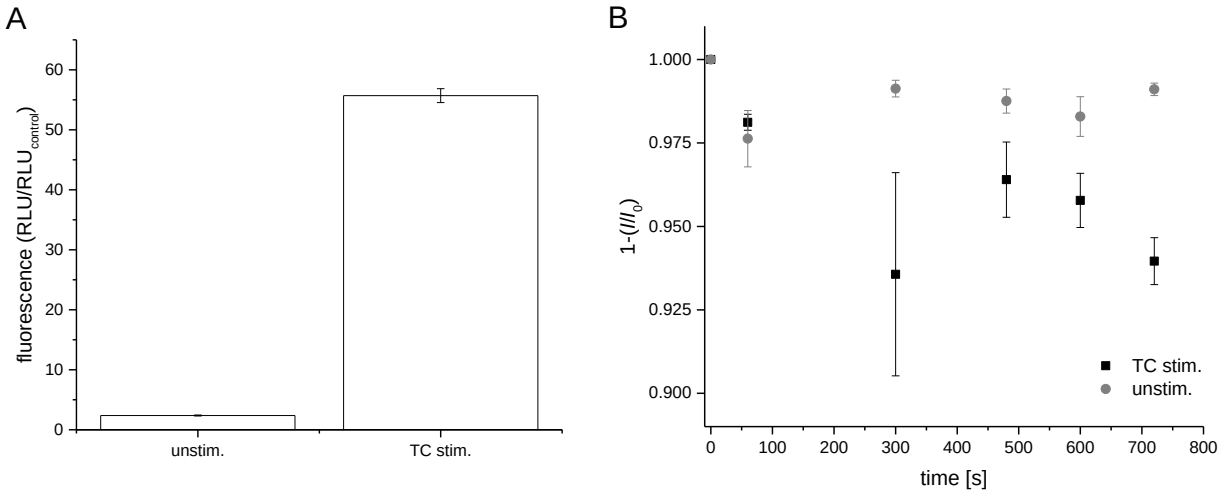

Figure 32: A) Fold change of the measured AmplexRed fluorescence signal from TC stimulated and unstimulated Nox4-HEK293. Data represent RLU from n=3 independent measurements ±SD corrected for the blank value (measurement performed without cells). B) $Ru(NH_3)_6^{3+}$ ion reduction currents measured at SAM modified gold electrodes in DPV in relation to the exposure time (60 to 720 seconds) to TC stimulated or unstimulated Nox4-HEK293. Data represent $n \geq 3$ independent measurements ±SD. The measured currents *(I)* were standardized to the currents measured at the clean electrode (I_0). Measurements were performed 24 hours after the TC stimulation.

Exposure of the sensor electrodes towards 10^{-3} to 10^{-5} M H_2O_2 in water did not have a measurable impact on the integrity of the SAM in DPV measurements (see chapter 4.1.2.). The changes that are induced by the TC stimulated Nox4-HEK293 can therefore not be attributed to H_2O_2 itself. As hypothesized for the signal regain at electrodes exposed to stimulated Nox5 cells, it is most likely that the released H_2O_2 forms secondary ROS that interact with the SAM. The control measurements with unstimulated cells demonstrate that the H_2O_2 is required as a precursor molecule to initiate SAM modification processes. Besides it has been proposed that Nox4 does not exclusively release H_2O_2 but that the claim is due to unspecific ROS detection methods or failure to detect superoxide caused by membrane compartmentalization of the generation product [295]. In fact it has been claimed that the Nox4 product consist of 90% H_2O_2 and 10% superoxide [295].

The extracellular ROS released by all three cell types (HaCaT, Nox4-HEK293, Nox5-HEK293) failed to modify the SAM of the sensor electrode on a large scale. Results published before on human peripheral blood mononuclear cells (PBMC) reported an increase of up to 9.6% at alkanethiol modified sensor electrodes after 20 minutes exposure to 200 ng/mL lipopolysaccharides (LPS) stimulated cells. The LPS from Gram-negative bacteria (*Salmonella typhimurium*) provoked the production of reactive oxygen species (oxygen burst). However, the recovery of current at the sensor electrode after 5 minutes exposure was also only at 0.4%. [2] In our experimental setting, we could not detect a further current increase at the electrodes after 12 minutes exposure. However, as could be demonstrated by the AmplexRed and the L-012 measurements the released ROS from the HEK293 cells did decrease after stimulation again.

Therefore, the period for ROS detection was limited and the degree of SAM degradation could not be enhanced beyond a certain exposure time.

We could detect small changes in the SAMs DPV behavior induced by the ROS released from Nox4-HEK293 and Nox5-HEK293 upon stimulation. The small changes leave little room to investigate the impact of the investigated plant compounds on the process. In fact, measurements that included prior incubation of the cells with AA yielded inconclusive results. Therefore, the investigation of the plant compounds' cellular effects with the electrochemical assay was not persuaded further in this work. Instead, the *in-vitro* data of the electrochemical assay were in the following compared to data on cellular redox parameters (proliferation under *t*BHP/H_2O_2 stimulation, GSH/GSSG ratio, total GSH content, mitochondrial ROS concentration) obtained by established cellular assays on C6 glioma and HaCaT cells.

4.3.2. Cellular effects of the plant compounds

4.3.2.1. Effects on metabolic activity and proliferation

The effects of the plant substances on the metabolic activity and on the cell proliferation of HaCaT cells were evaluated. For this purpose, the conversion of WST-8 by the cells was assessed. Since the conversion is dependent on the dehydrogenases activity in viable cells, the assays results combine information on the cell number and the enzyme activity. Therefore, the data is interpreted as the metabolic activity measured in the specific culture plate well. Figure 33 A demonstrates the dependency of the measured signal on the number of cells. In a range of 500 to 10,000 cells platted per well the fluorescence signal measured after 24 hours increases linear with the cell number (linear correlation; Pearson R^2=0.987). Incubation of the cells with 50 to 1,000 µM *t*BHP or H_2O_2 for 2 hours decreased the metabolic activity within the well in comparison to untreated control cells in a concentration dependent manner (figure 33 B). The impact of *t*BHP at higher concentrations was more pronounced than the effect of H_2O_2. This observation was reported before for HaCaT cells [296]. The phenomenon can be explained by the rapid metabolization of H_2O_2 preventing a depletion of total glutathione [296], in contrast to the treatment with organic peroxides. The higher stability of *t*BHP on the other hand results in a persistent stimulation of the cells.

In the following we stimulated the HaCaT cells with 100 µM *t*BHP to obtain a measurable effect on the metabolic activity without being lethal to too many cells (metabolic activity after 2 hours with 100 µM *t*BHP: 87±5%). We also tested the effects of DMSO and EtOH as possible solvents for the plant compounds on the metabolic activity of the cells (figure 33 C). At 2% v/v neither DMSO nor EtOH influenced the metabolic activity of the cells in a significant way (one-sided t-test, $p<0.05$). At concentrations > 5% v/v the substances significantly reduced the cellular activity and concentrations > 10% v/v were lethal to the cells. From these results, we conclude that dilution

of the plant substances with a final DMSO concentration of 0.8% v/v had no significant effects on the metabolic activity of the cells.

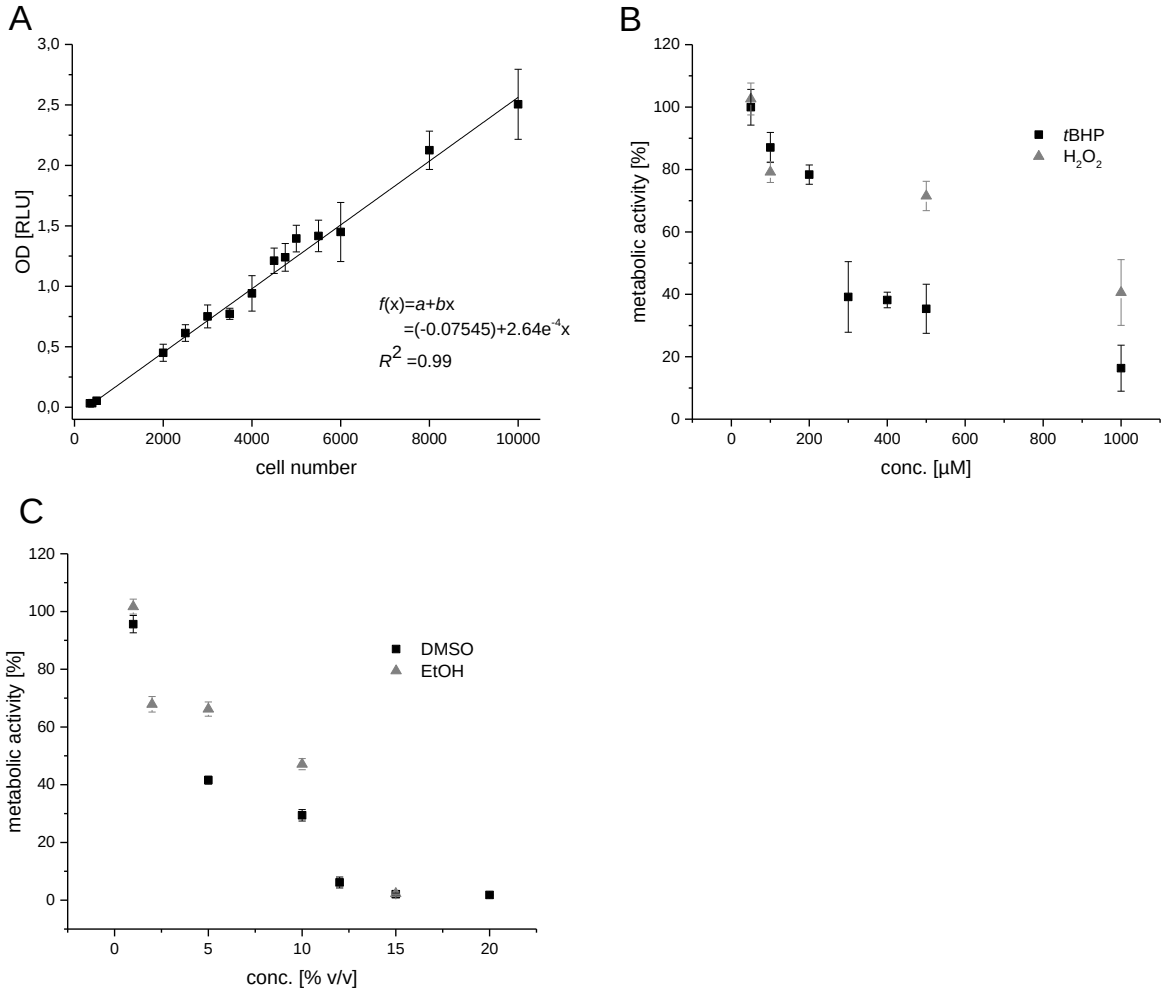

Figure 33: A) Dependency of the OD values measured in the WST-8 assay on the number of platted HaCaT cells (linear fit; Pearson R^2=0.987). B) Impact of different concentrations of *t*BHP and H_2O_2 (50 to 1000 µM) on the metabolic activity of HaCaT cells. C) Impact of different concentrations of ethanol (EtOH) and DMSO (1 to 20% v/v) on the metabolic activity of HaCaT cells. Data are presented as mean±SD of $n \geq 3$ replicates; the incubation time with DMSO, EtOH, *t*BHP and H_2O_2 was 2 hours.

Incubation of the cells for 24 hours with 100 µM of the individual plant compounds had different effects on the metabolic activity. For AA and CA a significantly increased metabolic activity was measured (149±7%; 127±13%; oneway ANOVA; Bonferroni correction; $p<0.05$). FA, rutin and trolox had no significant effects (97±3%; 101±9%; 104±5 %) and EGCG, kaempferol and quercetin reduced the metabolic activity (78±5%; 41±6%; 92±4%; figure 34 A). Reducing the concentration of EGCG, kaempferol and quercetin altered the effects of the substances on the metabolic activity of the cells. At 10 µM quercetin and EGCG affected the activity positively and the negative effect of kaempferol was reduced to a remaining metabolic activity of 94.6±4% of the control (figure 34 B). In the following the experiments the concentration of quercetin, EGCG and kaempferol was therefore reduced to 10 µM.

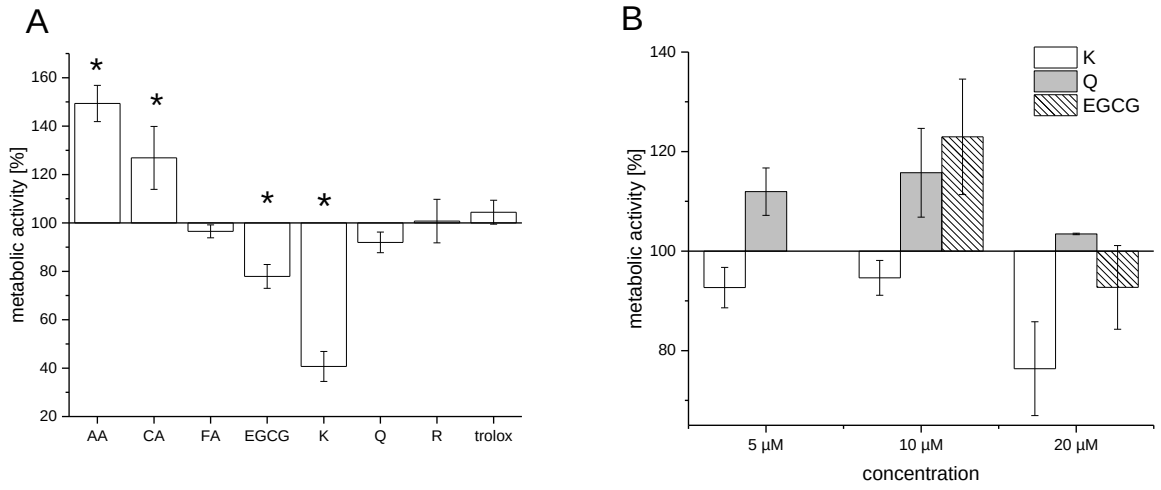

Figure 34: A) Metabolic activity of HaCaT cells incubated 24 hours with different plant substances at a concentration of 10^{-4} M. * mark mean values significantly different from the control (one way ANOVA, Bonferroni correction; $p<0.05$). B) Metabolic activity of HaCaT cells incubated 24 hours with 5, 10 or 20 µM K, Q or EGCG. The metabolic activity is related to the measured values of untreated control cells. Data are presented as mean±SD of $n\geq3$ replicates. AA: ascorbic acid, CA: caffeic acid, FA: ferulic acid, EGCG: epigallocatechin gallate, K: kaempferol, Q: quercetin, R: rutin

After 24 hours incubation with the plant substances (100 or 10 µM) the cells were stimulated with 100 µM *t*BHP. In the control group the treatment reduced the metabolic activity by 18.5±7%. The treatment had the same effect on cells that were previously incubated with AA, CA, FA, EGCG, kaempferol or quercetin. However, the extent of reduction indicated a trend towards higher values for cells incubated with FA, EGCG and kaempferol (22.8±8%; 23±5%; 25.1±11%). On the other side the mean value for the reduction in activity induced by *t*BHP treatment in cells incubated with AA, CA, quercetin, rutin and trolox was lower than the control mean value (9.9±5%; 10.2±9%; 12±7%;0.7±2%; 1.4±15%). The differences in the decreased viability of the cells upon *t*BHP stimulation were statistically not significant (figure 35 C). However, since the initial activities measured in treated cells were in some cases higher, the remaining metabolic activity after *t*BHP stimulation was significantly higher for cells treated with AA (132.8±8%) and CA (113.9±12%) than for control cells (84.7±8%) (one-way ANOVA; Bonferroni correction; $p<0.05$; figure 35 B).

Incubation of the cells with GP extract let to slightly increased mean metabolic activity values of the cells in comparison to the control ones, though the differences were not significant (30 µg/mL: 111.7±13%; 60 µg/mL: 109.3±8%; 120 µg/mL: 108±10%). After *t*BHP stimulation the cells treated with the GP extract exhibited significantly higher metabolic activities than the untreated control cells. This effect could be demonstrated at all three tested concentrations (30, 60, 120 µg/mL) (figure 35 A).

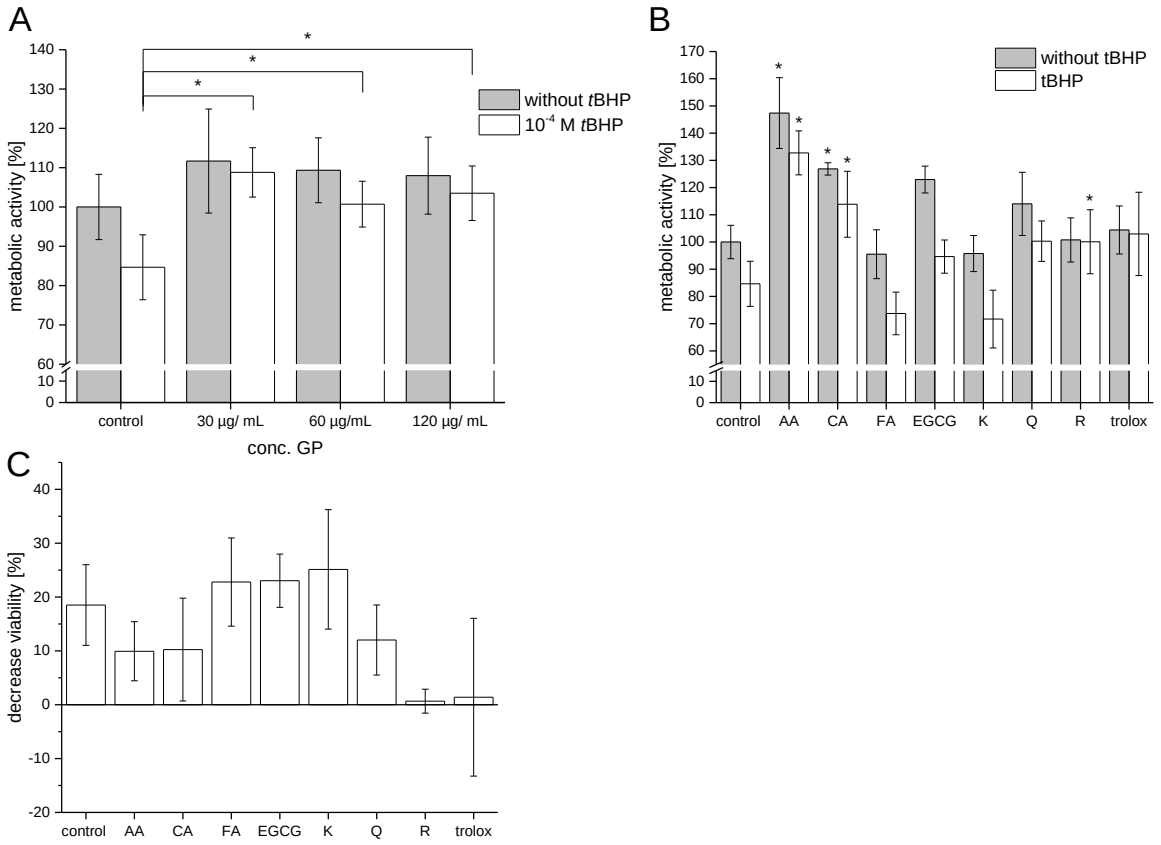

Figure 35: A) Comparison of the metabolic activites of HaCaT cells after 24 hours incubation with 0 (control), 30, 60 or 120 µg/mL GP extract with or without 1 hour stimulation by 10^{-4} M *t*BHP. B) Data from cells incubated with different plant extracts together with C) the resulting change in metabolic activity for the individual plant compounds. The concentrations for treatment were 10^{-4} M for AA, CA, FA, rutin (R) and trolox and 10^{-5} M for EGCG, kaempferol (K) and quercetin (Q); * mark mean values significantly different from the control (one-way ANOVA, Bonferroni correction; $p<0.05$).

As mentioned before increased absorbance measured in the WST-8 assay can either be due to a higher cell number (higher proliferation/ lower mortality rate) or higher enzymatic activity. Independent data on the cell number were obtained by cell counting, based on the separation of the cells by their physical properties. The technique allows to quantify the total number of cells in a sample (cells/mL) as well as to distinguish viable and dead cells (viability [%]). For cells treated with the different cell substances, the viability after 24 hours was between 96 and 88 %. The viability of cells treated with FA was significantly lower than from control cells (88±5% vs. 945±2%; $p<0.05$). The viability of cells treated with the other plant substances did not significantly differ from the control (figure 36 A). Stimulation of the control cells with 10^{-4} M *t*BHP for 2 hours decreased the viability of control cells to 86.9±2%. The viability of cells previously treated with plant substances ranged after *t*BHP stimulation between 85 and 95 %. The values are not significantly different from the control (AA: 92.6%; CA: 94.9±2%; FA: 90±2%; EGCG: 94±1%; kaempferol: 87±3%; quercetin: 93±1%; rutin: 92±1%; trolox: 85±7%; GP 30 µg/mL: 90±4; GP 60 µg/mL 93±2%; GP 120 µg/mL 89±1%; figure 36 A). The number of viable cells per mL after

48 hours growth was significantly increased for cells that were incubated for 24 hours with 100 µM AA and CA (control: 4.5±0.6 × 10^5 cells/mL vs. AA: 9.4±0.6 × 10^5 cells/mL vs. CA: 6±0.6 × 10^5 cells/mL; $p<0.05$; Bonferroni correction). Treatment with 100 µM *t*BHP for 2 hours decreased the number of viable cells in the control samples as well as in cells treated with AA, CA, FA, kaempferol and rutin. The number of viable cells were significantly higher after *t*BHP stimulation in cells treated with AA and significantly lower for cells treated with kaempferol in comparison to *t*BHP treated control cells (figure 36 B).

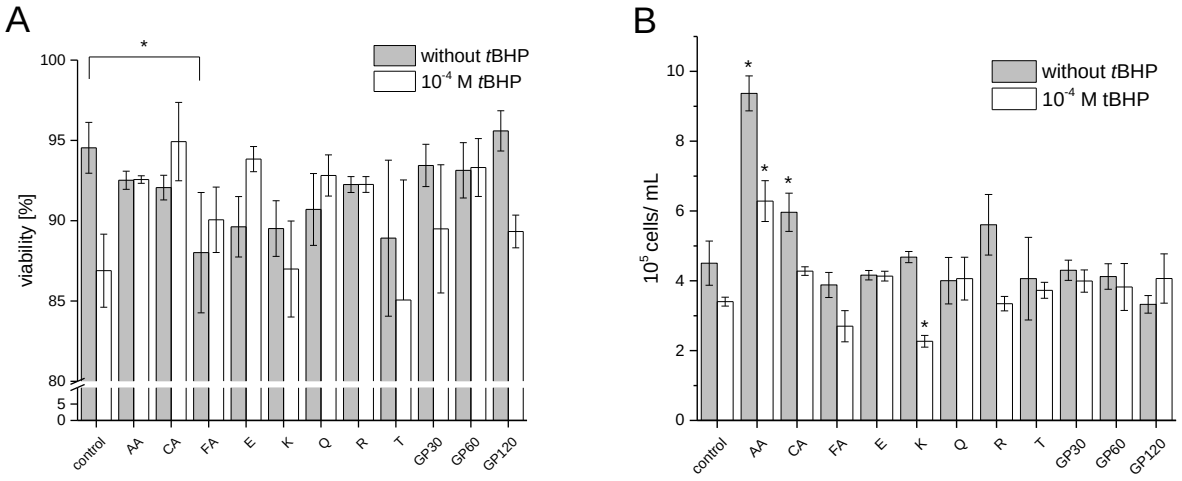

Figure 36: A) Viability of HaCaT cells grown for 48 hours with different plant compounds and upon stimulation with 100 µM *t*BHP for 2 hours and B) the corresponding cell number in the samples determined with a CASY cell counter. Data represent the mean of $n \geq 3$ samples ±SD. * mark significant difference to the corresponding control (with or without *t*BHP treatment; $p<0.05$)

The metabolic activity obtained with the WST-8 assay is correlated to the number of viable cells per mL obtained by cell counting (correlation coefficient 0.955; figure 37). The comparison between the two methods lead to the conclusion that, as expected, for HaCaT cells the metabolic activity measured is in fact mainly dependent on the number of viable cells in a sample and to a lesser extent on the activity of intracellular dehydrogenases.

The tendency of AA and CA to increase the proliferation of HaCaT cells is demonstrated with both methods (WST-8 and CASY cell count) as well as the negative effects of kaempferol in combination with *t*BHP on the cell number.

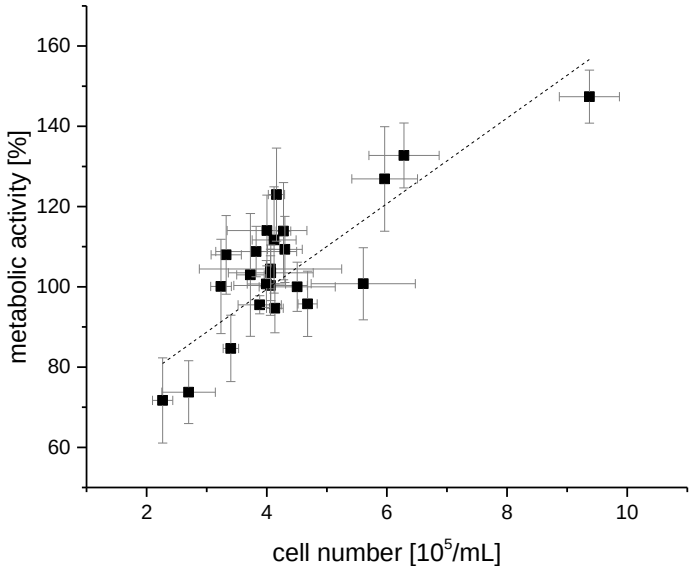

Figure 37: Correlation between the cell numbers measured with a CASY cell counter to the metabolic activity measured with the WST-8 assay (correlation coefficient=0.955). Data represent the mean of $n \geq 3$ samples $\pm$SD.

It has been reported before that trolox can influence cell proliferation by modulation of intracellular ROS levels in tumor cells both in a positive [297] and in a negative direction [298]. However, in HaCaT cells trolox failed to exert any significant effects on cell proliferation. In order to investigate the cell line specific effects of trolox further, we tested the effects of trolox on cell proliferation in a second setting with HyPer expressing C6 glioma cells. The experiments were performed on wild type cells (WT) as well as on tafazzin knock out cells (TAZ). Tafazzin is a mitochondrial acyltransferase that is involved in the remodeling of cardiolipin (CL), a phospholipid with four fatty acyl chains that can change in their composition [299]. The knock-down of tafazzin has been reported before to decrease cell proliferation in C6 glioma cells [300] as well as in neonatal ventricular fibroblasts [301]. We saw the same effect in our cell population. The total number of viable cells was significantly lower in TAZ cells at all time points in comparison to WT cells (figure 38 A+B).

Incubation with 50 µM trolox did not affect the cell proliferation of TAZ cells. In WT cells trolox treatment increased the cell number after 24, 72 and 96 hours significantly, but the observed effect was little (19$\pm$1-fold increase vs. 20.7$\pm$0.4-fold increase after 96 hours incubation, figure 38 A). Additional stimulation with 50 µM H_2O_2 every 24 hours increased the differences between trolox treated and untreated calls. The cell proliferation was significantly enhanced in WT cells incubated with trolox + H_2O_2 in comparison to cells treated only with H_2O_2 (figure 38 B). In TAZ cells a significant positive effect of trolox + H_2O_2 treatment on cell proliferation was seen after 96 hours growth time (5.5$\pm$0.1-fold increase vs. 6.6$\pm$0.3-fold increase, figure 38 B). The absolute cell number after 96 hours was reduced in WT cells grown without trolox upon H_2O_2 stimulation

(16.0±0.5-fold increase vs. 18.9±0.8-fold increase). In TAZ cells the H_2O_2 treatment reduced the number of viable cells counted after 96 hours regardless of the additional treatment with trolox. H_2O_2 stimulated WT cells grown with trolox reached similar cell numbers after 96 hours like the unstimulated WT cells (21±1 vs. 20.7±0.4-fold increase).

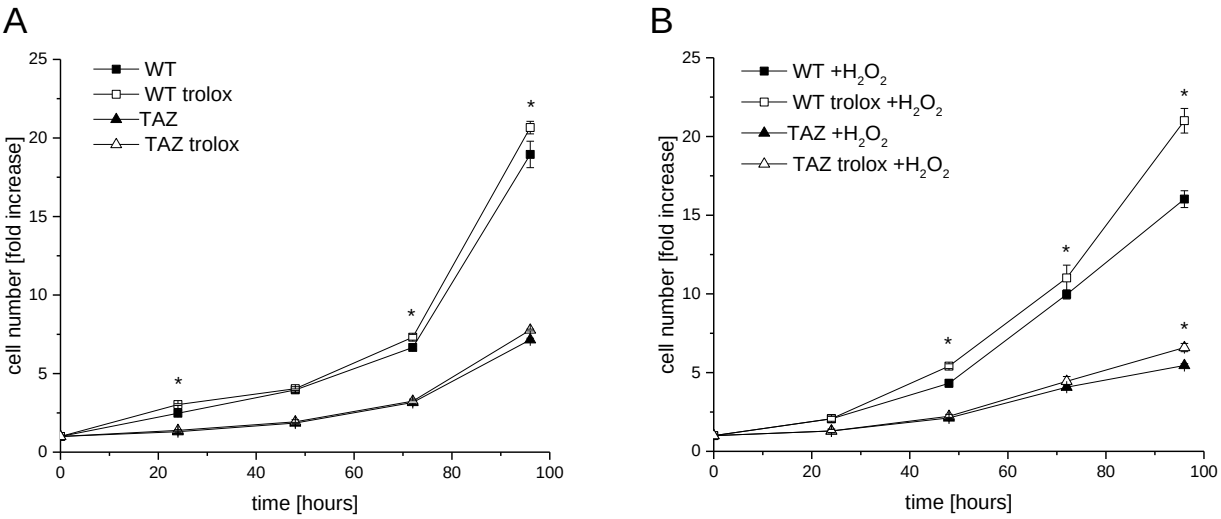

Figure 38: A) Cell number increase of WT and TAZ C6 glioma cells grown with or without 50 µM trolox over 96 hours and B) with additional stimulation by 50 µM H_2O_2 every 24 hours. Data represent the mean fold change in relation to the initial cell number at t=0 hours of n=4 samples; * mark significant differences between the same cell type at the corresponding time ($p<0.05$)

The data indicate that unlike HaCaT cells C6 glioma cells exhibit higher proliferation in the presence of trolox. In unstimulated cells the effect is only observed in WT cells. Additional stimulation of the cells with H_2O_2 increases the impact of trolox on the proliferation in TAZ as well as in WT cells. Overall, WT cells profit more from the incubation with trolox than TAZ cells regarding cell proliferation. Further effects of the TAZ knock down are discussed in chapter 4.3.2.4.

4.3.2.2. Effects on intracellular GSH/GSSG ratio

As described in the introduction glutathione is s a highly abundant LMWA in eukaryotic cells. The ratio of GSH to GSSG is often taken as a measure for the intracellular redox status. We determined the GSH/ GSSG ratio in HaCaT cells after incubation with the different plant substances and after additional stimulation with *t*BHP with a commercially available assay. The assay relies on a luminescence-based detection system to quantify the total glutathione (GSH + GSSG) as well as the reduced GSH concentration (GSSG) in the cell. With a standard curve obtained from a dilution series of GSH, the calculation of absolute concentrations in µM from the obtained luminescence values in RLU was performed (figure 39). The plotted data was fitted to a linear function ($f(x)=a+bx$ with a=3.7e^5, b=2.11e^6, R^2=0.997). The linear section of the curve (0 to 8µM GSH) was used for calculations. The obtained graph demonstrates the linear dependency of the

measured luminescence to the actual GSH concentration in a sample. The values correspond well to the data provided by the manufacturer [223] as well as to previous results from our institute [224]. However, the intercept of the linear fit with the y-axis was at $3.7e^5$ RLU. Luminescence values below this point yielded negative concentration values. This phenomena has been observed before [224]. Therefore, we worked in the following with the GSH/ GSSG ratios obtained from the measured RLUs.

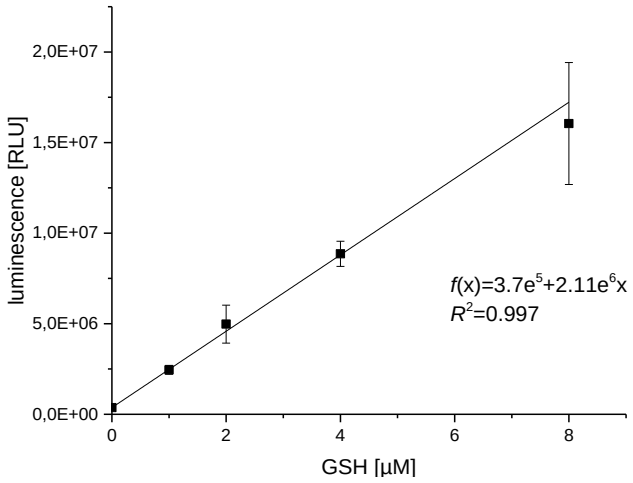

Figure 39: Luminescence values of samples containing different concentrations of GSH. The graph represent data from n>3 samples ±SD. The fitted linear function with a correlation coefficient of R^2=0.997 is shown in the graph.

Comparison of the ratios within cells incubated with the different cell substances for 24 hours to untreated control cells showed some differences between the treatments. Cells that were incubated with 60 µg/mL GP extract had significantly higher GSH/GSSG ratio compared to untreated control cells (figure 40 A, ANOVA, Bonferroni correction, $p<0.05$). The higher ratio indicates that lower amounts of GSSG were present in the individual cells or that the decrease in GSH was less pronounced in GP treated cells than in control cells. In cells treated with 120 µg/mL GP extract as well as in cells treated with AA or rutin a tendency towards higher GSH/GSSG ratios was measured. Treatment with the other plant compounds did not alter the ratio significantly. The exceptions were quercetin treated cells, which exhibited a tendency for lower ratios.

Additional stimulation of the cells with *t*BHP decreased the ratio within the cells in a concentration dependent manner (50 to 200 µM, figure 40 B). From the data we conclude that the *t*BHP stimulus is reflected in a decreased GSH/GSSG ratio within the cells. However, the effect induced by 100 µM *t*BHP was diminished in cells incubated before with CA, trolox (T), FA, EGCG, kaempferol (K), and rutin (R). Only the incubation with high GP concentrations (120 µg/mL) or quercetin failed to have any effects. The decrease of the GSH/GSSG ratio was significantly smaller for cells treated with rutin or GP extract (30 or 60 µg/mL) in comparison to untreated cells stimulated with 100 µM *t*BHP (ANOVA, Bonferroni correction, $p<0.05$, figure 40 B). The data indicate that rutin and

GP extract could diminish the effect of the *t*BHP stimulation on the intracellular GSH pool. Since the GSH/GSSG ratio was higher after *t*BHP stimulation in those cells, it seems that the substances could reduce the oxidation/depletion of the intracellular GSH caused by *t*BHP.

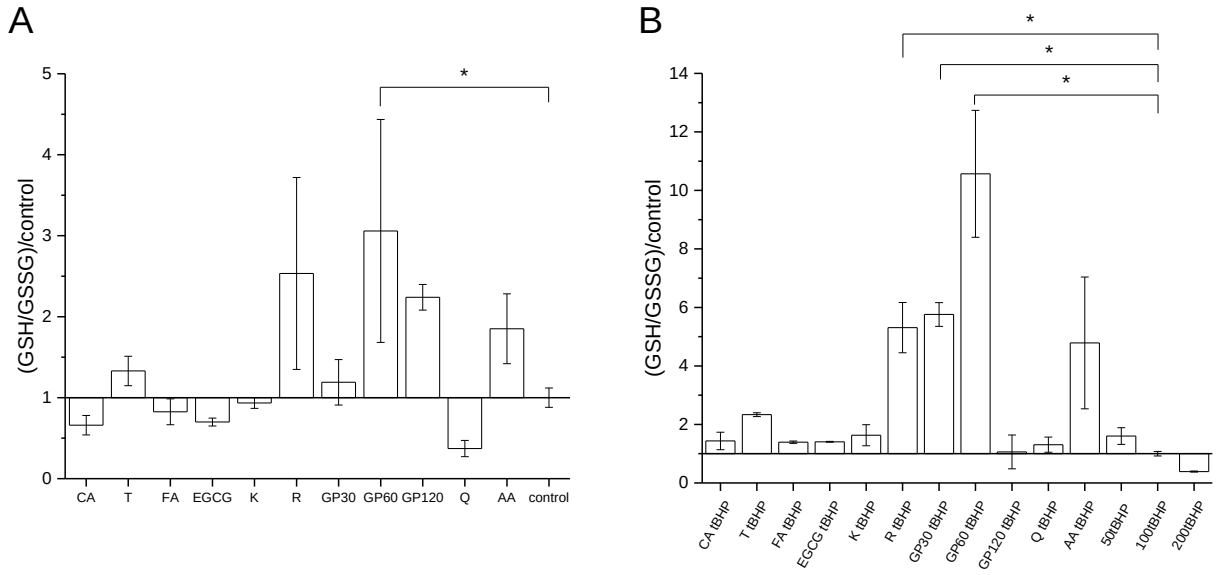

Figure 40: A) GSH/GSSG ratio determined in HaCaT cells after 24 hours incubation with different plant substances. The ratios are normalized to the ratios obtained for untreated control cells. B) Normalized GSH/GSSG ratios determined in cells that were additionally stimulated with 100 µM *t*BHP for 2 hours (control) or 50 µM or 200 µM *t*BHP. Data are represented as mean values of $n \geq 3$ replicates $\pm$SD; * mark significant different mean values from the corresponding control (ANOVA, Bonferroni correction, $p<0.05$).

The absolute values for the GSH/GSSG content calculated from the RLU values in our experiment varied between 3 and 110. This extent of variation is in good agreement with previously published work using LC–MS/MS for quantification [302]. Other published data, obtained with the assay we used, showed the great variety of the GSH/GSSG ratio between different cell types (0.8 in mouse skin tissue [303] to 90 in L2 cell line [304]). The great variety makes the comparison of absolute values troublesome. However, the method allows detection of relative changes in the GSH/GSSG ratio. The reduction of the ratio due to external stressors, such as menadione [302], ozone [304], or *t*BHP has been reported for different cell types and tissues.

In most studies the increase of the GSH/GSSG ratio is considered as an "indicator of oxidative stress" ([305],[303]). Besides a correlation between an increased cellular GSH efflux and the progression of apoptosis has been reported [306]. Coming from that perspective, the assay results suggest a protective effect of GP and AA against *t*BHP induced effects in HaCaT cells.

Exhibition of mouse skin tissue to UV-A radiation has similar effects on the intracellular GSH/GSSG pool as the treatment with *t*BHP [303]. However, the effects witnessed in mouse skin cells could be diminished by quercitrin (glycosylated form of quercetin), while this plant compound failed to

show any protective effect on the GSH/GSSG pool in our experimental setting. This demonstrates that the protective effects described for any substance is not only tissue specific but also stimulus dependent. In this case, it demonstrates that quercetin cannot per se reduce the decrease of the GSH/GSSG ratio in skin cells, but specifically does this upon UV-A stimulation.

Alterations of the intracellular GSH/GSSG ratio can have multiple causes: the inhibited biosynthesis of GSH [307], the increased oxidation of GSH [308], the inhibition of GSSG reduction [309], the increased binding of GSH to proteins (signaling) or xenobiotic substrates (detoxification), the increased efflux of GSH from the cell [305], or the increased efflux of GSSG from cell compartments [309].

In this case, the different GSH/GSSG ratios are caused by a variation in the cellular GSH content as well as variations in the GSSG content. Looking at the individual fluorescence values measured for GSH (total GSH−GSSG) and GSSG, cells treated with trolox, rutin or GP extract showed a slight increase of intracellular GSH that was couplet to a decrease in GSSG. Cells treated with CA, EGCG, kaempferol (K) or 50 µM *t*BHP had higher GSH content but also slightly increased GSSG in comparison to the control cells. Cells treated with quercetin or AA exhibited lower GSH values but the corresponding GSSG values were also lower than in the control cells. A reduction of GSH coupled to an increased GSSG concentration in comparison to the control was detected in cells incubated with FA and untreated cells stimulated with 100 or 200 µM *t*BHP.

The great variability in the GSH/GSSG ratios detected in these assays are contradictory to GSH/GSSG ratios obtained with genetically encoded sensors that are in the range of 50000 to 1. The ratios measured with genetically encoded sensors indicate that the intracellular concentration of GSSG is much smaller than assessed with the described assay. The observation is supported by LC–MS (liquid chromatography–mass spectroscopy) analysis of GSH and GSSG concentration in HaCaT cells, where the GSSG content was always below the detection limit (0.1 µM) [310]. Furthermore, it has been proposed that the cell actively prevents the accumulation of GSSG either by reducing it or by excretion from the cell/cell compartment [309]. Therefore, the GSH/GSSG ratio would always remain constant in the cell. The reduced GSH/GSSG ratios upon cell stimulation, as demonstrated by our data and reported before in the literature [224], [302], [304], [311], are not in agreement with this statement. Either, the changes must be due to biased results from sample preparation or from the detection method. One possible explanation would be that the assays sensitivity to distinguish accurately GSH from GSSG is not sufficient for the small amounts of GSSG expected in a cell. In this case, reduction of the total GSH pool can be misinterpreted as a decrease in the measured ratio. Another explanation would be that working

in oxygen containing atmosphere causes oxidation of GSH after cell lysis. In any case, three major limitations of the presented GSH/GSSG assay need to be considered:

i. Cell lysis might cause some oxidation of GSH during sample preparation. This can lead to an overestimation of intracellular GSSG.
ii. The assay is conceptualized as an end-point assay. The snapshot of the current state cannot reflect dynamic cellular processes that regulate the intracellular GSH/GSSG ratio, like the efflux of GSH [305].
iii. The assay does not detect the amount of GSH bound to proteins (glutathionylation).

Considering this, we treat the results of the assay only as indicative values for the comparison of treatments.

4.3.2.3. Effects on intracellular GSH content

In a second approach to assess the intracellular GSH pool we quantified the amount of total GSH (GSH/GSSG) in HaCaT cells incubated with the different plant compounds and additional stimulation with 100 µM *t*BHP. From the absorption values of a dilution series of GSH a standard curve was obtained. The plotted data was fitted to a non-linear function $f(x)=(a-d)/(1+((x/c)^b))+d$ with a=0.00630, b=1.31085, c=12.9516, d=2.07567 (xmgrace software, figure 41 A) to calculate the GSH concentration in the corresponding samples. The function reached a plateau at 100 µM GSH. The measured absorption values of the samples were all in the linear part of the function. Therefore, we could determine the GSH concentration/ mg Protein. The obtained values are shown in figure 41 B. The highest concentration of GSH was determined in the samples of HaCaT cells incubated with CA (13±1.0 nmol/mg protein), followed by the control cells (12±1 nmol/mg protein), kaempferol treated cells (11.6±0.5 nmol/mg protein) and trolox treated cells (9.4±0.2 nmol/mg protein). The observation that treatment of HaCaT cells with trolox does not have a significant impact on the intracellular GSH content is in agreement with previously published results [312]. In the samples of cells incubated with rutin, EGCG, GP extract and FA the GSH content was significantly lower in comparison to the control cells (9.1±0.2, 8±1, 7.7±0.8, 6±2 nmol/mg protein).

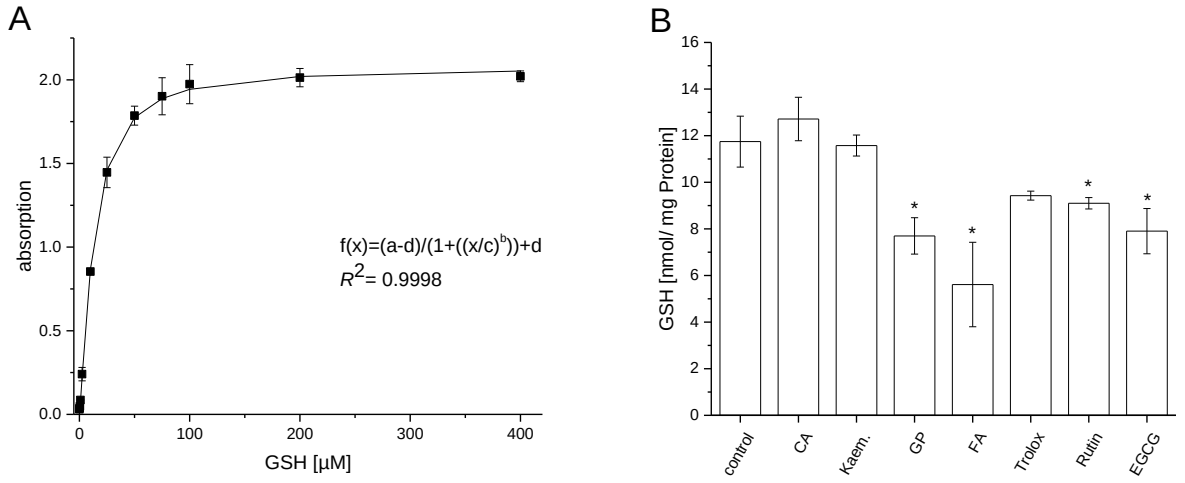

Figure 41: A) absorbance values measured from samples with known GSH concentration. The black line represents the non-linear fitted function $f(x)=(a-d)/(1+((x/c)^b))+d$ with a=0.0063, b=1.3109, c=12.9516, d=2.0757; B) the GSH concentration/mg Protein calculated from the fitted function for HaCaT cells incubated for 24 hours with different plant compounds; data represent the mean of n=3 samples ±SD; * mark a significant difference to the control (ANOVA, Bonferroni correction, $p<0.05$)

The values of intracellular GSH concentrations per mg protein reported in the literature are tissue specific. However, the measured values correspond to concentrations reported before in HaCaT cells [310]. Taking the sample size into account the presented data need to be supported by further experiments.

Data from the GSH/GSSG assay suggested that GP extract and rutin diminished the effect of *t*BHP treatment on the ratio within HaCaT cells. The detected changes in the ratio were not only due to the increase of GSSG within the cells, but also caused by a change in the GSH concentration. The two assays correspond on the results that FA treatment decreased the amount of GSH in the cells. However, results from the assay suggest that incubation of the cells with GP extract, rutin, or EGCG increased the amount of GSH in the cells, which is contradictory to the data of this assay. An explanation for this discrepancy might be the risk of reducing intracellular GSH during cell lysis in the GSH/GSSG assay (see chapter 4.3.2.2.).

4.3.2.4. Effects on mitochondrial ROS concentration

As mentioned in the introduction the use of genetically encoded sensors for the determination of intracellular redox parameters has the advantage that measurements can be performed without cell lysis. In C6 glioma cells the H_2O_2 concentration at the mitochondria upon stimulation with different concentrations of external H_2O_2 (5 to 50 µM) was measured via the fluorescence signal of the encoded mitoHyPer sensor normalized to the cell number. The studies were performed on C6 glioma tafazzin knock out cells (TAZ) as well as on the corresponding wild-type (WT) cells.

As mentioned before tafazzin is a mitochondrial acyltransferase [299]. As such, tafazzin is essential in adapting CL composition to the cellular environment [313] (e.g. changes in the lipid environment [300]). Tafazzin knock out in C6 glioma cells affects the mitochondrial energy metabolism and decreased their proliferation rate, as demonstrated in this work (see chapter 4.3.2.1.) in concordance with previous studies [300].

In TAZ cells the basal level of H_2O_2 was higher than in the corresponding WT cells (1.3 times higher fluorescence ratio). Elevated mitochondrial ROS levels have been reported before in TAZ knockdown cells [314], [315]. One hypothesis is that TAZ knock-down prevents the proper organization of the mitochondrial respiratory chain components in supramolecular assemblies (respiratory supercomplexes)[316]. The absence of supercomplexes enhances the production of superoxide and diminishes the energy production rate from mitochondria, because electron transfer becomes less efficient [317].

The observed elevated H_2O_2 levels slightly increased in TAZ cells upon stimulation with extracellular H_2O_2 but reached a plateau after stimulation with 20 µM H_2O_2 at 1.3-fold increase of the fluorescence signal. Further increase of external H_2O_2 was not translated into higher H_2O_2 levels measured at the mitochondria. In comparison stimulation of the WT cells let to an increase up to 1.4 times of the initial fluorescence signal at 30 µM external H_2O_2 (figure 42 B+E) Since the basal level of H_2O_2 measured in WT cells is lower, the dynamic window of the intracellular H_2O_2 concentrations is wider in these cells.

Incubation of WT cells with kaempferol, trolox, CA and FA let to a decrease of basal mitochondrial H_2O_2 levels in comparison to the control. This could also be observed upon stimulation with H_2O_2 (figure 36 A). The reduction was most pronounced in cells incubated with trolox and kaempferol. Incubation with FA and CA had similar effects on unstimulated cells and on cells treated with 15 µM H_2O_2. At higher H_2O_2 stimulation (50 µM) the substances were less effective to reduce mitochondrial ROS levels (figure 42 C). Quercetin failed to have any significant effect on the intracellular concentrations measured. Incubation of the cells with GP extract reduced the H_2O_2 concentration at 60 µg/mL but failed to do so at lower concentrations (30 µg/mL).

Incubation of TAZ cells with kaempferol, trolox or GP extract (30 and 60 µg/mL) reduced the basal level of mitochondrial H_2O_2 in the cells. At 15 µM external H_2O_2 stimulus cell incubated with these substances as well as with quercetin exhibited still significantly lower values as control cells. At higher external H_2O_2 concentrations (50 µM) only kaempferol, trolox and FA incubated cells had significantly lower mitochondrial levels than the control cells (figure 42 D–F).

From all the plant compounds quercetin exhibited the lowest activity of reducing the intracellular H_2O_2 levels. The explanation might be the specific effects on the investigated cell line. Studies on

cancer cells suggest that the polyphenol possesses mitochondria-targeted anticancer drug (mitocan) properties [318]. Further, quercetin might promote cell survival or death in a cell type- and metabolism-specific manner. For example, by exerting anti-inflammatory activities in neurons, while inducing oxidative, kinase- and cell cycle-inhibitory, apoptosis-inducing effects in cancer cells [319]. Since, the investigated cell line is a cancer cell line (glioma), while HaCaT cells are spontaneously immortalized cells derived from healthy keratinocytes, it is plausible that the cells might react differently to the plant compound.

The average reduction of mitochondrial H_2O_2 reduction by the plant compounds was less pronounced in the TAZ cells than in WT cells. Especially at high exogenous H_2O_2 concentrations, most substances failed to induce a significant change. One possible explanation might be that the increased basal H_2O_2 levels measured in TAZ cells could inhibit the cells to cope with excessive loads of extracellular H_2O_2. In this case, supplementation with H_2O_2 reducing compounds fails to compensate the harmful effects. The observation that the variability of intracellular H_2O_2 concentrations in TAZ cells is reduced in comparison to WT cell indicate that the phenotype of the TAZ knock out is not *per-se* characterized by elevated intracellular H_2O_2 levels. It is rather a lack to adapt to external stimuli that characterize the cells at high external H_2O_2 levels.

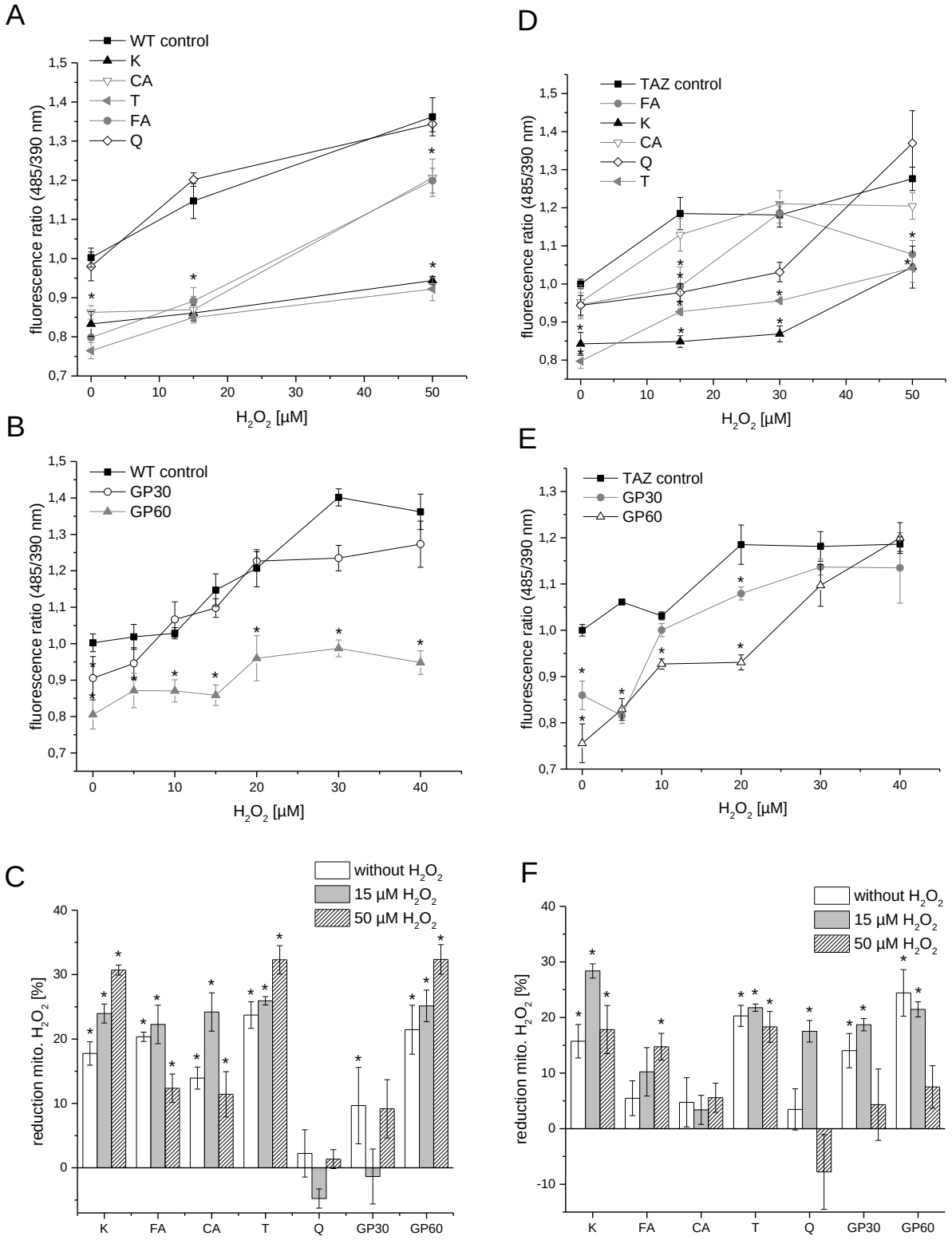

Figure 42: Mitochondrial H_2O_2 concentration measured in mitoHyPer expressing C6 glioma cells. The fluorescence ratios (485 to 390 nm), an indicator of H_2O_2 production, are shown normalized to the ratio of untreated cells in wild type cells (WT, A-C) and tafazzin knock-out cells (TAZ, D-F). Cells were grown with different plant compounds (A, D) and different concentrations of GP extract (30 or 60 µg/mL; B, D) for 24 hours before stimulation with 0 to 50 µM H_2O_2 directly before measurement of the fluorescence signal. The reduction of H_2O_2 in the cells incubated with the plant compounds in comparison to untreated cells are shown in C and F. Data represent the mean of $n \geq 4$ samples ±SEM. Significant differences to the corresponding control are marked with * (ANOVA, Bonferroni correction, $p<0.05$).

The data presented demonstrate that trolox significantly decreases mitochondrial H_2O_2 concentration. Data presented in chapter 4.3.2.1. demonstrate the effects of trolox in H_2O_2 stimulated C6 glioma cells on the cell proliferation. The reduction of H_2O_2 at the mitochondria might be an explanation for the increased proliferation of trolox treated cells. This phenomenon is especially interesting for the TAZ cells, because they exhibit a weaker proliferation compared to the WT cells [300]. Studies on TAZ knock-down cardiac myocytes demonstrated that treatment with mito-Tempo could normalize mitochondrial ROS production and cellular ATP levels along with other cellular dysfunctions [314]. Supplementation with mitochondrial ROS decreasing compounds might therefore be an approach to counteract TAZ dysfunction symptoms. Though the average benefit from the incubation with the plant compounds was lower for TAZ cells compared to the WT cells, treatment with substances reducing the H_2O_2 concentration at the mitochondria might beneficially influence proliferation of the cells. However, it is unlikely that supplementation with these substances can totally diminish the effects of TAZ knock-out, because studies indicate that tafazzin might also have a direct role in cell cycle control [300], [301].

4.3.2.5. Effects on extracellular metabolome

We evaluated the extracellular metabolome of HaCaT cells and C6 glioma cells (WT and TAZ) after 24 hours growth with the plant substances or GP extract. The measured metabolite concentrations divided by the initial concentration in the cell media yielded the fold change over 24 hours incubation. Since the plant substances affected the cell proliferation (see chapter 4.3.2.1.), the values were normalized to the cell number *n*.

HaCaT cells were cultivated in RPMI medium (see methods). The RPMI medium contains the amino acids histidine, tyrosine, hydroxyl-proline, threonine, oxo-proline, serine, glycine, cysteine, phenylalanine, lysine, asparagine, aspartate, methionine, glutamine, glutamate, isoleucine, valine and leucine. All of those amino acids serve as nutrients to the cells. Their concentration does therefore decrease over time. The same is observed for myo-inositol and glucose. On the other hand, the amount of the amino acids ornithine and alanine, which were initially not present in the medium, increased. The metabolites formiate, fumarate, fructose, pyruvate, 2-oxoglutarate, choline and lactate increased. In comparison to the control, the decrease of cysteine and glucose in the media was more pronounced in the cells treated with the different plant compounds. The increase of lactate and pyruvate was higher in the control cells. Comparing the different plant compound treatments with each other showed significant differences between kaempferol

treated cells and EGCG treated cells, where the metabolic profile of EGCG treated cells was closest to the control cells (one-way ANOVA, $p<0.05$, figure 43).

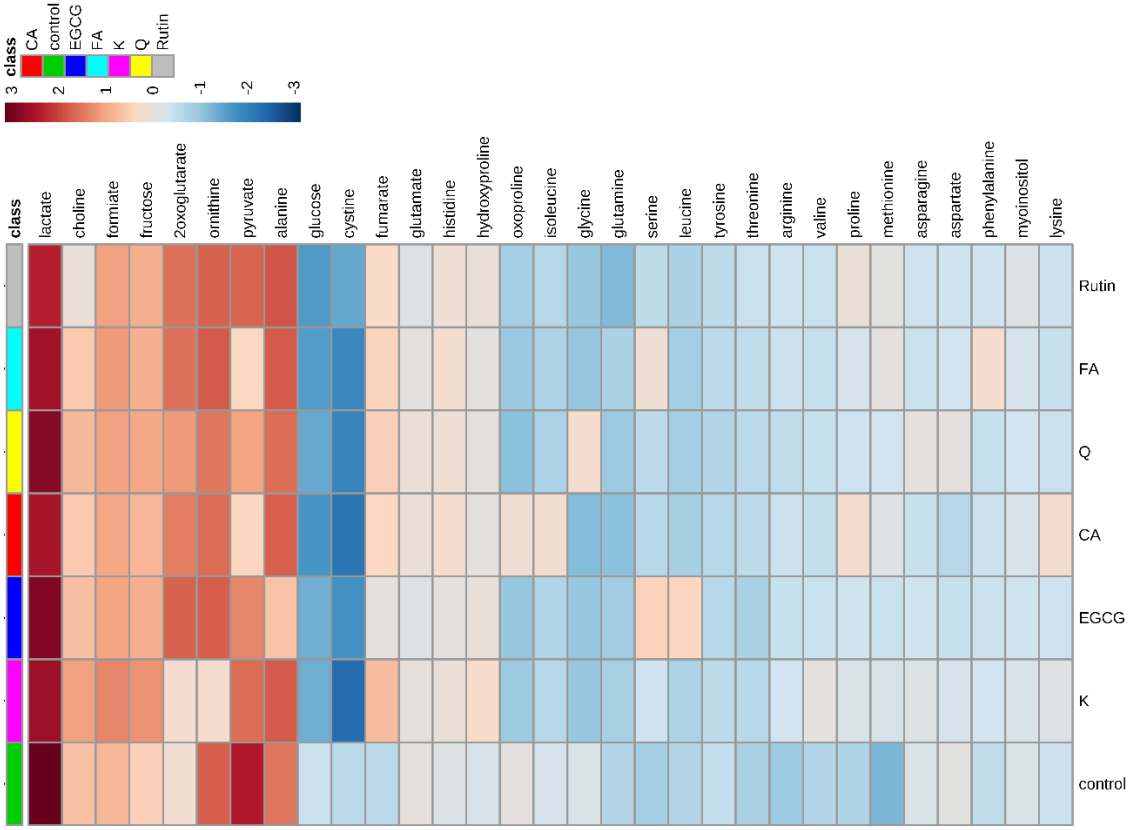

Figure 43: Extracellular metabolites measured in the medium of HaCaT cells. The absolute metabolite concentration (c) was divided by the initial concentration contained in the cell media (c_0). The illustrated heat maps show the Log_2 fold change of the metabolites normalized to the cell number (n) and the control treatment with rising concentrations in red and with decreasing concentrations in blue. The heat map illustrates data from HaCaT cells incubated with different plant substances for 24 hours with additional *t*BHP stimulation (100 µM for 2 hours).

A principle component analysis (PCA) on the normalized metabolites data revealed a distinction of kaempferol treated cells from the other cell samples by the first component, which contributes with 74.6% to the differences in variance found in the data set.

In the extracellular metabolome of HaCaT cells treated with 30, 60 and 120 µg/mL GP extract ornithine, alanine, formiate, pyruvate, choline and lactate increased. However, the increase of fumarate and 2-oxoglutarate was less pronounced. In comparison to the control the concentration of methionine did not increase to the same extent in the GP treated cell samples (figure 44). However, in general the metabolite concentrations from GP treated HaCaT cells did not differ much from untreated cells. The concentration of fumarate slightly decreases in control and GP treated cells, while a slight increase was detected in HaCaT cells treated with the different plant compounds.

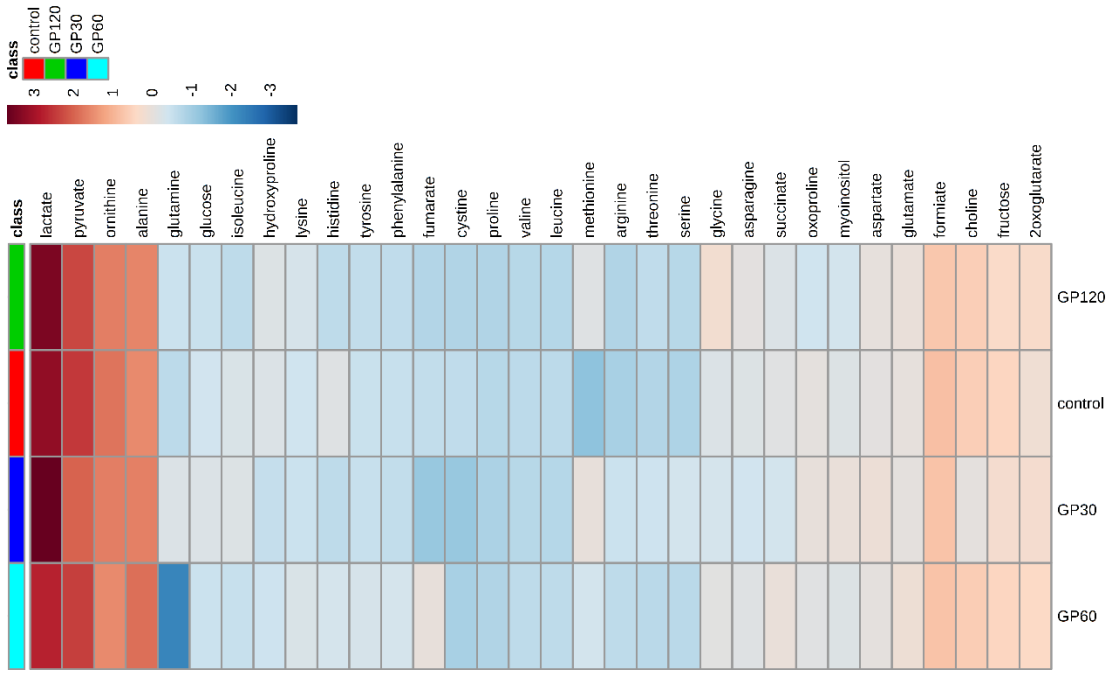

Figure 44: Extracellular metabolite concentrations in the medium of HaCaT cells treated with 0 (control), 30, 60 or 120 µg/mL GP (24 h). Data are presented as described in figure 43. The heat map illustrates the mean of n≥3 replicates.

Taking the results together, the extracellular metabolome reflects the expected outcome of HaCaT cells depending on glucose for energy generation producing lactate in the process. The slight increase of glucose consumption and lactate production in the HaCaT cells treated with the plant compounds might be an indicator for the beneficial impact of those substances on the metabolic activity of the cells. This assumption is in concordance with the data of the WST-8 assay on HaCaT cells presented in chapter 4.3.2.1.

C6 glioma WT and TAZ cells were cultivated in DMEM medium. In contrast to RPMI the cell medium does not contain glutamate, GSH, oxoproline or hydroxyproline. However, DMEM contains most of the other amino acids in higher concentrations. This can explain why the changes detected in the medium after 24 hours growth are not as pronounced as demonstrated before for the HaCaT cells. The highest increase after 24 hours was detected for lactate and alanine, which is in concordance with the changes detected in the medium of HaCaT cells. Further, an increase in fumarate was detected in the extracellular metabolite of glioma cells, which was more pronounced than for HaCaT cells. Glucose and cysteine levels did not decrease to the same extent in the medium of the glioma cells as seen for HaCaT cells (figure 45). One possible explanation could be the higher proliferation rate of HaCaT cells that entails higher metabolic activity.

Comparison of WT and TAZ cells revealed significant differences in the extracellular concentration of formiate, histidine, fructose, oxoproline, cysteine and succinate. The concentration of glucose

was significantly different in WT cells treated with GP in comparison to the untreated control (one-way ANOVA, $p<0.05$).

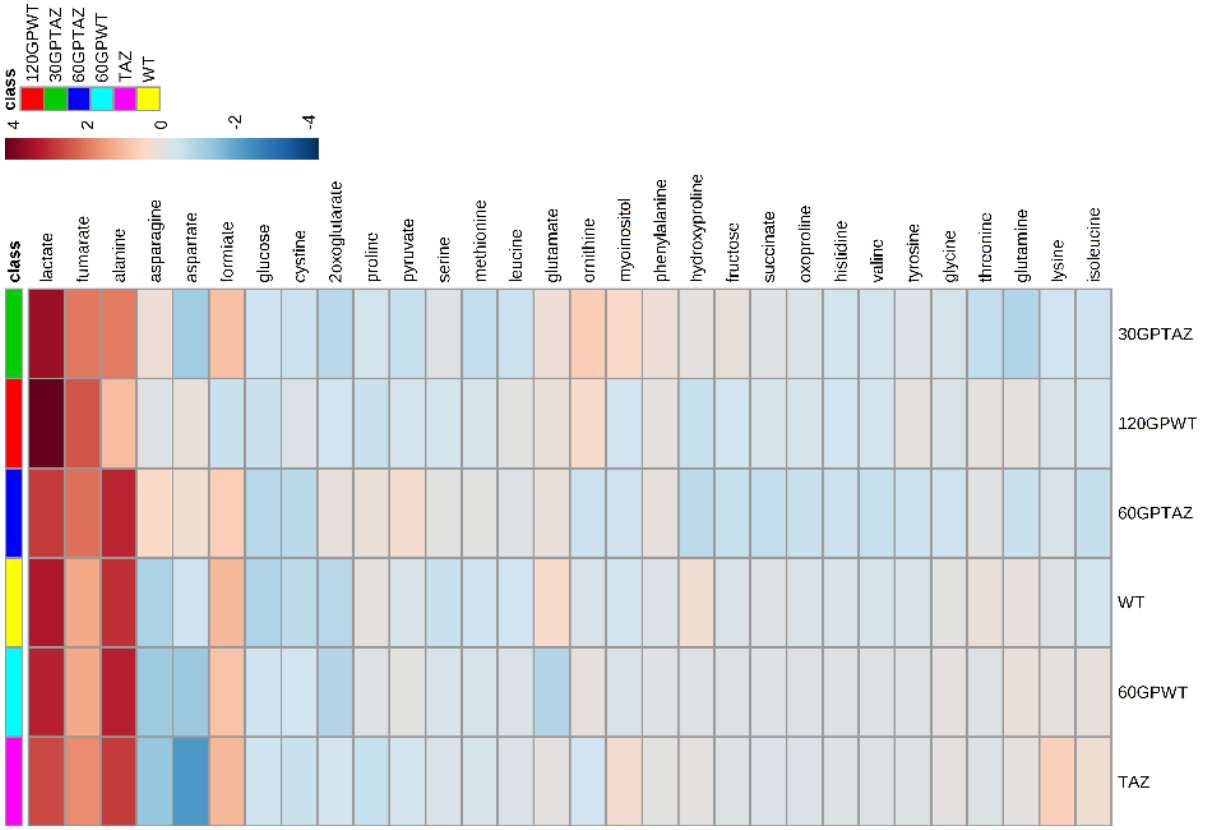

Figure 45: Concentration of extracellular metabolites measured in the medium of C6 WT and TAZ glioma cells. Cells were grown for 24 hours with 0, 30, 60 or 120 µg/mL GP extract. Data are presented as described in figure 43.

4.4. Comparison of the electrochemical assay with intracellular parameters

As mentioned before the direct evaluation of the plant substances in cell culture experiments with the electrochemical assay were not conclusive. However, we compared the results for the different redox parameters (proliferation under *t*BHP/H_2O_2 stimulation, GSH/GSSG ratio, protein bound GSH, mitochondrial ROS concentration) we obtained for C6 glioma and HaCaT cells with the *in-vitro* measurements of the electrochemical assay.

The effects of the individual plant substances on cellular parameters were very heterogeneous (table 7). In HaCaT cells only the effects on metabolic activity, determined with the WST-8 assay, and the cell proliferation were correlated to each other (see section 4.3.2.1.). The effects on GSH/GSSG ratio and on total GSH are not directly connected to each other. The heterogeneity of the effects of the plant substances on cellular parameters demonstrate the problems associated with correlating the observed effects to one property of the substance (in this case the radical scavenging activity *in-vitro*).

Table 7: Effects of the individual plant compounds on different cellular parameters in HaCaT cells and C6 glioma cells.

	GSH/GSSG	GSH total	HyPer		Proliferation (WST-8)
Cell line	**HaCaT (*t*BHP stimulated cells)**	**HaCaT**	**C6 glioma WT**	**C6 glioma TAZ**	**HaCaT**
AA	Increase	No data	No data	No data	Increase
CA	No effect	No effect	Reduction H_2O_2	No effect	Increase
FA	No effect	Reduction GSH	Reduction H_2O_2	Reduction H_2O_2	No effect
EGCG	No effect	Reduction GSH	No data	No data	Decrease
Kaempferol	No effect	No effect	Reduction H_2O_2	Reduction H_2O_2	Decrease
Rutin	No effect	Reduction GSH	No data	No data	No effect
trolox	No effect	No effect	Reduction H_2O_2	Reduction H_2O_2	No effect
Quercetin	No effect	No data	No effect	Reduction H_2O_2	No effect
GP extract	Increase (60, 120 µg/mL)	No data	Reduction H_2O_2 (60 µg/mL)	Reduction H_2O_2 (30, 60 µg/mL)	Increase

The electrochemical assay assesses the capacity of the substances to scavenge ROS (preferentially hydroxyl radicals) in the aqueous phase. However, various pathways can affect the intracellular parameters.

The cell experiments were designed in such way that the plant substances containing media was washed of before the cell assays. However, it is still possible that some compounds remained attached to the cell membrane and executed its action in this manner, e.g. by reducing the load of ROS that interacted with the cell. In this case, the direct ROS scavenging activity of the plant compound would be relevant. Assuming the washing steps removed most of the plant substances, the first barrier for them to induce some effects is to cross the cell membrane either directly or by activation of membrane receptors (induction of intracellular pathways).

The knowledge on the cellular uptake mechanisms for the investigated plant compounds is heterogeneous. AA can enter cells both in its reduced and oxidized form (ascorbate or dehydroascorbate), utilizing respectively sodium-dependent transporters (SVCT) or glucose transporters (GLUT) [68]. We assume that AA is adsorbed by C6 glioma as well as by HaCaT cells. Studies on the protective effects of CA and FA on UV-A induced damage in HaCaT cells reported intracellular effects of the substances that presuppose their cellular uptake [320], [321]. Further,

transcriptional studies in HaCaT cells demonstrated the intracellular effects of kaempferol [322]. Intracellular effects were also reported for EGCG[323], rutin, quercetin [324] and trolox [312] in the HaCaT cell line.

A study on human colon adenocarcinoma cells (HT-29) demonstrated that CA is absorbed, isomerized, and metabolized by those cells and that the substance can be found within the cells after 72 hours incubation, while derivates of CA were detected already after 1 hour in the cells [325]. It is very likely that the absorbance rates of the investigated plant substances varied in the different cell lines in a comparable manner. For all of the plant compounds investigated in this work cellular effects have been demonstrated before in other published work. We therefore assume, that in general a cellular uptake of the substances by eukaryotic cells is possible. However, as demonstrated for CA and FA in HepG2 cells [326], the uptake rate might differ.

5. Conclusion and outlook

In summary, we could optimize the pretreatment of polycrystalline gold electrodes for repetitive cycles of SAM formation and removal via oxygen radicals. We could provide some inside on the effects of the oxygen radical treatment on the SAM as well as on the underlying gold surface. The defects induced to the SAM by low oxygen radical concentrations were investigated with different techniques and demonstrated the minor impact on the formed SAM structure that were still detectable with DPV measurements. Our results demonstrate the different sensitivity of the SAM modified sensor electrode towards H_2O_2, $O_2^{-}\cdot$ and OH^{-}, making it an attractive tool for the evaluation of biologically relevant ROS.

The evaluation of different plant compounds with the electrochemical assay demonstrates its ability to assess the antioxidant activity of different secondary plant metabolite classes as well as of more complex plant extracts. Comparison of the results with established antioxidant assays showed some differences in the obtained ranking for the individual substances. The inter-assay variations between established assays demonstrate the impact of experimental parameters on the obtained results.

Measurements of extracellular ROS from different cell lines verified that physiologically high ROS concentrations could be detected with the electrochemical assay, as proposed previously [3]. However, due to the minor changes induced by cellular ROS the additional effects from plant substances were below the detection limit of the assay. Therefore, we conclude that the electrochemical assay is not sensitive enough to directly measure extracellular redox changes induced by the plant substances.

Additional studies on the effects of the plant substances on intracellular redox parameters could not always verify the antioxidant activity demonstrated *in-vitro*. However, it could be shown that the plant substances have an impact on certain cell parameters in different cell lines. To verify these observations repetition of the experiments with higher sample sizes are required. From the results, we conclude that intracellular antioxidant activities are concentration and cell line dependent and are not purely assessable from *in-vitro* measurements. The observed intracellular effects can not necessarily linked to the antioxidant activity observed *in-vitro*.

As a future perspective for the direct comparison of the intracellular and extracellular antioxidant activity of a substance e.g. with an electrochemical assay, the experimental setting should be more specific. That could be achieved by limiting the investigated antioxidant properties to one target site, like the cell membrane.

6. References

[1] R. A. Larson, "The antioxidants of higher plants," *Phytochemistry*, vol. 27, no. 4, pp. 969–978, Jan. 1988.

[2] F. Scholz *et al.*, "Indirect electrochemical sensing of radicals and radical scavengers in biological matrices.," *Angew. Chem. Int. Ed. Engl.*, vol. 46, no. 42, pp. 8079–81, Jan. 2007.

[3] M. Hilgemann *et al.*, "Electrochemical Assay to Quantify the Hydroxyl Radical Scavenging Activity of Medicinal Plant Extracts," *Electroanalysis*, vol. 22, no. 4, pp. 406–412, 2010.

[4] K. Krumova and G. Cosa, "Overview of reactive oxygen species," in *Singlet Oxygen : Applications in Biosciences and Nanosciences, Volume 1*, S. Nonell and C. Flors, Eds. Royal Society of Chemistry, 2016, pp. 1–21.

[5] B. Halliwell, "Free Radicals and Other Reactive Species in Disease," *eLS*, pp. 1–9, 2015.

[6] C. C. Winterbourn, "Reconciling the chemistry and biology of reactive oxygen species," *Nat. Chem. Biol.*, vol. 4, no. 5, pp. 278–286, 2008.

[7] T. Finkel and N. J. Holbrook, "Oxidants, oxidative stress and the biology of ageing.," *Nature*, vol. 408, no. 6809, pp. 239–247, 2000.

[8] C. Nathan and A. Cunningham-Bussel, "Beyond oxidative stress: an immunologist's guide to reactive oxygen species," *Nat. Rev. Immunol.*, vol. 13, no. 5, pp. 349–361, 2013.

[9] J. F. Turrens, "Superoxide production by the mitochondrial respiratory chain.," *Biosci. Rep.*, vol. 17, no. 1, pp. 3–8, 1997.

[10] M. Schrader and H. D. Fahimi, "Peroxisomes and oxidative stress," *Biochim. Biophys. Acta - Mol. Cell Res.*, vol. 1763, no. 12, pp. 1755–1766, 2006.

[11] J. D. Malhotra and R. J. Kaufman, "Endoplasmic Reticulum Stress and Oxidative Stress: A Vicious Cycle or a Double-Edged Sword?," *Antioxid. Redox Signal.*, vol. 9, no. 12, pp. 2277–2294, 2007.

[12] J. D. Lambeth, "NOX enzymes and the biology of reactive oxygen," *Nat. Rev. Immunol.*, vol. 4, no. 3, pp. 181–189, 2004.

[13] L. Miao and D. K. St. Clair, "Regulation of superoxide dismutase genes: Implications in disease," *Free Radic. Biol. Med.*, vol. 47, no. 4, pp. 344–356, 2009.

[14] E. Zito, "ERO1: A protein disulfide oxidase and H2O2 producer," *Free Radic. Biol. Med.*, vol. 83, pp. 299–304, 2015.

[15] S. J. Klebanoff, "Myeloperoxidase: friend and foe," *J. Leukoc. Biol.*, vol. 77, no. 5, pp. 598–625, 2005.

[16] E. G. Hrycay and S. M. Bandiera, *Involvement of Cytochrome P450 in Reactive Oxygen Species Formation and Cancer*, 1st ed., vol. 74. Elsevier Inc., 2015.

[17] Y. V. Grinkova, I. G. Denisov, M. A. McLean, and S. G. Sligar, "Oxidase uncoupling in heme monoxygenases: Human cytochrome P450 CYP3A4 in Nanodiscs," *Biochem Biophys Res Commun*, vol. 430, no. 4, pp. 1223–1227, 2013.

[18] S. Park, X. You, and J. A. Imlay, "Substantial DNA damage from submicromolar intracellular hydrogen peroxide detected in Hpx- mutants of Escherichia coli.," *Proc. Natl. Acad. Sci. U. S. A.*, vol. 102, no. 26, pp. 9317–22, 2005.

[19] G. R. Buettner, "The Pecking Order of Free Radicals and Antioxidants: Lipid Peroxidation, a-Tocopherol, and Ascorbate," *Arch. Biochem. Biophys.*, vol. 300, no. 2, pp. 535–543, 1993.

[20] M. Valko, M. Izakovic, M. Mazur, C. J. Rhodes, and J. Telser, "Role of oxygen radicals in DNA damage and cancer incidence," *Mol. Cell. Biochem.*, vol. 266, no. 1–2, pp. 37–56, 2004.

[21] A. K. Sharma, G. Taneja, D. Khanna, and S. K. Rajput, "Reactive oxygen species: friend or foe?," *RSC Adv.*, vol. 5, no. 71, pp. 57267–57276, 2015.

[22] D. Harman, "Free radical theory of aging," *Mutat. Res.*, vol. 275, no. 3–6, pp. 257–266, Sep. 1992.

[23] S. I. Liochev, "Reactive oxygen species and the free radical theory of aging," *Free Radic. Biol. Med.*, vol. 60, pp. 1–4, 2013.

[24] M. Chattopadhyay, V. K. Khemka, G. Chatterjee, A. Ganguly, S. Mukhopadhyay, and S. Chakrabarti, "Enhanced ROS production and oxidative damage in subcutaneous white adipose tissue mitochondria in obese and type 2 diabetes subjects," *Mol. Cell. Biochem.*, vol. 399, no. 1–2, pp. 95–103, 2015.

[25] N. Li, F. Frigerio, and P. Maechler, "The sensitivity of pancreatic beta-cells to mitochondrial injuries triggered by lipotoxicity and oxidative stress.," *Biochem. Soc. Trans.*, vol. 36, pp. 930–934, 2008.

[26] M. Mittal, M. R. Siddiqui, K. Tran, S. P. Reddy, and A. B. Malik, "Reactive oxygen species in inflammation and tissue injury.," *Antioxid. Redox Signal.*, vol. 20, no. 7, pp. 1126–67, 2014.

[27] Z. Radak, H. Y. Chung, E. Koltai, A. W. Taylor, and S. Goto, "Exercise, oxidative stress and hormesis," *Ageing Res. Rev.*, vol. 7, no. 1, pp. 34–42, 2008.

[28] S. K. Powers, W. B. Nelson, and M. B. Hudson, "Exercise-induced oxidative stress in humans: Cause and consequences," *Free Radic. Biol. Med.*, vol. 51, no. 5, pp. 942–950, 2011.

[29] J. Moskovitz, "Methionine sulfoxide reductases: ubiquitous enzymes involved in antioxidant defense, protein regulation, and prevention of aging-associated diseases," *Biochim. Biophys. Acta - Proteins Proteomics*, vol. 1703, no. 2, pp. 213–219, 2005.

[30] M. Valko, D. Leibfritz, J. Moncol, M. T. D. Cronin, M. Mazur, and J. Telser, "Free radicals and antioxidants in normal physiological functions and human disease.," *Int. J. Biochem. Cell Biol.*, vol. 39, no. 1, pp. 44–84, 2007.

[31] E.-M. Hanschmann, J. R. Godoy, C. Berndt, C. Hudemann, and C. H. Lillig, "Thioredoxins, Glutaredoxins, and Peroxiredoxins—Molecular Mechanisms and Health Significance: from Cofactors to Antioxidants to Redox Signaling," *Antioxid. Redox Signal.*, vol. 19, no. 13, pp. 1539–1605, 2013.

[32] G. Ferrer-Sueta, B. Manta, H. Botti, R. Radi, M. Trujillo, and A. Denicola, "Factors affecting protein thiol reactivity and specificity in peroxide reduction," *Chem. Res. Toxicol.*, vol. 24, no. 4, pp. 434–450, 2011.

[33] N. J. Adimora, D. P. Jones, and M. L. Kemp, "A Model of Redox Kinetics Implicates the Thiol Proteome in Cellular Hydrogen Peroxide Responses," *Antioxidants Redox Signal.*, vol. 13, no. 6, 2010.

[34] J.-M. Lü, P. H. Lin, Q. Yao, and C. Chen, "Chemical and molecular mechanisms of antioxidants: experimental approaches and model systems.," *J. Cell. Mol. Med.*, vol. 14, no. 4, pp. 840–860, 2010.

[35] W. M. Nauseef, "Biological roles for the NOX family NADPH oxidases," *J. Biol. Chem.*, vol. 283, no. 25, pp. 16961–16965, 2008.

[36] M. Kemp, Y.-M. Go, and D. P. Jones, "Non-equilibrium thermodynamics of thiol/disulfide redox systems: A perspective on redox systems biology," *Free Radic. Biol. Med.*, vol. 44, no.

6, pp. 921–937, 2008.

[37] D. P. Jones, “Redox sensing: Orthogonal control in cell cycle and apoptosis signalling,” *J. Intern. Med.*, vol. 268, no. 5, pp. 432–448, 2010.

[38] Y.-M. Go and D. P. Jones, “Thiol/disulfide redox states in signaling and sensing,” *Crit Rev Biochem Mol Biol*, vol. 48, no. 2, pp. 173–181, 2013.

[39] C. S. Sevier and C. A. Kaiser, “Ero1 and redox homeostasis in the endoplasmic reticulum,” *Biochim. Biophys. Acta - Mol. Cell Res.*, vol. 1783, no. 4, pp. 549–556, 2008.

[40] T. Ramming *et al.*, “A PDI-catalyzed thiol-disulfide switch regulates the production of hydrogen peroxide by human Ero1,” *Free Radic. Biol. Med.*, vol. 83, pp. 361–372, 2015.

[41] Z. Radak, Z. Zhao, E. Koltai, H. Ohno, and M. Atalay, “Oxygen Consumption and Usage During Physical Exercise: The Balance Between Oxidative Stress and ROS-Dependent Adaptive Signaling,” *Antioxid. Redox Signal.*, vol. 18, no. 10, pp. 1208–1246, 2013.

[42] J. M. Thornton, “Disulfide bridges in globular proteins,” *J. Mol. Biol.*, vol. 151, pp. 261–287, 1981.

[43] J. S. Richardson, “The anatomy and taxonomy of protein structure,” *Adv. Protein Chem.*, vol. 34, no. C, pp. 167–339, 1981.

[44] M. A. Wouters, S. W. Fan, and N. L. Haworth, “Disulfides as Redox Switches: From Molecular Mechanisms to Functional Significance,” *Antioxid. Redox Signal.*, vol. 12, no. 1, pp. 53–91, 2010.

[45] W. Maret, “Zinc Coordination Environments in Proteins as Redox Sensors and Signal Transducers,” *Antioxid. Redox Signal.*, vol. 8, no. 9–10, pp. 1419–1441, 2006.

[46] I. Jordan *et al.*, “A universal trend of amino acid gain and loss in protein evolution,” *Nature*, vol. 433, pp. 633–638, 2005.

[47] Houghton Mifflin Harcourt Publishing Company., *antioxidant*, 5th editio. Houghton Mifflin Harcourt Publishing Company, 2016.

[48] C. U. P. 2017, “Meaning of ‘antioxidant’ in the English Dictionary,” *Cambridge Dictionary*, 2017. [Online]. Available: https://dictionary.cambridge.org/dictionary/english/antioxidant.

[49] B. Halliwell, “How to Characterize a Biological Antioxidant,” *Free Radic. Res. Commun.*, vol. 9, no. 1, pp. 1–32, 1990.

[50] K. Asada, “Production and Scavenging of Reactive Oxygen Species in Chloroplasts and Their Functions,” *Plant Physiol.*, vol. 141, no. 2, p. 391 LP-396, Jun. 2006.

[51] C. Andre, Y. Larondelle, and D. Evers, “Dietary Antioxidants and Oxidative Stress from a Human and Plant Perspective: A Review,” *Curr. Nutr. Food Sci.*, vol. 6, no. 1, pp. 2–12, 2010.

[52] S. Hong-bo, C. Li-ye, C. A. Jaleeld, M. Hong-meie, and S. Ming-ana, “Higher plant antioxidants and redox signaling under environmental stresses,” *C. R. Biol.*, vol. 331, no. 6, pp. 433–441, 2008.

[53] W. Liu *et al.*, “Influence of Environmental Factors on the Active Substance Production and Antioxidant Activity in Potentilla fruticosa L. and Its Quality Assessment,” *Sci. Rep.*, vol. 6, p. 28591, Jul. 2016.

[54] J. Peñuelas and J. Llusià, “Effects of Carbon Dioxide, Water Supply, and Seasonality on Terpene Content and Emission by Rosmarinus officinalis,” *J. Chem. Ecol.*, vol. 23, no. 4, pp.

979–993, 1997.

[55] N. Miller, J. Sampson, L. Candeias, P. Bramley, and C. Rice-Evans, “Antioxidant activities of carotenes and xanthophylles,” *FEBS Lett.*, vol. 384, pp. 240–242, 1996.

[56] B. Demmig-Adams, “Antioxidants in Photosynthesis and Human Nutrition,” *Science (80-.).*, vol. 298, no. 5601, pp. 2149–2153, 2002.

[57] J. Von Lintig, “Provitamin A metabolism and functions in mammalian biology,” *Am. J. Clin. Nutr.*, vol. 96, no. 5, pp. 1234–1244, 2012.

[58] C. A. Williams and R. J. Grayer, “Anthocyanins and other flavonoids,” *Nat. Prod. Rep.*, pp. 539–573, 2004.

[59] C. A. Rice-Evans, N. J. Miller, and G. Paganga, “Structure-antioxidant activity relationships of flavonoids and phenolic acids,” *Free Radic. Biol. Med.*, vol. 20, no. 7, pp. 933–956, 1996.

[60] C. Rice-Evans, N. Miller, and G. Paganga, “Antioxidant properties of phenolic compounds,” *Trends Plant Sci.*, vol. 2, no. 4, pp. 152–159, 1997.

[61] S. V. Jovanovic, S. Steenken, M. Tosic, B. Marjanovic, and M. G. Simic, “Flavonoids as antioxidants,” *J. Am. Chem. Soc.*, vol. 116, no. 11, pp. 4846–4851, 1994.

[62] S. V Jovanovic and M. G. Simic, “Antioxidants in nutrition.,” *Ann. N. Y. Acad. Sci.*, vol. 899, pp. 326–334, 2000.

[63] C. A. Rice-evans, N. J. Miller, P. G. Bolwell, P. M. Bramley, and J. B. Pridham, “The Relative Antioxidant Activities of Plant-Derived Polyphenolic Flavonoids,” *Free Radic. Res.*, vol. 22, no. 4, pp. 375–383, 1995.

[64] S. V. Jovanovic, S. Steenken, Y. Hara, and M. G. Simic, “Reduction potentials of flavonoid and model phenoxyl radicals. Which ring in flavonoids is responsible for antioxidant activity?,” *J. Chem. Soc. Perkin Trans. 2*, no. 11, p. 2497, 1996.

[65] C. Manach, A. Scalbert, C. Morand, C. Rémésy, and L. Jiménez, “Polyphenols: food sources and bioavailability,” *Am. J. Clin. Nutr.*, vol. 79, no. 5, pp. 727–747, 2005.

[66] M. Galleano, S. V. Verstraeten, P. I. Oteiza, and C. G. Fraga, “Antioxidant actions of flavonoids: Thermodynamic and kinetic analysis,” *Arch. Biochem. Biophys.*, vol. 501, no. 1, pp. 23–30, 2010.

[67] N. Smirnoff, “Ascorbic acid: metabolism and functions of a multi-facetted molecule,” *Curr. Opin. Plant Biol.*, vol. 3, no. 3, pp. 229–235, 2000.

[68] A. Corti, A. F. Casini, and A. Pompella, “Cellular pathways for transport and efflux of ascorbate and dehydroascorbate,” *Arch. Biochem. Biophys.*, vol. 500, pp. 107–115, 2010.

[69] J. Mandl, A. Szarka, and G. B??nhegyi, “Vitamin C: Update on physiology and pharmacology,” *Br. J. Pharmacol.*, vol. 157, no. 7, pp. 1097–1110, 2009.

[70] A.-H. Harding, N. J. Wareham, and S. A. Bingham, “Plasma Vitamin C level, fruit and vegetable consumption, and the risk of new-onset type 2 diabetes mellitus,” *Arch. Int. Med.*, vol. 168, no. 14, pp. 1493–1499, 2008.

[71] J. Du, J. J. Cullen, and G. R. Buettner, “Ascorbic acid: Chemistry, biology and the treatment of cancer,” *Biochim. Biophys. Acta - Rev. Cancer*, vol. 1826, no. 2, pp. 443–457, 2012.

[72] X. Li, C. E. Cobb, K. E. Hill, R. F. Burk, and J. M. May, “Mitochondrial Uptake and Recycling of Ascorbic Acid,” *Arch. Biochem. Biophys.*, vol. 387, no. 1, pp. 143–153, 2001.

[73] M. Pohanka *et al.*, “Ascorbic Acid: An Old Player with a Broad Impact on Body Physiology Including Oxidative Stress Suppression and Immunomodulation: A Review,” *Mini-Reviews*

Med. Chem., vol. 12, no. 1, pp. 35–43, 2012.

[74] N. H. Williams and J. K. Yandell, *Outer-sphere electron-transfer reaction of ascorbate anions*, vol. 35. 1982.

[75] C. H. Foyer and G. Noctor, "Ascorbate and Glutathione: The Heart of the Redox Hub," *Plant Physiol.*, vol. 155, no. 1, pp. 2–18, 2011.

[76] R. Brigelius-Flohé and F. Galli, "Vitamin E: A vitamin still awaiting the detection of its biological function," *Mol. Nutr. Food Res.*, vol. 54, no. 5, pp. 583–587, 2010.

[77] M. Traber and J. Atkinson, "Vitamin E, antioxidant and nothing more.," *Free Radic. Biol. Med.*, vol. 43, pp. 4–15, 2007.

[78] M. G. Traber and E. a. Serbinova, "Biological Activities of Tocotrienols and Tocopherols," in *Antioxidant Food Supplements in Human Health*, 1st ed., L. Packer, M. Hiramatsu, and T. Yoshikawa, Eds. Academic Press, 1999, pp. 55–71.

[79] A. Azzi, "Molecular mechanism of α-tocopherol action," *Free Radic. Biol. Med.*, vol. 43, pp. 16–21, 2007.

[80] R. Brigelius-Flohé and K. J. A. Davies, "Is vitamin E an antioxidant, a regulator of signal transduction and gene expression, or a 'junk' food? Comments on the two accompanying papers: 'Molecular mechanism of α-tocopherol action' by A. Azzi and 'Vitamin E, antioxidant and nothing more' by M. Tra," *Free Radic. Biol. Med.*, vol. 43, no. 1, pp. 2–3, 2007.

[81] K. Herrmann and C. W. Nagel, "Occurrence and content of hydroxycinnamic and hydroxybenzoic acid compounds in foods," *Crit. Rev. Food Sci. Nutr.*, vol. 28, no. 4, pp. 315–347, Jan. 1989.

[82] M. N. Clifford, "Chlorogenic acids and other cinnamates–nature, occurrence and dietary burden," *J. Sci. Food Agric.*, vol. 79, no. 3, pp. 362–372, 1999.

[83] M.-E. Cuvelier, H. Richard, and C. Berset, "Comparison of the Antioxidative Activity of Some Acid-phenols: Structure-Activity Relationship.," *Biosci. Biotechnol. Biochem.*, vol. 56, no. 2, pp. 324–325, 1992.

[84] K. J. Lee, J. H. Choi, Y. P. Hwang, Y. C. Chung, and H. G. Jeong, "Protective effect of caffeic acid phenethyl ester on tert-butyl hydroperoxide-induced oxidative hepatotoxicity and DNA damage," *Food Chem. Toxicol.*, vol. 46, pp. 2445–2450, 2008.

[85] K. Natarajan, S. Singh, T. R. Burke, D. Grunberger, and B. B. Aggarwal, "Caffeic acid phenethyl ester is a potent and specific inhibitor of activation of nuclear transcription factor NF-kappa B.," *Proc. Natl. Acad. Sci. U. S. A.*, vol. 93, no. 17, pp. 9090–5, 1996.

[86] G. F. Sud'ina, O. K. Mirzoeva, M. A. Pushkareva, G. A. Korshunova, and N. V Sumbatyan, "Caffeic acid phenethyl ester as a lipoxygenase inhibitor with antioxidant properties," *Fed. Eur. Biochem. Soc.*, vol. 329, no. 1, pp. 21–24, 1993.

[87] J. D. Lambert and R. J. Elias, "The antioxidant and por-oxidant activities of green tea polyphenols: a role in cancer prevention," *Arch. Biochem. Biophys.*, vol. 501, no. 1, pp. 65–72, 2011.

[88] R. F. Boyer, J. S. McArthur, and T. M. Cary, "Plant phenolics as reductants for ferritin iron release," *Phytochemistry*, vol. 29, no. 12, pp. 3717–3719, 1990.

[89] C. B. Summers and G. W. Felton, "Prooxidant Effects of Phenolic Acids on the Generalist Herbivore Helicoverpa zea (Lepidoptera:Noctuidae): Potential Mode of Action for Phenolic Compounds in Plant Anti-herbivore Chemistry," *Insect Biochem. Mol. Biol.*, vol. 24, no. 9, pp. 943–953, 1994.

[90] E. Graf, “Antioxidant potential of ferulic acid.,” *Free Radic. Biol. Med.*, vol. 13, pp. 435–448, 1992.

[91] S. Itagaki *et al.*, “In vitro and in vivo antioxidant properties of ferulic acid: A comparative study with other natural oxidation inhibitors,” *Food Chem.*, vol. 114, no. 2, pp. 466–471, 2009.

[92] J. H. Chen and C.-T. Ho, “Antioxidant Activities of Caffeic Acid and Its Related Hydroxycinnamic Acid Compounds,” *J. Agric. Food Chem.*, vol. 45, no. 7, pp. 2374–2378, 1997.

[93] Y.-Y. Bian *et al.*, “Ferulic acid renders protection to HEK293 cells against oxidative damage and apoptosis induced by hydrogen peroxide,” *Vitr. Cell. Dev. Biol. - Anim.*, 2015.

[94] G.-C. Dong *et al.*, “A potent inhibition of oxidative stress induced gene expression in neural cells by sustained ferulic acid release from chitosan based hydrogel,” *Mater. Sci. Eng. C*, vol. 49, pp. 691–699, 2015.

[95] S. Sang *et al.*, “Synthesis and structure identification of thiol conjugates of (-)-epigallocatechin gallate and their urinary levels in mice,” *Chem. Res. Toxicol.*, vol. 18, no. 11, pp. 1762–1769, 2005.

[96] H. Zhang, D. Cao, W. Cui, M. Ji, X. Qian, and L. Zhong, “Molecular bases of thioredoxin and thioredoxin reductase-mediated prooxidant actions of (-)-epigallocatechin-3-gallate,” *Free Radic. Biol. Med.*, vol. 49, no. 12, pp. 2010–2018, 2010.

[97] Y. Wang, H. Zhang, A. Holmgren, W. Tian, and L. Zhong, “Inhibitory effect of green tea extract and (-)-epigallocatechin-3-gallate on mammalian thioredoxin reductase and HeLa cell viability,” *Oncol. Rep.*, vol. 20, pp. 1479–1487, 2008.

[98] H. S. Kim, M. J. Quon, and J. a. Kim, “New insights into the mechanisms of polyphenols beyond antioxidant properties; lessons from the green tea polyphenol, epigallocatechin 3-gallate,” *Redox Biol.*, vol. 2, pp. 187–195, 2014.

[99] K. Min and T. K. Kwon, “Anticancer effects and molecular mechanisms of epigallocatechin-3-gallate,” *Integr. Med. Res.*, vol. 3, no. 1, pp. 16–24, 2014.

[100] J. M. Calderón-Montaño, E. Burgos-Morón, C. Pérez-Guerrero, and M. López-Lázaro, “A review on the dietary flavonoid kaempferol.,” *Mini Rev. Med. Chem.*, vol. 11, pp. 298–344, 2011.

[101] M. A. Gates, S. S. Tworoger, J. L. Hecht, I. De Vivo, B. Rosner, and S. E. Hankinson, “A prospective study of dietary flavonoid intake and incidence of epithelial ovarian cancer,” *Int. J. Cancer*, vol. 121, no. 10, pp. 2225–2232, Nov. 2007.

[102] U. Nöthlings *et al.*, “A food pattern that is predictive of flavonol intake and risk of pancreatic cancer,” *Am. J. Clin. Nutr.*, vol. 88, no. 6, pp. 1653–1662, 2015.

[103] G. An, J. Gallegos, and M. E. Morris, “The Bioflavonoid Kaempferol Is an Abcg2 Substrate and Inhibits Abcg2-Mediated Quercetin Efflux,” *Drug Metab. Dispos.*, vol. 39, no. 3, p. 426 LP-432, Mar. 2011.

[104] J. C. R. Vellosa *et al.*, “Antioxidant and cytotoxic studies for kaempferol, quercetin and isoquercitrin ,” *Eclética Química* , vol. 36. scielo , pp. 7–20, 2011.

[105] V. A. Roginsky, T. K. Barsukova, A. A. Remorova, and W. Bors, “Moderate antioxidative efficiencies of flavonoids during peroxidation of methyl linoleate in homogeneous and micellar solutions,” *J. Am. Oil Chem. Soc.*, vol. 73, no. 6, pp. 777–786, 1996.

[106] X.-K. Fang, J. Gao, and D.-N. Zhu, “Kaempferol and quercetin isolated from Euonymus alatus improve glucose uptake of 3T3-L1 cells without adipogenesis activity,” *Life Sci.*, vol.

82, no. 11, pp. 615–622, 2008.

[107] M. Sugahara, J. Nakanishi, and Y. Katsuta, “Kaempferol enhanced the intracellular thioredoxin system in normal cultured human keratinocytes.,” *Biosci. Biotechnol. Biochem.*, vol. 74, no. 8, pp. 1701–3, 2010.

[108] E.-J. Yang, G.-S. Kim, M. Jun, and K.-S. Song, “Kaempferol attenuates the glutamate-induced oxidative stress in mouse-derived hippocampal neuronal HT22 cells,” *Food Funct.*, vol. 5, no. 7, pp. 1395–1402, 2014.

[109] C.-N. Wang, C.-W. Chi, Y.-L. Lin, C.-F. Chen, and Y.-J. Shiao, “The Neuroprotective Effects of Phytoestrogens on Amyloid β Protein-induced Toxicity Are Mediated by Abrogating the Activation of Caspase Cascade in Rat Cortical Neurons,” *J. Biol. Chem.*, vol. 276, pp. 5287–5295, 2001.

[110] Y. J. Lee *et al.*, “Kaempferol protects HIT-T15 pancreatic beta cells from 2-deoxy-D-ribose-induced oxidative damage,” *Phyther. Res.*, vol. 24, no. 3, pp. 419–423, Mar. 2010.

[111] P. Rajendran, T. Rengarajan, N. Nandakumar, R. Palaniswami, Y. Nishigaki, and I. Nishigaki, “Kaempferol, a potential cytostatic and cure for inflammatory disorders,” *Eur. J. Med. Chem.*, vol. 86, pp. 103–112, 2014.

[112] D. Kashyap, A. Sharma, H. S. Tuli, K. Sak, S. Punia, and T. K. Mukherjee, “Kaempferol – A dietary anticancer molecule with multiple mechanisms of action: Recent trends and advancements,” *J. Funct. Foods*, vol. 30, pp. 203–219, 2017.

[113] K. P. Devi *et al.*, “Kaempferol and inflammation: From chemistry to medicine,” *Pharmacol. Res.*, vol. 99, pp. 1–10, 2015.

[114] M. J. T. J. Arts, J. Sebastiaan Dallinga, H.-P. Voss, G. R. M. M. Haenen, and A. Bast, “A new approach to assess the total antioxidant capacity using the TEAC assay,” *Food Chem.*, vol. 88, no. 4, pp. 567–570, 2004.

[115] B. Yang, K. Arai, and F. Kusu, “Electrochemical behaviors of quercetin and kaempferol in neutral buffer solution.,” *Anal. Sci.*, vol. 17, no. 8, pp. 987–989, 2001.

[116] I. B. Afanas’ev, A. I. Dcrozhko, A. V. Brodskii, V. A. Kostyuk, and A. I. Potapovitch, “Chelating and free radical scavenging mechanisms of inhibitory action of rutin and quercetin in lipid peroxidation,” *Biochem. Pharmacol.*, vol. 38, no. 11, pp. 1763–1769, 1989.

[117] H. M. Awad, M. G. Boersma, S. Boeren, P. J. van Bladeren, J. Vervoort, and I. M. C. M. Rietjens, “The Regioselectivity of Glutathione Adduct Formation with Flavonoid Quinone/Quinone Methides Is pH-Dependent,” *Chem. Res. Toxicol.*, vol. 15, no. 3, pp. 343–351, Mar. 2002.

[118] A. W. Boots, N. Kubben, G. R. M. M. Haenen, and A. Bast, “Oxidized quercetin reacts with thiols rather than with ascorbate: Implication for quercetin supplementation,” *Biochem. Biophys. Res. Commun.*, vol. 308, no. 3, pp. 560–565, 2003.

[119] M. Russo, C. Spagnuolo, I. Tedesco, S. Bilotto, and G. L. Russo, “The flavonoid quercetin in disease prevention and therapy: Facts and fancies,” *Biochem. Pharmacol.*, vol. 83, no. 1, pp. 6–15, 2012.

[120] G. D’Andrea, “Quercetin: A flavonol with multifaceted therapeutic applications?,” *Fitoterapia*, vol. 106, pp. 256–271, 2015.

[121] P. Iacopini, M. Baldi, P. Storchi, and L. Sebastiani, “Catechin, epicatechin, quercetin, rutin and resveratrol in red grape: Content, in vitro antioxidant activity and interactions,” *J. Food Compos. Anal.*, vol. 21, no. 8, pp. 589–598, 2008.

[122] Y. Hanasaki, S. Ogava, and S. Fukui, "The Correlation Between Active Oxygens Scavanging and Antioxidative Effects of Flavonoids," *Free Radic. Biol. Med.*, vol. 16, no. 6, pp. 845–850, 1994.

[123] N. Kamalakkannan and P. S. M. Prince, "Rutin improves the antioxidant status in streptozotocin-induced diabetic rat tissues," *Mol. Cell. Biochem.*, vol. 293, no. 1, p. 211, 2006.

[124] A. Saija, M. Scalese, M. Lanza, D. Marzullo, F. Bonina, and F. Castelli, "Flavonoids as antioxidant agents: Importance of their interaction with biomembranes," *Free Radic. Biol. Med.*, vol. 19, no. 4, pp. 481–486, 1995.

[125] H. Tsuchiya, "Structure-dependent membrane interaction of flavonoids associated with their bioactivity," *Food Chem.*, vol. 120, no. 4, pp. 1089–1096, 2010.

[126] M. Blumert and J. Liu, *Jiaogulan: China's "Immortality Herb."* Badger, CA 93603: Torchlight Publishing, Inc., 1999.

[127] V. Razmovski-Naumovski, T. Huang, V. Tran, G. Li, C. Duke, and B. Roufogalis, "Chemistry and Pharmacology of Gynostemma pentaphyllum," *Phytochem. Rev.*, vol. 4, no. 2, pp. 197–219, 2005.

[128] Y. Zhao, Z. Xie, Y. Niu, H. Shi, P. Chen, and L. (Lucy) Yu, "Chemical compositions, HPLC/MS fingerprinting profiles and radical scavenging properties of commercial Gynostemma pentaphyllum (Thunb.) Makino samples," *Food Chem.*, vol. 134, no. 1, pp. 180–188, 2012.

[129] X. Y. Shang, Y. Zhang, Y. L. Bai, C. L. Xu, W. N. Niu, and C. G. Qin, "Extraction and antioxidant activities of polysaccharides from Gynostemma pentaphyllum makino," *Asian J. Chem.*, vol. 25, no. 16, pp. 9092–9096, 2013.

[130] Z. Xie *et al.*, "Chemical composition and anti-proliferative and anti-inflammatory effects of the leaf and whole-plant samples of diploid and tetraploid Gynostemma pentaphyllum (Thunb.) Makino," *Food Chem.*, vol. 132, no. 1, pp. 125–133, 2012.

[131] D. Samec, L. Valek-Zulj, S. Martinez, J. Gruz, A. Piljac, and J. Piljac-Zegarac, "Phenolic acids significantly contribute to antioxidant potency of Gynostemma pentaphyllum aqueous and methanol extracts," *Ind. Crops Prod.*, vol. 84, pp. 104–107, 2016.

[132] J. H. Kim and Y. N. Han, "Dammarane-type saponins from Gynostemma pentaphyllum," *Phytochemistry*, vol. 72, no. 11–12, pp. 1453–1459, 2011.

[133] S. Lin-Na and S. Yong-Xiu, "Effects of polysaccharides from Gynostemma pentaphyllum (Thunb.), Makino on physical fatigue," *Afr. J. Tradit. Complement. Altern. Med.*, vol. 11, no. 3, pp. 112–117, 2014.

[134] X. Shang, Y. Chao, Y. Zhang, C. Lu, C. Xu, and W. Niu, "Immunomodulatory and antioxidant effects of polysaccharides from Gynostemma pentaphyllum Makino in immunosuppressed mice," *Molecules*, vol. 21, no. 8, 2016.

[135] Y. Niu *et al.*, "Characterization of a Novel Alkali-Soluble Heteropolysaccharide from Tetraploid Gynostemma pentaphyllum Makino and Its Potential Anti-in fl ammatory and Antioxidant Properties," *J. Agric. Food Chem.*, vol. 62, pp. 3783–3790, 2014.

[136] F. Aktan, S. Henness, B. D. Roufogalis, and A. J. Ammit, "Gypenosides derived from Gynostemma pentaphyllum suppress NO synthesis in murine macrophages by inhibiting iNOS enzymatic activity and attenuating NF-??B-mediated iNOS protein expression," *Nitric Oxide - Biol. Chem.*, vol. 8, no. 4, pp. 235–242, 2003.

[137] J. Su *et al.*, "Hypolipidemic mechanism of gypenosides via inhibition of pancreatic lipase and reduction in cholesterol micellar solubility," *Eur. Food Res. Technol.*, vol. 242, no. 3,

pp. 305–312, 2016.

[138] S. Megalli, F. Aktan, N. M. Davies, and B. D. Roufogalis, “Phytopreventative Effects Of Gynostemma Pentaphyllum In Rats,” *J. Pharmacol. Pharm. Sci.*, vol. 8, no. 3, pp. 507–515, 2005.

[139] M. Wang, F. Wang, Y. Wang, X. Ma, M. Zhao, and C. Zhao, “Metabonomics study of the therapeutic mechanism of gynostemma pentaphyllum and atorvastatin for hyperlipidemia in rats,” *PLoS One*, vol. 8, no. 11, pp. 1–10, 2013.

[140] S.-H. Park *et al.*, “Antiobesity Effect of Gynostemma pentaphyllum Extract (Actiponin): A randomized, double-blind, placebo-controlled trial,” *Clin. Trials Behav. Pharmacother. devices, Surg.*, vol. 22, no. 1, pp. 63–71, 2014.

[141] M. A. Tanner, X. Bu, J. A. Steimle, and P. R. Myers, “The Direct Release of Nitric Oxide by Gypenosides Derived from the Herb Gynostemma pentaphyllum,” *Nitric Oxide Biol. Chem.*, vol. 3, no. 5, pp. 359–365, 1999.

[142] C. Liao *et al.*, “Gypenoside L inhibits autophagic flux and induces cell death in human esophageal cancer cells through endoplasm reticulum stress-mediated Ca2+ release,” *Oncotarget*, vol. 7, no. 30, p. 47387—47402, 2016.

[143] S. Xing, M. Jang, Y. Wang, and X. Piao, “A new dammarane-type saponin from Gynostemma pentaphyllum induces apoptosis in A549 human lung carcinoma cells,” *Bioorg. Med. Chem. Lett.*, vol. 26, no. 7, pp. 1754–1759, 2016.

[144] K. Tsui *et al.*, “Flavonoids from Gynostemma pentaphyllum Exhibit Differential Induction of Cell Cycle Arrest in H460 and A549 Cancer Cells,” *Molecules*, vol. 19, pp. 17663–17681, 2014.

[145] L. Schild, B. H. Chen, P. Makarov, K. Kattengell, K. Heinitz, and G. Keilhoff, “Selective induction of apoptosis in glioma tumour cells by a Gynostemma pentaphyllum extract,” *Phytomedicine*, vol. 17, no. 8–9, pp. 589–597, 2010.

[146] Y. Li, W. Lin, J. Huang, Y. Xie, and W. Ma, “Anti-cancer effects of Gynostemma pentaphyllum (Thunb.) Makino (Jiaogulan),” *Chin. Med.*, vol. 11, no. 1, p. 43, 2016.

[147] R. H. Mu *et al.*, “Antidepressant-like effects of standardized gypenosides: involvement of brain-derived neurotrophic factor signaling in hippocampus,” *Psychopharmacology (Berl).*, vol. 233, no. 17, pp. 3211–3221, 2016.

[148] M. He *et al.*, “Inhibitory effects of gypenosides on seven human cytochrome P450 enzymes in vitro,” *Food Chem. Toxicol.*, vol. 57, no. 528, pp. 262–265, 2013.

[149] L. Shang *et al.*, “Gypenosides protect primary cultures of rat cortical cells against oxidative neurotoxicity,” *Brain Res.*, vol. 1102, pp. 163–174, 2006.

[150] E. Bendary, R. R. Francis, H. M. G. Ali, M. I. Sarwat, and S. El Hady, “Antioxidant and structure–activity relationships (SARs) of some phenolic and anilines compounds,” *Ann. Agric. Sci.*, vol. 58, no. 2, pp. 173–181, 2013.

[151] J. S. Wright, E. R. Johnson, and G. A. DiLabio, “Predicting the activity of phenolic antioxidants: Theoretical method, analysis of substituent effects, and application to major families of antioxidants,” *J. Am. Chem. Soc.*, vol. 123, no. 6, pp. 1173–1183, 2001.

[152] N. J. Miller, C. Rice-Evans, M. J. Davies, V. Gopinathan, and A. Milner, “A Novel Method for Measuring Antioxidant Capacity and its Application to Monitoring the Antioxidant Status in Premature Neonates,” *Clin. Sci.*, vol. 84, no. 4, pp. 407–412, 1993.

[153] I. F. F. Benzie and J. J. Strain, “The Ferric Reducing Ability of Plasma (FRAP) as a Measure of ‘Antioxidant Power’: The FRAP Assay,” *Anal. Biochem.*, vol. 239, no. 1, pp. 70–76, 1996.

[154] M. Blois, “Antioxidant determinations by the use of a stable free radical,” *Nature*, vol. 181, pp. 1199–1200, 1958.

[155] S. B. Kedare and R. P. Singh, “Genesis and development of DPPH method of antioxidant assay,” *J. Food Sci. Technol.*, vol. 48, no. 4, pp. 412–422, 2011.

[156] J. Muff, L. R. Bennedsen, and E. G. Søgaard, “Study of electrochemical bleaching of p-nitrosodimethylaniline and its role as hydroxyl radical probe compound,” *J. Appl. Electrochem.*, vol. 41, no. 5, pp. 599–607, 2011.

[157] I. Popov and G. Lewin, “Antioxidative homeostasis: characterisation by means of chemiluminescent technique,” *Methods Enzymol.*, vol. 300, pp. 437–456, 1999.

[158] V. Fogliano, G. Verde, Veronica Randazzo, and A. Ritieni, “Method for Measuring Antioxidant Activity and Its Application to Monitoring the Antioxidant Capacity of Wines,” *J. Agric. Food Chem.*, vol. 47, no. 3, pp. 1035–1040, 1999.

[159] A. Hamelin, “Underpotential deposition of lead on single crystal faces of gold,” *J. Electroanal. Chem. Interfacial Electrochem.*, vol. 165, no. 1–2, pp. 167–180, 1984.

[160] B. Ou, J. Hampsch-Woodill, Maureen Flanagan, E. K. Deemer, R. L. Prior, and D. Huang, “Novel Fluorometric Assay for Hydroxyl Radical Prevention Capacity Using Fluorescein as the Probe,” *J. Agric. Food Chem.*, vol. 50, no. 10, pp. 2772–2777, 2002.

[161] K. Mishra, H. Ojha, and N. K. Chaudhury, “Estimation of antiradical properties of antioxidants using DPPH - assay: A critical review and results,” *Food Chem.*, vol. 130, no. 4, pp. 1036–1043, 2012.

[162] D. Huang, O. U. Boxin, and R. L. Prior, “The chemistry behind antioxidant capacity assays,” *J. Agric. Food Chem.*, vol. 53, no. 6, pp. 1841–1856, 2005.

[163] K. Schlesier, M. Harwat, V. Böhm, and R. Bitsch, “Assessment of antioxidant activity by using different in vitro methods.,” *Free Radic. Res.*, vol. 36, no. 2, pp. 177–187, 2002.

[164] D. J. Charles, *Antioxidant Properties of Spices, Herbs and Other Sources*. Springer New York, 2012.

[165] A. G. Krainev and D. J. Bigelow, “Comparison of 2,2[prime or minute]-azobis(2-amidinopropane) hydrochloride (AAPH) and 2,2[prime or minute]-azobis(2,4-dimethylvaleronitrile)(AMVN) as free radical initiators: a spin-trapping study,” *J. Chem. Soc. Perkin Trans. 2*, no. 4, pp. 747–754, 1996.

[166] G. W. Winston, F. Regoli, A. J. Dugas, J. H. Fong, and K. A. Blanchard, “A Rapid Gas Chromatographic Assay for Determining Oxyradical Scavenging Capacity of Antioxidants and Biological Fluids,” *Free Radic. Biol. Med.*, vol. 24, no. 3, pp. 480–493, 1998.

[167] C. C. Winterbourn, “The challenges of using fluorescent probes to detect and quantify specific reactive oxygen species in living cells,” *Biochim. Biophys. Acta - Gen. Subj.*, vol. 1840, no. 2, pp. 730–738, 2014.

[168] B. Zhao, F. A. Summers, and R. P. Mason, “Photooxidation of Amplex Red to resorufin: implications of exposing the Amplex Red assay to light,” *Free Radic. Biol. Med.*, vol. 53, no. 5, pp. 1080–1087, Sep. 2012.

[169] J. Serrano, M. Jové, J. Boada, M. J. Bellmunt, R. Pamplona, and M. Portero-Otín, “Dietary antioxidants interfere with Amplex Red-coupled-fluorescence assays,” *Biochem. Biophys. Res. Commun.*, vol. 388, no. 2, pp. 443–449, 2009.

[170] D. Andina, J.-C. Leroux, and P. Luciani, “Ratiometric Fluorescent Probes for the Detection of Reactive Oxygen Species,” *Chem. - A Eur. J.*, pp. 13549–13573, 2017.

[171] Y. Nishinaka, Y. Aramaki, H. Yoshida, H. Masuya, T. Sugawara, and Y. Ichimori, “A New Sensitive Chemiluminescence Probe, L-012, for Measuring the Production of Superoxide Anion by Cells,” *Biochem. Biophys. Res. Commun.*, vol. 193, no. 2, pp. 554–559, 1993.

[172] J. Zielonka, J. D. Lambeth, and B. Kalyanaraman, “On the use of L-012, a luminol-based chemiluminescent probe, for detecting superoxide and identifying inhibitors of NADPH oxidase: A re-evaluation,” *Free Radic. Biol. Med.*, vol. 65, pp. 1310–1314, 2013.

[173] A. A. Pakhomov and V. I. Martynov, “GFP Family: Structural Insights into Spectral Tuning,” *Chem. Biol.*, vol. 15, no. 8, pp. 755–764, 2008.

[174] V. V. Belousov *et al.*, “Genetically encoded fluorescent indicator for intracellular hydrogen peroxide,” *Nat. Methods*, vol. 3, no. 4, pp. 281–286, 2006.

[175] K. A. Lukyanov and V. V. Belousov, “Genetically encoded fluorescent redox sensors,” *Biochim. Biophys. Acta - Gen. Subj.*, vol. 1840, no. 2, pp. 745–756, 2014.

[176] I. Mehmeti, S. Lortz, and S. Lenzen, “The H2O2-sensitive HyPer protein targeted to the endoplasmic reticulum as a mirror of the oxidizing thiol-disulfide milieu,” *Free Radic. Biol. Med.*, vol. 53, no. 7, pp. 1451–1458, 2012.

[177] V. V Belousov *et al.*, “Genetically encoded fluorescent indicator for intracellular hydrogen peroxide,” *Nat. Methods*, vol. 3, p. 281, Mar. 2006.

[178] W. Gehrmann and M. Elsner, “A specific fluorescence probe for hydrogen peroxide detection in peroxisomes.,” *Free Radic. Res.*, vol. 45, no. 5, pp. 501–6, 2011.

[179] H. Østergaard, A. Henriksen, F. G. Hansen, and J. R. Winther, “Shedding light on disulfide bond formation: engineering a redox switch in green fluorescent protein,” *EMBO J.*, vol. 20, no. 21, p. 5853 LP-5862, Nov. 2001.

[180] G. T. Hanson *et al.*, “Investigating Mitochondrial Redox Potential with Redox-sensitive Green Fluorescent Protein Indicators,” *J. Biol. Chem.* , vol. 279, no. 13, pp. 13044–13053, Mar. 2004.

[181] C. T. Dooley, T. M. Dore, G. T. Hanson, W. C. Jackson, S. J. Remington, and R. Y. Tsien, “Imaging Dynamic Redox Changes in Mammalian Cells with Green Fluorescent Protein Indicators,” *J. Biol. Chem.* , vol. 279, no. 21, pp. 22284–22293, May 2004.

[182] M. Gutscher *et al.*, “Real-time imaging of the intracellular glutathione redox potential,” *Nat. Methods*, vol. 5, p. 553, May 2008.

[183] M. Gutscher *et al.*, “Proximity-based Protein Thiol Oxidation by H2O2-scavenging Peroxidases,” *J. Biol. Chem.* , vol. 284, no. 46, pp. 31532–31540, Nov. 2009.

[184] J. S. Beckman and W. H. Koppenol, “Nitric oxide, superoxide, and peroxynitrite: the good, the bad, and ugly,” *Am. J. Physiol. Physiol.*, vol. 271, no. 5, pp. C1424–C1437, Nov. 1996.

[185] J. P. Crow and H. B. T.-M. in E. Ischiropoulos, “[17] Detection and quantitation of nitrotyrosine residues in proteins: In vivo marker of peroxynitrite,” in *Nitric Oxide Part B: Physiological and Pathological Processes*, vol. 269, Academic Press, 1996, pp. 185–194.

[186] M. Fedorova, R. C. Bollineni, and R. Hoffmann, “Protein carbonylation as a major hallmark of oxidative damage: Update of analytical strategies,” *Mass Spectrom. Rev.*, vol. 33, no. 2, pp. 79–97, Mar. 2014.

[187] I. Dalle-Donne, G. Aldini, M. Carini, R. Colombo, R. Rossi, and A. Milzani, “Protein carbonylation, cellular dysfunction, and disease progression,” *J. Cell. Mol. Med.*, vol. 10, no. 2, pp. 389–406, Apr. 2006.

[188] E. Augustyniak *et al.*, “Validation of protein carbonyl measurement: A multi-centre study,”

Redox Biol., vol. 4, pp. 149–157, 2015.

[189] G. L. Milne, E. S. Musiek, and J. D. Morrow, "F_2-Isoprostanes as markers of oxidative stress *in vivo* : An overview," *Biomarkers*, vol. 10, no. sup1, pp. 10–23, 2005.

[190] G. P. C. Drummen, L. C. M. Van Liebergen, J. A. F. Op den Kamp, and J. A. Post, "C11-BODIPY581/591, an oxidation-sensitive fluorescent lipid peroxidation probe: (Micro)spectroscopic characterization and validation of methodology," *Free Radic. Biol. Med.*, vol. 33, no. 4, pp. 473–490, 2002.

[191] M. N. Peyrat-Maillard, S. Bonnely, and C. Berset, "Determination of the antioxidant activity of phenolic compounds by coulometric detection," *Talanta*, vol. 51, no. 4, pp. 709–716, 2000.

[192] H. Hotta, S. Nagano, M. Ueda, Y. Tsujino, J. Koyama, and T. Osakai, "Higher radical scavenging activities of polyphenolic antioxidants can be ascribed to chemical reactions following their oxidation," *Biochim. Biophys. Acta - Gen. Subj.*, vol. 1572, pp. 123–132, 2002.

[193] A. René, M. L. Abasq, D. Hauchard, and P. Hapiot, "How do phenolic compounds react toward superoxide ion? A simple electrochemical method for evaluating antioxidant capacity," *Anal. Chem.*, vol. 82, no. 20, pp. 8703–8710, 2010.

[194] C. Cren-Olivé, P. Hapiot, J. Pinson, and C. Rolando, "Free radical chemistry of flavan-3-ols: Determination of thermodynamic parameters and of kinetic reactivity from short (ns) to long (ms) time scale," *J. Am. Chem. Soc.*, vol. 124, no. 47, pp. 14027–14038, 2002.

[195] C. P. Andrieux, P. Hapiot, and J. M. Saveant, "Mechanism of superoxide ion disproportionation in aprotic solvents," *J. Am. Chem. Soc.*, vol. 109, no. 12, pp. 3768–3775, 1987.

[196] B. Prieto-Simón, M. Cortina, M. Campàs, and C. Calas-Blanchard, "Electrochemical biosensors as a tool for antioxidant capacity assessment," *Sensors Actuators B Chem.*, vol. 129, no. 1, pp. 459–466, Jan. 2008.

[197] K. Tammeveski, T. T. Tenno, A. A. Mashirin, E. W. Hillhouse, P. Manning, and C. J. McNeil, "Superoxide electrode based on covalently immobilized cyt c: modelling studies," *Free Radic. Biol. Med.*, vol. 25, pp. 973–978, 1998.

[198] M. K. Beissenhirtz, F. W. Scheller, and F. Lisdat, "A superoxide sensor based on a multilayer cyt c electrode," *Anal. Chem.*, vol. 76, pp. 4665–4671, 2004.

[199] Y. Tian, L. Mao, T. Okajima, and T. Ohsaka, "Superoxide dismutase-based third-generation biosensor for superoxide anion," *Anal. Chem.*, vol. 74, pp. 2428–2434, 2002.

[200] L. Campanella, G. Favero, L. Persi, and M. Tomassetti, "New biosensor for superoxide radical used to evidence molecules of biomedical and pharma- ceutical interest having radical scavenging properties," *J. Pharm. Biomed. Anal.*, vol. 23, pp. 69–76, 2000.

[201] V. Lvovich and A. Scheeline, "Amperometric sensors for simultaneous super- oxide and hydrogen peroxide detection," *Anal. Chem.*, vol. 69, pp. 454–462, 1997.

[202] L. D. Mello, S. Hernandez, G. Marrazza, M. Mascini, and L. T. Kubota, "Investigations of the antioxidant properties of plant extracts using a DNA-electrochemical biosensor.," *Biosens. Bioelectron.*, vol. 21, no. 7, pp. 1374–82, Jan. 2006.

[203] I. Gualandi, L. Guadagnini, S. Zappoli, and D. Tonelli, "A Polypyrrole Based Sensor for the Electrochemical Detection of OH Radicals," *Electroanalysis*, vol. 26, no. 7, pp. 1544–1550, Jul. 2014.

[204] E. Kibena, K. Tammeveski, L. Matisen, U. Hasse, and F. Scholz, "OH radical degradation of

blocking aryl layers on glassy carbon and gold electrodes leads to film thinning on glassy carbon and pinhole films on gold," *Electrochem. commun.*, vol. 29, pp. 33–36, Apr. 2013.

[205] F. Scholz, *Electroanalytical methods*, 2nd ed. Heidelberg: Springer Berlin Heidelberg, 2010.

[206] J. Tkac and J. J. Davis, "An optimised electrode pre-treatment for SAM formation on polycrystalline gold," *J. Electroanal. Chem.*, vol. 621, no. 1, pp. 117–120, 2008.

[207] C. Lefrou and R. Cornut, "Analytical expressions for quantitative scanning electrochemical microscopy (SECM)," *ChemPhysChem*, vol. 11, no. 3, pp. 547–556, 2010.

[208] J. H. Scofield, "Hartree-Slater subshell photoionization cross-sections at 1254 and 1487 eV," *J. Electron Spectros. Relat. Phenomena*, vol. 8, no. 2, pp. 129–137, 1976.

[209] P. E. Laibinis, R. L. Graham, H. A. Biebuyck, and G. M. Whitesides, "X-ray Damage to CF3CO2-Terminated Organic Monolayers on Si/Au: Principal Effect of Electrons," *Science (80-.).*, vol. 254, no. 5034, pp. 981–983, 1991.

[210] R. Jogireddy *et al.*, "Structural Analysis of HS(CD2)12(O- CH2-CH2)6OCH3 Monolayers on Gold by Means of Polarization Modulation Infrared Reflection Absorption Spectroscopy . Progress of the Reaction with Bromine," *Langmuir*, vol. 26, no. 1, pp. 362–370, 2010.

[211] X. He, W. G. Aker, M. Pelaez, Y. Lin, D. D. Dionysiou, and H. M. Hwang, "Assessment of nitrogen-fluorine-codoped TiO2 under visible light for degradation of BPA: Implication for field remediation," *J. Photochem. Photobiol. A Chem.*, vol. 314, no. August, pp. 81–92, 2016.

[212] L. Schild, A. Roth, G. Keilhoff, A. Gardemann, and R. Brödemann, "Protection of hippocampal slices against hypoxia/hypoglycemia injury by a Gynostemma pentaphyllum extract.," *Phytomedicine*, vol. 16, no. 8, pp. 734–43, 2009.

[213] T. C. Genaro-Mattos, L. T. Dalvi, R. G. Oliveira, J. S. Ginani, and M. Hermes-Lima, "Reevaluation of the 2-deoxyribose assay for determination of free radical formation," *Biochim. Biophys. Acta - Gen. Subj.*, vol. 1790, no. 12, pp. 1636–1642, 2009.

[214] H. E. Miller, "A simplified method for the evaluation of antioxidants," *J. Am. Oil Chem. Soc.*, vol. 48, no. 2, pp. 91–91, 1971.

[215] S. Schneider, N. Srirangan, M. Wurster, U. Lindequist, and M. Lalk, "Cytotoxic activity of aquatic fungus Pseudohalonectria lignicola on two different human cell lines," *Planta Med*, vol. 80, no. 16, p. P1N20, 2014.

[216] L. Serrander *et al.*, "NOX4 activity is determined by mRNA levels and reveals a unique pattern of ROS generation," *Biochem. J.*, vol. 406, no. 1, pp. 105–114, 2007.

[217] PromoKine, "Colorimetric Cell Viability Kit I (WST-8)," Heidelberg, 2014.

[218] H. Tominaga *et al.*, "A water-soluble tetrazolium salt useful for colorimetric cell viability assay," *Anal. Commun.*, vol. 36, no. 2, pp. 47–50, 1999.

[219] C. J. Adams and B. Storrie, "A simple DNA-dependent fluorescence enhancement assay for cell number.," *J. Histochem. Cytochem.*, vol. 29, no. 2, pp. 326–328, Feb. 1981.

[220] N. (InCelligence) Kühl-Erb, "Zellkultur - Zellzählung," 2018. [Online]. Available: http://www.incelligence.de/zellkultur/zellzaehlung/zellzaehlung-anleitung. [Accessed: 10-Jan-2018].

[221] K. Dörries and M. Lalk, "Metabolic footprint analysis uncovers strain specific overflow metabolism and D-isoleucine production of Staphylococcus aureus COL and HG001," *PLoS One*, vol. 8, no. 12, 2013.

[222] A. Leonard, P. Gierok, K. Methling, A. Gómez-Mejia, S. Hammerschmidt, and M. Lalk, "Metabolic inventory of Streptococcus pneumoniae growing in a chemical defined environment," *Int. J. Med. Microbiol.*, Jan. 2018.

[223] Promega, "GSH / GSSG-Glo ™ Assay technical manual," Madison, USA, 2011.

[224] A. Lammers, "Untersuchung zum Redox-Metabolismus in einem humanen Zellkulturmodell mittels GSH/GSSG-Assay," University of Greifswald, 2015.

[225] T. P. M. Akerboom and H. B. T.-M. in E. Sies, "[48] Assay of glutathione, glutathione disulfide, and glutathione mixed disulfides in biological samples," in *Detoxication and Drug Metabolism: Conjugation and Related Systems*, vol. 77, Academic Press, 1981, pp. 373–382.

[226] M. M. Bradford, "A rapid and sensitive method for the quantitation of microgram quantities of protein utilizing the principle of protein-dye binding," *Anal. Biochem.*, vol. 72, no. 1, pp. 248–254, 1976.

[227] S. E. Creager, L. A. Hockett, and G. K. Rowe, "Consequences of microscopic surface roughness for molecular self-assembly," *Langmuir*, vol. 8, no. 3, pp. 854–861, Mar. 1992.

[228] D. Thal, H. Kahlert, J. Chinnaya, P. Ahrens, and U. Hasse, "Impact of gold-1-decanethiol-SAM formation and removal cycles on the surface properties of polycrystalline gold and SAM quality," *J. Solid State Electrochem.*, pp. 1–6, 2017.

[229] U. Hasse, K. Fricke, D. Dias, G. Sievers, H. Wulff, and F. Scholz, "Grain boundary corrosion of the surface of annealed thin layers of gold by OH· radicals," *J. Solid State Electrochem.*, vol. 16, no. 7, pp. 2383–2389, May 2012.

[230] A. M. Nowicka, U. Hasse, M. Hermes, and F. Scholz, "Hydroxyl radicals attack metallic gold.," *Angew. Chem. Int. Ed. Engl.*, vol. 49, no. 6, pp. 1061–3, Feb. 2010.

[231] M. H. Schoenfisch and J. E. Pemberton, "Air Stability of Alkanethiol Self-Assembled Monolayers on Silver and Gold Surfaces," *J. Am. Chem. Soc.*, vol. 120, no. 18, pp. 4502–4513, May 1998.

[232] J. D. C. Jacob, T. R. Lee, and S. Baldelli, "In Situ Vibrational Study of the Reductive Desorption of Alkanethiol Monolayers on Gold by Sum Frequency Generation Spectroscopy," *J. Phys. Chem. C*, vol. 118, pp. 29126–29134, 2014.

[233] O. Chailapakul and R. M. Crooks, "Synthesis and Characterization of Simple Self-Assembling, Nanoporous Monolayer Assemblies: A New Strategy for Molecular Recognition," *Langmuir*, vol. 9, no. 4, pp. 884–888, 1993.

[234] J. Richer and J. Lipkowski, "Measurement of Physical Adsorption of Neutral Organic-Species at Solid Electrodes," *J. Electrochem. Soc.*, vol. 133, no. 1, pp. 121–128, 1986.

[235] I. Zawisza and J. Lipkowski, "Layer by layer characterization of 1-octadecanol films on a Au(III) electrode surface. 'In situ' polarization modulation infrared reflection absorption spectroscopy and electrochemical studies," *Langmuir*, vol. 20, no. 11, pp. 4579–4589, 2004.

[236] J. Dai *et al.*, "Some thoughts on the existence of ion and water channels in highly dense and well-ordered CH3-terminated alkanethiol self-assembled monolayers on gold.," *Biosens. Bioelectron.*, vol. 24, no. 5, pp. 1074–82, Jan. 2009.

[237] C. S. Ltd, "XPS Spectra manual," 2013. [Online]. Available: http://www.casaxps.com/help_manual/manual_updates/xps_spectra.pdf.

[238] Y. Ning, H. Xie, H. Xing, W. Deng, and D. Yang, "Comparison of Self-Assembled Monolayers ofn-Alkanethiols and Phenylthioureas on the Surface of Gold," *Surf. Interface Anal.*, vol. 24,

no. 9, pp. 667–670, Sep. 1996.

[239] U. Gelius *et al.*, "Molecular Spectroscopy by Means of ESCA III. Carbon compounds," *Phys. Scr.*, vol. 2, no. 1–2, pp. 70–80, Jul. 1970.

[240] A. Widrig and M. D. Porter, "The electrochemical desorption of n-alkanethiol from polycrystalline Au and Ag electrodes monolayers," *J. Electroanal. Chem.*, vol. 310, pp. 335–359, 1991.

[241] A. T. Hubbard, *Encyclopedia of Surface and Colloid Science* -, no. Bd. 1. Taylor & Francis, 2002.

[242] H. Wano and K. Uosaki, "In Situ dynamic monitoring of electrochemical oxidative adsorption and reductive desorption processes of a self-assembled monolayer of hexanethiol on a Au(111) surface in KOH ethanol solution by scanning tunneling microscopy.," *Langmuir*, vol. 21, no. 9, pp. 4024–33, Apr. 2005.

[243] R. A. MacPhail, H. L. Strauss, R. G. Snyder, and C. A. Elliger, "Carbon-hydrogen stretching modes and the structure of n-alkyl chains. 2. Long, all-trans chains," *J. Phys. Chem.*, vol. 88, no. 3, pp. 334–341, Feb. 1984.

[244] R. G. Snyder, H. L. Strauss, and C. A. Elliger, "Carbon-hydrogen stretching modes and the structure of n-alkyl chains. 1. Long, disordered chains," *J. Phys. Chem.*, vol. 86, no. 26, pp. 5145–5150, Dec. 1982.

[245] D. M. Small, "Lateral chain packing in lipids and membranes.," *J. Lipid Res.* , vol. 25, no. 13, pp. 1490–1500, Dec. 1984.

[246] X. Bin, I. Zawisza, J. D. Goddard, and J. Lipkowski, "Electrochemical and PM-IRRAS Studies of the Effect of the Static Electric Field on the Structure of the DMPC Bilayer Supported at a Au(111) Electrode Surface," *Langmuir*, vol. 21, no. 1, pp. 330–347, Jan. 2005.

[247] I. Zawisza, X. Bin, and J. Lipkowski, "Potential-Driven Structural Changes in Langmuir−Blodgett DMPC Bilayers Determined by in situ Spectroelectrochemical PM IRRAS," *Langmuir*, vol. 23, no. 9, pp. 5180–5194, Apr. 2007.

[248] M. Moskovits, "Surface selection rules," *J. Chem. Phys.*, vol. 77, no. 9, pp. 4408–4416, Nov. 1982.

[249] D. L. Allara and R. G. Nuzzo, "Spontaneously organized molecular assemblies. 2. Quantitative infrared spectroscopic determination of equilibrium structures of solution-adsorbed n-alkanoic acids on an oxidized aluminum surface," *Langmuir*, vol. 1, no. 1, pp. 52–66, Jan. 1985.

[250] D. L. Allara and J. D. Swalen, "An infrared reflection spectroscopy study of oriented cadmium arachidate monolayer films on evaporated silver," *J. Phys. Chem.*, vol. 86, no. 14, pp. 2700–2704, Jul. 1982.

[251] R. G. Nuzzo, L. H. Dubois, and D. L. Allara, "Fundamental studies of microscopic wetting on organic surfaces. 1. Formation and structural characterization of a self-consistent series of polyfunctional organic monolayers," *J. Am. Chem. Soc.*, vol. 112, no. 2, pp. 558–569, Jan. 1990.

[252] G. Wittstock, M. Burchardt, S. E. Pust, Y. Shen, and C. Zhao, "Scanning electrochemical microscopy for direct imaging of reaction rates," *Angew. Chemie - Int. Ed.*, vol. 46, no. 10, pp. 1584–1617, 2007.

[253] A. J. Bard and M. V Mirkin, *Scanning Electrochemical Microscopy, Second Edition*. Taylor & Francis, 2012.

[254] R. Cornut and C. Lefrou, "New analytical approximation of feedback approach curves with

a microdisk SECM tip and irreversible kinetic reaction at the substrate," *J. Electroanal. Chem.*, vol. 621, no. 2, pp. 178–184, 2008.

[255] J. Spreight, *Lange`s Handbook of Chemistry*, 16th ed. New York: McGraw-Hill Education, 2005.

[256] D. Oyamatsu, S. Kuwabata, and H. Yoneyama, "Underpotential deposition behavior of metals onto gold electrodes coated with self-assembled monolayers of alkanethiols," *J. Electroanal. Chem.*, vol. 473, no. 1, pp. 59–67, 1999.

[257] N. B. Zolotoy and G. V Karpov, "The Conventional Method of the Determination of Enthalpy Change at Ion Solvation in Solutions: Is It Correct?," *J. Phys. Chem. B*, vol. 104, no. 31, pp. 7468–7470, Aug. 2000.

[258] P. Krysinski, M. R. Moncelli, and F. Tadini-Buoninsegni, "A voltammetric study of monolayers and bilayers self-assembled on metal electrodes," *Electrochim. Acta*, vol. 45, no. 12, pp. 1885–1892, Feb. 2000.

[259] S. Amemiya, A. J. Bard, F.-R. F. Fan, M. V. Mirkin, and P. R. Unwin, "Scanning Electrochemical Microscopy," *Annu. Rev. Anal. Chem.*, vol. 1, no. 1, pp. 95–131, 2008.

[260] M. Hilgemann *et al.*, "Electrochemical Assay to Quantify the Hydroxyl Radical Scavenging Activity of Medicinal Plant Extracts," *Electroanalysis*, vol. 22, no. 4, pp. 406–412, Feb. 2010.

[261] I. Böse, "Anwendung neuartiger elektrochemischer Methoden zur Untersuchung der Radikalfängereigenschaften von biogenen Antioxidantie," 2011.

[262] A. Nadezhdin and H. B. Dunford, "Oxidation of nicotinamide adenine dinucleotide by hydroperoxyl radical. A flash photolysis study," *J. Phys. Chem.*, vol. 83, no. 15, pp. 1957–1961, 1979.

[263] K. Krumova and G. Cosa, "Chapter 1 Overview of Reactive Oxygen Species," in *Singlet Oxygen: Applications in Biosciences and Nanosciences, Volume 1*, vol. 1, The Royal Society of Chemistry, 2016, pp. 1–21.

[264] G. V. Buxton, C. L. Greenstock, W. P. Helman, and A. B. Ross, "Critical Review of rate constants for reactions of hydrated electrons, hydrogen atoms and hydroxyl radicals (·OH/·O−in Aqueous Solution," *J. Phys. Chem. Ref. Data*, vol. 17, no. 2, pp. 513–886, 1988.

[265] M. Arora, "Cell Culture Media: A Review," *Mater. Methods*, vol. 3, Mar. 2013.

[266] D. Wang, L. Zhao, H. Ma, H. Zhang, and L.-H. Guo, "Quantitative Analysis of Reactive Oxygen Species Photogenerated on Metal Oxide Nanoparticles and Their Bacteria Toxicity: The Role of Superoxide Radicals," *Environ. Sci. Technol.*, p. acs.est.7b00473, 2017.

[267] Y. Li, W. Zhang, J. Niu, and Y. Chen, "Mechanism of photogenerated reactive oxygen species and correlation with the antibacterial properties of engineered metal-oxide nanoparticles," *ACS Nano*, vol. 6, no. 6, pp. 5164–5173, 2012.

[268] E. L. Bastos, P. Romoff, C. R. Eckert, and W. J. Baader, "Evaluation of Antiradical Capacity by H2O 2-Hemin-Induced Luminol Chemiluminescence," *J. Agric. Food Chem.*, vol. 51, no. 25, pp. 7481–7488, 2003.

[269] P. F. Rosewell and E. H. White, "Luminol Chemoluminescence," in *Chemi- and Bioluminescence*, Burr, Ed. New York: Dekker, Marcel, 1985, p. 215.

[270] C. Lu, G. Song, and J.-M. Lin, "Reactive oxygen species and their chemiluminescence-detection methods," *TrAC Trends Anal. Chem.*, vol. 25, no. 10, pp. 985–995, 2006.

[271] I. Parejo, C. Codina, C. Petrakis, and P. Kefalas, “Evaluation of scavenging activity assessed by Co(II)/EDTA-induced luminol chemiluminescence and DPPH· (2,2-diphenyl-1-picrylhydrazyl) free radical assay,” *J. Pharmacol. Toxicol. Methods*, vol. 44, no. 3, pp. 507–512, 2000.

[272] I. Parejo, C. Petrakis, and P. Kefalas, “A transition metal enhanced luminol chemiluminescence in the presence of a chelator,” *J. Pharmacol. Toxicol. Methods*, vol. 43, no. 3, pp. 183–190, 2000.

[273] M. J. G. Hastings *et al.*, “MEASUREMENT OF LUMINOL-DEPENDENT CHEMILUMINESCENCE,” pp. 147–153, 1982.

[274] I. Kraljić and C. N. Trumbore, “p-Nitrosodimethylaniline as an OH Radical Scavenger in Radiation Chemistry,” *J. Am. Chem. Soc.*, vol. 87, no. 12, pp. 2547–2550, 1965.

[275] L. R. Fukumoto and G. Mazza, “Assessing Antioxidant and Prooxidant Activities of Phenolic,” *J. Agric. Food Chem.*, vol. 48, no. 8, pp. 3597–3604, 2000.

[276] G. J. Marco, “A rapid method for evaluation of antioxidants,” *J. Am. Oil Chem. Soc.*, vol. 45, no. 9, pp. 594–598, Sep. 1968.

[277] A. L. Dawidowicz and M. Olszowy, “Influence of some experimental variables and matrix components in the determination of antioxidant properties by $β$-carotene bleaching assay: experiments with BHT used as standard antioxidant,” *Eur. Food Res. Technol.*, vol. 231, no. 6, pp. 835–840, 2010.

[278] V. Kuellmer, “Ascorbic Acid,” in *Kirk-Othmer Encyclopedia of Chemical Technology*, K. Othmer, Ed. New York: John Wiley & Sons, Ltd., 2001.

[279] M. J. (ed. . O’Neil, *The Merck Index - An Encyclopedia of Chemicals, Drugs, and Biologicals*. Whitehouse Station, NJ: Merck and Co., Inc., 2006.

[280] J. Chappell and K. Hahlbrock, “Transcription of plant defence genes in response to UV light or fungal elicitor,” *Nature*, vol. 311, p. 76, Sep. 1984.

[281] A. Seidell, *Solubilities of Organic compounds*, 3rd ed. New York: D. an Nostrand Company, Inc., 1941.

[282] J. B. Zvezdanović, J. S. Stanojević, D. Z. Marković, and D. Cvetković, “Irreversible UV-induced quercetin and rutin degradation in solution studied by UV spectrophotometry and HPLC chromatography,” *J. Serbian Chem. Soc.*, vol. 77, no. 3, pp. 297–312, 2012.

[283] A. LAVOLA, R. JULKUNEN-TIITTO, P. APHALO, T. DE LA ROSA, and T. LEHTO, “The effect of u.v.-B radiation on u.v.- absorbing secondary metabolites in birch seedlings grown under simulated forest soil conditions,” *New Phytol.*, vol. 137, pp. 617–621, 1997.

[284] S. D. Lin, E. H. Liu, and J. L. Mau, “Effect of different brewing methods on antioxidant properties of steaming green tea,” *LWT - Food Sci. Technol.*, vol. 41, pp. 1616–1623, 2008.

[285] X. Chen and D. U. Ahn, “Antioxidant activities of six natural phenolics against lipid oxidation induced by Fe2+ or ultraviolet light,” *J. Am. Oil Chem. Soc.*, vol. 75, no. 12, pp. 1717–1721, 1998.

[286] P. Mladěnka *et al.*, “In vitro analysis of iron chelating activity of flavonoids,” *J. Inorg. Biochem.*, vol. 105, no. 5, pp. 693–701, 2011.

[287] K. MacÁková *et al.*, “Iron reduction potentiates hydroxyl radical formation only in flavonols,” *Food Chem.*, vol. 135, no. 4, pp. 2584–2592, 2012.

[288] M. J. Laughton, B. Halliwell, P. J. Evans, J. Robin, and S. Hoult, “Antioxidant and pro-oxidant actions of the plant phenolics quercetin, gossypol and myricetin: Effects on lipid

peroxidation, hydroxyl radical generation and bleomycin-dependent damage to DNA," *Biochem. Pharmacol.*, vol. 38, no. 17, pp. 2859–2865, 1989.

[289] Y. J. Hyun *et al.*, "Photoprotective effect of Undaria crenata against ultraviolet B-induced damage to keratinocytes," *J. Biosci. Bioeng.*, vol. 116, no. 2, pp. 256–264, 2013.

[290] L. Gan *et al.*, "Fullerenes as a tert-Butylperoxy Radical Trap, Metal Catalyzed Reaction of tert-Butyl Hydroperoxide with Fullerenes, and Formation of the First Fullerene Mixed Peroxides C60(O)(OOtBu)4 and C70(OOtBu)10," *J. Am. Chem. Soc.*, vol. 124, no. 45, pp. 13384–13385, Nov. 2002.

[291] F. Virgili, M. P. Santini, R. Canali, R. R. Polakowska, A. Haake, and G. Perozzi, "Bcl-2 Overexpression in the HaCaT Cell Line is Associated With A Different Membrane Fatty Acid Composition and Sensitivity to Oxidative Stress," *Free Radic. Biol. Med.*, vol. 24, no. 1, pp. 93–101, 1998.

[292] Z. Huang, Y. Senoh, S. Katoh, and N. Miwa, "Preventive effects of a water-soluble derivative of chroman moiety of vitamin E on lipid hydroperoxide-induced cell injuries and DNA cleavages through repressions of oxidative stress in the cytoplasm of human keratinocytes," *J. Cell. Biochem.*, vol. 92, no. 3, pp. 425–435, Jun. 2004.

[293] L. Serrander *et al.*, "NOX5 is expressed at the plasma membrane and generates superoxide in response to protein kinase C activation," *Biochimie*, vol. 89, no. 9, pp. 1159–1167, 2007.

[294] I. Takac *et al.*, "The E-loop is involved in hydrogen peroxide formation by the NADPH oxidase Nox4," *J. Biol. Chem.*, vol. 286, no. 15, pp. 13304–13313, 2011.

[295] Y. Nisimoto, B. A. Diebold, D. Constentino-Gomes, and J. D. Lambeth, "Nox4: A hydrogen peroxide-generating oxygen sensor," *Biochemistry*, vol. 53, no. 31, pp. 5111–5120, 2014.

[296] D. A. Vessey, K.-H. Lee, and K. L. Blacker, "Characterization of the Oxidative Stress Initiated In Cultured Human Keratinocytes by Treatment with Peroxides," *J. Invest. Dermatol.*, vol. 99, no. 6, pp. 859–863, Dec. 1992.

[297] Q. X. Diao *et al.*, "Vitamin E promotes breast cancer cell proliferation by reducing ROS production and p53 expression.," *Eur. Rev. Med. Pharmacol. Sci.*, vol. 20, no. 12, pp. 2710–7, Jun. 2016.

[298] L.-G. Yang, X.-A. Tian, X.-Y. Li, J.-G. Huang, N.-Q. Liu, and Q.-L. Sun, "Trolox induces inhibition of cell proliferation and apoptosis in human colon cancer cells," *Bangladesh J. Pharmacol. Vol 10, No 4*, Nov. 2015.

[299] M. A. Kiebish, X. Han, H. Cheng, J. H. Chuang, and T. N. Seyfried, "Cardiolipin and electron transport chain abnormalities in mouse brain tumor mitochondria: lipidomic evidence supporting the Warburg theory of cancer," *J. Lipid Res.* , vol. 49, no. 12, pp. 2545–2556, Dec. 2008.

[300] T. Ohlig *et al.*, "Effects of siRNA-dependent knock-down of cardiolipin synthase and tafazzin on mitochondria and proliferation of glioma cells," *Biochim. Biophys. Acta - Mol. Cell Biol. Lipids*, vol. 1863, no. 4, pp. 379–387, 2018.

[301] Q. He, M. Wang, N. Harris, and X. Han, "Tafazzin knockdown interrupts cell cycle progression in cultured neonatal ventricular fibroblasts," *Am. J. Physiol. Circ. Physiol.*, vol. 305, no. 9, pp. H1332–H1343, Nov. 2013.

[302] S. Sentellas, O. Morales-Ibanez, M. Zanuy, and J. J. Albertí, "GSSG/GSH ratios in cryopreserved rat and human hepatocytes as a biomarker for drug induced oxidative stress," *Toxicol. Vitr.*, vol. 28, no. 5, pp. 1006–1015, 2014.

[303] Y. Yin *et al.*, "Quercitrin protects skin from UVB-induced oxidative damage," *Toxicol. Appl.*

Pharmacol., vol. 269, no. 2, pp. 89–99, 2013.

[304] M. Chalfant and K. Bernd, "Detecting Ozone-Induced Changes in Cellular Redox Balance via GSH / GSSG-Glo ™ Assay," Davidson, 2011.

[305] Y.-Y. He, J.-L. Huang, D. C. Ramirez, and C. F. Chignell, "Role of Reduced Glutathione Efflux in Apoptosis of Immortalized Human Keratinocytes Induced by UVA," *J. Biol. Chem.* , vol. 278, no. 10, pp. 8058–8064, Mar. 2003.

[306] R. Franco and J. A. Cidlowski, "SLCO/OATP-like Transport of Glutathione in FasL-induced Apoptosis: GLUTATHIONE EFFLUX IS COUPLED TO AN ORGANIC ANION EXCHANGE AND IS NECESSARY FOR THE PROGRESSION OF THE EXECUTION PHASE OF APOPTOSIS ," *J. Biol. Chem.* , vol. 281, no. 40, pp. 29542–29557, Oct. 2006.

[307] R. Singh, A. S. Karakoti, W. Self, S. Seal, and S. Singh, "Redox-Sensitive Cerium Oxide Nanoparticles Protect Human Keratinocytes from Oxidative Stress Induced by Glutathione Depletion," *Langmuir*, vol. 32, no. 46, pp. 12202–12211, Nov. 2016.

[308] J. J. Inbaraj and C. F. Chignell, "Cytotoxic Action of Juglone and Plumbagin: A Mechanistic Study Using HaCaT Keratinocytes," *Chem. Res. Toxicol.*, vol. 17, no. 1, pp. 55–62, Jan. 2004.

[309] G. M. Gordillo, A. Biswas, S. Khanna, J. M. Spieldenner, X. Pan, and C. K. Sen, "Multidrug Resistance-associated Protein-1 (MRP-1)-dependent Glutathione Disulfide (GSSG) Efflux as a Critical Survival Factor for Oxidant-enriched Tumorigenic Endothelial Cells," *J. Biol. Chem.* , vol. 291, no. 19, pp. 10089–10103, May 2016.

[310] S. Jacquoilleot *et al.*, "Glutathione metabolism in the HaCaT cell line as a model for the detoxification of the model sensitisers 2,4-dinitrohalobenzenes in human skin," *Toxicol. Lett.*, vol. 237, no. 1, pp. 11–20, 2015.

[311] O. Zitka *et al.*, "Redox status expressed as GSH:GSSG ratio as a marker for oxidative stress in paediatric tumour patients," *Oncol. Lett.*, vol. 4, no. 6, pp. 1247–1253, Dec. 2012.

[312] H. Masaki, Y. Okano, Y. Ochiai, K. Obayashi, H. Akamatsu, and H. Sakurai, *α-Tocopherol Increases the Intracellular Glutathione Level in HaCaT Keratinocytes*, vol. 36. 2002.

[313] M. Schlame, Y. Xu, and M. Ren, "The Basis for Acyl Specificity in the Tafazzin Reaction," *J. Biol. Chem.* , Feb. 2017.

[314] Q. He, N. Harris, J. Ren, and X. Han, "Mitochondria-targeted antioxidant prevents cardiac dysfunction induced by tafazzin gene knockdown in cardiac myocytes," *Oxid. Med. Cell. Longev.*, vol. 2014, 2014.

[315] G. Wang *et al.*, "Modeling the mitochondrial cardiomyopathy of Barth syndrome with induced pluripotent stem cell and heart-on-chip technologies," *Nat. Med.*, vol. 20, no. 6, pp. 616–623, 2014.

[316] G. Paradies, V. Paradies, V. De Benedictis, F. M. Ruggiero, and G. Petrosillo, "Functional role of cardiolipin in mitochondrial bioenergetics," *Biochim. Biophys. Acta - Bioenerg.*, vol. 1837, no. 4, pp. 408–417, 2014.

[317] E. Maranzana, G. Barbero, A. I. Falasca, G. Lenaz, and M. L. Genova, "Mitochondrial Respiratory Supercomplex Association Limits Production of Reactive Oxygen Species from Complex I," *Antioxid. Redox Signal.*, vol. 19, no. 13, pp. 1469–1480, Apr. 2013.

[318] S. Gorlach, J. Fichna, and U. Lewandowska, "Polyphenols as mitochondria-targeted anticancer drugs," *Cancer Lett.*, vol. 366, no. 2, pp. 141–149, Apr. 2018.

[319] F. Dajas, "Life or death: Neuroprotective and anticancer effects of quercetin," *J. Ethnopharmacol.*, vol. 143, no. 2, pp. 383–396, 2012.

[320] G. Yang *et al.*, “Caffeic Acid Directly Targets ERK1/2 to Attenuate Solar UV-Induced Skin Carcinogenesis,” *Cancer Prev. Res.*, vol. 7, no. 10, p. 1056 LP-1066, Oct. 2014.

[321] P. Thanyawan, O. Tasanee, and P. Uraiwan, “Caffeic Acid and Ferulic Acid Inhibit UVA-Induced Matrix Metalloproteinase-1 through Regulation of Antioxidant Defense System in Keratinocyte HaCaT Cells,” *Photochem. Photobiol.*, vol. 88, no. 4, pp. 961–968, Apr. 2012.

[322] B. Y. Kang *et al.*, “Transcriptional profiling in human HaCaT keratinocytes in response to kaempferol and identification of potential transcription factors for regulating differential gene expression,” *Exp. &Amp; Mol. Med.*, vol. 40, p. 208, Apr. 2008.

[323] C. Weixing, D. Zigang, V. Susanne, T. B. N., and B. G. Tim, “Inhibition of ultraviolet B–induced c-fos gene expression and p38 mitogen-activated protein kinase activation by (-)-epigallocatechin gallate in a human keratinocyte cell line,” *Mol. Carcinog.*, vol. 24, no. 2, pp. 79–84, Mar. 1999.

[324] E.-R. Lee, Y.-J. Kang, J.-H. Kim, H. T. Lee, and S.-G. Cho, “Modulation of Apoptosis in HaCaT Keratinocytes via Differential Regulation of ERK Signaling Pathway by Flavonoids,” *J. Biol. Chem.* , vol. 280, no. 36, pp. 31498–31507, Sep. 2005.

[325] L. D. Murad, N. da C. P. Soares, C. Brand, M. C. Monteiro, and A. J. Teodoro, “Effects of Caffeic and 5-Caffeoylquinic Acids on Cell Viability and Cellular Uptake in Human Colon Adenocarcinoma Cells,” *Nutr. Cancer*, vol. 67, no. 3, pp. 532–542, Apr. 2015.

[326] R. Mateos, L. Goya, and L. Bravo, “Uptake and Metabolism of Hydroxycinnamic Acids (Chlorogenic, Caffeic, and Ferulic Acids) by HepG2 Cells as a Model of the Human Liver,” *J. Agric. Food Chem.*, vol. 54, no. 23, pp. 8724–8732, Nov. 2006.

Eigenständigkeitserklärung

Hiermit erkläre ich, dass diese Arbeit bisher von mir weder an der Mathematisch-Naturwissenschaftlichen Fakultät der Ernst-Moritz-Arndt-Universität Greifswald noch einer anderen wissenschaftlichen Einrichtung zum Zwecke der Promotion eingereicht wurde.

Ferner erkläre ich, dass ich diese Arbeit selbstständig verfasst und keine anderen als die darin angegebenen Hilfsmittel und Hilfen benutzt und keine Textabschnitte eines Dritten ohne Kennzeichnung übernommen habe.

Unterschrift des Promovenden

Acknowledgements

"None of us is as smart, enduring or strong as all of us."

Keeping that thought in mind, I would like to thank all the people who contributed to the work and created the conditions making it possible.

Especially, I would like to thank Dr. Heike Kahlert for her professional advice, supervision and encouragement throughout the work.

Further, I would like to thank the group of Prof. Fritz Scholz, especially Chinnaya Jeyabharathi, Nico Heise, Paula Ahrens, Anja Albrecht and Gabriele Meyer, for their everyday support and advice.

Besides, I am grateful for the support of the group of Prof. Michael Lalk, especially of Simone Seefeldt, Stefanie Schneider, Anne Leonard and Daniel Schultz. The same holds true for the people from the group of Prof. Uwe Lendeckel and Dr. Christopher Horst Lillig, namely Manuela Gellert, Daniel Trnka and Sahra Gürtler.

I also thank Prof. Gunther Wittstock and Dr. Izabella Brand for hosting me at the University of Oldenburg and Prof. Dr. K. L. N. Phani for having me at the Central Electrochemical Research Institute in India. Thank you for the prosperous collaboration.

For mutual support, professional advice and fruitful collaborative work I thank my research training group 1947/“BiOx”. Being part of a graduate college greatly increased my resources at hand in an intellectual, social and technical way. The financial support of my work within the RTG by the DFG is gratefully acknowledged.

Finally, I thank my friends and family for continuous support, encouragement and motivation throughout the work.

All the ones mentioned above hold a large share in the presented work.